



Characterization of Performance in the
Monitoring of UASB Reactor

This is to certify that the


dissertation entitled

presented by

May Meiliang Wu

has been accepted towards fulfillment
of the requirements for

Ph.D degree in Environmental Engineering


Co-Major professor

Date 2-3-95


Co-Major Professor

LIBRARY
Michigan State
University

PLACE IN RETURN BOX to remove this checkout from your record.
TO AVOID FINES return on or before date due.

DATE DUE	DATE DUE	DATE DUE
_____	_____	_____
_____	_____	_____
_____	_____	_____
_____	_____	_____
_____	_____	_____
_____	_____	_____
_____	_____	_____

MSU is An Affirmative Action/Equal Opportunity Institution

c:\circ\dteduea.pm3-p.1

**CHARACTERIZATION OF PERFORMANCE AND MONITORING
OF THE UPFLOW ANAEROBIC SLUDGE BLANKET REACTOR**

Volume I

By

May Meiliang Wu

A DISSERTATION

Submitted to
Michigan State University
in partial fulfillment of the requirements
for the degree of

DOCTOR OF PHILOSOPHY

Department of Civil and Environmental Engineering

1995

ABSTRACT

CHARACTERIZATION OF PERFORMANCE AND MONITORING OF THE UPFLOW ANAEROBIC SLUDGE BLANKET REACTOR

By

May Meiliang Wu

Upflow Anaerobic Sludge Blanket (UASB) reactors have numerous applications for wastewater treatment in the food industry. Anaerobic granules used in UASB reactor systems are aggregates of microbial consortia performing anaerobic degradation (hydrolysis, acetogenesis and methanogenesis) of organic carbon present in waste water. The high microbial density of these granules and the resultant high rate of biological treatment process allow excellent treatment performance in small reactor volumes. The wide range of potential applications coupled with the complexity of the UASB process demonstrate the importance of developing strong engineering and scientific knowledge to achieve stable and controlled performance. This study focused on describing overall performance of an UASB reactor treating a synthetic brewery waste using anaerobic

granules. Work included characterization of UASB reactor hydraulics, metabolic performance, monitoring and modeling of UASB reactor performance.

Hydraulics of an UASB reactor was studied using LiCl as tracer and stimulus-response technique to evaluate effects of organic and hydraulic flux on reactor mixing. Three existing flow models were evaluated using the experimental data. Two new models were developed to describe the UASB reactor hydraulics at low and high OLR. UASB reactors represented non-ideal flow reactors for the experimental conditions tested (ranging from 4-10 kgCOD/m³bed-d OLR and 12 hrs-2days HRT). Increased gas production, a result of increased OLR, reduced dead volume and improved reactor mixing at a HRT of 12 hrs.

Substrate utilization kinetic studies were conducted for anaerobic granules collected from the UASB reactor treating a synthetic brewery waste. Mass transfer within liquid boundary layer and within granules and temperature effects on acetate utilization were evaluated. Whole granules, partially disrupted granules and granule flocs, developed by mechanically disrupting granules, were tested. Temperature was varied from 26°C to 37°C. Substrate used for mass transfer experiments included acetate, propionate and ethanol. Intrinsic kinetic parameters k_m and K_s , for acetate, propionate and ethanol, were estimated using granule flocs. The effectiveness factors of whole granules, η , were 0.32, 0.41, 0.75, for acetate, propionate and ethanol, respectively.

Microbial conversion of ethanol using anaerobic granules was conducted to examine the fate of substrate, metabolic intermediates, and final products during ethanol degradation. Free energy analysis was performed for 14 major potential reactions. Based on the observation of n-propanol production, the n-propanol pathway was studied using

^{13}C bicarbonate to evaluate the role of CO_2 in formation of n-propanol during ethanol degradation. Anaerobic granule physical structure and microbial populations were examined using light and Confocal microscopy.

Responses of the trace gases H_2 and CO and reactor performance during various hydraulic loading rates, organic loading rates and variation in feed composition at pseudo-steady state of an UASB reactor were examined. Unsteady state monitoring experiments were conducted to study the potential use of H_2 and CO as indicators for the UASB reactor system, to detect onset of unstable conditions (organic overloading) and system failure. Statistical analyses were performed.

A dynamic mathematical model incorporating reactor hydraulics, substrate utilization kinetics and mass transfer within granules was developed for the UASB reactor. Numerical methods were used to solve the model. Sensitivity analyses for model parameters were performed. The model was calibrated using data from the acetate impulse experiment and then evaluated with acetate step increase experiments.

ACKNOWLEDGMENTS

My gratitude goes first to Dr. Robert Hickey, my principal advisor for his encouragement, advice and guidance during my study.

I would like to express my sincere appreciation to Dr. Thomas Voice and Dr. Craig Criddle , for their advice, assistance, valuable comments and interest in the outcome of this research. Thanks is extended to Dr. James Tiedje and Dr. William Saul for their patience and help during this research.

Many persons collaborated with me on innumerable occasions during this research at Michigan Biotechnology Institute. I want to thank Dr. Wei-min Wu for helpful and stimulating discussions, Jeff Cook for his skill and dedication in the laboratory, Dan Wagner for the reactor fabrication. Thanks also extended to Dr. Jain-Er Lin, Dr. Michèle van der Walle and Leslie Neilson for their help during this journey.

I also like to thank US EPA and New York State Energy Research Authority, especially to Barry Liebowitz, for the financial support.

Finally, I would like to thank my husband for his encouragement, understanding and support, and our son, Joseph, without him, this study could be finished one year earlier.

TABLE OF CONTENTS

Chapter	Page
LIST OF TABLES	xi
LIST OF FIGURES	xv
1. INTRODUCTION	1
2. BACKGROUND	3
A. Methanogenesis and methane production	3
B. Substrate transport and utilization within anaerobic granules	7
C. Process monitoring and dynamic modeling.....	9
3. OBJECTIVES AND PROCEDURAL OVERVIEW	14
A. Objectives	14
A-1. Overall objectives.....	14
A-2. UASB reactor hydraulics	14
A-3. Metabolic performance of an UASB reactor	15
A-4. Monitoring and modeling UASB reactors	15
B. Experimental approaches.....	16
B-1. UASB reactor hydraulics	16
B-2. Metabolic performance of an UASB reactor	16
B-3. Monitoring and modeling UASB reactors	16
4. THEORETICAL DEVELOPMENT	18
A. A dynamic model of UASB reactor with granular sludge.....	18
A-1. Reactor hydraulics and fluid flow model.....	18
A-1.1. Parallel CSTRs and a dispersion PFR in series with a PFR (modell)	19
A-1.11. Dispersion model	20
A-1.12. Mixed flow and plug flow model	22

A-1.2. Two CSTRs in series followed by a PFR (Van der Meer model)	24
A-1.3. One CSTR and a dispersion PFR in series model (model 2)	26
A-2. Integrated reaction-diffusion and hydraulic model	27
A-2.1. Reaction-diffusion model	28
A-2.2. Development of a dynamic model including a flow model combined with a reaction-diffusion model for UASB reactors	32
5. HYDRAULIC CHARACTERISTICS OF AN UASB REACTOR WITH GRANULAR SLUDGE	34
A. Introduction.....	34
B. Organic loading and hydraulic flux effect ...	38
B-1. UASB reactor	38
B-2. Tracer study	39
B-3. Organic loading and hydraulic flux effects	39
C. Evaluation of existing fluid flow models and model development	41
C-1. Modeling at low OLR	42
C-2. Modeling at high OLR.....	43
D. Discussion	46
6. KINETICS OF SUBSTRATE UTILIZATION BY BREWERY GRANULES	66
A. Introduction.....	66
B. Intrinsic kinetics of acetate, propionate, ethanol utilization	71
B-1. Description of the laboratory batch system	71
B-2. Experiment design and methods	71
B-3. Kinetic parameter estimation for acetate, propionate, ethanol and H ₂	73
C. Mass transfer on brewery granule ...	76
C-1. Liquid film resistance	76
C-2. Effect of granule size on substrate diffusion	77
D. Temperature effect	79
E. Threshold and reaction thermodynamics during acetate and H ₂ utilization	80
F. Discussion	82
7. IDENTIFICATION OF GRANULE STRUCTURE, MAJOR MICROBIAL GROUPS AND PATHWAYS	107
A. Introduction	107

B. Ethanol degradation	111
B-1. Carbon and electron balance	114
B-2. Energetics of ethanol degradation	116
C. Pathway of n – propanol formation	117
C-1. Reaction thermodynamics of n-propanol formation	118
C-2. ¹³ C experiment on n-propanol formation	121
D. Identification of granule structures and major microbial groups	124
E. Discussion	125
 8. MONITORING UASB REACTOR TREATING SYNTHETIC BREWERY WASTE	156
A. Introduction.....	156
B. Monitoring CO and H ₂ at pseudo-steady state operation	160
B-1. On-line monitoring system and bench UASB reactor	160
B-2. Pseudo-steady state experiment	161
B-3. Statistics of H ₂ , CO and process variables	163
B-3.1 General statistics analysis	163
B-3.11 Mean, coefficient of variance, population distribution and standard error	163
B-3.12 Confidence level and mean versus OLR	164
B-3.13 Correlations	165
B-3.14 Analysis of variances and multiple comparison tests	165
B-3.2 OLR, HRT and feed concentration effect	166
B-3.3 Spectra analysis	167
B-4. Reaction energetics	169
C. Unsteady state OLR perturbations and response patterns	172
C-1. OLR variation at 2, 5, 8, 10 KgCOD/M ³ bed-d	172
C-2. OLR variation at 5,10,15, 20 KgCOD/M ³ bed-d	173
C-3. OLR random variation at 10, 15, 20, 25, 30, 60, 104 KgCOD/M ³ bed-d	174
C-4. OLR variation at 10, 30, 40, 50, 60 KgCOD/M ³ bed-d	178
D. Discussion	183
 9. MODELING UASB REACTOR USING A DYNAMIC MODEL INCLUDING REACTOR HYDRAULICS, REACTION AND DIFFUSION	227
A. Introduction	227
B. Development of a dynamic model	232
B-1. Model development, solution technique, and parameters	232

B-2. Simulation of UASB responses during acetate impulse	236
B-3. Model prediction during acetate step increases	238
C. Sensitivity analysis	240
D. Discussion	243
10. SUMMARY AND CONCLUSIONS	260
A. UASB reactor hydraulics	260
B. Kinetics of substrate utilization within the brewery granules	261
C. Microbial populations and granule structure	262
D. Monitoring UASB reactor	262
E. Dynamic modeling of UASB reactor	264
11. RECOMMENDATIONS FOR FUTURE RESEARCH	265
APPENDICES	
A. Medium and feed composition	266
B. Material and methods	270
B-1. Activity assays for acetate, propionate, ethanol using brewery granules	270
B-1.1. Inoculum and media	270
B-1.1.1. Inoculum preparation and biomass estimation	270
B-1.1.2. Medium preparation and inoculum transfer techniques	271
B-1.2. Assays for intrinsic kinetic parameters for acetate, propionate, and ethanol	271
B-2. Residence time distribution(RTD) experiment on laboratory bench-scale UASB reactor	272
B-3. Tracer recovery test for adsorption on granular sludge	273
B-4. Unsteady state perturbation experiment using the laboratory bench-scale UASB reactor	274
B-5. Dissolved hydrogen and carbon monoxide measurements	275
B-5.1. Trace gas analyzer ICM program	275
B-5.2. Procedure for dissolved H ₂ and CO measurements	275
B-6. Isotopic assay for determining n – propanol pathway	277
B-6.1. Protocol for extraction of n-propanol	277
B-7. Microscopy	278

C. Quality assurance and quality control	279
C-1. Monitoring and sample recording during laboratory bench – scale UASB reactor operation	279
C-2. Sampling, storage, analysis and calibration	281
C-2.1. VFAs, ethanol, and n – propanol	281
C-2.2. Formate.....	284
C-2.3. Gas phase analysis	285
C-2.31. Gas sampling loop and instrumentation	285
C-2.32. CO and H ₂ analysis and calibration.....	286
C-2.33. Dissolved H ₂ and CO	290
C-2.34. CH ₄	291
C-2.35. Gas production	292
C-2.36. CO ₂	293
C-2.4. Total suspended solids(TSS) and volatile suspended solids(VSS)	293
C-2.5. Total solids(TS) and volatile solids(VS) for granules	294
C-2.6. Lithium	295
C-3. Data sheets	296
D. Determination of Monod kinetic parameters <i>km</i> and <i>Ks</i> by nonlinear least square method	301
D-1. Differential form	301
D-2. Integrated form	302
E. Fortran program of dynamic hydraulic-reaction-diffusion modeling	305
References	318

LIST OF TABLES

Table VB-1.	Operational conditions of bench-scale UASB reactor during hydraulic experiments.	62
Table VB-2.	RTD experimental design.	62
Table VB-3.	Effect of organic loading rate on UASB reactor hydraulic characteristics.	63
Table VB-4.	Effect of recirculation on UASB reactor hydraulic characteristics.	64
Table VB-5.	Fluidization index of UASB reactor under different hydraulic operating conditions and granule sizes.....	65
Table VIB-1.	Environmental and operational conditions used for the bench-top reactor	98
Table VIB-2.	Sampling frequency for the acetate utilization assays	99
Table VIB-3.	Sampling frequency for the propionate utilization assays	99
Table VIB-4.	Summary of literature values of acetate and propionate utilization kinetics compare to results from this study	100
Table VIB-5.	Kinetics of ethanol and hydrogen utilization by the brewery granules compared to reported values in the literature	101
Table VIC-1.	Experimental design of liquid film resistance experiment for the brewery granules	102

Table VIC-2.	Estimated unsteady state effectiveness factor for substrate utilization using brewery granules	102
Table VID-1.	Estimated km of whole granules and flocs at 37°C, 31°C and 26°C, in gAcetate/gVS-d	103
Table VIE-1.	Acetate threshold and calculated minimum available Gibb's free energy during acetate metabolism	103
Table VIE-2.	Reported acetate threshold values.....	104
Table VIE-3.	Reported hydrogen threshold values for different hydrogenotrophic anaerobes	105
Table VIIB-1.	Possible reactions involving ethanol, acetate, methane, carbon monoxide, hydrogen, formate and carbon dioxide during ethanol fermentation and their standard Gibb's free energy changes	149
Table VIIC-1.	Possible reactions involving ethanol, n-propanol and propionate during ethanol degradation and their standard Gibb's free energy changes	150
Table VIIC-2.	Substrate and major products acetate and propionate concentrations varied with propanol during ethanol assay changes	151
Table VIIC-3.	GC/MS results from ¹³ C labeled ethanol assay.....	152
Table VIIC-4.	Gibb's free energy profiles of major reactions during initial hours of ethanol degradation	153
Table VIIIB-1.	Operational conditions of the bench-scale UASB reactor during pseudo-steady state experiment	216
Table VIIIB-2.	OLR, HRT and feed concentration at pseudo-steady state experiments	217
Table VIIIB-3.	Maximum frequency of acetate, propionate, CO ₂ , H ₂ , gas production and methane at different OLR. (calculated from periodogram).....	218

Table VIIIB-4.	Time phase between each pair of monitoring variables in frequency	219
Table VIIIB-5.	Fisher's white noise test results for each variable at different organic loading rate	220
Table VIIIB-6.	Range of mean, coefficient of variances and standard error of monitoring variables during pseudo-steady state experiment	221
Table VIIIB-7.	OLR, HRT and feed concentration effect on H ₂ , CO and performance variables	222
Table VIIIB-8.	Gibb's free energy change for propionate oxidation and methanogenesis at standard conditions	223
Table VIIIB-9.	Analysis of variance of each monitoring variables among OLRs operated at pseudo-steady state	224
Table VIIIB-10.	Results from Duncan's multiple range test and LSD test on means of monitoring variables (grouped by OLR)	225
Table VIIIB-11.	Head space and dissolved H ₂ and CO in the bench-scale UASB reactor	226
Table IXB-1.	Experimental conditions of the bench-scale UASB reactor during the acetate impulse and step OLR increase experiments	256
Table IXB-2.	Model parameters used in simulation	257
Table IXB-3.	Results obtained from acetate impulse and step OLR increase and Lithium Chloride impulse	258
Table IXB-4.	Comparison of UASB reactor hydraulics and mass transfer during Lithium Chloride and acetate impulse and acetate step OLR increase	259
Table A-1.	Mineral medium composition	266
Table A-2.	Composition of trace mineral solution	267

Table A-3.	Synthetic brewery waste feed composition, Feed I ...	268
Table A-4.	Synthetic brewery waste feed composition, Feed II, III, IV	268
Table A-5.	PBBM	269
Table B-1.	Typical sequency program during unsteady state perturbation experiment	274
Table B-2.	Unsteady state monitoring parameters setting for Paragon and ICM	275
Table C-1.	List of information recorded on Daily Monitoring Sheets	280
Table C-2.	Analytical methods for samples from laboratory bench-scale UASB and batch experiments	282
Table C-3.	GC operational conditions for VFAs analysis	283
Table C-4.	Reduced Gas Analyzer operating conditions	287
Table C-5.	ICM parameters programming	289
Table C-6.	Steady state daily monitoring sheet	299
Table C-7.	Unsteady state monitoring sheet	300

LIST OF FIGURES

Figure II-1.	Carbon and electron flow in methanogenic environments. Metabolic groups involved: I. hydrolytic and fermentative bacteria; II. Proton-reducing acetogenic bacteria; III. methanogenic bacteria a) hydrogenophilic b) acetophilic; IV. homoacetogenic bacteria; V. Fatty acid-synthesizing bacteria. After Zehnder et al.[1981].....	12
Figure II-2.	Effect of hydrogen partial pressure on the Gibb's free energy changes of conversion of ethanol, propionate, acetate and hydrogen during methane formation. After McCarty [1981].....	13
Figure IVA-1.	Flow chart of model 1 describing UASB reactor at low gas production.	19
Figure IVA-2.	Flow chart of Van der Meer model.	24
Figure IVA-3.	A shematic representation of model 2 describing UASB reactor at high gas production.	26
Figure IVA-4.	Mass transport, diffusion and reaction within a slab of biofilm.	28
Figure IVA-5.	A crossection of a granule with radius R, active layer thickness δ and substrate profile S.	30
Figure VB-1.	Schematic representation of fluid flow models evaluated in this work.	52
Figure VB-2.	Effect of organic loading rate on hydraulic behavior at 2gpm/sqft.	53
Figure VB-3.	Effect of organic loading rate on hydraulic behavior at 5gpm/sqft.	53

Figure VB-4.	Comparison of effect at two surface upflow rates and an organic loading rate of 10 gCOD/Lbed-d.	54
Figure VB-5.	Comparison of effect at two surface upflow rates and an organic loading rate of 5 gCOD/Lbed-d.	54
Figure VC-1.	Measured data compare with ideal CSTR at OLR 4gCOD/Lbed-d and HRT 99 hrs.	55
Figure VC-2(a).	Results obtained using the CHolette-Cloutier model at OLR 4 gCOD/Lbed-d and HRT 99 hrs.	55
Figure VC-2(b).	Results obtained using the Hall model at OLR 4 gCOD/Lbed-d and HRT 99 hrs.	56
Figure VC-2(c).	Results obtained using the Van der Meer model at OLR 4 gCOD/Lbed-d and HRT 99 hrs.	56
Figure VC-3.	Representation of Model 1 used to describe UASB hydraulics at low OLR and high HRT.	57
Figure VC-4.	Results obtained using the Model 1 at OLR 4 gCOD/Lbed-d and HRT 99 hrs.	57
Figure VC-5.	Measured data compare with ideal CSTR at OLR 10 gCOD/Lbed-d and HRT 11 hrs.	58
Figure VC-6(a).	Results obtained using the Cholette-Cloutier model at OLR 10 gCOD/Lbed-d and HRT 11 hrs.....	58
Figure VC-6(b).	Results obtained using the Hall model at OLR 10 gCOD/Lbed-d andHRT 11 hrs.	59
Figure VC-6(c).	Results obtained using the Van der Meer model at OLR 10 gCOD/Lbed-d and HRT 11 hrs.....	59
Figure VC-7.	Model 2 describes UASB at high OLR and low HRT	60
Figure VC-8.	Results obtained using the Model 2 at OLR 10 gCOD/Lbed-d and HRT 11 hrs.	60

Figure VC-9.	Results obtained using the Model 1 at an OLR 10 gCOD/Lbed-d and HRT 11 hrs.	61
Figure VC-10.	Results obtained using the Model 2 at an OLR 4 gCOD/Lbed-d and HRT 99 hrs.	61
Figure VIB-1.	Schematic diagram of bench-top CSTR set-up	88
Figure VIB-2.	Acetate utilization by brewery granules and fitted Monod kinetics	89
Figure VIB-3.	Propionate utilization by brewery granules and fitted Monod kinetics	89
Figure VIB-4.	Ethanol utilization by brewery granule and fitted Monod kinetics	90
Figure VIB-5.	Hydrogen consumption by brewery granules	90
Figure VIC-1.	Acetate utilization rate at various impeller speeds. acetate=7mM, biomass=2g, pH=7.0, temp.=37°C ...	91
Figure VIC-2.	Acetate utilization by whole granules, disrupted granules and flocs in batch assays(31°C). Time scale was adjusted by biomass(VS,g). The slope represents substrate utilization rate in mMAcetate/gVS-h	92
Figure VIC-3.	Acetate utilization by whole granules, disrupted granules and flocs in batch assay(37°C). Time scale was adjusted by biomass(VS,g). The slope represents substrate utilization rate in mMAcetate/gVS-h	93
Figure VIC-4.	Acetate utilization rate at different acetate concentrations and granule sizes. T=37°C.	94
Figure VIC-5.	Size distribution of disrupted granules	94
Figure VID-1.	Acetate utilization at 37°C, 31°C, 26°C by whole granules. Time scale was adjusted by biomass(VS,g). The slope represents utilization rate in mMAcetate/gVS-h	95
Figure VID-2.	Acetate consumption rate of flocs and whole granules at 37°C, 31°C, 26°C. bars represent standard deviations	96

Figure VID-3.	Linearization of km and temperature effects for acetate utilization by flocs. $y=33.44793 - 9888.54 x$ $r^2=0.95$	96
Figure VID-4	Linearization of km and temperature effects for acetate utilization by whole granules. $y=25.658 - 7854.31 x$ $r^2=0.95$	97
Figure VIIB-1.	Substrate and products concentration profile (ethanol, acetate, methane and carbon monoxide) during ethanol fermentation.....	132
Figure VIIB-2.	Substrate and products concentration profile (hydrogen and formate) during ethanol fermentation	133
Figure VIIB-3.	Substrate and products concentration profile (propionate, propanol and carbon dioxide) during ethanol fermentation.....	133
Figure VIIB-4.	Electron balance of substrate and products during ethanol degradation in batch CSTR study using brewery granules	134
Figure VIIB-5.	Gibb's free energy changes during ethanol degradation: reactions 1,3,6 and 15	135
Figure VIIB-6.	Gibb's free energy changes during ethanol degradation: reactions 2,4,5 and 7	135
Figure VIIB-7.	Carbon balance of substrate and products during ethanol assay using brewery granules(flocs) in batch CSTR	136
Figure VIIC-1.	Gibb's free energy variations of ethanol oxidation reactions	137
Figure VIIC-2.	Gibb's free energy variations of n-propanol formation and consumption reactions during ethanol degradation by brewery granules	137

Figure VIIC-3.	Gibb's free energy variations of propionate formation reactions during ethanol degradation by brewery granules	138
Figure VIIC-4.	Gibb's free energy variations of propionate consumption during ethanol degradation by brewery granules	138
Figure VIIC-5.	Typical progress curves of ethanol and acetate during ethanol degradation using whole granules. (experiment stopped after 71hrs)	139
Figure VIIC-6.	Typical progress curves of propionate and n-propanol during ethanol degradation using whole granules. (experiment stopped after 71hrs)	139
Figure VIIC-7.	Possible reactions occurring during initial 11 hours in ethanol assay based on available free energy analyses using brewery granule flocs. a). $t=0.5$ to 5 hr., b). $t=6-8$ hr., c). $t=9-11$ hr.	140
Figure VIID-1.	Low magnification thin section microscopy of granules from bench UASB reactor-layered structures: a) cross section view of granule A. magnification 44, b) cross section view of granule B. magnification 65, c) a section of a granule, higher cell density in the outer-layer. magnification 167	142
Figure VIID-2.	Heterogeneous microbial distributions in outer-layer of a granule. (Olympus BH-2 epifluorescence microscope) magnification 1790. a) finger looking structure, spaces in between serve as gas vent. Clusters of different rods distributed through out the entire layer. b) another section of the outer-layer	144
Figure VIID-3.	Transparent layer: spaces between outer layer and central core of a granule. (Olympus BH-2 epifluorescence microscope. magnification 1790)	145
Figure VIID-4.	Decreased cell density in the central core of a granule. (Olympus BH-2 epifluorescence microscope. magnification 1790)	146

Figure VIID-5.	Confocal laser beam microscopy of predominant species in brewery granules a) <i>Methanothrix</i> -like rods, b) <i>Desulfovibrio</i> -like rods	147
Figure VIID-6.	Confocal laser beam microscopy of predominant species in brewery granules c) <i>Desulfohalobium</i> -like big rods ...	148
Figure VIIIB-1.	Schematic representation of the bench-scale UASB reactor and the on-line data acquisition system	189
Figure VIIIB-2.	Typical profiles for acetate, propionate, CO, H ₂ , methane and gas production at pseudo-steady state. (OLR 15 kgCOD/m ³ bed-d, HRT 1.5d, feed concentration 13.7 kgCOD/m ³)	190
Figure VIIIB-3.	Bivariant plot of CO versus acetate at each pseudo-steady state	191
Figure VIIIB-4.	Bivariant plot of H ₂ versus acetate at each pseudo-steady state	192
Figure VIIIB-5.	Mean and confidence intervals of methane and gas production during pseudo-steady state operation	193
Figure VIIIB-6.	Mean and confidence intervals of H ₂ and CO during pseudo-steady state operation	194
Figure VIIIB-7.	Free energy change of propionate oxidation and methanogenesis during pseudo-steady state operation. (head space CO and H ₂ used for calculation)	195
Figure VIIIB-8.	Free energy change of propionate oxidation and methanogenesis during pseudo-steady state operation. (dissolved CO and H ₂ used for calculation)	196
Figure VIIIB-9.	Mean and confidence intervals of acetate and propionate during pseudo-steady state operation	197
Figure VIIIB-10.	Schematic diagram of correlations among monitoring variables at pseudo-steady state operations (based on results from correlation analysis; (+) – positive correlation; (-) – negative correlation; correlation test at $\alpha=0.01$)	198

Figure VIIIC-1.	Applied OLR and HRT and reactor methane content variation during OLR variation experiments (OLR: 5-15kgCOD/m ³ bed-d)	199
Figure VIIIC-2.	Hydrogen, carbon monoxide and gas production rate during OLR variation experiments (OLR: 5-15 kgCOD/m ³ bed-d)	200
Figure VIIIC-3.	Acetate, propionate and pH during OLR variation experiments (OLR: 5-15 kgCOD/m ³ bed-d)	201
Figure VIIIC-4.	Applied OLR and HRT and reactor methane content variation during OLR variation experiments (OLR: 5-25kgCOD/m ³ bed-d)	202
Figure VIIIC-5.	Hydrogen, carbon monoxide and gas production rate during OLR variation experiments (OLR: 5-25 kgCOD/m ³ bed-d)	203
Figure VIIIC-6.	Acetate, propionate, butyrate, isobutyrate and pH during OLR variation experiments (OLR: 5-25 kgCOD/m ³ bed-d)	204
Figure VIIIC-7.	Volatile suspended solids (VSS) during OLR variation experiment (OLR: 5-25 kgCOD/m ³ bed-d)	205
Figure VIIIC-8.	Applied OLR and HRT and reactor H ₂ responses during OLR variation experiments (OLR:10-104 kgCOD/m ³ bed-d)	206
Figure VIIIC-9.	Gas production rate, CO and methane content during OLR variation experiments (OLR:10-104 kgCOD/m ³ bed-d)	207
Figure VIIIC-10.	Acetate, propionate and soluble COD during OLR variation experiment (OLR: 10-104 kgCOD/m ³ bed-d)	208
Figure VIIIC-11.	pH, total suspended solids (Tss) and volatile suspended solids (Vss) during OLR variation experiments (OLR: 10-104 kgCOD/m ³ bed-d)	209

Figure VIIIC-12.	Four and five carbon compounds measured during OLR variation experiment (OLR:10-104 kgCOD/m ³ bed-d)	210
Figure VIIIC-13.	Applied OLR and HRT and reactor methane content variation during loading experiment (OLR: 10-60 kgCOD/m ³ bed-d)	211
Figure VIIIC-14.	Gas production rate, H ₂ and CO responses during OLR variation experiments (OLR:10-60 kgCOD/m ³ bed-d)	212
Figure VIIIC-15.	Acetate, propionate, butyrate and isobutyrate during OLR variation experiment (OLR:10-60 kgCOD/m ³ bed-d)	213
Figure VIIIC-16.	Ethanol, n-propanol, valerate, isovalerate and 2-methyl-butyrate during OLR variation experiments (OLR: 10-60 kgCOD/m ³ bed-d). 2MB: 2-methyl-butyrate	214
Figure VIIIC-17.	pH variation during OLR experiment (OLR:10-60 kgCOD/m ³ bed-d)	215
Figure VIIIC-18.	Carbon monoxide gas production from acetoclastic methanogenesis	187
Figure IXB-1.	Model simulation of acetate concentration during an acetate impulse and measured data from a bench-scale UASB reactor	249
Figure IXB-2.	Model simulation results of effluent acetate concentration during a step increase in acetate inlet concentration compared to measured data from the bench UASB reactor	249
Figure IXB-3.	Effect of reaction and diffusion in modeling data from the acetate impulse experiment	250
Figure IXB-4.	Model comparisons: one or two CSTRs and the newly developed hydraulic model with reaction and diffusion.....	250

Figure IXC-1.	Effect of maximum substrate utilization rate, k_m , on UASB reactor response during the acetate impulse experiment	251
Figure IXC-2.	Effect of half velocity constant, K_s , on UASB reactor response during the acetate impulse experiment	251
Figure IXC-3.	Effect of variation in granule radius R on UASB response during acetate impulse at different initial substrate concentrations (S_0).....	252
Figure IXC-4.	Effect of diffusion coefficient, D , on acetate concentration curve during acetate impulse	252
Figure IXC-5.	Effect of variations in diffusion coefficient, D , on UASB response during acetate impulse at different initial substrate concentration (S_0)	253
Figure IXC-6.	Effect of mass transfer coefficient, K_L , on UASB response during acetate impulse	253
Figure IXC-7.	Effect of dead volume, V_d , on acetate impulse modeling	254
Figure IXC-8.	Effect of by-pass flow $(1-f)Q$ on UASB response curve during acetate impulse	254
Figure IXC-9.	Effect of dispersion factor, $\frac{D_p}{L^2}$ ($\times 10$), on UASB response during an acetate impulse	255
Figure IXC-10.	Comparison of dispersion PFR and PFR (dispersion factor is zero) during acetate impulse modeling.....	255
Figure C-1.	Response of work file 7 and 8 to low concentration of acetate	297
Figure C-2.	Response of workfile 7 and 8 to high concentration of acetate	297
Figure C-3.	Schematic diagram of on-line gas volume measurement	298

CHAPTER 1. INTRODUCTION

Anaerobic processes have been used for wastewater treatment for more than a century. Over the past twenty years, anaerobic treatment has attracted considerably greater attention due to the development of high-rate anaerobic process, advanced monitoring and control technologies, and new discoveries in anaerobic microbiology.

Many studies have been performed using high-rate anaerobic processes such as UASB (Upflow Anaerobic Sludge Blanket) reactors, anaerobic fluidized bed reactors and anaerobic filters. UASB reactors with their ability to operate at short retention times (6-12 hrs), high organic loading rates ($10-15 \text{ kgCOD/m}^3\text{-d}$), and high removal efficiency, have broad applications in food industry world wide. They have seen considerable application in the USA and Netherlands. Anaerobic granules in UASB reactor systems are aggregates of microbial consortia comprised of 3-5 major groups of organisms. These granules have the advantages of high volumetric densities of microorganisms. This high density of biomass accumulation allows excellent treatment performance in small reactor volumes. All three major steps in the process of anaerobic degradation (hydrolysis, acetogenesis and methanogenesis) are involved in treating brewery wastewater. The complexity of the UASB process and wide range of potential applications demonstrate the importance of

In biological wastewater treatment processes, the primary goal of characterizing a process is to combine the knowledge of physico-chemical and microbial kinetics to allow a better understanding of the degradation process. Studying UASB reactors, includes better understanding the responses of system variables, their inherent properties, the physico-chemical-biological characteristics, along with on-line monitoring. Such research should result in the ability to control the process with great confidence. This can further improve system performance and avoid gross process failure. This research focuses on an overall description of UASB reactor performance in treating a synthetic brewery waste using anaerobic granules, including 1) characterization of UASB reactor hydraulics, 2) determination of metabolic performance of the anaerobic granules and 3) monitoring and modeling of UASB reactor performance.

CHAPTER 2. BACKGROUND

A. Methanogenesis and Methane Production

Methanogenesis is the terminal step in anaerobic degradation once inorganic electron acceptors such as nitrate and sulfate are exhausted. It is, therefore, the most important process in anaerobic freshwater lake sediments, sewage sludge, or the rumen, where the supply of nitrate or sulfate is small compared with the input of organic substrates. Chemically speaking, the entire, rather complex, process of anaerobically transforming complex organic substances to methane and carbon dioxide is a disproportionation of organic carbon into its most oxidized and its most reduced form. Carbon and electron flow in methanogenic environments can be described by a three step process (Figure II-1). Complex organic matter is first broken down to alcohol's, carboxylic acids (long chain fatty acids) through hydrolysis and fermentation. These compounds are further converted to acetate and H_2 during acetogenesis. Finally, methane is produced from the acetate and H_2/CO_2 . Major metabolic groups involved are: hydrolytic and fermentative bacteria (I), proton-reducing acetogens (II), methanogens (hydrogenotrophic and acetoclastic) (III) and the homoacetogenic bacteria (IV). Depending on the beginning substrate, acetoclastic methanogenesis contributes to about 70%-80% of the methane produced. The remaining 20%-30% of methane is formed by hydrogenotrophic methanogenesis. The percentage of methane in the gas mixture formed depends on the oxidation state of the substrate used. Carbohydrates are converted to equal amounts of methane and carbon dioxide, methanol and lipids to more methane than carbon dioxide, and no methane can be obtained from urea hydrolysis. During brewery waste water

and no methane can be obtained from urea hydrolysis. During brewery waste water treatment, all three steps of the anaerobic degradative process are involved. Theoretically, about 75% methane and 25% CO₂ are produced from degradation of the brewery waste used in this study.

Anaerobic degradation of complex organics requires the interactions of different groups of microorganism to form a “network” for a complete conversion of the organics to CO₂ and CH₄. These interactions are sensitive to environmental changes (i.e. waste type, waste strength, toxicity, etc.). Variation of environmental conditions could result in significant changes in microbial populations within the system and affect performance. Methanogenic bacteria are very sensitive to pH variations. A low pH environment can inhibit methane production to a great extent. Many toxicants were inhibitory to this group of organisms.

Methanogens are specialized for a unique form of energy metabolism. The central metabolic pathway in autotrophic methanogens involved the stepwise reduction of a one-carbon unit which was derived from the growth substrate such as CO₂. Acetoclastic methanogenesis is dependent upon the ability of the cell to cleave the acetate molecule, reduce the methyl substituent and oxidize the carboxyl substituent.

Unique coenzymes found in methanogens include factor F₄₂₀, MFR (methanofuran, carbon dioxide reduction factor), methanopterin, nickel-containing factor F₄₃₀, mobile factor (required by *Methanomicrobium mobile*), component B of the methylreductase system. These coenzymes play a major role in the methanogenic pathways.

Methanogenesis from acetate to methyl coenzyme M (CH₃-S-CoM) involves coenzyme M

as a methyl equivalent carrier, carbon monoxide dehydrogenase (CODH) oxidizes the carboxyl carbon, and cobamides. Methanogenesis from CO_2 and H_2 involves three coenzymes - MFR, H_4MPT , and Coenzyme M - as carbon carriers during the sequential reduction of CO_2 to CH_4 . The terminal reduction of $\text{CH}_3\text{-S-CoM}$ by hydrogen involves two additional cofactors, component B and factor F_{430} of the $\text{CH}_3\text{-S-CoM}$ methylreductase system which reduces the methyl moiety to methane.

Methanogens are limited to simple growth substrates and can only obtain limited amounts of energy from these substrates. A comparison of the free energy changes of hydrolysis of ATP (-31.8 kJ/mol) and those of methane formation from the substrates hydrogen and carbon dioxide (135.6 kJ/mol of CH_4), formate (-130.1 kJ), methanol (-104.9 kJ), methylamines (about -74 kJ), carbon monoxide (196.7 kJ) and acetate -31.0 kJ) lead to the conclusion that only small amounts of energy are available to these organisms [Daniels et al. 1984] [Thauer et al. 1977]. Membranes of methanogens are important in proton-dependent energy coupling. This includes a membrane-associated, proton-dependent ATPase coupled to a sodium/proton antiporter. A Na^+ gradient is maintained by an Na^+/H^+ antiporter implicated in ATP synthesis. Active transport has been described in transport coenzyme M, nickel and amino acids. Hydrogenase is central to methanogen bioenergetics. Methanogenesis and its energetics have been thoroughly reviewed [Jones et al., 1987] [Daniels et al., 1984].

Many of the bacteria of groups I, III and IV have been cultivated and studied in detail in the past. Not much is known about the bacteria of group II because they are difficult to cultivate independently; a sink for the reducing equivalents they produce is

required if the acetogenic reactions are to have favorable energetics. The Gibbs' free energy change $\Delta G'$ of a single chemical reaction



can be written in the form

$$\Delta G' = \Delta G^{\circ'} + RT \ln \left(\frac{c^{\gamma} d^{\delta}}{a^{\alpha} b^{\beta}} \right) \quad \dots \quad (\text{II-2})$$

Lowercase letters a, b, c, d signify molar concentrations of compounds A, B, C, D . Primes denote evaluation in aqueous solution at pH 7. The standard free energy change $\Delta G^{\circ'}$ denotes the free energy change in aqueous solution with all other reactants and products present at 1 M concentration, at 1 atmosphere and 273K. In a closed system, the reaction will proceed from left to right if and only if G' is negative.

Since the proton reducing acetogenic bacteria (group II) catalyze reactions which are thermodynamically endergonic under standard conditions, they can be cultivated only in the presence of hydrogen-scavenging bacteria such as methanogens, which maintain a sufficiently low hydrogen partial pressure to allow substrate degradation [Wolin, 1976]. A scheme that visualizes the thermodynamically delicate situation of ethanol and propionate degrading bacteria is given in Figure II-2. In order for propionate to be converted to acetate, the H_2 partial pressure must be maintained lower than 10^{-4} atm. Methanogenic hydrogen consumers, however, require a H_2 level higher than 10^{-6} atm to maintain a negative $\Delta G'$ for methanogenesis. The lower bound of H_2 reflects a minimum energy. Energy requirements form the basis of the concept of substrate thresholds. A threshold is the substrate concentration below which a specific organism can no longer use that substrate as the primary growth substrate.

B. Substrate transport and utilization within anaerobic granules

Reaction kinetics within biofilm systems (including anaerobic granules) often involves mass-transfer into biofilms and simultaneous substrate utilization. The effect of mass-transfer or diffusion on a specific system can be described by a coupled reaction-diffusion relationship. When using mixed cultures, substrate utilization can be generally described by Monod equation ($\frac{dS}{dt} = \frac{kmXS}{Ks + S}$) when there are no mass transfer limitations.

For Monod limiting substrate kinetics, when the substrate concentration is small ($S \ll Ks$), substrate utilization rate is proportional to $\frac{km}{Ks}$, the ratio of specific maximum substrate utilization rate km to half velocity constant Ks , times the biomass concentration, X and substrate concentration, S . The reaction rate approaches a constant Kmx when the substrate concentration becomes very large ($S \gg Ks$). Kinetic parameters km and Ks reflect the intrinsic properties of microorganisms for a specific substrate.

In a biofilm system, calculation of the observed rate of substrate disappearance requires evaluation of the concentration profile of substrate within the biofilm. Substrate must first traverse the external film or liquid boundary layer from bulk liquid and subsequently diffuses into biofilms where the biochemical reactions occur. The external mass transfer (substrate flux, Ns in mass per unit time per unit area) of substrate from the bulk liquid to the interface of liquid film and biofilm, is described by the following equation:

$$Ns = K_L (S_o - S) \quad \dots \quad (II-3)$$

where K_L is the mass transfer coefficient. S and S_0 are the substrate concentrations at the interface and in the bulk liquid, respectively. The diffusion of substrate follows Fick's law, or in X axis direction

$$\frac{\partial S}{\partial t} = -D \frac{\partial^2 S}{\partial x^2} \quad \dots \quad (\text{II-4})$$

where D is substrate diffusivity. The observed overall reaction rate (apparent rate) in the bulk liquid therefore, is a function of both reaction and mass transfer. Substrate concentrations within the biofilm varies with time and position. At steady state, the rate of substrate transported into the biofilm is balanced by substrate consumption so that a substrate profile within the biofilm is established. There are several factors affecting substrate utilization under a mass transfer limited biofilm system: 1) biofilm thickness or granule diameter 2) intrinsic kinetic parameters 3) temperature and pH 4) substrate concentration in the bulk liquid 5) diffusion and mass transfer coefficients 6) liquid film thickness. Using a dimensional analysis, the mass transfer limitation in the biofilm system can be described by an effectiveness factor, η . The η is defined as the ratio of observed reaction rate at the surface of the biofilm to the reaction rate without mass transfer limitation, or the intrinsic reaction rate. When η is lower than 1, the system is mass transfer limited. When η approaches 1, reaction becomes rate limiting. The effectiveness factor is influenced mostly by biofilm thickness or granule size. A detailed description of effectiveness factor and its evaluation is described elsewhere [Bailey and Ollis, 1986]. Mass diffusion through biofilm appears species dependent. The diffusivity of different species varies [Bennett and Myers, 1982]. For the same substrate, the diffusivity changes with temperature. Within the biofilm, diffusion is described by an effectiveness diffusion coefficient which combines influences of the substrate diffusivity in the bulk liquid, particle

porosity, tortuosity factor and restricted diffusion situation in pores, internal surface chemistry and charge.

C. Process monitoring and dynamic modeling

Process monitoring is performed to detect changes of key parameters from a target level or to observe the variability of the process. Monitoring can be combined with control measures to maintain a process at a certain level of performance. Monitoring is accomplished using process indicators. The functions of process indicators are: 1) to tell how the process is operating currently 2) to tell how the process may behave in the near future 3) to identify periods of poor operation when assignable causes exist. Ideal process indicators should be: 1) sensitive with low noise 2) easy to measure 3) have intrinsic meaning 4) provide early warning and 5) be amenable to on-line measurement.

Anaerobic wastewater treatment processes, in general, are pH and temperature sensitive, vulnerable to toxicants, and require a certain range of hydrogen concentration to maintain a balance between hydrogen producers and hydrogen utilizers. For best performance of high rate systems, the process must be monitored on a real-time basis. Various methods have been developed to detect variations in anaerobic wastewater treatment process, including on-line or off-line, liquid, solid or gas phases monitoring. Conventional process indicators in anaerobic system have been reactor liquid pH, effluent VFA and COD, gas production and methane production. Another category of monitoring has focused on parameters that have intrinsic meaning for biological consortia. These include using enzymatic, immunological or gene probe assays, lipid composition analysis,

F_{420} (growth factor), and fatty acids methyl ester (FAME) variation among methanogens.

Most of these methods are off line and time consuming. With improvements in monitoring technology and instrumentation, on-line monitoring in anaerobic wastewater treatment becomes increasingly available. In recent years, there has been considerable interest in the trace gases - CO and H_2 - for on-line monitoring. A computerized, on-line monitoring system along with process indicators that are simple, sensitive and reflect microbial or biochemical variations can contribute significantly to the operation of high rate anaerobic treatment process. Successful process monitoring allows application of a control strategy and can prevent system failure.

Mathematical modeling is still more of an art than a science. Several different approaches are possible; based on existing information, hypothesis formulation in the literature or theoretical knowledge from other branches of engineering and science. These lead to an explanation of phenomena known to occur in the field but not predicted by existing models. In wastewater treatment processes mathematical modeling can serve many purposes. Modeling serves as a conceptual framework upon which to build and test hypotheses, and it allows for exploration of the impact of a wide range of system variables, thereby extending knowledge. Modeling allows the development of control strategies by facilitating the investigation of treatment system response to a wide range of inputs without jeopardizing actual system performance. Dynamic modeling for bioreactors is used to describe unsteady-state reactor performance and to characterize transient behavior. The application of mathematical structured models to anaerobic waste treatment process was initially based on substrate utilization and growth of biomass. These simple

models, although not a great advance over empirical equations for design and operating treatment systems, were a step forward. These models were not, however, satisfactory in describing dynamic behavior and treatment of complex organic waste under different reactor flow conditions. For these cases, a more complex structured model is necessary. A structured model is one which considers the biomass and substrate to be divided into several components with biomass growth mediating the conversion of substrate to intermediates and final products. Physical, chemical and biological interactions during this process within the boundary volume (i.e. the reactor) are considered. Because of the unique characteristics of the bacteria in anaerobic treatment systems (low growth rates, high sensitivity to environmental factors and complex syntrophic populations) and variations of reactor configurations, use of such modeling approach becomes especially important.

To mathematically describe the biological processes, the kinetics, stoichiometries, mass transport and hydraulic relationships are incorporated into process material balances. This results in a family of simultaneous mathematical equations (a model) which can be used to describe and predict system performance under a variety of conditions.

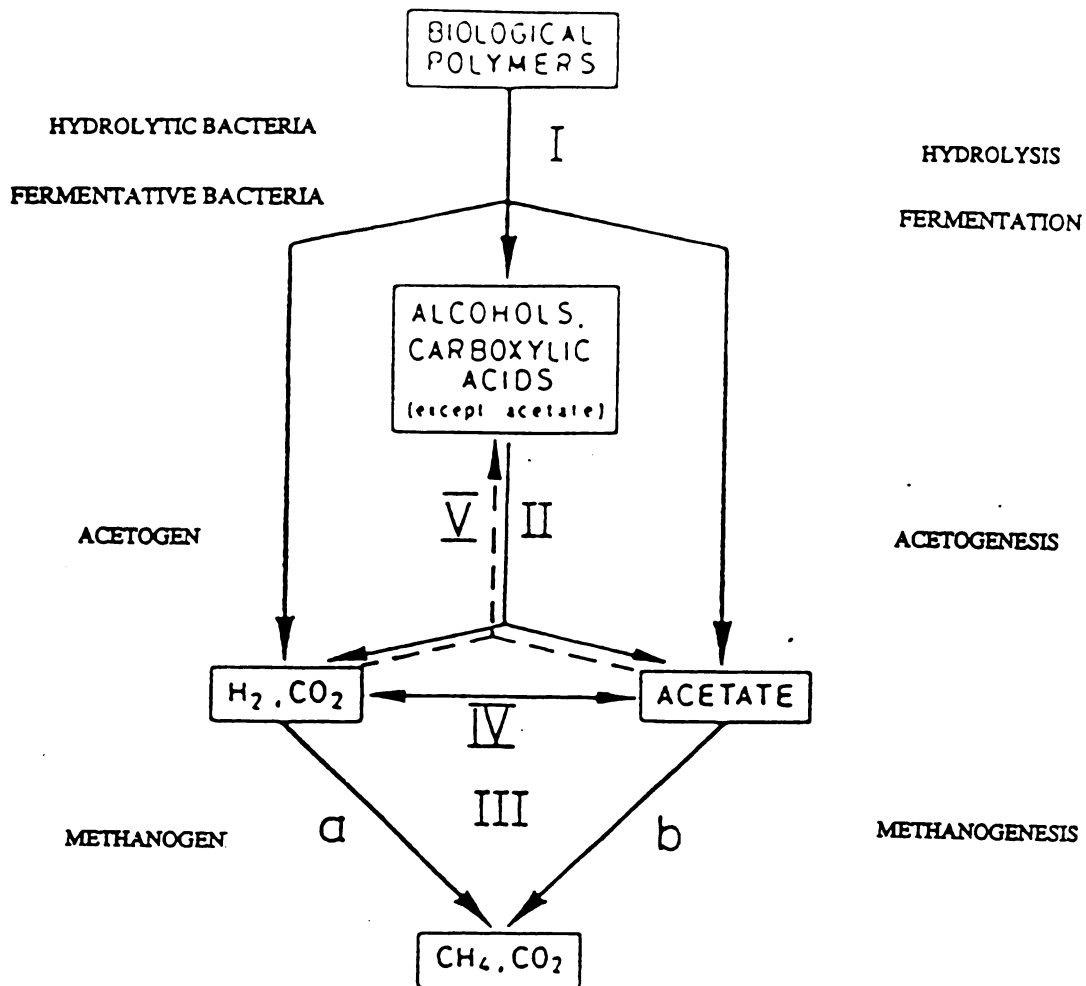


Figure II-1. Carbon and electron flow in methanogenic environments. Metabolic groups involved: I. hydrolytic and fermentative bacteria; II. Proton-reducing acetogenic bacteria; III. methanogenic bacteria a) hydrogenophilic b) acetophilic; IV. homoacetogenic bacteria; V. Fatty acid-synthesizing bacteria. After Zehnder et al.[1981].

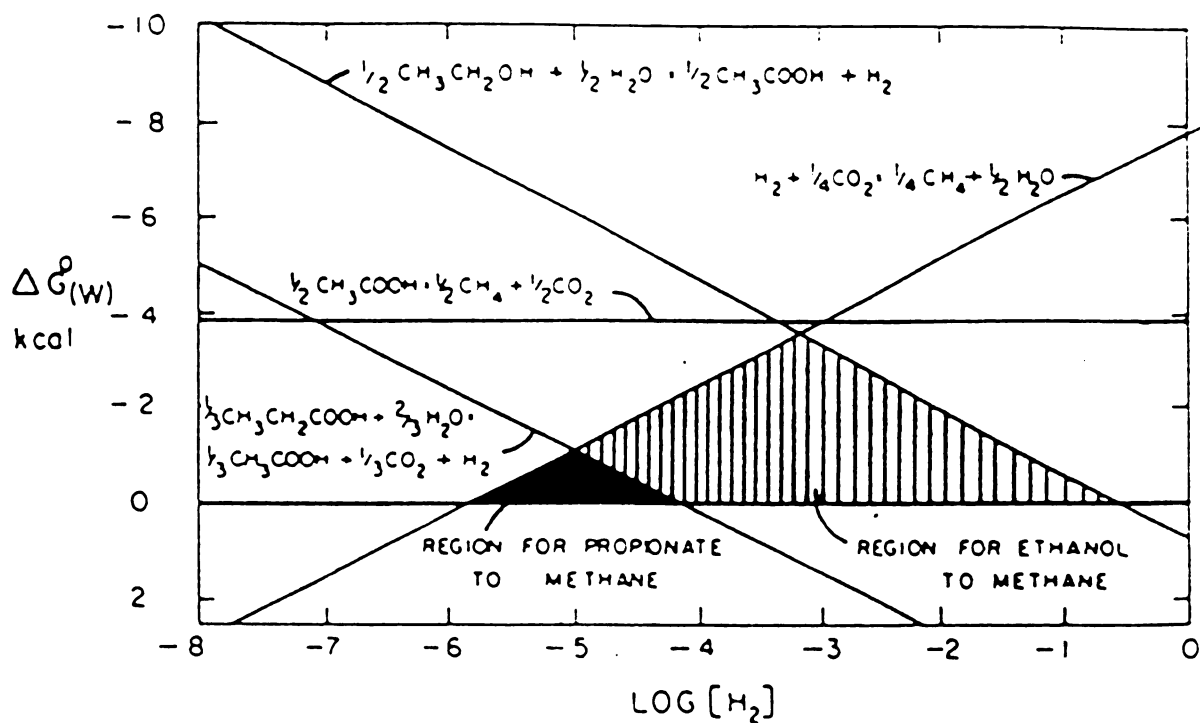


Figure II-2. Effect of hydrogen partial pressure on the Gibb's free energy changes of conversion of ethanol, propionate, acetate and hydrogen during methane formation. After McCarty[1981].

CHAPTER 3. OBJECTIVES AND PROCEDURAL OVERVIEW

A. Objectives

A-1. Overall objectives

The goal of this study is primarily to extend engineering knowledge in the area of anaerobic treatment. The primary objective is to develop the information base needed to improve process monitoring, control and design of UASB reactors. Specific tasks within this objective include:

- characterize the UASB reactor in terms of its hydraulic, kinetic, and mass transfer aspects
- monitor UASB reactor overall performance under pseudo-steady state and dynamic conditions and develop a dynamic mathematic model to describe performance of the UASB reactor

A-2. UASB reactor hydraulics

The **objectives** of this portion of work are

- examine the effect of organic loading rate and hydraulic flux on UASB reactor hydraulics
- evaluation of existing flow models
- development of improved flow models for the UASB reactor

A-3. Metabolic performance of an UASB reactor

The **objectives** of this portion of work are

- examine the metabolic activity of brewery granules using different substrates
- examine mass transfer and diffusional limitations within the granules during substrate utilization
- examine the effect of temperature and substrate flux on overall substrate utilization
- examine acetate threshold during methanogenesis
- identify granule structure and predominant microbial groups
- identify pathway(s) of ethanol fermentation including n-propanol formation

A-4. Monitoring and modeling UASB reactors

The **objectives** of this portion of work are

- examine the impact of hydraulic loading, organic loading and organic composition on responses of H_2 and CO in the UASB reactor and relate these to reactor performance
- examine the potential of using H_2 and CO to detect onset of unstable conditions and system failure
- develop a dynamic mathematical model for UASB reactors by integrating reactor hydraulic, kinetic and mass transfer information

B. Experimental approaches

B-1. UASB reactor hydraulics

Experiments were conducted using a tracer study followed by flow modeling. An inert tracer, lithium chloride was used. An impulse of the tracer was imposed on the reactor system and the response measured (residence time distribution curves).

Several existing models were evaluated. Then improved models were developed and compared with these previous models.

B-2. Metabolic performance of biomass from an UASB reactor

Experiments were conducted in a batch CSTR (Multigen Bench-Top Fermentor). Liquid film boundary layer mass transfer limitation was examined by controlling mixing in the reactor. Temperature was controlled in order to examine temperature effects.

Anaerobic granules were disintegrated to help examine the extent of diffusional limitations. Substrates analyzed include ethanol, propionate, acetate and H_2 (during ethanol degradation)..

Microscopy was performed to examine the internal physical structure and biological properties of anaerobic granules. Labeled substrate was used in determining the potential pathways of n-propanol production during ethanol degradation.

B-3. Monitoring and modeling UASB reactors

These experiments were conducted in a bench-scale UASB reactor equipped with an on-line data acquisition system for monitoring H_2 , CO, methane content, and gas

production rate. During pseudo-steady state, the reactor was operated at various combinations of OLR, HRT and feed composition. During unsteady state operation, organic overloading was imposed on the reactor. The responses of H_2 and CO and the system performance were examined using statistical analysis.

Dynamic modeling was based on single substrate and one microbial population. A series of mass balances were established describing reactor mass transport and transformations. A hydraulic flow model and a diffusion-reaction model were incorporated into the dynamic model. The problem was solved numerically by developing a computer program (FORTRAN) and using subroutines from IMSL. Model calibration and verification were performed by a separate set of data gathered from the UASB reactor. Parameters sensitivities were analyzed.

CHAPTER 4. THEORETICAL DEVELOPMENT

A. A dynamic model of UASB reactor with granular sludge

A-1. Reactor hydraulics and fluid flow model

Reactor flow can be ideally described by two flow patterns: plug flow (PFR) and complete mixed flow (CSTR). In reality, real reactors never fully follow these flow patterns. In most cases deviations from these ideal flow patterns can be considerable. This deviation can be caused by channeling of fluid flow, or by creation of stagnant regions in the reactor. These problems of nonideal flow are intimately tied to those of scale-up because the question of whether to conduct pilot-scale testing and at what scale rests in large part on how much control we have of all the major variables for the process. Often the uncontrolled factor in scale-up is the magnitude of the nonideality of flow. Ignoring this factor may lead to gross errors in design.

Nonideal flow behavior such as short circuiting and dead volume may be present in UASB reactors. In this section, nonideal flow in a bench-scale UASB reactor was considered to consist of different regions interconnected in various ways. The modeling is accomplished using a combination of dispersion model and a network of ideal reactors (PFR or CSTR), connected in series or parallel. Since biogas production from the degradation of organic material affect reactor fluid mixing, several fluid flow models were developed (Chapter V) to describe UASB reactor flow under low and high biogas production regimes. Theoretical derivations of these flow models are presented in this section.

A-1.1 Parallel CSTRs and a dispersion PFR in series with a PFR (model 1)

Under conditions of low gas production, the UASB can be characterized as two CSTRs and a dispersion plug flow reactor in parallel followed by a plug flow reactor, as indicated by Figure IVA-1.

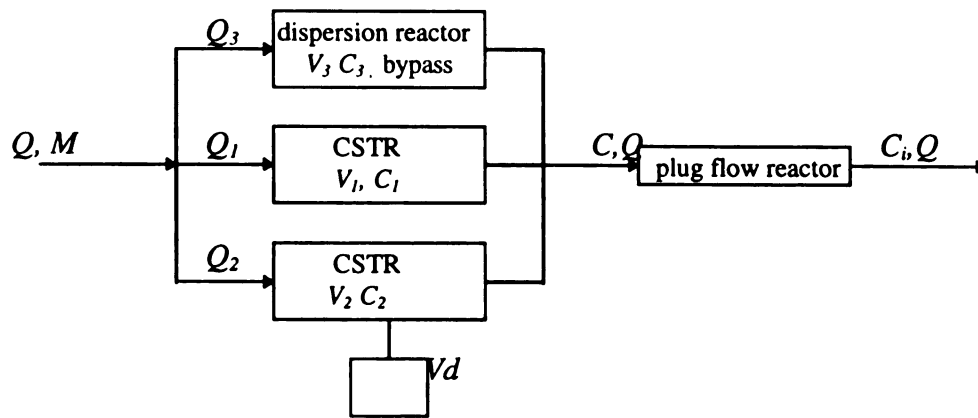


Figure IVA-1. Flow chart of model 1 describing UASB reactor at low gas production.

In this model, M is the amount of mass input into the system; V is volume; Q is flow rate; C is concentration; Vd is dead space. The by-pass flow is characterized by a dispersion model which is in-between mixing in actual flow and a diffusional process. Two parallel CSTRs and a dead volume describe the granular bed. The first CSTR describes the main mixing region in the bed (V_1). The other CSTR describes a small volume between this main mixing volume and a dead space. The dispersion reactor and CSTRs are followed by a plug flow reactor representing the clarification zone above the sludge bed.

A-1.11 Dispersion model

The mixing process involves a shuffling or redistribution of material either by slippage or eddies. This is repeated a considerable number of times during the flow of fluid through the reactor. We can consider these disturbances to be statistical in nature, somewhat as in molecular diffusion. For molecular diffusion in still water the governing differential equation is given by Fick's law

$$\frac{\partial C}{\partial t} = D_f \left[\frac{\partial^2 C}{\partial X^2} + \frac{\partial^2 C}{\partial Y^2} + \frac{\partial^2 C}{\partial Z^2} \right] \quad \dots \quad (\text{IV-1})$$

where C is concentration in reactor; t is time; D_f is diffusion coefficient. In an analogous manner we may consider all the contributions to backmixing of fluid flowing in the X , Y and Z directions to be described by a similar form of expression, or

$$\frac{\partial C}{\partial t} = D_p \left[\frac{\partial^2 C}{\partial X^2} + \frac{\partial^2 C}{\partial Y^2} + \frac{\partial^2 C}{\partial Z^2} \right] \quad \dots \quad (\text{IV-2})$$

where the parameter D_p , which we call the axial dispersion coefficient, uniquely characterizes the degree of backmixing occurring. Since here only one dimensional dispersion is considered, the above equation is reduced to

$$\frac{\partial C}{\partial t} = D_p \left[\frac{\partial^2 C}{\partial X^2} \right] \quad \dots \quad (\text{IV-3})$$

In the case when advection (bulk flow) is also present, a moving coordinate system (X, t axis) should be introduced. This X coordinate moves along with the stream at the mass average velocity, u . The fixed coordinate system (X', t') is defined by $X' = X + ut$, $t' = t$, where t is time. By differentiation, we have

$$dX' = dX,$$

$$\frac{dX'}{dt} = u,$$

$$dt' = dt,$$

$$\frac{dt'}{dX} = 0$$

Hence

$$\frac{\partial C}{\partial t} = \frac{\partial C}{\partial X'} \frac{\partial X'}{\partial t} + \frac{\partial C}{\partial t'} \frac{\partial t'}{\partial t} = u \frac{\partial C}{\partial X'} + \frac{\partial C}{\partial t'}$$

$$\frac{\partial C}{\partial X} = \frac{\partial C}{\partial X'} \frac{\partial X'}{\partial X} + \frac{\partial C}{\partial t'} \frac{\partial t'}{\partial X} = \frac{\partial C}{\partial X'}$$

Substituting the relations into equation IV-3, the equation for dispersion and advection in a fixed coordinate system has the form

$$\frac{\partial C}{\partial X'} u + \frac{\partial C}{\partial t'} = D_p \frac{\partial^2 C}{\partial X'^2}$$

or

$$\frac{\partial C}{\partial t'} = D_p \frac{\partial^2 C}{\partial X'^2} - u \frac{\partial C}{\partial X'} \quad 0 < t', 0 < X' < L \quad \dots \quad (\text{IV-4})$$

Let $Z = \frac{X'}{L}$, where L is the length of dispersion plug flow reactor. Equation (IV-4)

becomes

$$\frac{\partial C}{\partial t'} = \left(\frac{D_p}{L^2} \right) \frac{\partial^2 C}{\partial Z^2} - \left(\frac{u}{L} \right) \frac{\partial C}{\partial Z} \quad 0 < t', 0 < Z < 1 \quad \dots \quad (\text{IV-5})$$

The dimensionless form of the above differential equation is:

$$\frac{\partial C}{\partial \theta} = \left(\frac{D_p}{uL} \right) \frac{\partial^2 C}{\partial Z^2} - \frac{\partial C}{\partial Z} \quad \dots \quad (\text{IV-6})$$

where $\theta = \frac{t'}{\bar{t}} = \frac{t' u}{L}$; \bar{t} is mean residence time. The dimensionless group $\frac{D_p}{uL}$, called the

vessel dispersion number, is the parameter which measures the extent of axial dispersion.

When $\frac{D_p}{uL} \rightarrow 0$, the dispersion is negligible, hence conditions approach plug flow. When

$\frac{D_p}{uL} \rightarrow \infty$, the dispersion is large and hence conditions approach completely mixed flow.

Under an idealized impulse the solution to equations IV-5 and IV-6 yields a symmetric concentration curve

$$\frac{C}{C_o} = \frac{L}{2\sqrt{\pi t' D_p}} \exp \left[-\frac{u^2 \left(\frac{L}{u} - t' \right)^2}{4t' D_p} \right] \quad \dots \quad (\text{IV-7})$$

$$\frac{C}{C_o} = \frac{1}{2\sqrt{\frac{\pi \theta D_p}{uL}}} \exp \left[-\frac{(1-\theta)^2}{4\theta \left(\frac{D_p}{uL} \right)} \right] \quad \dots \quad (\text{IV-8})$$

Equation (IV-8) is a normalized form of equation (IV-7). The UASB reactor by-pass flow in this model is described by above dispersion plug flow equations.

A-1.12 Mixed flow and plug flow model

The granular bed is characterized by two parallel CSTRs. The clarification zone is best characterized by a plug flow reactor. A mass balance is performed, after an inert tracer impulse, on the liquid volume of the CSTRs with time t' , which lead to the following expressions:

$$V_1 \frac{dC_1}{dt'} = -Q_1 C_1 \text{ with initial condition } C_1(0) = \frac{Q_1}{Q} \frac{M}{V_1} \quad \dots \quad (\text{IV-9})$$

and

$$V_2 \frac{dC_2}{dt'} = -Q_2 C_2 \text{ with initial condition } C_2(0) = \frac{Q_2}{Q} \frac{M}{V_2} \dots \quad (\text{IV-10})$$

Integrating the above equations gives

$$C_1 = \frac{Q_1}{Q} \frac{M}{V_1} \exp\left[-\frac{Q_1}{V_1} t'\right] \dots \quad (\text{IV-11})$$

$$C_2 = \frac{Q_2}{Q} \frac{M}{V_2} \exp\left[-\frac{Q_2}{V_2} t'\right] \dots \quad (\text{IV-12})$$

or

$$\frac{C_1}{C_o} = \frac{Q_1}{Q} \frac{V}{V_1} \exp\left[-\frac{Q_1}{V_1} t'\right] \dots \quad (\text{IV-13})$$

$$\frac{C_2}{C_o} = \frac{Q_2}{Q} \frac{V}{V_2} \exp\left[-\frac{Q_2}{V_2} t'\right] \dots \quad (\text{IV-14})$$

where $C_o = \frac{M}{V}$ is effluent concentration at $t'=0$ in an ideal CSTR. Applying a mass balance

on the whole system gives

$$QC = Q_3 C_3 + Q_2 C_2 + Q_1 C_1 \dots \quad (\text{IV-15})$$

Substituting equations IV-7, 13 and 14 into equation IV-15, the UASB hydraulic model equation has the form

$$\frac{C_i}{C_o} = \frac{A}{\sqrt{t'}} \exp\left[-\frac{B}{t'} (T_d - t' + T_{d1})^2\right] + C \exp[-D(t' - T_{d1})] + E \exp[-F(t' - T_{d1})] \dots \quad (\text{IV-16})$$

where C_i is effluent concentration of the UASB reactor at time i ; $A = \frac{Q_3 L}{2C_o Q \sqrt{\pi D_p}}$;

$$B = \frac{u^2}{4D_p}; C = \left(\frac{Q_1}{Q}\right)^2 \frac{V}{V_1}; D = \frac{Q_1 V}{Q V_1}; T_{d1} \text{ is lag time of plug flow reactor}; T_d = \frac{L}{u};$$

$$E = \left(\frac{Q_2}{Q}\right)^2 \frac{V}{V_2}; F = \frac{Q_2 V}{Q V_2}.$$

A-1.2 Two CSTRs in series followed by a PFR (Van der Meer model)

At higher organic loading rates (ea. 10 kgCOD/m³bed-d), increased biogas production enhances the extent of mixing within the granular bed. The UASB can be described by the Van der Meer model, in which two CSTRs and a plug flow reactor are in series. By-pass and dead volume are present. The model is shown as follows:

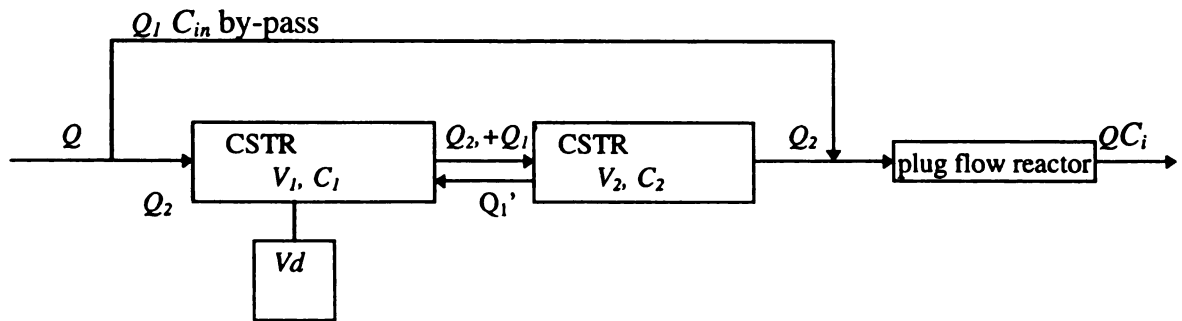


Figure IVA-2. Flow chart of Van der Meer model

The by-pass stream is assumed to not occupy any fluid volume. One of the CSTR (V_1) represents the sludge bed in which the granular sludge is relatively compact and well settled. The other CSTR describes the sludge blanket with upper layer granules and is

more fluidized. The plug flow reactor represents the clarification zone. Performing a mass balance on the mass contained within the liquid volume in CSTRs with time t , in the case of a conservative tracer impulse, results in the following expressions:

$$V_1 \frac{dC_1}{dt} = -(Q_2 + Q_1')C_1 + Q_1' C_2 \quad \dots \quad (\text{IV-17})$$

$$V_2 \frac{dC_2}{dt} = (Q_2 + Q_1')C_1 - (Q_2 + Q_1')C_2 \quad \dots \quad (\text{IV-18})$$

$$QC_i = Q_2 C_2 + Q_1 C_{in} \quad \dots \quad (\text{IV-19})$$

where $Q = Q_1 + Q_2$, $V = V_1 + V_2 + V_d + V_{pf}$. Initial conditions are:

$$C_1(0) = \frac{M}{V}, C_2(0) = 0.$$

Solutions to equation IV-17 and 18 have the form

$$C_1 = A_1 \exp[\lambda_1 t] + B_1 \exp[\lambda_2 t] \quad \dots \quad (\text{IV-20})$$

$$C_2 = A_2 \exp[\lambda_1 t] + B_2 \exp[\lambda_2 t] \quad \dots \quad (\text{IV-21})$$

$$\text{where } A_1 + B_1 = C_1(0) \quad \dots \quad (\text{IV-22})$$

$$A_2 + B_2 = C_2(0) \quad \dots \quad (\text{IV-23})$$

When considering PFR following the CSTRs, and normalize C and t for the whole system, the effluent tracer concentration of the UASB is given by

$$\frac{C_i}{C_0} = \frac{A_2}{C_0} \exp[-HRT\lambda_1(\theta - T_d)] + \frac{B_2}{C_0} \exp[-HRT\lambda_2(\theta - T_d)] \quad \dots \quad (\text{IV-24})$$

where $\theta = \frac{t}{HRT}$; T_d is normalized delay time as a result of plug flow or $\frac{RT_{PF}}{HRT}$. To

simplify, let $C = \frac{A_2}{C_0}$, $D = \frac{B_2}{C_0}$, $E = -HRT\lambda_1$, $F = -HRT\lambda_2$. Equation IV-24 becomes

$$\frac{C_i}{C_0} = C \exp[-E(\theta - T_d)] + D \exp[-F(\theta - T_d)] \quad \dots \quad (\text{IV-25})$$

A-1.3 One CSTR and a dispersion PFR in series model (model 2)

A second model (model 2) was developed to describe the UASB reactor hydraulics at high OLR. Compared to Van der Meer model, this model uses a simpler expression of one CSTR for granular bed. The clarifier section is represented by a dispersion PFR. Both by-pass flow and dead volume are present. Model 2 has the following form

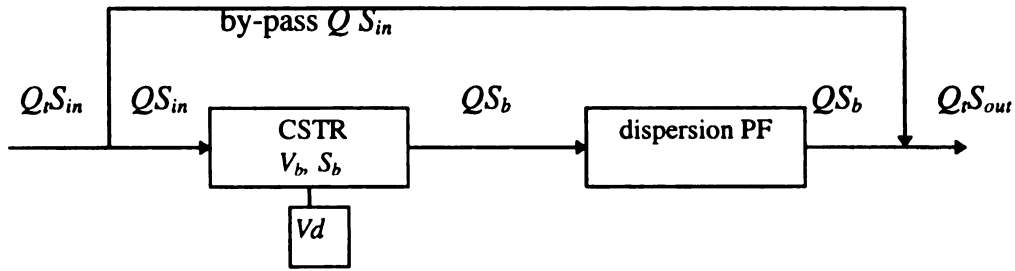


Figure IVA-3. A schematic representation of model 2 describing UASB reactor at high gas production.

For the case of addition of an impulse of a conservative tracer the CSTR of the model 2 can be expressed by the following equations

$$V_b \frac{dC}{dt} = V_b E(t) - QfC(t) \quad \dots \quad (\text{IV-26})$$

$$E(t) = \begin{cases} \frac{Mf}{V_b T_{in}}, & \text{if } 0 \leq t \leq T_{in} \\ 0, & \text{if } T_{in} \leq t \end{cases} \quad \text{For impulse} \quad \dots \quad (\text{IV-27})$$

where $C(t)$ is concentration within CSTR; V_b is working volume of CSTR ($=V-V_d$); V_d is dead volume within CSTR; $E(t)$ is an input function; S_b is bulk tracer concentration; f is

fraction; Q_f is the flow fraction that enters the main stream; M_f is fraction of mass input that go through reactor working volume; T_{in} is tracer injection time.

Clarifier is described by a dispersion plug flow reactor. Only vertical direction advection and dispersion were considered in this part. Equation (IV-5) is rewritten to have the form

$$\frac{\partial C_{pf}}{\partial t} = \frac{D_p}{L} \frac{\partial^2 C_{pf}}{\partial Z^2} - \frac{u}{L} \frac{\partial C_{pf}}{\partial Z}, \quad t > 0, \quad 0 < Z < l, \quad \dots \quad (IV-28)$$

$$\text{BC: } C_{pf}(0, t) = C(t) \quad \dots \quad (IV-29)$$

$$\text{IC: } C_{pf}(Z, 0) = C_o \quad \dots \quad (IV-30)$$

where C_{pf} is concentration in dispersion PFR; X is a vertical coordinate. An inert tracer response after a impulse to the UASB reactor can be predicted by solving equations IV-26 to 30.

A-2. Integrated reaction-diffusion and hydraulic model

Substrate transport and consumption within granular sludge bed can be described by a reaction-diffusion model. The model can be then integrated with reactor hydraulic characteristics discussed above (Section A-1.3; Chapter IV), in order to characterize the dynamic behavior of UASB reactors under organic impulse and step OLR increase events (Chapter IX). The theoretical development of this dynamic coupled reaction-diffusion-hydraulic model is presented in this section.

A-2.1 Reaction-diffusion model

The kinetic properties of the granular sludge bed in an UASB reactor depend upon coupled mass transfer and biochemical reaction processes. A reaction-diffusion type model can be used to describe the interaction of mass transport and reaction of the granules, to determine the overall activities. The mass transport and biochemical reaction interactions in a slab of biofilm is presented in Figure IVA-4.

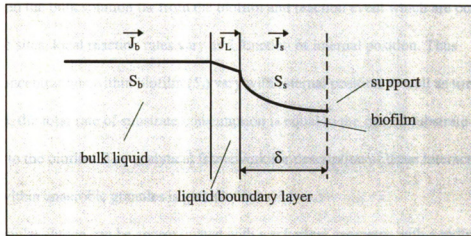


Figure IVA-4. Mass transport, diffusion and reaction within a slab of biofilm

Substrate (S_b) transport from bulk liquid to a stagnant film or boundary layer which is at the outside of the biofilm. A concentration gradient is established across the liquid film. Substrate is then concurrently diffuse through the biofilm and consumed (S_s). By continuity of mass, at the interface of bulk liquid–boundary layer and boundary layer–granule, the fluxes are equal. Thus, $J_b = J_L$ at bulk–boundary layer interface, and $J_L = J_s$ at boundary layer–biofilm interface. This phenomena results in a substrate profile indicated in

Figure IVA–4. This profile can be described quantitatively in terms of the following parameters: bulk substrate concentration (S_b), intrinsic kinetic parameters (k_m , K_s), effective diffusion coefficient (D), the mass transfer coefficient through boundary layer (K_L) and biofilm thickness (δ). Mixing or flow of substrate solution adds a convective transport contribution to the movement of substrate from bulk solution to the external surface. As indicated in Figure IVA–4, reaction occurs within the biofilm at rates which are determined by the concentrations within the slab. Because of concentration gradients arise between the bulk solution far from the biofilm and reaction event which are occurring at the active sites, local reaction rates vary as a function of internal position. Thus substrate concentrations within biofilm (S_i) vary with internal position as well as time. At steady state, the total rate of substrate consumption is equal to the rate of substrate transport into the biofilm. The analytical framework for description of these interacting processes within anaerobic granules is given below.

Granular sludge can be approximated with a spherical geometry with a radius of R . Assuming that substrate diffuses through a layer of the granules with a constant thickness of δ (active layer) as observed from microscopy (Chapter VII D). This active layer (δ) was composed of different group of microorganisms involved in anaerobic degradation of a complex waste, and formed as a result of a long period of acclimation to this waste at a certain range of OLR. There are only traces of substrate beyond that layer (central core), indicated from much lower cell density at that area compared to the cell density in outer layer (Chapter VII D). The assumption is therefore made that diffusion and reaction in the central core are small compared to that in the active layer and can be ignored. Due to the

slow growth rate of methanogens the growth and decay of granule biomass were ignored. Substrate concentration profiles through the granules are symmetric about the center of the granules. A basic model is shown in Figure IVA-5. Several assumptions are made: 1) effective substrate diffusivity within the granules is constant and 2) the reaction can be described using Monod kinetics.

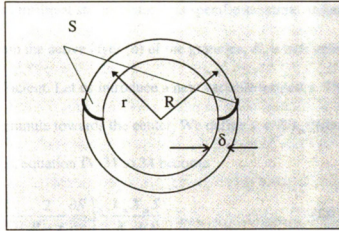


Figure IVA-5. A cross-section of a granule with radius R , active layer thickness δ and substrate profile S .

The shell balance on substrate S in coordinate r , results in a second-order partial differential equation

$$\frac{\partial S}{\partial t} = D \left(\frac{\partial^2 S}{\partial r^2} + \frac{2}{r} \frac{\partial S}{\partial r} \right) - \frac{k_m X_m S}{K_s + S} \quad \dots \quad (\text{IV-31})$$

with boundary conditions

$$(i) \quad D \frac{\partial S}{\partial r} + K_i S = K_i S_b \quad r=R \quad \dots \quad (\text{IV-32})$$

$$(ii) \quad \frac{\partial S}{\partial r} = 0, \quad r=R-\delta \quad \dots \quad (\text{IV-33})$$

and initial condition

$$(i) S(r,0) = S_s(r) \quad r \in (R-\delta, R) \quad \dots \quad (IV-34)$$

where term $D\left(\frac{\partial^2 S}{\partial r^2} + \frac{2}{r} \frac{\partial S}{\partial r}\right)$ is the rate at which substrate diffuses into the granules;

$\frac{k_m X_m S}{K_s + S}$ is substrate reaction rate; D is effective substrate diffusivity; S_s is substrate

concentration within biofilm at steady state; k_m is specific substrate utilization rate; X_m is

biomass density within the active layer (δ) of the granules; K_s is half velocity constant; K_l

is mass transfer coefficient. Let us introduce a new variable termed x . The x axis originates

from the surface of granule towards the center. We define $x = R-r$, then $dr = -dx$. By

changing of variables, equation IV-31 to 34 become

$$\frac{\partial S}{\partial t} = D\left(\frac{\partial^2 S}{\partial x^2} - \frac{2}{R-x} \frac{\partial S}{\partial x}\right) - \frac{k_m X_m S}{K_s + S} \quad \dots \quad (IV-35)$$

$$\text{BCs: (i) } -D \frac{\partial S}{\partial x} + K_l S = K_l S_b, \quad x=0 \quad \dots \quad (IV-36)$$

$$(ii) \frac{\partial S}{\partial x} = 0, \quad x=\delta \quad \dots \quad (IV-37)$$

$$\text{IC: (i) } S(x,0) = S_s(x) \quad x \in (0, \delta) \quad \dots \quad (IV-38)$$

At steady state $\frac{\partial S}{\partial t} = 0$ for equation IV-35, thus we have following second-order ordinary

differential equation

$$D\left(\frac{\partial^2 S_s}{\partial x^2} - \frac{2}{R-x} \frac{\partial S_s}{\partial x}\right) = \frac{k_m X_m S_s}{K_s + S_s} \quad \dots \quad (IV-39)$$

$$\text{BCs: (i) } -D \frac{\partial S_s}{\partial x} + K_l S_s = K_l S_{b0}, \quad x=0 \quad \dots \quad (IV-40)$$

where
and
ground

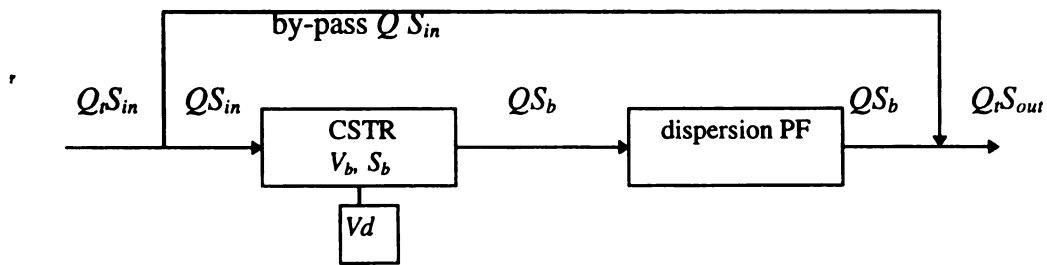
as s
hy
di
re
as

$$(ii) \quad \frac{\partial S_x}{\partial x} = 0, \quad x = \delta \quad \dots \quad (IV-41)$$

where S_{bo} is the steady state substrate concentration in bulk liquid. Equations IV-35 to 38 and 39 to 41 can be solved numerically for a description of substrate variation within the granular bed of UASB reactor at unsteady state and steady state, respectively.

A-2.2 Development of a dynamic model including a flow model combined with a reaction-diffusion model for UASB reactors

As discussed earlier in section IV A-1.1, UASB reactor flow can be characterized as several CSTRs, PFRs and dispersion PFR interconnected in series or in parallel. The hydraulic model (model 2) developed in section A-1.3 is integrated into the reaction-diffusion model presented above (section A-2.1) to develop a dynamic model for UASB reactors. A schematic representation of the dynamic model is presented in Figure IVA-3, as follows:



A mass balance can be performed on the substrate within the boundary volume of the CSTR, at organic impulse and step increase:

$$V_b \frac{dS_b}{dt} = V_b E(t) - Q f S_b(t) - K_L A_r (S_b - S(0, t)) \quad \dots \quad (IV-42)$$

$$\text{IC: } S_b(0) = S_{bo} \quad \dots \quad (\text{IV-43})$$

$$E(t) = \begin{cases} \frac{Mf}{VbT_{in}}, & \text{if } 0 \leq t \leq T_{in} \\ 0, & \text{if } T_{in} \leq t \end{cases} \quad \text{For an impulse } \dots \quad (\text{IV-44})$$

$$E(t) = \begin{cases} QfS_{bkgd}, & \text{if } 0 < t < T_{stp1} \\ QfS_{stp1}, & \text{if } T_{stp1} \leq t < T_{stp2} \\ QfS_{stp2}, & \text{if } T_{stp2} \leq t \end{cases} \quad \text{For a step increase } \dots (\text{IV-45})$$

where V_b is working volume of the CSTR; V_d is dead volume of CSTR; $E(t)$ is an input function; A_r is total granule surface area; S_b is bulk substrate concentration; S is substrate concentration within the granules at unsteady state; Qf is the flow fraction that enters the main stream; Mf is fraction of mass input that go through reactors working volume; S_{bkgd} is feed concentration before step increase; S_{stp1} is feed concentration at first step increase; S_{stp2} is feed concentration at second step increase. T_{stp1} is the time that the first step is initiated; T_{stp2} is the time that the second step is initiated. T_{in} is the substrate injection time.

In clarifier section very few granules were observed. Thus, the reaction term was neglected. For the substrate concentration within the PFR, S_d , the dispersion PFR described in equation IV-28 to 30 is rewritten as:

$$\frac{\partial S_d}{\partial t} = \frac{D_p}{L^2} \frac{\partial^2 S_d}{\partial Z^2} - \frac{u}{L} \frac{\partial S_d}{\partial Z}, \quad t > 0, \quad 0 < Z < 1 \quad \dots \quad (\text{IV-46})$$

$$\text{BC: } S_d(0, t) = S_b(t) \quad \dots \quad (\text{IV-47})$$

$$\text{IC: } S_d(Z, 0) = S_{bo} \quad \dots \quad (\text{IV-48})$$

The UASB reactor responses under organic impulse and step increases can be simulated by simultaneously solving equations IV-35 to 48, using numeric method (Appendix E).

CHAPTER 5. HYDRAULIC CHARACTERISTICS OF AN UPFLOW ANAEROBIC SLUDGE BLANKET (UASB) REACTOR

A. Introduction

A number of high rate anaerobic treatment systems have been developed over the past two decades. Despite the demonstrated benefits of these processes, hydraulic mixing efficiency problems are frequently observed. These must be taken into account when scaling up from laboratory reactors to pilot- and full-scale systems. Clogging and short-circuiting in anaerobic reactors are major concerns since these problems can lead to reduction in the volume of active biomass and, therefore, reduced removal efficiency. The Upflow Anaerobic Sludge Blanket (UASB) system is the most widely used high-rate anaerobic process. The UASB process is generally reported to have good hydraulic mixing [Hall 1984, 1985]. The design of UASB reactors has been primarily based on empirical relationships or using the assumption that the process behaves as a continuously stirred tank reactor (CSTR). How well these systems approximate ideal CSTRs has not been adequately evaluated under different organic and hydraulic loading rates.

Several studies have been conducted in attempt to characterize reactor hydraulics. Macmullen and Weber presented an analytical study for short-circuiting in CMF (completely mixed flow) reactors in series in early 30's [Macmullen and Weber,1935]. Cholette and Cloutier [1959] described three factors influencing reactor fluid flow mixing patterns: effective volume, short circuiting, and plug flow. Van der Meer[1979], studying the hydraulic characteristics of UASB reactors at bench-, pilot-, and full-scale, observed that biogas production, due to increases in organic loading rate, did not result in significantly altered fluid flow patterns. He further suggested that dead volume can be

reduced by control of the amount of sludge and internal recirculation. In treating cane sugar wastewater, it was observed that at low organic loading rates, adequate mixing of an UASB reactor contents did not take place [Manjunath, D.L. et al,1989]. Bolle et al.[1986] developed a model in which both sludge bed and sludge blanket can be described as completely mixed flow reactors (CSTRs) with short-circuiting flow paths, while the settler volume was best described as a plug flow reactor. Short-circuiting flow through the sludge bed was a function of the bed height. Hall [1985] suggested that gas production has a major impact on mixing under low hydraulic retention time(HRT<1day) conditions. Other researchers considered dead volume and mixing-zone volume without by-passing flow[Monteith and Stephenson, 1981][Xu,1983].

Three different models which have been used to describe reactor hydraulics, are summarized in Figure VB–1. Cholette and Cloutier[1959] modified the CSTR model to include the effects of dead volume and short circuiting, resulting in the following expression:

$$\frac{C_i}{C_o} = \frac{f_1}{f_2} \exp \left\{ -\frac{f_1 Q}{f_2 V} t_i \right\} \quad \dots \quad (V-1)$$

where C_i – effluent concentration at time i ; C_o – effluent concentration at time=0 in an ideal

CSTR; $f_1 = \frac{V_1}{V}$, where V_1 – mixing volume (V_m), V – total volume; $f_2 = \frac{Q_1}{Q}$, Q_1 –

working flow rate, Q – total flow rate; t_i – time ; $V=V_1 + V_d$, where V_d – dead volume;

$Q=Q_1 + Q_2$, where Q_2 – bypass flow rate. Van der meer[1979] presented a general flow

model scheme (Figure VB–1) based on two coupled CSTR's; one was for the sludge bed

and the other for the sludge blanket portion of the reactor volume with back mixing in

between. A dead volume and short circuit portion were also assumed to be present in the sludge bed, followed by a plug flow (PF) reactor representing the liquid layer above the sludge blanket. Hall [1985] proposed a parallel mixing hydraulic model for UASB reactors (Figure VB-1). Instead of assuming flow could short-circuit directly to the effluent from the inlet without mixing, a mixed bypass flow zone, parallel to the working zone, was assumed. The reported model equation is:

$$\frac{C_i}{C_o} = \frac{B_1}{B_2 + B_3} \exp\left\{-\frac{B_1}{B_2} \theta_i\right\} + \frac{1 - B_1}{B_2 + B_3} \exp\left\{-\frac{1 - B_1}{B_3} \theta_i\right\} \quad \dots (V-2)$$

where $B_1 = \frac{Q_2}{Q}$, where Q_2 —by-pass flow; $B_2 = \frac{V_1}{V}$, where V_1 —active volume; $B_3 = \frac{V_d}{V}$,

where V_d —dead volume; $\theta_i = \frac{t_i}{HRT}$; V_2 —bypass volume; $Q_1 + Q_2 = Q$; $V_1 + V_2 + V_d = V$ (total

volume). Hall concluded that the hydraulics in an UASB can be well described by the CSTR model, but that some deviation does exist during the initial period in tracer experiments. Fluid-flow model parameter estimates were accomplished using both linear regression and the nonlinear least square techniques [Chapman, 1983]. The hydraulics in a UASB reactor with granular sludge is similar to that observed in liquid-solid fluidized bed reactors (FBR). Richardson and Zaki [1954] discussed in detail various factors that affect fluidization and presented an empirical correlation between particle velocity and bed voidage during fluidization. Iza et al. [1988] demonstrated that the hydraulic behavior of a pilot scale FBR could be described by this correlation. The Richardson-Zaki equation was modified by Fouda and Capes [1977] for describing the fluidization of non-spherical particles. Other correlations have been developed based on Reynolds number and particle velocity [Garside et al., 1977] and Galileo number, Reynolds number and bed voidage

[Wen and Yu,1966]. Andrews and Tien [1979] observed that the growth of biomass causes the bed in FBR system to expand. This phenomena can be described by a linear function of biomass with bed expansion.

Tracer studies are commonly used for the study of fluid flow [Levenspiel,1972]. Rebhun and Argaman presented a tracer analysis for a reactor which including dead volume, mixing volume and a plug flow reactor using F curve techniques [Rebhun and Argaman,1965]. Riemer et al. [1980] suggested the diffusion of tracer dye into and out of biological films could cause tailing in the residence time distribution curve. Stevens et al.[1986] presented a model that accounts for the diffusion of a tracer within a biofilm.

UASB reactors can be operated over a wide range of HRTs depending on the design organic loading rate and influent substrate concentration. The organic loading rate relates directly to biogas production in the sludge bed. The formation of gas bubbles contributes to the mixing intensity in the sludge bed zone. Flow recirculation rate also exerts an influence on the hydraulic behavior. If the reactor upflow rate is high enough, it will also affect the sludge bed hydraulics. Accumulation of biomass may cause dead volume and reduce active working volume. How strong these influences are and the interactions between them under different operational conditions has not been systematically studied.

The present work investigated the hydraulic characteristics of a laboratory-scale UASB reactor operated at different HRTs, ranging from 11 hours to 5.6 days, organic loading rates ranging from 5 to 15 kgCOD/m³bed-d, and surface upflow velocities ranging from 2 to 5 gpm/sqft (0.14 to 0.34 cm/s) of reactor cross-sectional area. The initial hypothesis was that at low OLRs, effluent recirculation would play a major role in mixing;

at high OLR, the biogas production would be the predominant factor affecting mixing. This hypothesis was examined using two sets of experiments: 1) tracer studies of the UASB at various organic loading and hydraulic flux rates and 2) fluid flow modeling and model evaluation at low and high OLR.

B. Organic loading rate and hydraulic flux effects

The UASB reactor during this portion of study was operated at OLRs between 5 and 15 kgCOD/m³bed-d. The hydraulic flux rate was varied from 2 to 5 gpm/sqft. The UASB is considered to be linear system with respect to hydraulic behavior during the entire residence time distribution (RTD) period. That is, the changes of response under various operational conditions are consistent for the whole RTD curve. Since the only major discrepancies from CSTR behavior exist during the early period of the overall HRT[1985], this study focused on residence time distribution during the initial period of the system HRT. This is the time period where differences in behavior would be expected as a result of changes in substrate concentration, flow rate, etc.

B-1. UASB reactor

An all-glass, water-jacketed bench-scale UASB reactor (shown schematically in Figure VIIB-1) with an empty bed volume of 3.1L was used for all hydraulic experiments. The unit was sealed from the atmosphere to prevent oxygen entry. Influent flow was pumped upward through the reactor continuously (using a Watson-Marlow model 503U tubing pump), contacted with the granular sludge bed and discharged via effluent tubing. Mixing was provided by both biogas production and by hydraulic

recirculation. The recycle flow was pumped back to the bottom of the reactor and mixed with the feed just prior entering the reactor proper. Gas/liquid/solid separation was accomplished using a gas collector at the top of the reactor. A concentrated synthetic brewery waste, based on a waste analysis of a full-scale UASB plant where the granules used in this study were taken from, was used as the influent feed (see appendix A). Seed granular sludge was acclimated with the synthetic waste for more than six months prior to initiating hydraulic studies. The granules ranged in size from 1 to 3mm in diameter. Operational conditions of the bench-scale UASB are presented in Table VB-1.

B-2. Tracer study

Residence time distribution (RTD) studies were performed using the tracer techniques described by Levenspiel [1972]. Lithium was used as a conservative tracer material. For these experiments, 122mg of lithium chloride was injected into the recirculation tubing just before the reactor inlet to produce an impulse input. Samples were collected at a sampling port in the recirculation tubing as the flow exited the reactor proper. The sampling frequency used was 1 minute for the recirculation effect study. Samples were centrifuged, and the supernatant collected for analysis. Lithium concentration was determined by ion chromatography (Dionex model 4000). The pseudo-steady state residence time distribution experimental design is shown in Table VB-2.

B-3. Organic loading and hydraulic flux effects

It was assumed that pseudo-steady state conditions were reached after a minimum of three hydraulic retention times at each OLR, and the control parameters,(i.e. pH, gas

production, methane concentration and effluent volatile fatty acids), varied less than 10% from the mean. Changes in the OLR were made by varying the influent feed rate while maintaining a constant feed concentration. The sludge-bed volume was fixed such that the unexpanded (settled) volume in the reactor was 1.5L throughout these experiments. The degree of the fluidization of the sludge blanket was controlled by the hydraulic recirculation rate.

The matrix of residence time distribution experiments for the early period of overall hydraulic retention time for each organic loading and recirculation rate is presented in Table VB-2. The effluent from the reactor was tracked for more than one recirculation after adding a pulse of lithium to the reactor. For each OLR, HRT and surface upflow rate, biogas production and bed height (fluidized) were monitored. Dispersion number and bed expansion were then calculated. Statistical comparisons were performed on the experiment data. The RTD results are presented in Figures VB-2 to 5, and Tables VB-3 and 4. The gas production rate increased proportionally with the OLR (2.8 times; Table VB-3) as expected. Dispersion number as well as bed expansion (V_b/V_r) varied primarily with surface upflow rate. A multiple comparison test was performed on dispersion numbers (averaged) at four OLRs. The least significant difference at the 0.05 level was 0.1008, which means the reactor hydraulic mixing patterns under four OLRs tested were not significantly different. A similar test was conducted for the dispersion numbers (averaged) at two surface upflow rates. Results indicate a significant difference (Table VB-4). The tracer profiles during the early period of an impulse varied considerably with surface upflow rate (Figure VB-4 and 5). These profiles varied slightly with OLR (Figure

VB-2 and 3). The extent of mixing was predominantly affected by effluent recirculation, or surface upflow rate. For the final experimental condition (15gCOD/L-d, HRT=2d), the combination of high gas production and high hydraulic loading rate(5gpm/sqft) resulted in excessive loss of solids, and required termination of the experiment. This result shows the influence of gas production at high organic loading rates. The mixing provided by the gas bubbles becomes increasingly important compared to hydraulic flux effects when the HRT is low. This is in agreement with results reported by Hall [1985].

C. Evaluation of existing fluid flow models and model development

Modeling experiments were performed using stimulus-response technique at OLRs of 4 and 10 kgCOD/m³bed-d and HRT ranging from 11 to 99 hrs. The surface upflow velocity used was 2 gpm/sqft. The Cholette-Cloutier model, Hall's parallel CSTR model and the Van der Meer model were evaluated and compared. Two new hydraulic models (model 1 and model 2) have been developed to describe the hydraulic behavior of UASB under low and high OLR. Residence time distribution (E curve) of an inert tracer following an impulse was used for modeling. The F curve (the integration of E curve) analysis was employed for determination of tracer recovery and dead volume. In a dimensionless plot of F curve, the area between $F=1$ and $F(\theta)$ equals 1 for ideal CSTRs. An area that is less than 1 indicates the existence of dead volume. Sampling frequencies here were 10% of the HRT. Model parameters estimation of the Cholette-Cloutier model, Hall's parallel CSTR model, the Van der Meer model and the model 1 were performed using a software SYSTAT. For the model 2, a computer simulation program written with FORTRAN and IMSL were developed. The theoretical development of the models and

the simulation program are presented in Chapters IV and IX, respectively.

C-1. Modeling at low OLR

For the UASB reactor operated at OLR of 4 kgCOD/m³bed-d and HRT of 99 hrs, 11 mg of lithium chloride was injected into the reactor inlet to produce an impulse. Approximately 90.4% of lithium applied was recovered during the initial 1.4 HRT. There is a big discrepancy between measured data and ideal CSTR behavior under the operating conditions tested (Figure VC-1). Description of this non-ideal flow was attempted using four models: 1) the Cholette-Cloutier model, 2) the Hall model 3) the Van der Meer model and 4) model 1 developed during this study. This model 1 (Figure VC-3) includes a dispersion plug flow reactor for the by-pass flow, two parallel CSTRs for the granular bed and a plug flow reactor for the clarifier. Granular sludge bed has a mixing region, dead volume and a by-pass flow region. The first CSTR describes the main mixing region of the bed (V_1). The other CSTR describes the volume in-between this volume and the stagnant region, or dead volume (V_d). Following parallel CSTRs and a dispersion PF, is a plug flow reactor. The model is expressed as the following equation (for derivation see Chapter IV A-1.1):

$$\frac{C_i}{C_o} = \frac{A}{\sqrt{t'}} \exp \left[-\frac{B}{t'} (T_d - (t' - T_{d1}))^2 \right] + C \exp[-D(t' - T_{d1})] + E \exp[-F(t' - T_{d1})] \quad \dots \quad (\text{IV-16})$$

where C_i - tracer concentration in the effluent at time i ; C_o - effluent concentration at $t'=0$

in an ideal CSTR; $A = \frac{Q_3 L}{2 C_o Q \sqrt{\pi D_p}}$; D_p - axial dispersion coefficient; u - fluid velocity; L -

length of dispersion plug flow reactor: $B = \frac{u^2}{4D_p}$; $T_d = \frac{L}{u}$; $C = \left(\frac{Q_1}{Q} \right)^2 \frac{V}{V_1}$; $D = \frac{Q_1 / Q}{V_1 / V}$;

T_{d1} - lag time of plug flow reactor; $E = \left(\frac{Q_2}{Q} \right)^2 \frac{V}{V_2}$; $F = \frac{Q_2 / Q}{V_2 / V}$. Detailed development of

this flow model are provided in Chapter IV A-1.1.

Results obtained using above referenced models are shown in Figures VC-2(a), (b), (c) and Figure VC- 4. The first few data points in the tracer study represent the bypass flow, expressed as a delta function. This initial portion of the RTD curve was not fit well by any of the existing models. Following this initial portion of the curve an exponential decay curve was observed; this was described reasonably well by the Cholette-Cloutier, Hall and the Van der Meer models. The model developed during this work (model 1) fit the experimental data, including the initial portion of the data extremely well.

C-2. Modeling at high OLR

The bench-scale UASB was operated at an OLR of 10 kgCOD/m³bed-d and HRT of 11 hours. Lithium chloride (160mg) was injected at the base of the reactor. Recovery of LiCL was 100% at 5.3 HRT. As expected, when the OLR was increased, gas production increased. This in turn produced better mixing within the sludge bed. Thus a model with a larger mixing volume would describe the UASB well. Initial results show the UASB does not represent an ideal CSTR (Figure VC-5). Parameters of Cholett-Cloutier, Hall and Van der Meer models and model 1 were estimated with this data set (Figure VC-6(a), (b), (c) and 9). Van der Meer's model describes the UASB reactor with good fit. Cholett-Cloutier's, Hall's models and model 1 were unable to fit the data. An attempt was made to

describe the reactor hydraulics at high OLR using one CSTR, with bypass flow, in series with PFR. The model parameters showed no physical significance. A second model 1(model 2) was developed. The structure of model 2 is composed of a single CSTR with dead volume and by-pass flow to represent the granular bed, followed by a dispersion plug flow reactor (Figure VC-7). This model was developed for high OLR operation because of the different hydraulic regime, the result of increased gas production. In practice, we are looking for a model as simple and meaningful as possible. There are several differences or simplifications between model 2 and the Van der Meer model. Since the interface layer of sludge bed and sludge blanket in a UASB reactor is usually not distinguishable by visual inspection and uneasy to determine, the two CSTRs which describe the sludge bed and sludge blanket in Van der Meer model are simplified to one CSTR. The clarification zone above the sludge blanket is represented by a dispersion plug flow rather than a simple plug flow reactor, because increased gas production during the high OLR contributes to increased mixing in this layer. By-pass flow, instead of going through the bed only, pass to the end of the reactor. A computer program written with FORTRAN and using IMSL has been developed for model 2. Finite difference [Ames, 1977] was used as solution technique. Equations of this model are:

$$V_b \frac{dC}{dt} = V_b E(t) - QfC(t) \quad \dots \quad (\text{IV-26})$$

$$E(t) = \begin{cases} \frac{Mf}{V_b T_{in}}, & \text{if } 0 \leq t \leq T_{in} \\ 0, & \text{if } T_{in} \leq t \end{cases} \quad \text{For impulse} \quad \dots \quad (\text{IV-27})$$

$$\frac{\partial C_{pf}}{\partial t} = \frac{D_p}{L} \frac{\partial^2 C_{pf}}{\partial Z^2} - \frac{u}{L} \frac{\partial C_{pf}}{\partial Z}, \quad t > 0, 0 < Z < 1, \quad \dots \quad (\text{IV-28})$$

$$\text{BC: } C_{pf}(0,t)=C(t) \quad \dots \quad (\text{IV-29})$$

$$\text{IC: } C_{pf}(Z,0)=C_o \quad \dots \quad (\text{IV-30})$$

where $C(t)$ is concentration within CSTR; C_{pf} is concentration within dispersion plug flow reactor; V_b is working volume of CSTR ($=V-V_d$); V_d is dead volume within the CSTR; $E(t)$ is an input function; S_b is bulk tracer concentration; f is fraction; Qf is the flow fraction that enters the main stream; Mf is fraction of mass input that go through reactor working volume; T_{in} is tracer injection time; C_{pf} is concentration in dispersion PFR; X is a vertical coordinate; D_p is dispersion coefficient; u is flow velocity within the reactor; L is the length of the PFR. Detailed derivations are provided in Chapter IV A–1.3. Model 2 fit the tracer data reasonably well (Figure VC–8). The estimated working volume (excluding the plug flow region), plug flow volume, dead volume and by-pass flow were 91% and 97% of the total reactor volume, 2% and 3% of the total volume, 7% of total volume and zero, and 24% and 31% of the total flow, for the model 2 and the Van der Meer model, respectively (Figure VC–6(c) and 8). Dead volume in Van der Meer model was estimated from F curve analyses. The dispersion factor ($\frac{D_p}{L^2}$) was 0.001 for model 2. A ratio of flow velocity (u) to the length of the PFR ($\frac{u}{L}$) of 0.635 was observed. Model 2 does not describe the UASB hydraulics under low OLR (4kgCOD/m³bed-d, Figure VC-10) because of differences in hydraulic regime between low and high OLR. This hydraulic model is used in the dynamic modeling of UASB reactor during organic perturbations (Chapter IX). The two factors, $\frac{D_p}{L^2}$ and $\frac{u}{L}$ will be compared with that obtained from dynamic modeling.

D. Discussion

UASB reactors do not represent CSTRs under the experimental conditions tested. Hydraulic flux had a strong influence on the mixing efficiency of the UASB system at HRTs of 2 to 5.6 days, applied OLR of 5 to 10 kgCOD/m³bed-d and an upflow velocity between 2 and 5 gpm/sqft, based on dispersion number analysis. By comparing Figure VB-2 with Figure VB-3, one can observe that at the recirculation rate of 2 gpm/sqft, an increase in the organic loading rate by a factor of 2.8, did not significantly change the hydraulic characteristics, despite a 2.8 fold increase in biogas production (280ml/hr additional production, Table VB-3). An increase in the recirculation rate (surface upflow rate) of 2.5 times did, however, significantly improve mixing at OLR of 5 to 10 kgCOD/m³bed-d. This is demonstrated by examining the calculated dispersion numbers (based on one turnover) shown in Table VB-4. A dispersion number larger than 0.02 is generally considered to be significant in a closed plug flow system. Under high reactor hydraulic loading rates (5 gpm/sqft) the dispersion number was 0.1, double that observed at the lower hydraulic loading rate (0.05) of ca. 2 gpm/sqft. Results from student t tests showed that the dispersion number for the two different surface upflow rate were significantly different (Table VB-4). Multiple comparisons (Least significant difference test) for dispersion numbers under four organic loadings revealed a $Lsd_{(0.05)} = 0.1008 > \text{all differences of means}$ (Table VB-3). This indicates that the differences among the dispersion numbers for the four organic loading rates was not significant. During the initial period the reactor exhibits a pattern of plug flow with high dispersion under all operating conditions tested. The degree of mixing increased with increased recirculation and resultant increase in the expansion of the granular bed. Distribution curves were flatter for

the higher upflow rate, indicating that increased internal circulation smoothed the RTD curve by providing greater mixing, and more homogenous distribution. A lower peak ratio of C_i/C_o was observed at the higher flow rates (Figure VB-3). This ratio should approach 1.0 for an ideal CSTR, but only reached 0.69 (on average) in the experiment at a surface upflow rate of 5gpm/sqft. This indicates that some flow by-pass occurred. A peak C_i/C_o ratio of greater than 1 was observed for runs at the lower surface upflow rate. This indicates the presence of a significant amount of dead volume, probably as a result of insufficient expansion of and channeling through the granular bed. This dead volume was reduced at higher internal recirculation (surface upflow) rates. It thus appears that recirculation serves to decrease dead-volume but concurrently increases the degree of short-circuiting that occurs.

However, at the same range of upflow velocities, HRTs of 11-99 hours and OLRs of 4-10 kgCOD/m³bed-d, the organic loading rate has shown to have a major influence on mixing, observed from modeling experiment (model 1 and 2). It is thus appeared that the organic loading effect was not consistent. The mixing experiment (V B) was conducted focused on dispersion number per cycle at the initial period of the RTD curve, thus local effect; while the modeling experiment (V C) examined the whole RTD curve and the descriptions were more general. Under the variations of OLR flux and hydraulic flux, granular bed expansion were increased (7% and 14%, respectively), demonstrated that both OLR and SUV (surface upflow velocity) affected reactor mixing, and the hydraulic flux had a stronger effect. This improvement of mixing through increased gas production was supported by modeling experiment where SUV was fixed, as described by the models 1 and 2. Dispersion number failed to detect this change suggesting it is not a good tool

for evaluating reactor hydraulics.

A correlation of fluidization index (n) with bed voidage and superficial velocity (or empty bed velocity) (U_{bs}), has been used to describe fluidized bed expansion [Wen and Yu,1966] [Fouda and Capes,1977] [Garside and Al-Dibouni,1977]. The bed voidage can be related to superficial velocity in reactor by the Richardson-Zaki equation:

$$U_{bs} = U_i \varepsilon$$

where U_{bs} - superficial velocity (empty bed velocity), U_i - terminal particle settling velocity, ε - bed voidage, n - index. The correlation between the index n with reactor system variables can be determined by following relationships:

$$n = 4.65 + 19.5 \frac{d}{D} \quad \text{Re} < 0.2$$

$$n = (4.35 + 17.5 \frac{d}{D}) \text{Re}^{-0.3} \quad 0.2 \leq \text{Re} < 1.0$$

$$n = (4.4 + 18 \frac{d}{D}) \text{Re}^{-0.1} \quad 1.0 \leq \text{Re} < 200$$

$$n = 2.39 \quad 500 \leq \text{Re}$$

where d - granule diameter, D - reactor diameter, Re - Reynolds number. The index for the two sizes of granules observed in this study ($d=3\text{mm}, 1\text{mm}$, respectively) for two different upflow velocities is presented in Table VB–5. By visual observation, the lower portion of the bed (sludge bed) tended to have larger granules and appeared as a compact nearly static bed; the upper part of the bed (sludge blanket) had smaller granules and fluidization could be maintained quite well. Results presented in Table VB–5 reflect the fact that the hydraulics were greatly different between the sludge bed and sludge blanket, with lower Reynolds number values in the sludge bed region. This resulted in non-uniform

expansion and different n values for the sludge bed and sludge blanket region. The poor expansion of the sludge bed is likely the primary cause of the dead volume observed during experiments with low OLRs and high HRTs. This may contribute, in part, to the differences between UASB reactor performance and that expected from ideal CSTR behavior.

All three existing models (Cholette-Cloutier's, Hall's and Van der Meer's) failed to describe the UASB reactor at low applied OLRs (4 kgCOD/m³bed-d). Model 1, however, fit the experimental data well. The duration for the net working flow (total flow rate minus by-pass flow rate, $0.91Q$) go through the working volume (total reactor volume minus

dead space, $0.78V$) is 0.86HRT ($0.86 = \frac{0.78V}{0.91Q} = \frac{0.78}{0.91} \text{HRT}$). This means the time the fluid

stayed within the reactor was 14% less than would be anticipated. By-pass flow has been observed in the bench-scale UASB reactor, especially between the bed and the glass wall of the reactor. Nine percent of the total flow entering the reactor by passed the working volume region. At low OLR, the sludge bed was relatively compact due to low gas production and thus poor mixing within the bed. In fact, compact clusters of large granules in sludge bed were often observed. The calculated dead space of 22% of total reactor volume suggests a significant portion of the granule bed has not being used for treatment. The space between the main working volume and the dead volume was described by a small CSTR (1% of total volume and total flow). The clarification zone above the sludge blanket in the bench-scale UASB reactor was about 20% of the total volume. There was essentially no granular sludge in this portion of the reactor although some granules pass upward through this volume when buoyed by attached gas bubbles and

downward through this region after gas/solid separation occurred. However, the gas bubbles produced continuously migrate from the sludge bed, due to degradation of organic materials, up through this region. This contributes to extent of mixing in this region. At the top layer of this region, gas and solids are separated. Obviously, the hydraulics in this zone could be different from both the sludge bed and sludge blanket. Ideally, this portion of the flow could be described as a dispersion–plug flow or a plug flow and a CSTR. In the case of low OLR, a plug flow reactor and a CSTR joined with sludge bed work well, as was predicted by the model 1 (Figure VC– 4). At high OLR, a dispersion PFR is better describing the clarification volume in UASB (Figure VC-8). The plug flow reactor has 2% of total reactor volume at low OLR. This means majority space in the clarifier was well mixed by the gas bubbles. The model 1 appears adequate in describing the non-ideal behavior of UASB reactor at low applied OLRs.

At high OLRs, the bench UASB does not behave as an ideal CSTR. Neither Cholette-Cloutier's and Hall's model nor model 1 describe the UASB hydraulics well. The Van der Meer model and model 2 fit the data well (Figure VC–6(c) and 8). The reactor working volume from these two models were close (3% difference in the total volume). By comparison, the by–pass flow estimated by model 2 (22% of the total flow) is more reasonable than that estimated with Van der Meer model (31% of the total flow). A 31% by-pass flow means a maximum about 70% of organics removal can be achieved. However, operational data from the UASB reactor showed a COD removal efficiency of 80% and above. Thus the UASB reactor tested is unlikely to have 30% of total flow bypassed. Model 2 has less compartments (one less CSTR) than does the Van der Meer model and thus a reduced set of differential equation which resulted in much simpler

computations. Apparently, the higher the OLR, the more gas is produced and the larger the mixing volume becomes. By comparing these results with the results from the low OLR modeling, one can observe that the volume of CSTR increased 17%, from 74% (model 1, Figure VC-4) to 91% (model 2, Figure VC-8), of total reactor volume. The increased mixing space is mostly a result of a reduction in the dead volume (22%). This means more granules in the bed were exposed to the incoming substrate. The by-product of this improving is a 13% increase in by-pass flow. The fit obtained with the different flow models changed significantly when the OLR was increased from 4 to 10 kgCOD/m³bed-d, and the HRT decreased from 99 to 11 hrs. The two parallel CSTRs became one CSTR, a dispersion plug flow by-pass stream reduced to a simple by-pass flow, and a PFR is replaced by a dispersion PFR (Figure VC-3 and 7), suggesting improved axial mixing in the reactor. This is main reason that model 2 did not fit data obtained at low OLR (Figure VC-10).

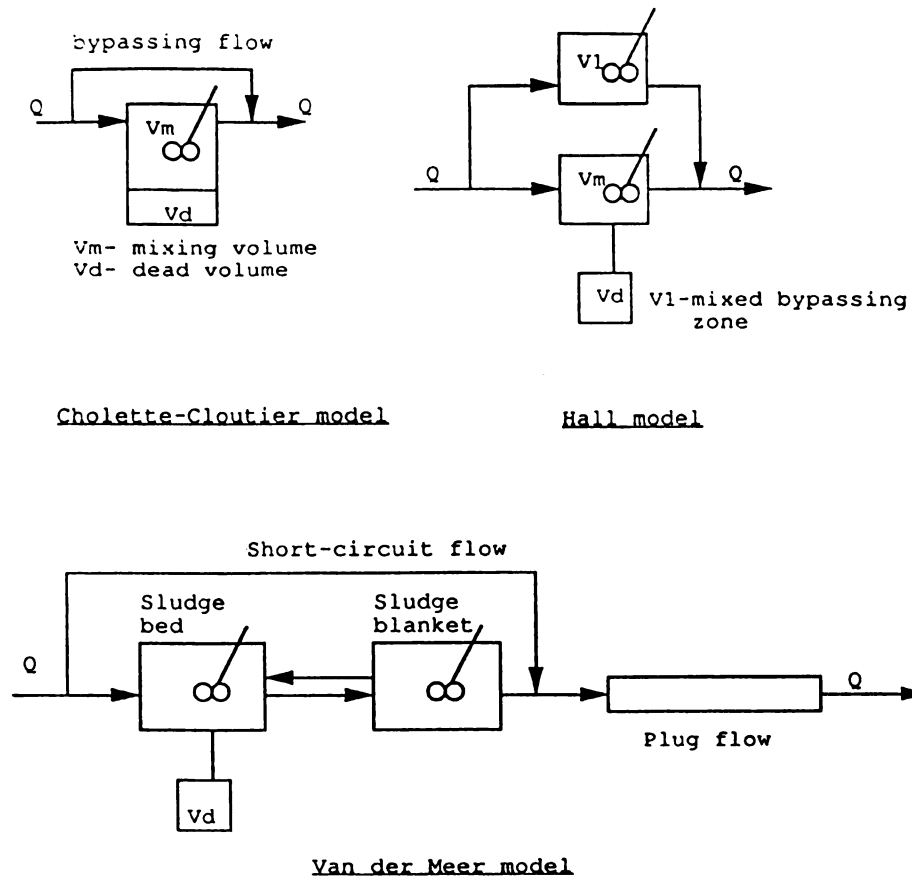


Figure VB-1. Schematic representation of fluid flow models evaluated in this work

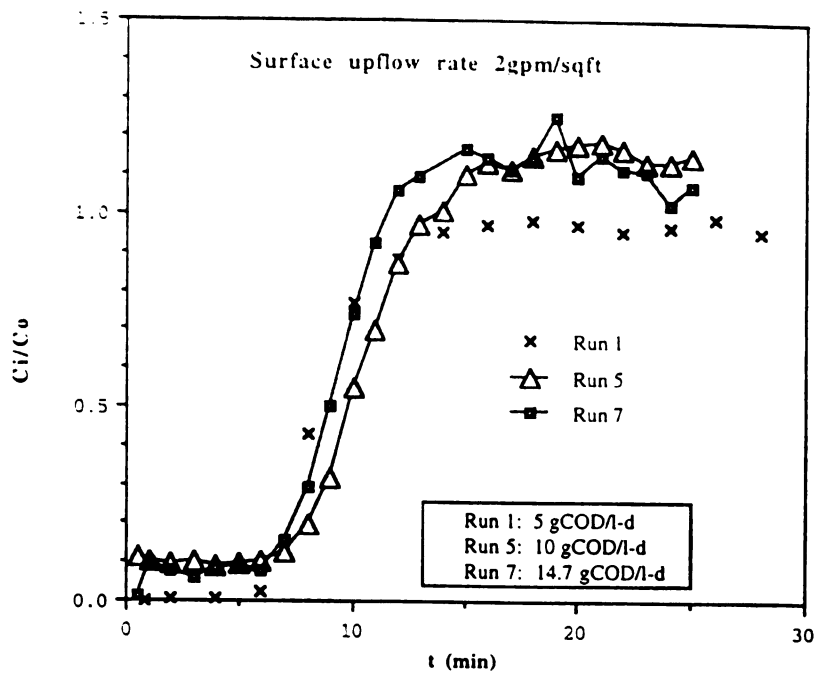


Figure VB-2. Effect of organic loading rate on hydraulic behavior at 2gpm/sqft

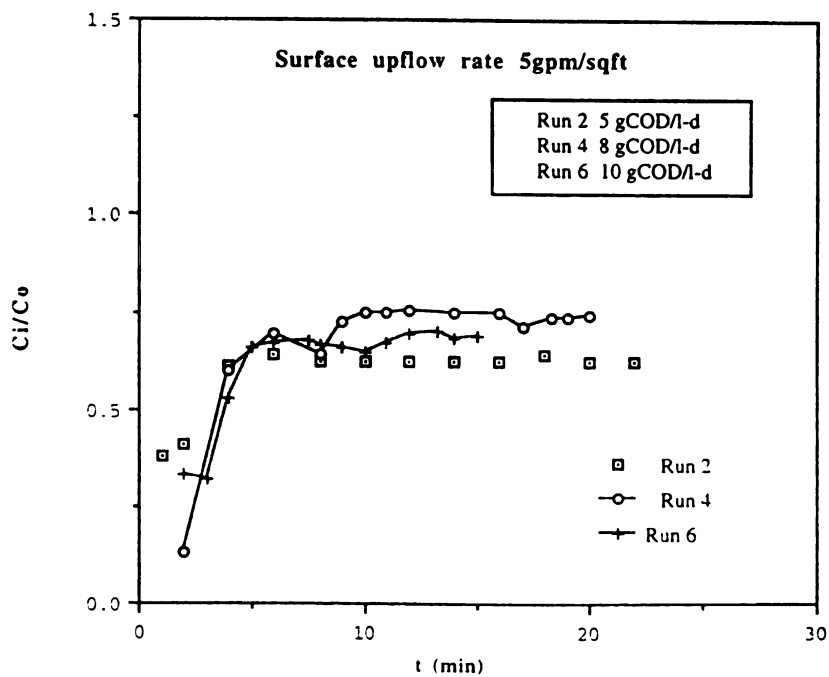


Figure VB-3. Effect of organic loading rate on hydraulic behavior at 5 gpm/sqft

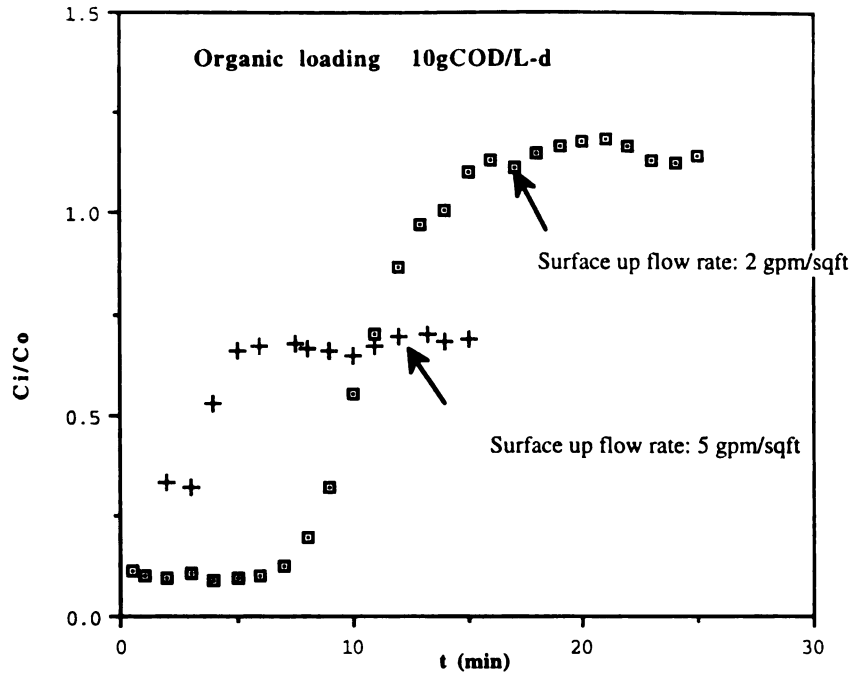


Figure VB-4. Comparison of effect at two surface upflow rates and an organic loading rate of 10 gCOD/Lbed-d

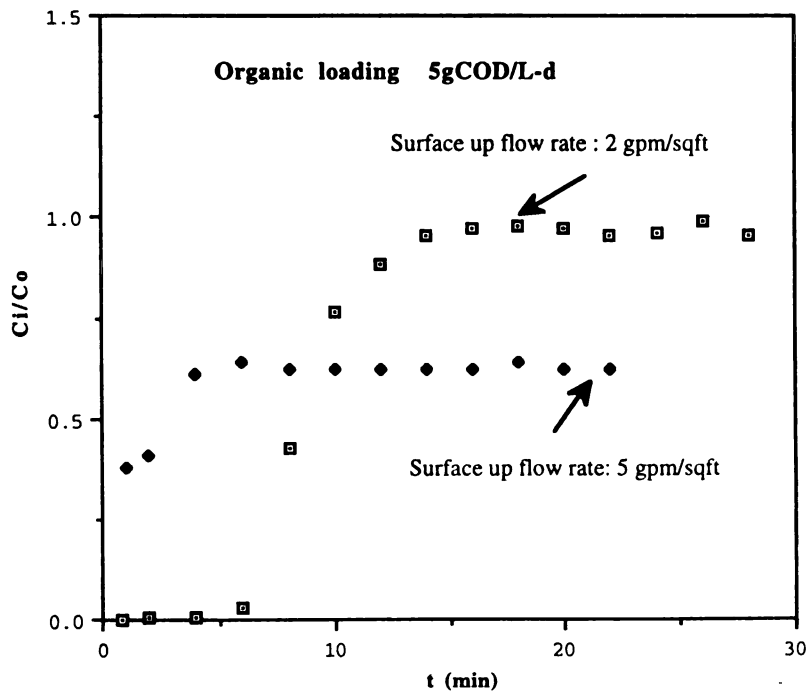


Figure VB-5. Comparison of effect at two surface upflow rates and an organic loading rate of 5 gCOD/Lbed-d

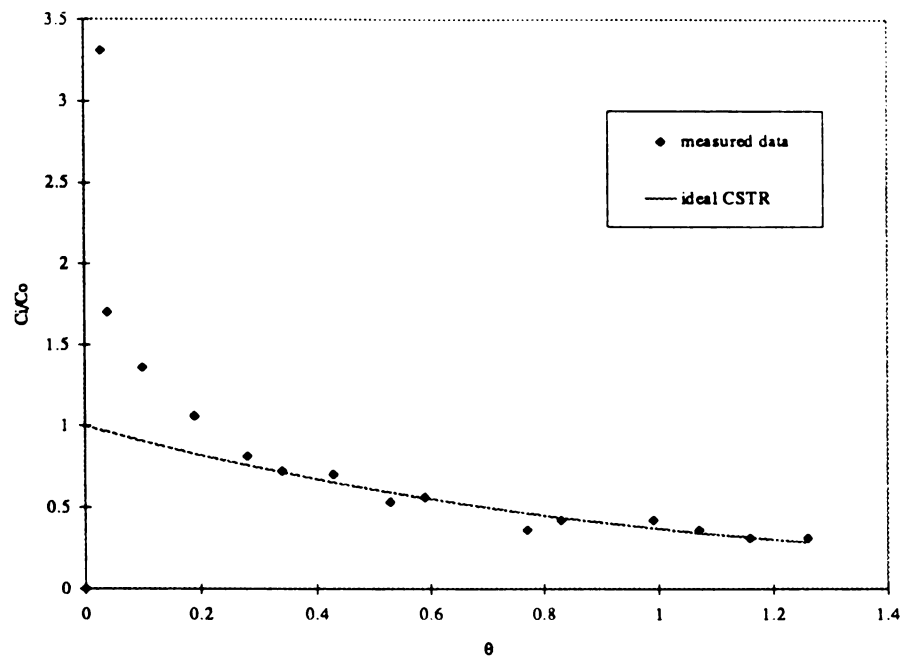


Figure VC-1. Measured data compare with ideal CSTR at 4 gCOD/Lbed-d and HRT 99 hrs.

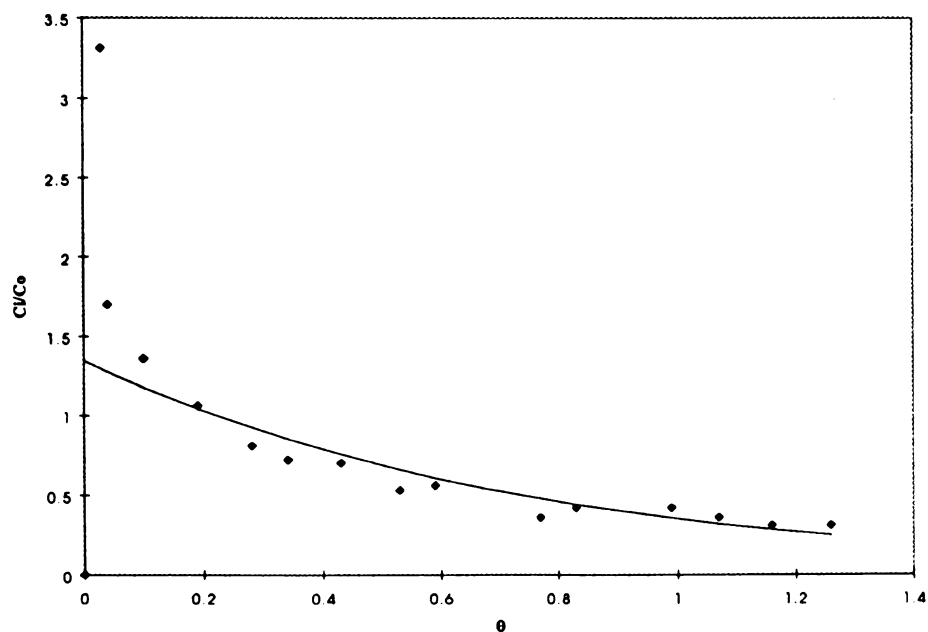


Figure VC-2(a) Results obtained using the Cholette-Cloutier model at OLR 4gCOD/Lbed-d and HRT 99hrs.

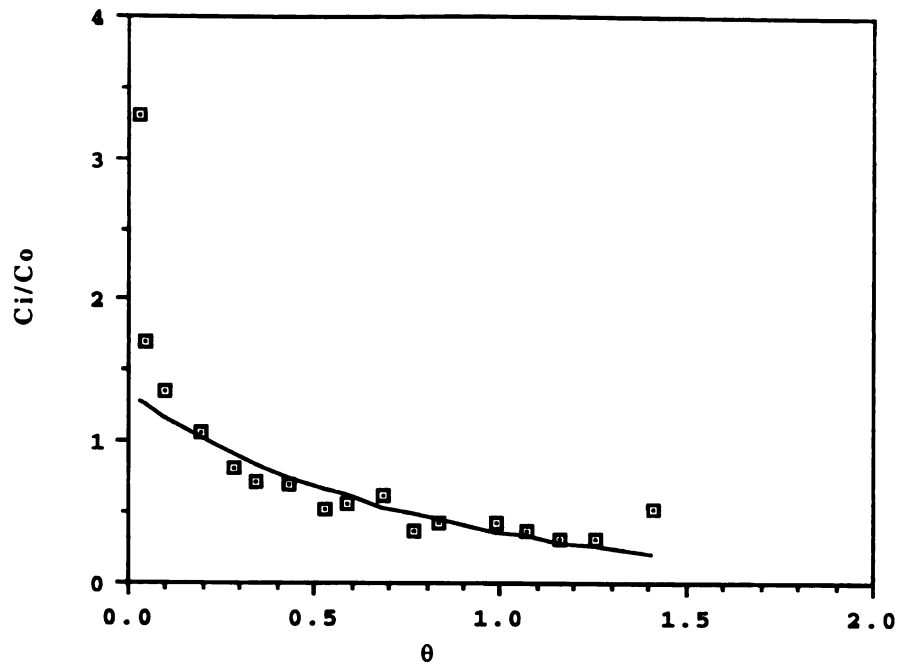


Figure VC-2(b). Results obtained using the Hall model at OLR 4gCOD/Lbed-d and HRT 99hrs.

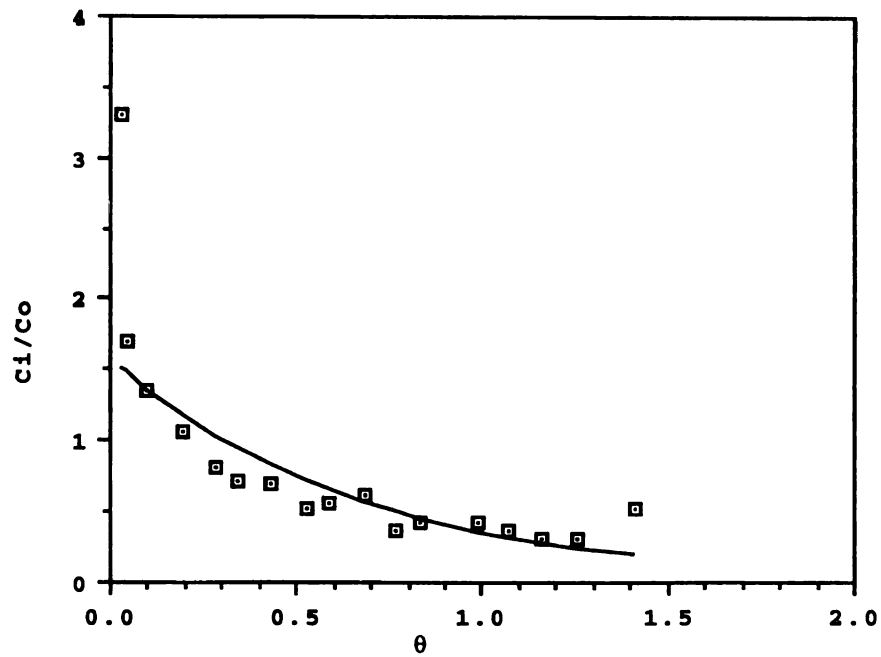


Figure VC-2(c). Results obtained using the Van der Meer model at OLR 4gCOD/Lbed-d and HRT 99hrs.

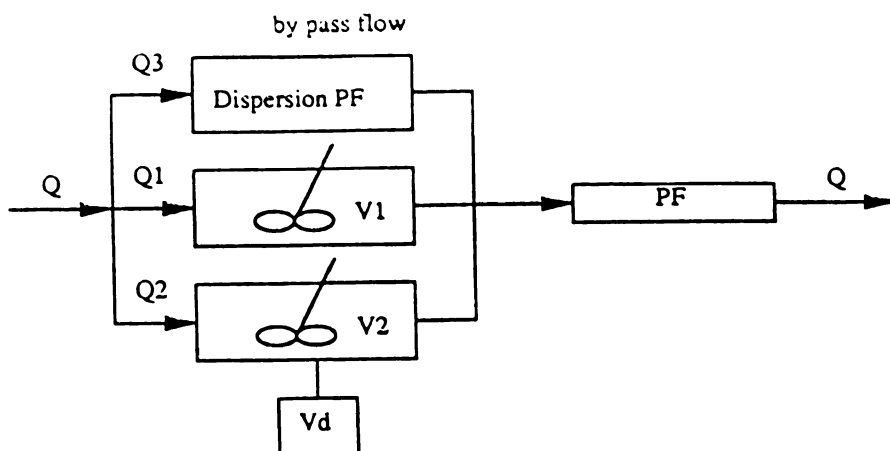


Figure VC-3. Representation of Model 1 used to describe UASB hydraulics at low OLR and high HRT

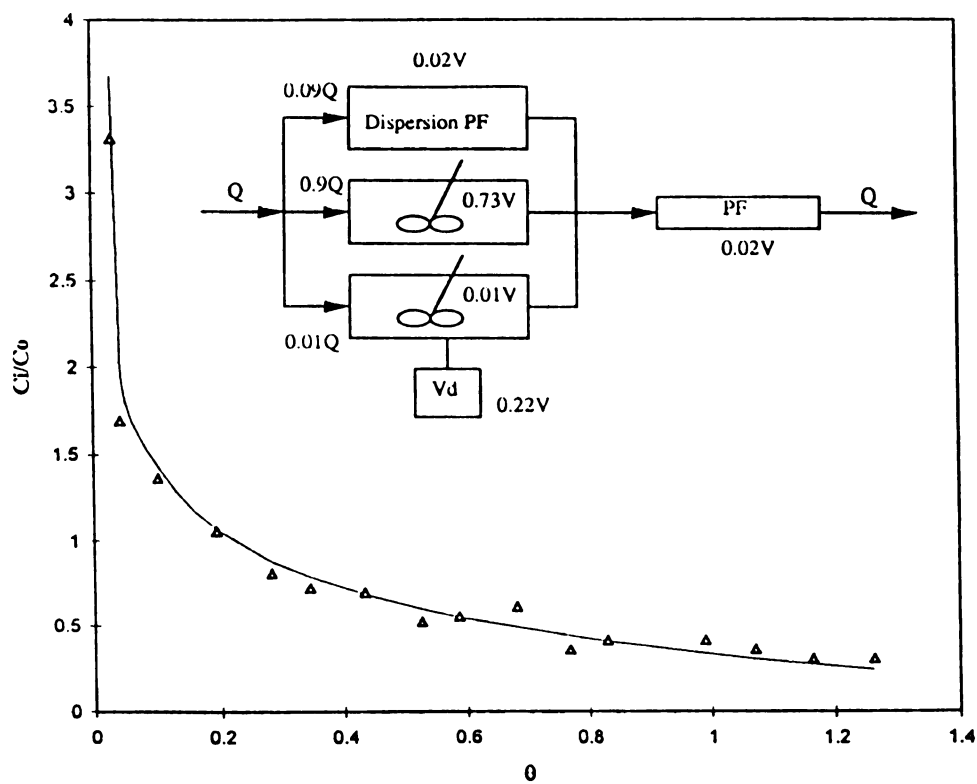


Figure VC-4. Results obtained using the new model at OLR 4gCOD/Lbed-d and HRT 99hrs.

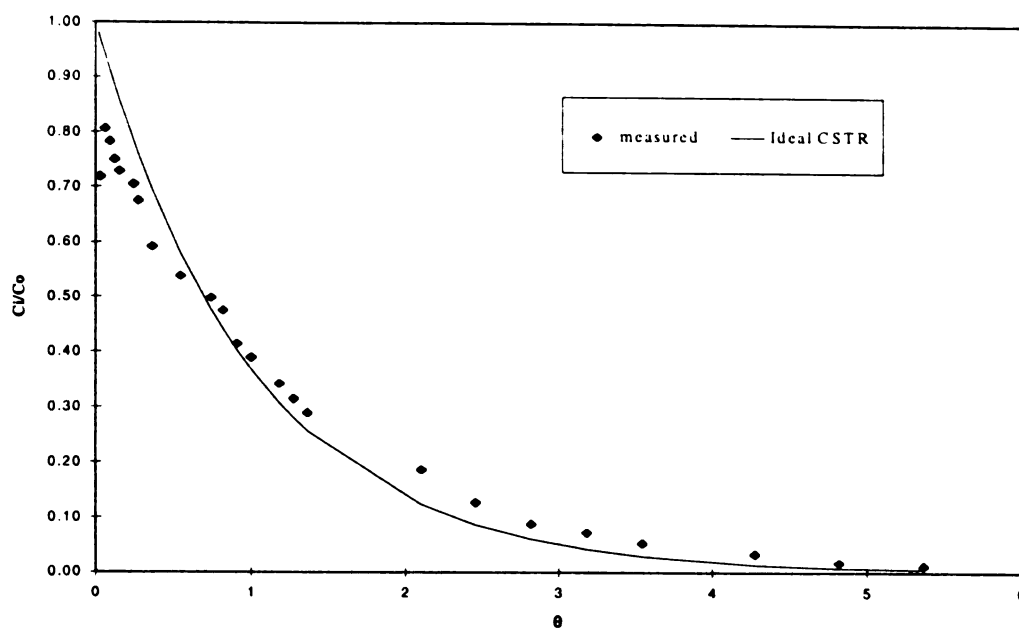


Figure VC-5. Measured data compare with ideal CSTR at OLR 10gCOD/Lbed-d and HRT 11hrs.

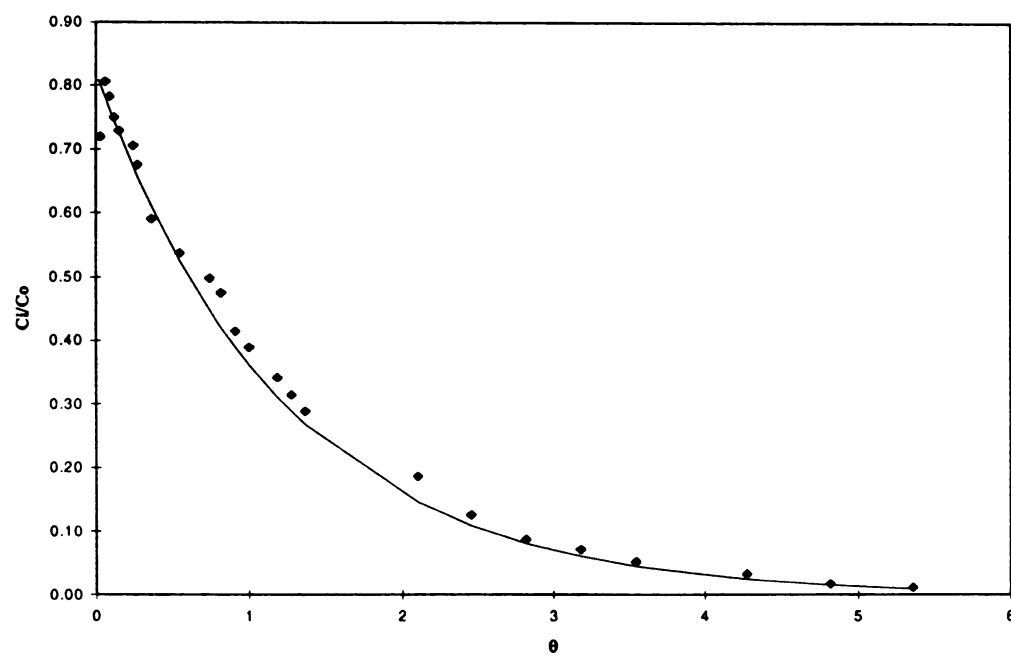


Figure VC-6(a). Results obtained using the Cholette-Cloutier model at OLR 10gCOD/Lbed-d and HRT 11hrs.

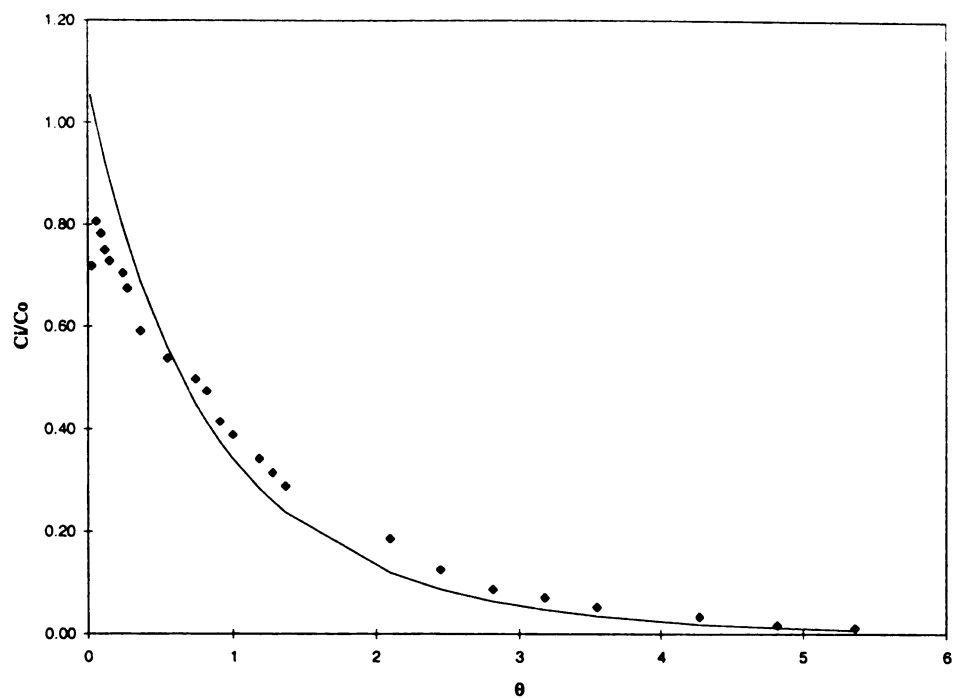


Figure VC-6(b). Results obtained using the Hall model at OLR 10gCOD/Lbed-d and HRT 11 hrs.

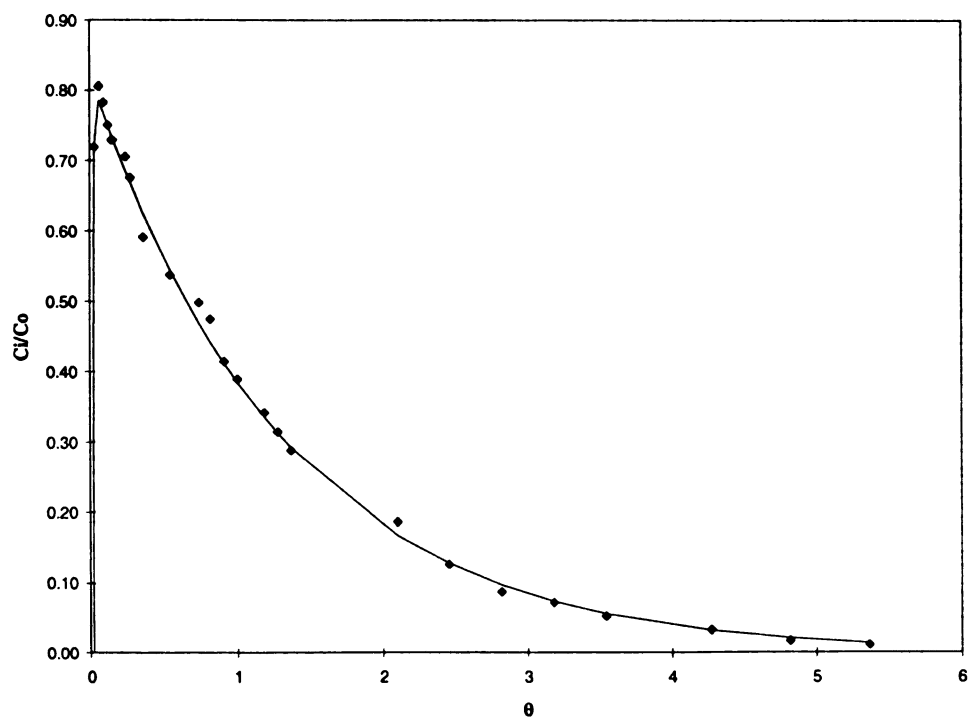


Figure VC-6(c). Results obtained using the Van der Meer model at OLR 10gCOD/Lbed-d and HRT 11 hrs.

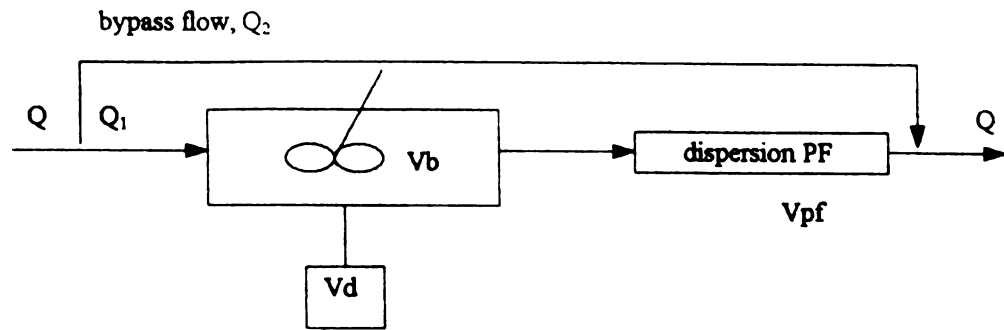


Figure VC-7. Model 2 describes UASB at high OLR and low HRT

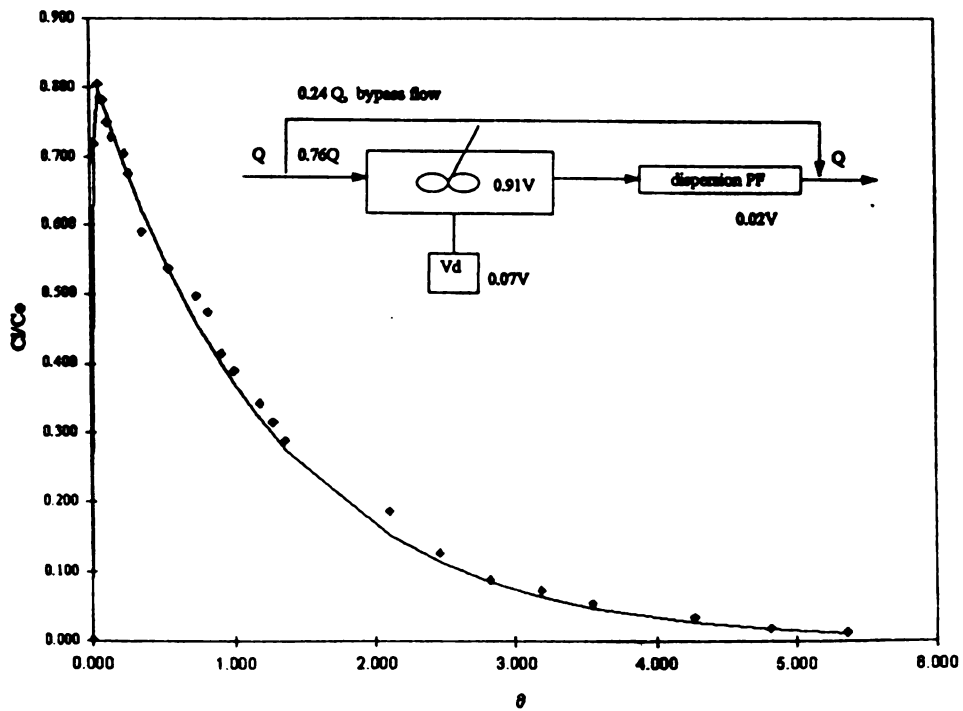


Figure VC-8. Results obtained using the model 2 at OLR 10gCOD/Lbed-d and HRT 11hrs.

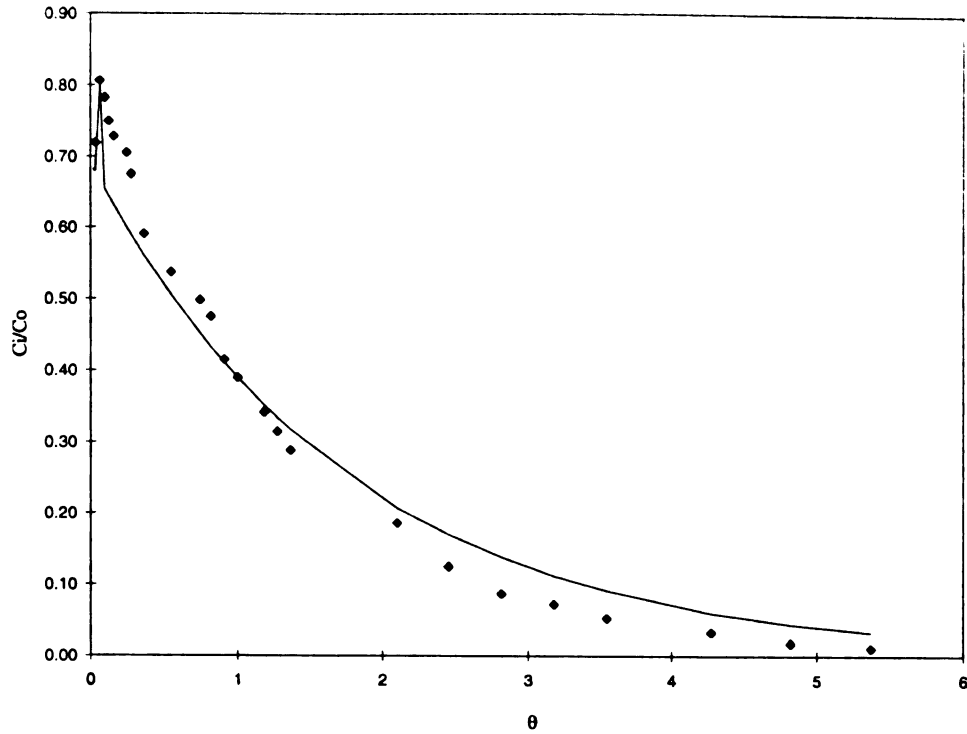


Figure VC-9. Results obtained using the model 1 at an OLR 10 gCOD/Lbed-d and HRT 11hrs.

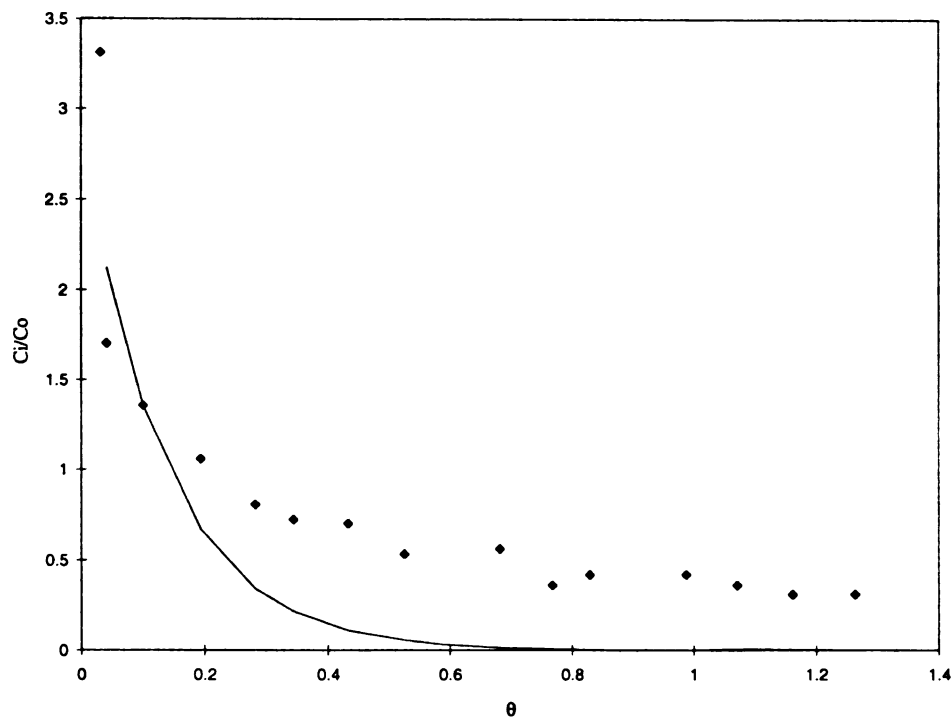


Figure VC-10. Results obtained using the model 2 at an OLR 4 gCOD/Lbed-d and HRT 99hrs.

Table VB-1. Operational conditions of bench-scale UASB reactor during hydraulic experiments

Parameters	Range
Influent COD (g/l)	14.1
Organic Loading (gCOD/L-d)	5 - 15
Biogas production (l/l-d)*	2.5 - 7.0
Reactor surface	
upflow rate (gpm/sqft)	2 - 5
upflow velocity (cm/s)	0.14 - 0.34
pH	6.82 - 7.0
Bed expansion	
(percent of total volume)	63% - 77%

* based on sludge bed volume (unexpanded)

Table VB-2. RTD Experimental Design

Run . No.	HRT (d)	Organic Loading (gCOD/L-d)	Surface upflow rate (gpm/sqft)
1	5.6	5	2
2	5.6	5	5
3	3.6	8	2
4	3.6	8	5
5	2.9	10	2
6	2.9	10	5
7	2.0	15	2
8	2.0	15	5

Table 3. Effect of organic loading rate on
UASB reactor hydraulic characteristics

Organic loading (gCOD/l-d)	Surface upflow rate (gpm/sqft)	Vb/Vt (%)	Dispersion number per cycle	HRT (d)	Biogas production (ml/hr)
5.2	2	60.0	0.051	5.6	155
	5	80.0	0.11		156
8.0	2	61.6	0.069	3.6	253
	5	74.5	0.097		257
10.0	2	62.9	0.045	2.9	305
	5	77.0	0.102		300
14.7	2	68.4	0.048	2.20	440
	2.2	69.0	0.049		444

* Vb - Sludge blanket volume

Vt - Reactor total volume

* Dispersion number (D/uL) based on one turn over.

* Multiple comparison test for dispersion number under four
organic loading rate: $Lsd_{0.05}=0.1008$ NS

Table VB-4. Effect of Recirculation on UASB Reactor Hydraulic Characteristics^a

Surface Upflow rate (gpm/sqft)	Vb/Vt (%)	Dispersion number per cycle	C/Colt=0	Student t test results
2	63.2	0.053	1.07	
5	77.2	0.103	0.69	df=5 t=6.986*** significant

a. mean value of experimental trials at each surface upflow rate

Table VB-5. Fluidization index of UASB reactor under different hydraulic operating conditions and granule sizes

U_{bs}^a (gpm/sqft)	Granule $d=3^{mm}$		Granule $d=1^{mm}$	
	Sludge bed		Sludge blanket	
	Re	n	Re	n
2	5.23	4.63	710	2.93
5	12.70	4.24	710	2.93

a. empty bed velocity

CHAPTER 6. KINETICS OF SUBSTRATE UTILIZATION BY BREWERY GRANULE

A. Introduction

Recent work investigating granules systems from Upflow Anaerobic Sludge Blanket (UASB) reactors has focused on defining the composition, kinetics and mass transfer within the anaerobic granules. Metabolic performance of granular sludge has been extensively studied [Zinder,et al.1984] [Koster,1986] [Koster and Cramer,1987] [Koster,et al.1986] [Fukuzaki,et al.1990a,1990b,1991] [Wu,1991a] [Wu,et al.1991b] [Peterson and Ahring,1991] [DeBeer,et al.1992][van Lier, et al.1993]. Kinetic studies of the granules were proceeded by studies using both defined cultures [Smith and Mah,1980] [Zehnder,1980] [Ahring and Westermann,1985] [Ahring and Westermann,1987] [Zinder,et al.1987] [Huser,et al,1982] [Patel,1984] and mixed cultures [Lawrence and McCarty,1969] [Kugelman and Chin,1971][Lin,et al,1989] [Gujerw and Zehnder,1983] [Chang,et al,1982,1983] [Zinder,1984] [Smith,1987] [Kaspar,1978] [Heyes,1983]. Various substrates were examined, including acetate, propionate, butyrate, isobutyrate, valerate, ethanol, methanol, formate, H_2 - CO_2 and glucose [Wu,1991a] [Schmidt,et al. 1993].

Metabolic performance, granule physical, chemical and biological composition, species distribution as well as ultrastructure were observed to be related to the wastewaters the granules were grown on /acclimated to. Substrate conversion rates were observed to be closely related to the composition of the wastewater that the granules were acclimated to. In one study, sulfate reduction accounted for 28% and 60% of ethanol and propionate conversion, respectively, but did not play a significant role in the metabolism of

H_2 , formate and acetate [Wu, et al. 1991b]. Schmidt and co-workers [Schmidt, et al. 1993] reported that addition of hydrogen utilizing methanogen and sulfate reducing bacteria to disintegrated granules improved both propionate and butyrate degradation rates. It was also observed that interspecies formate transfer does not play an important role for stimulation of propionate and butyrate degradation [Schmidt, et al. 1993].

Due to the complexity of substrate and product transfer processes within granules, a result of mass transfer limitation, description of substrate conversion rates of the granule has been characterized using apparent substrate utilization rates. The kinetics of substrate utilization by anaerobic granules appears to be considerably different from dispersed cells or biofilms with slab geometry for which explicit solutions are available [Bailey and Ollis, 1986]. Substrate flux, temperature, pH, granule size, and liquid film all contribute to the observed overall substrate utilization rate. A mathematic model was developed to describe the substrate utilization and mass transfer within biofilms [Williamson and McCarty, 1976] [Rittmann and McCarty, 1980]. Thermophilic granules grown on acetate from an UASB reactor were examined for mass transfer resistance [Schmidt and Ahring, 1991]. Disintegrated granules showed a higher specific methanogenic activity than intact granules when H_2/CO_2 were used as substrates. The reduction in mass transfer resistance depended on the method used to disrupt the granules when acetate was used as substrate. An effective diffusion coefficient for acetate in anaerobic sludge, measured using a diaphragm diffusion cell, was reported to be 22-33% of the diffusion coefficient in pure water [Nilsson and Karlsson, 1989]. DeBeer and coworkers [DeBeer et al., 1992] measured the pH profile inside granules using a pH micro-electrode. The pH inside was higher than in the bulk liquid. An unsteady state effectiveness factor, η , of 0.57-0.62 was

reported for acetate conversion based on the acetate profile which was calculated using the pH profile data. Alphenaar and co-workers [Alphenaar, et al., 1993] have shown that substrate transport limitations and substrate release (diffusion) velocity all increased with granule sizes. Overall effective diffusion coefficient was observed to be 40-80% of the diffusion coefficient in pure water in this study. An effectiveness factor was reported to be 0.48-0.67 during propionate degradation using whole granule and disintegrated granules [Schmidt and Ahring, 1993]. Numeric methods have been used for determining effectiveness factors with Michaelis-Menten kinetics and high Thiele moduli [Chang, 1982]. Controversies on the effect of diffusional and mass-transfer resistances to substrate utilization still exist [Henze and Harremoës, 1983]. No diffusional limitations in biofilms of 2.6 µm was reported [Kennedy and Droste, 1986]. Other researchers concluded that diffusion is not rate limiting during acetate utilization [DeBeer et al., 1992]. The degradation rate of propionate and butyrate in granules from a thermophilic UASB reactor decreased 35 and 25%, respectively, after disintegration of the granules [Schmidt and Ahring, 1993]. Overall, however, diffusional and mass transfer resistances within the granular sludge, its role and significance with respect to the utilization rates of different substrates, its interaction with temperature effect and granule size, have not been fully investigated to date. A detailed discussion of modeling anaerobic granular sludges for substrate utilization including liquid film mass transfer, diffusion limitations, intrinsic kinetics is presented in chapter IV.

Considerable work has been performed on studying reaction thermodynamics and substrate thresholds of anaerobic bacteria, particularly methanogens. From a thermodynamic point of view, threshold levels represent the minimal energy required for a particular

reaction to proceed. This minimal energy is required for ATP synthesis. Schink [1988][1992] suggested that during butyrate oxidation in anaerobic systems, a minimum of 20 kJ/mol is required for each reaction step. This is approximately 1/3 of energy required for formation of 1 mole ATP (75 KJ/mole ATP) [Schink, 1992]. The remaining energy is conserved via a membrane electron chain in a process of reversed electron flow. This reduces the H_2 concentration and through energy sharing process anaerobes are able to conserve and utilize a minimal amount of energy for growth. The minimal energy for a reaction is species dependent.

It is believed that the substrate threshold model provides a description of population competition in different habitats. The prevailing population for a particular substrate may be determined by the substrate concentration level within that environment. Bacteria will not consume a substrate when it falls below the threshold level. Different organisms each have their own threshold for a particular substrate. The organisms with a threshold at or lower than the environment level of a particular substrate are able to out compete other organisms for the substrate (assuming no other factors are involved). This competition could occur between different species or among the species. Lovely [1985] observed that a *Methanobacterium* did not consume H_2 below a threshold of 6.5 Pa. Cord-Ruwisch [1988] demonstrated that hydrogenotrophic anaerobic bacteria compete for H_2 . Successful competition was a function of the redox potential and electron transfer efficiency. Acetate decarboxylation is performed by two methanogens: *Methanosarcina* and *Methanotrix* [Zehnder et al. 1980] [Mah 1978]. After extensive study of anaerobic acetate decarboxylation, Westermann [1989], Zinder [1990], Hang and Zinder [1989] indicated a high acetate threshold (1–2.5mM) for *Methanosarcina* sp. and a low level (12

–75 μ M) for *Methanothrix sp.* The higher the electron transfer efficiency between electron donor and electron acceptor the lower the substrate threshold. Large amounts of electron transfer produce high energy yields, thus lowering the H₂ threshold required for energy conservation. The high acetate threshold *Methanosarcina sp.* conserve more free energy from acetoclastic methanogenesis than the low acetate threshold *Methanothrix sp.* does. In this case, the *Methanothrix sp.* require less energy to carry out the biochemical reactions and thus are more energy efficient.

In this study, granules obtained from a system treating brewery wastewater were characterized for the kinetics of substrate utilization, liquid film resistance and diffusional resistance. Temperature effects, reaction thermodynamics and substrate thresholds of the populations within the granules during acetoclastic methanogenesis were examined in order to better understand the physicochemical and biological process occurring. Experiments were performed using a batch-mode CSTR (Chapter VI B). Operational conditions were the same as indicated in section B except as otherwise specified. The carbon source used was acetate for mass transfer, temperature effects and threshold determinations. Acetate, propionate and ethanol were used for intrinsic kinetics and diffusion limitation studies. The mineral medium used and inoculum preparation are described in Appendix A and B1, respectively. Biomass determination and microscopy protocols are presented in Appendix B7 and C2, respectively. A linear regression was used to estimate the initial rate of degradation of each substrate. These analytical techniques are detailed in Appendix C2.

B. Intrinsic kinetics of acetate, propionate, ethanol and H₂ utilization

B-1. Description of laboratory batch system

Activity assays for brewery granular sludge were performed in a two-liter Multigen Convertible Bench-Top Reactor (Model F1000, New Brunswick Scientific Co.). A schematic representation of the system used is depicted in Figure VIB-1. The reactor was operated in batch mode. Temperature was controlled with a heating system equipped with a thermosensor. Reactor mixing was provided by two impellers, with a speed range of 100 to 1000rpm. The reactor was sealed with a rubber ring top to prevent air from entering the vessel. The reactor head space was connected, using small diameter tubing, to a flask that was used as a water seal. Sampling and drainage ports were sealed with butyl rubber stoppers and aluminum crimps. Target compounds were introduced through the injection port using 3ml to 25ml syringes (depending on the starting concentrations desired) equipped with 21-gauge needles. Liquid samples were taken from the sampling port using a 1ml syringe and a 21-gauge needle. Operational conditions are presented in Table VIB-1.

B-2. Experimental design and methods

To minimize diffusional resistance within the granules, which could mask the intrinsic properties of substrate utilization, the activity assays for acetate, propionate, ethanol and H₂ were performed using fine floc particles (~33µm in diameter) obtained by disrupting granules from a laboratory bench-scale UASB reactor (Figure VIII-1). These granules had been acclimated for more than six months to a synthetic brewery waste. The composition of this synthetic waste was based on the results of a one week sampling

program at the brewery (Appendix A). The anaerobic technique used to produce the flocs is described in Appendix B1. The Multigen reactor was operated using the mixing condition, determined during a separate experiment (Chapter VI, section C), required to ensure that the liquid film mass transfer resistance was minimized. Single carbon sources, acetate, propionate and ethanol, which are major components in the brewery waste, were used to assess the activity for each group of microorganisms (acetoclastic methanogens, propionate degraders, and ethanol utilizers, respectively). Sodium salts of propionate and acetate were used. Medium, stock solutions and the inoculum preparation technique used are described in detail in Appendix A and B1. Acetate and propionate degradation rate assays were performed using a series of substrate concentrations. The initial concentrations used covered the entire range of Monod kinetics, from the expected K_s to a value 10 times higher. This was done to allow observation of both the zero and the first order reaction periods. The sampling frequencies used, which were varied with initial doses used, are presented in Tables VIB-2 and VIB-3 for acetate and propionate, respectively. Assays were repeated at low and high concentration ranges. Substrate consumption was modeled using Monod kinetics. The maximum specific substrate utilization rate, k_m , and half velocity constant, K_s , for acetate and propionate were estimated by applying a non-linear least square technique (software SYSTAT) on the differential form of the Monod equation.

$$-\frac{\partial S}{\partial t} = V_i = \frac{k_m X S_i}{K_s + S_i} \quad \dots \quad (\text{VI-1})$$

where S -substrate (mM), t -time (hr), V_i -utilization rate of substrate I (mM/h), k_m -maximum substrate utilization rate (g/gVS-d), X -biomass as volatile solids (gVS),

K_s -half velocity constant (mM).

Ethanol utilization assays were performed by injection of a concentrated solution (20mM) into the reactor to obtain a high initial substrate concentration. Concentrations of ethanol and H_2 were then tracked over time. The progress curve for ethanol degradation, adjusted for an initial lag period, was fitted to the integrated form of the Monod equation. A non-linear least squares technique was used to evaluate k_m and K_s .

$$t_i = \frac{I}{k_m X} \left[K_s L n \frac{S_o}{S_i} + (S_o - S_i) \right] \quad \dots \quad (VI-2)$$

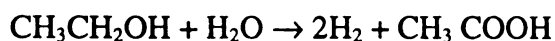
where t_i -time (hr), $i = 1, 2, 3, \dots n$, k_m -maximum substrate utilization rate (g/gVS-d), X -biomass at the conclusion (gVS), K_s -half velocity concentration (mM), S_o -initial substrate concentration (mM), S_i -substrate concentration at time t_i (mM). For details of ethanol assay refer to Chapter VII. For all kinetic parameters estimated, the quantity of curve fitting is judged by r^2 .

Analytical methods for acetate, propionate, ethanol and H_2 are given in Appendix C. Derivation of the non linear least squares procedure for equations VI-1 and VI-2 are provided in Appendix D. Microscopic observations were performed using an epifluorescence microscope (Olympus, BH-2, Appendix B7). Biomass was collected and dry weight determined after each assay.

B-3. Kinetic parameter estimation for acetate, propionate, ethanol and H_2

The initial acetate concentrations used ranged from 0.27mM to 8.65mM and for propionate from 0.1mM to 2.1mM. At each initial concentration, substrate conversion was measured with time. The linear range was chosen for calculation of the initial rate at that

substrate concentration using a linear regression. Kinetic parameters (K_s, km) were determined using initial utilization rates and the corresponding substrate concentrations from these assays. The ethanol degradation rate was measured at an initial concentration of 20mM. Concentrations of ethanol and H_2 were then tracked over time. Kinetic parameters for ethanol (K_s, km) and H_2 (K_s) were solved analytically using the integrated form of Monod equation. The H_2 consumption rate was calculated considering the observed H_2 disappearance rate and a calculated H_2 production rate from ethanol, based on the stoichiometric relationship:



and the following equation:

$$\frac{dH_2}{dt} = \left[\frac{dH_2}{dt} \right]_{app} + 2 \frac{dETOH}{dt} \quad \dots \quad (VI-3)$$

where $\left[\frac{dH_2}{dt} \right]_{app}$ is the apparent hydrogen consumption rate, that is, the change of hydrogen concentration with time in the system. $\frac{dETOH}{dt}$ is ethanol consumption rate. The influence of n-propanol and propionate on the hydrogen consumption rate were ignored, because the concentrations of n-propanol and propionate (<0.4mM and <0.7mM, respectively) were relatively low compared to that of ethanol (20mM).

The fitted curves for acetate, propionate, ethanol and H_2 utilization are presented in Figures VIB–2 to VIB–5. The estimated half velocity constant, K_s , and maximum specific utilization rate, km , for acetate, propionate and ethanol were 0.45mM, 0.40mM, and 3.37mM, and 5.11g/gVS-d, 6.25g/gVS-d, and 5.49g/gVS-d, respectively. The apparent K_s for H_2 was 150 ppm or 5.9 μ M (gas phase concentration). The H_2

consumption rate was 5.4 mM/gVS-h. Fitted curves had r^2 of 0.993 for acetate, 0.986 for propionate, 0.950 for ethanol and 0.820 for hydrogen, respectively. Background acetate, propionate, and ethanol levels were less than 0.1mM.

C. Mass transfer within brewery granules

C-1. Liquid film resistance

Mass transfer through the liquid film around the granules was studied using a bench-top Multigen reactor system (Figure VIB-1). Granules were collected from a laboratory bench-scale UASB reactor treating a synthetic brewery waste (Figure VIII-1). Reactor environmental and operational conditions are shown in Table VIB-1. Sodium acetate was the sole carbon and energy source used in for mass transfer experiments. Acetate utilization was initially measured at different mixing levels. The experimental design is listed in Table VIC-1. Impeller speeds were varied from 200 to 800rpm to determine the point at which liquid film diffusion was minimized. The initial acetate consumption utilization rate was determined by linear regression.

A graphical presentation of acetate utilization at different mixing levels is given in Figure VIC-1. The error bar ($\pm 1SD$) at 600rpm represents results of three different experimental runs. Acetate utilization rate increased with increasing impeller speed. Above 600rpm, the variation of acetate utilization rate became small, indicating negligible influence of liquid film on acetate consumption at or above 600rpm. At a speed of 800rpm, a liquid vortex formed within the reactor and the granules became physically disrupted. To ensure liquid film resistance was minimized for studying diffusional effect without disrupting the physical integrity of the granules, an impeller speed of 600rpm was chosen for all subsequent experiments.

C-2. Effect of granule size on substrate diffusion

In this portion of the work, the specific utilization rates for different granule sizes were compared to examine the effect of diffusional resistance on substrate utilization. Mass transfer limitation is described by the effectiveness factor, η , which was estimated by determining the ratio of apparent substrate utilization rate of whole granules, to the intrinsic substrate utilization rates obtained previously (Chapter VI section B). The η included diffusional resistance only. Theoretical development of reaction–diffusion function within the granule is given in Chapter IV.

All three major carbon sources in the brewery waste, acetate, propionate and ethanol, were studied. Three sizes of granules were used; whole granules (1.8–3.0 mm, average 2.5mm), partially disrupted granules (0.1–3.0mm, average 1.1mm) and flocs (20–75mm, average 33mm). Whole granules were mechanically disrupted, without filtering, to produce granules with an average size of 1.1mm. These were further fractionated into small flocs (average size of 33 μ m). A typical size distribution of partially disrupted granules is presented in Figure VIC–5. The partially disrupted granules had a size ranging from 0.1mm to 3.0mm, with an average size of 1.1mm. Both partially disrupted granules and flocs were prepared immediately before each experiment. Methods of formation of disrupted granules and flocs are described in Appendix B. The reactor impeller speed for the diffusion experiments was 600rpm. Particle sizes were measured using a microscope (Appendix B). Biomass concentration and particle size were determined at the conclusion of each assay.

To start each experiment, a concentrated substrate solution was injected into the reactor to obtain a starting substrate concentration of 6mM acetate, 8mM propionate and

30mM ethanol. Background substrate levels prior to the addition of substrate were less than 0.1mM for each substrate for all assays. Apparent substrate utilization by the granules was measured with time. The initial rate was determined using a linear regression. All experiments were conducted in duplicate.

Typical progress curves of acetate utilization, using different sized granules, are shown in Figures VIC-2 and VIC-3. A Monod type curve of acetate utilization versus granule size and concentration is given in Figure VIC-4. Utilization rates closely followed the granule size for the range studied. The apparent specific acetate utilization rate for the flocs was much higher than that of whole granules. The maximum apparent specific substrate utilization rate (zero order portion of the Monod curve) of the whole granules was only 1/3 of the rate observed for the flocs. The estimated unsteady state effectiveness factors, η , were calculated to be 0.32, 0.41 and 0.75 for acetate, propionate and ethanol, respectively (Table VIC-2).

D. Temperature Effects

The effect of temperature on substrate utilization was also examined using acetate as the sole carbon and energy source. The inocula used included whole granules and flocs. Assays were conducted at 26°C, 31°C and 37°C. An initial acetate concentration of 6mM was used for all assays. A time course of substrate utilization was obtained and apparent specific substrate utilization rate determined for each assay. At the conclusion of each assay, biomass and particle sizes were determined and fluorescence microscopy observations were performed (Appendix B). A typical acetate utilization curve for whole granules at 26°C, 31°C, 37°C is presented in Figure VID–1. Because of the heat generated by the mixing system during the experiment, it was impossible to maintain a temperature of 26°C for an entire assay. Only a few hours worth of data were available at 26°C. Estimated apparent specific utilization rates for whole granules and flocs at the three temperatures, are presented in Table VID–1. As expected, the rates increased with increasing temperature. A plot of acetate utilization rate versus temperature is presented in Figure VID–2. Effectiveness factors of granules for acetate utilization were 0.36, 0.35 and 0.32 at 26°C, 31°C and 37°C, respectively. To characterize the effect of temperature, an attempt was made to describe results obtained from the flocs using the Van't Hoff-Arrhenius equation. A linearized plot of temperature versus specific acetate utilization rate is presented in Figure VID–3. A linear regression on natural log of km resulted in a typical Arrhenius equation ($r^2=0.95$)

$$km = 3.359 \times 10^{14} \exp \left[\frac{-9888.54}{T} \right] \quad \dots \quad (\text{VI-4})$$

where km is in g/gVS-d, T in °K, applied range {26°C, 37°C}

The above equation can be rewritten as :

$$\ln \left[\frac{km_2}{km_1} \right] = \frac{E}{R} \left[\frac{1}{T_1} - \frac{1}{T_2} \right] \quad \dots \quad (\text{VI-5})$$

where E is activation energy. Estimated activation energy was 19380 Kcal/mole, within the common range of anaerobic wastewater treatment systems [Metcalf&Eddy, 1991].

Another form of this equation gives

$$\frac{km_{37}}{km_{27}} = 1.12^{37-27} \quad \dots \quad (\text{VI-6})$$

with the assumption that $\frac{E}{RT_1T_2}$ in equation (4) is constant and where $1.12 = e^{\frac{E}{RT_1T_2}}$. For the whole granules this constant was 1.09. The estimated activation energy was 15400 cal/mole.

E. Threshold and reaction thermodynamics of substrate utilization

A study of minimum acetate and hydrogen levels and reaction thermodynamics was conducted. Substrate threshold levels were determined by measuring the concentration at which further substrate utilization did not proceed. The pH and temperature were recorded in order to determine the minimal Gibb's free energy for acetate decarboxylation and hydrogen oxidation. It was assumed that the end products during acetoclastic methanogenesis was stoichiometrically 1:1 for CO_2 and CH_4 . A separate GC program was used to accurately quantitate low concentrations of acetate (Appendix C). Hydrogen from the headspace of the Multigen reactor was analyzed using a Reduced Gas Analyzer (Trace Analytical, RGD2) equipped with a mercuric oxide reaction

bed (Appendix C).

Results of acetate threshold and minimal Gibb's free energy during acetate metabolism are presented in Table VIE-1. There were no significant differences in the acetate threshold and minimal free energy levels for the different granule sizes (flocs and whole granules). The threshold acetate level ranged from 4–70 μ M. This threshold values agrees well with reported literature values (Table VIE-2). The minimal Gibb's free energy available for acetate decarboxylation ranged from –1.40 to –4.44kcal/mol acetate (–5.9 to –18.6kJ/mol), with an average of –2.53kcal/mol acetate (–10.6kJ/mol). The H₂ threshold concentrations were observed to vary from 5.2 to 26.3ppm. These values are within the literature values but fall into the lower bound of previously reported values (Table VIE-3). The minimum Gibb's free energy available for H₂ oxidation was calculated to be –1.3kcal/mol H₂ (–5.4kJ/mol).

F. Discussion

For our defined reactor system, operated under controlled hydrodynamic conditions, we assumed that results obtained using flocs (33 μ m diameter) were representative of the intrinsic kinetics of the brewery granules. Results from substrate utilization assays using flocs were well described by Monod kinetics. A summary of kinetic parameters for acetate, propionate, ethanol and H₂ obtained from different sources is presented in Tables VIB-4 and VIB-5 for comparison. Results obtained for acetate, propionate and H₂ intrinsic kinetics during this study agree well with reported literature values. The maximum specific utilization rate, k_m , obtained using flocs, for each substrate is at the higher bound of previously reported values for propionate and acetate (6.25, 5.11, g/gvs-d). The K_s values are at the lower bound of reported values for acetate (0.45mM), ethanol (3.37mM) which were probably a result of minimized diffusion limitations. The K_s for hydrogen (5.9 μ M) agreed well with Robinson and Tiedje [1982]. There was a discrepancy in the half velocity constant K_s observed for ethanol (3.37mM, this study) compared to other work (100mM, [Smith, 1987]). This could be the result of variations in experimental conditions. A single carbon source (ethanol or propionate) was used in previous study compared to a complex substrate mixture in this work. Differences in the predominant ethanol utilization population could also account for these differences in kinetic constants.

The mixing intensity applied during the liquid film mass transfer experiments can be expressed using the Reynolds numbers (N_R). Reynolds number was calculated according to following equation:

$$N_R = \frac{D^3 n \rho}{\mu} \quad \dots \quad (\text{VI-7})$$

where D —impeller diameter, (0.05556m); n —rpmx60; ρ —density of reactor fluid, (1000 kg/m³); μ —viscosity, (0.6965N⁵/m²). At N_R range of 53000–106000, which corresponds to an impeller speed of 200–400rpm, liquid–film mass transfer resistance still had a significant influence on substrate utilization (Figure VIC–1). A Reynolds Number of 159,000 (600rpm) was necessary to ensure good mixing and minimize liquid film resistance. Beyond that point, the effect of liquid film on mass transfer could be neglected. When the Reynolds number was increased to greater than 186,000 (700rpm), physical disruption of the granules occurred. An assumption was made that physical properties, density (ρ) and viscosity (μ) of the reactor fluid could be approximated by that of water. The region of Reynolds number applied in this study was much higher than that of the bench–scale UASB reactor. Hydraulic characterization experiments for the UASB reactor indicated when N_R was 700, 74% of the reactor total volume represents CSTR (model 1;Chapter V). It would appear, therefore, that liquid–film mass transfer resistance played a strong role in substrate utilization in the UASB reactor system.

Substrate utilization of partially disrupted or whole granules could not be adequately described using Monod kinetics due to the effect of mass transfer resistance. The apparent utilization rate decreased as the granule size increased (Figure VID–2). At low concentrations, the differences in rates between whole granules and flocs were small. As the initial substrate concentration increased, the influence of concentration on substrate utilization rate appeared stronger. At 6mM acetate, the apparent utilization rate of the flocs was 3 times the rate of whole granules. This phenomenon is typical for cell systems

with mass transfer limitations.

Temperature had a strong influence on the specific utilization rate of acetate (Table VID–1). This impact was greatest when the temperature exceeded 31°C. The magnitude of change in the utilization rate generally correlated with the granule size. Whole granules were less sensitive to temperature changes while flocs were most affected. When the temperature was increased from 31°C to 37°C, substrate utilization by the flocs increased by ca. 3.0 g/gVS-d, and whole granules, 0.7 g/gVS-d (Table VID–1). The apparent utilization rate does not increase exponentially with temperature when there are significant mass transfer limitations. Variation of effectiveness factor under the temperature range (0.32 to 0.36) was not significant. This also demonstrated that effects of temperature on substrate utilization were much less than the effects of diffusional limitations within the granules. Substrate utilization is influenced by temperature and diffusion when substrate concentration is fixed. The magnitude of this influence depends strongly on biofilm size, geometry, and the diffusion coefficient of the particular system. In slab geometry biofilm systems, substrate flux (J) increases with the square root of the maximum specific utilization rate (km), or $J \propto km^{1/2}$ [Rittmann and McCarty, 1980]. For free cell systems, $J \propto km$ as indicated by Monod kinetics. Since km is a function of temperature, as specified by Van't Hoff-Arrhenius equation, biofilm systems such as granules are less affected by temperature changes than dispersed cell systems. The influence of km on substrate flux in granular sludge system is more complex due to the geometry and does not have an explicit analytical solution [Bailey and Ollis, 1986]. The behavior of flocs was well described by the Van't Hoff-Arrhenius equation (Figure VID–3). This strongly supports the assumption that results obtained using flocs represent the intrinsic kinetics of the organisms in the

granules. As the size of granules increases diffusion limitations become more significant than temperature. Thus the response to changes in temperature was limited for whole granules. The differences between flocs and whole granules was smoothed in linerization results (Van't Hoff-Arrhenius equation) of flocs and whole granules (Figure VID-3, and 4) primarily due to log transformation.

A substrate threshold was observed for anaerobic utilization of acetate and H_2 during the experiment. The observed acetate threshold concentration ($17\mu M$) agreed well with literature values. The H_2 threshold (13.4ppm) fell into the lower bound of values reported in the literature. These results demonstrated that acetate decarboxylation and H_2 oxidation by methanogens can be described well by the threshold model. Substrate threshold reflected energy conservation for a specific species from the substrate. Minimal free energy requirements during methanogenesis were well below the available energy required for ATP synthesis. This is common in anaerobic system and is possibly due to the energy sharing processes. The specific growth rate (μ) and substrate affinity (half saturation constant) (K_s), play an role in the threshold level or minimal energy required for a reaction step to occur. *Methanothrix sp.* have a half saturation constant K_s of 0.7mM – 0.5mM (Table VIB-4, expressed as K_s). Acetate thiokinase found in *Methanothrix soghngeii* has a substrate affinity K_m close to 0.7mM [Kohler and Zehnder, 1984]. High level of acetate kinase with a K_m for acetate of 3mM was observed for *Methanosarcina barkeri* [Kenealy and Zeikus, 1982]. The low K_m of acetate thiokinase in *Methanothrix* indicates a high substrate affinity. These findings suggested the activation of the specific enzyme has a strong influence on the overall affinity of *Methanothrix sp.* and *Methanosarcina sp.* for acetate. Another important parameter in determining the

predominant organism in an environment is the specific growth rate, μ_{\max} .

Methanosarcina sp. has a higher μ_{\max} (1.8g/molCH₄) than *Methanothrix sp.* (1.1g/molCH₄) does [Zinder et al.,1987]. At acetate levels lower than 1mM, *Methanothrix sp.* can out-compete *Methanosarcina sp.* due to their high affinity for acetate. When the acetate level is elevated, both organisms are able to utilize acetate. *Methanosarcina sp.*, by virtue of its higher growth rate, is favored. Other factors such as growth factors and key vitamin can be important factors as well. In sediments, where acetate concentration are low (less than 400 μ M), *Methanothrix sp.* are generally the predominant methanogen (Table VIE-2). *Methanosarcina sp.*, are not able to compete effectively for acetate; they use other substrates for growth (i.e. methanol and methylamines). When the acetate concentration is at a level of 3–5mM such as in some sludge digestors, *Methanosarcina sp.* out-compete *Methanothrix sp.* and become the predominant acetoclastic methanogens. Changes in the acetate level can resulted in variations in populations of acetoclastic methanogen over a long period of time, despite the fact that the growth rates for methanogens are relatively low. In UASB reactor systems, the acetate concentration depends on operational conditions such as organic loading rate, hydraulic retention time, type of substrate, temperature, pH, and bacteria interactions. Under the selected operational conditions, the concentration of acetate in the laboratory bench-scale UASB reactor was maintained at 0.01mM–0.5mM. Therefore, it is reasonable that *Methanothrix sp.* were the prevailing population of acetoclastic methanogens (Chapter VII) in the brewery granules.

Similar phenomena occur for H₂ utilization within the anaerobic consortia, where

the syntrophic relationships between H_2 producers and H_2 consumers are established to maintain a minimal H_2 level. Different groups of hydrogenotrophic anaerobic bacteria can compete for H_2 as an electron acceptor. This preference, energetically, is nitrate and fumarate > sulfate > CO_2/CH_4 > sulfur > CO_2 /acetate. It was reported that the H_2 thresholds ranges from 0.33 to 950 ppm according to this order of electron acceptor energetics[Cord-Ruwisch,1988]. Both sulfate reducers and hydrogenotrophic methanogens were observed to be present in the brewery granules, with *Methanobacterium sp.* being the predominant H_2 utilizer (Chapter VII). The H_2 concentration in the bench-scale UASB varied between 10 and 200ppm. Either sulfate reducers or hydrogenotrophic methanogens could be potentially responsible for controlling the H_2 level (Table VIE-3). During the propionate and ethanol degradation assays, there was no sulfate supplied. The hydrogenotrophic methanogens were, therefore, the main H_2 consumers in these assays. A H_2 threshold level of 50–260ppm was observed under these assays conditions. It would appear, therefore, that the *Methanobacterium sp.* may have controlled the H_2 concentration in the system.

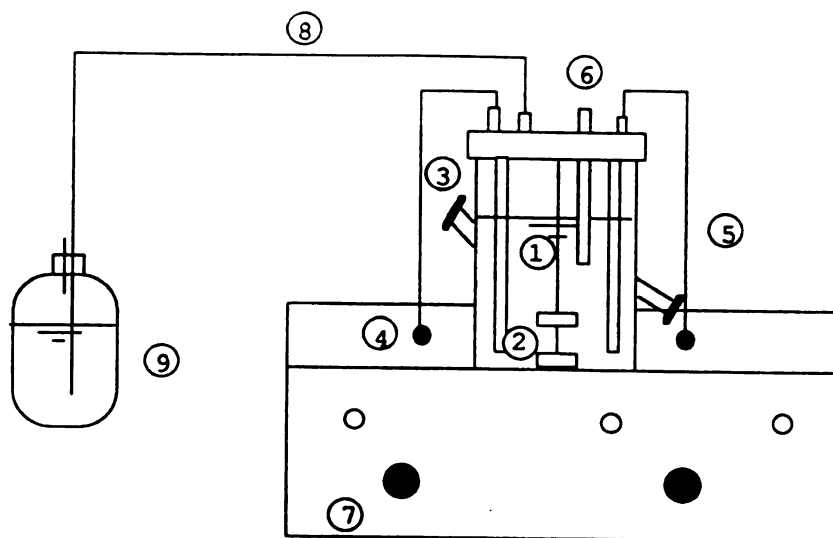


Figure VIB-1. Schematic diagram of bench-top CSTR set-up

- | | |
|------------------------|-----------------------------|
| ① 2 L Multigen reactor | ⑤ Thermosensor |
| ② Impellers | ⑥ Thermometer |
| ③ Sampling port | ⑦ Impeller speed controller |
| ④ Heating wire | ⑧ Gas line |
| | ⑨ Water seal |

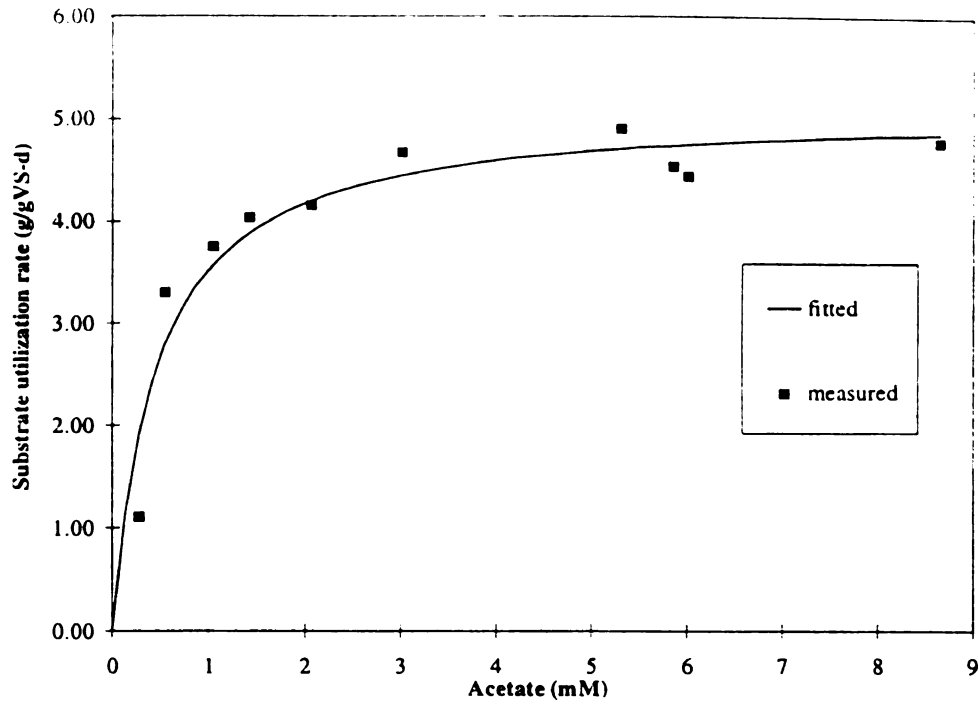


Figure VIB-2. Acetate utilization by brewery granules flocs and fitted Monod kinetics. $K_s=0.45$ mM, $k_m=5.11$ g/gVS-d.

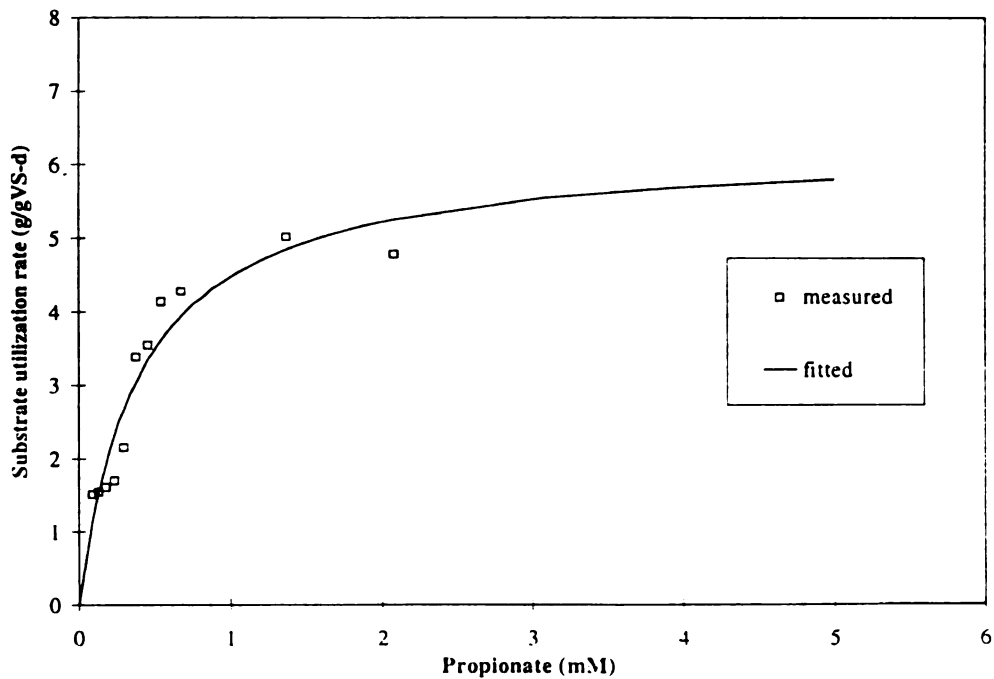


Figure VIB-3. Propionate utilization by brewery granules flocs and fitted Monod kinetics. $K_s=0.40$ mM, $k_m=6.25$ g/gVS-d.

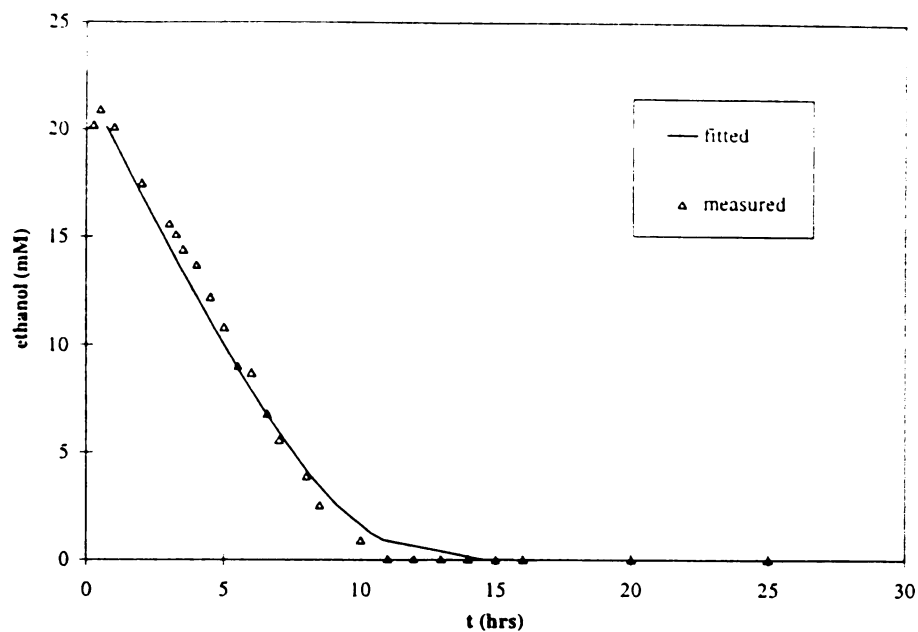


Figure VIB-4. Ethanol utilization by brewery granule flocs with fitted Monod kinetics. $K_s=5.49\text{g/gVS-d}$, $k_m=3.37\text{mM}$.

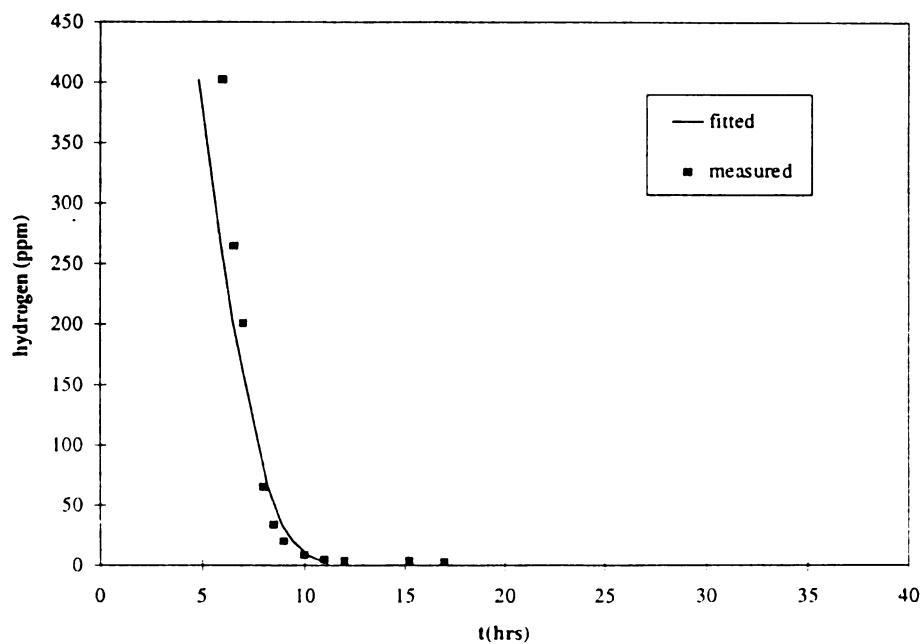


Figure VIB-5. Hydrogen consumption by brewery granule flocs during ethanol conversion. $K_s=5.9\text{ }\mu\text{M}$, hydrogen consumption rate= 5.4mM/gVS-h .

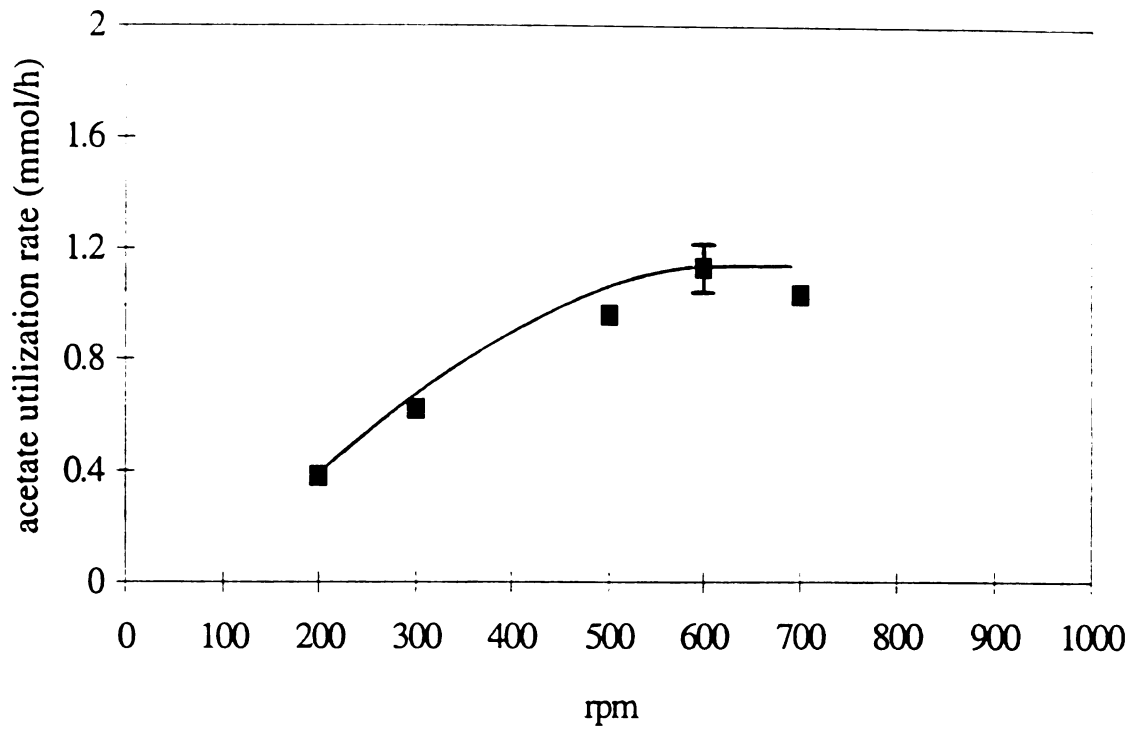


Figure VIC-1. Acetate utilization rate at various impeller speeds. acetate =7mM, biomass=2g, pH=7.0, temperature=37°C.

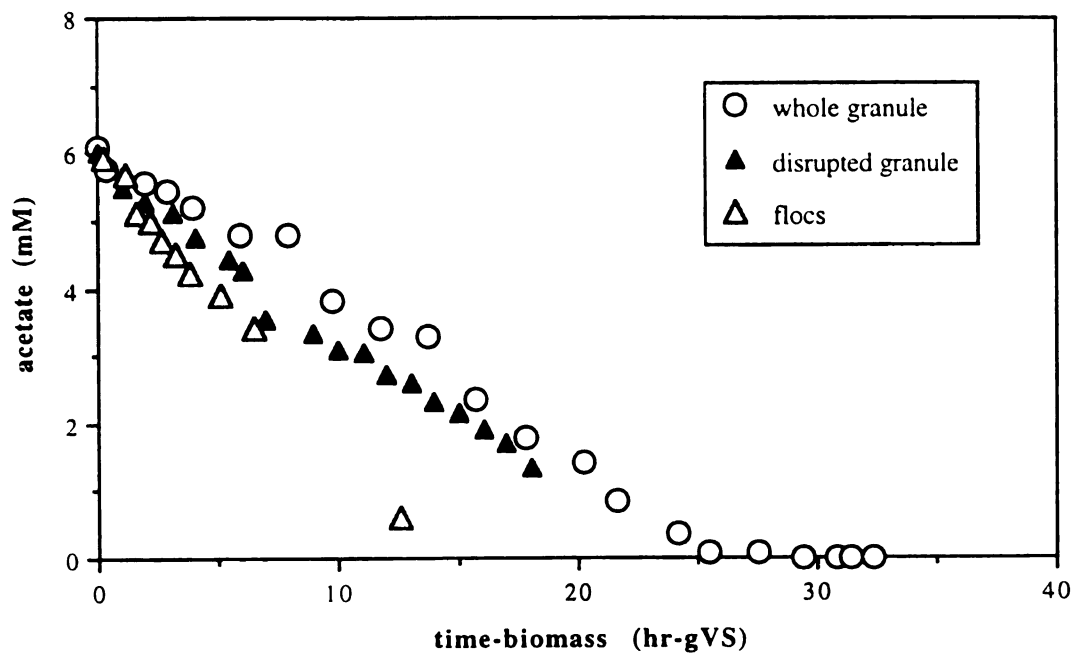


Figure VIC-2. Acetate utilization by whole granules, disrupted granules and flocs in batch assays (31°C). Time scale was adjusted by biomass(VS, g). The slope represents utilization rate in mMacetate/gVS-h.

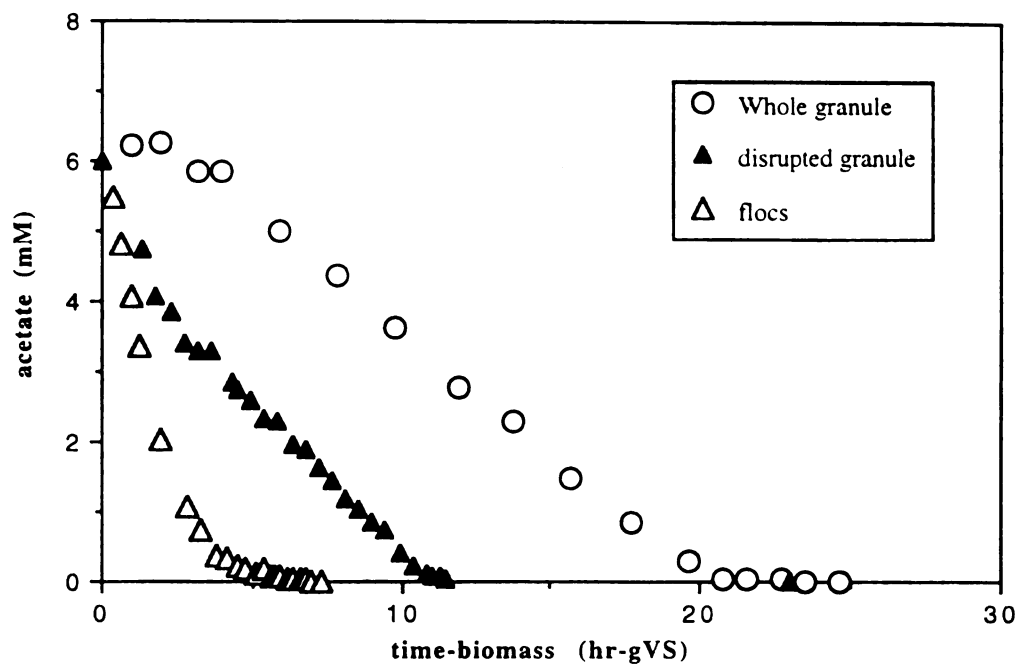


Figure VIC-3. Acetate utilization by whole granules, disrupted granules and flocs in batch assays (37°C). Time scale was adjusted by biomass(VS, g). The slope represents utilization rate in mM acetate/gVS-h.

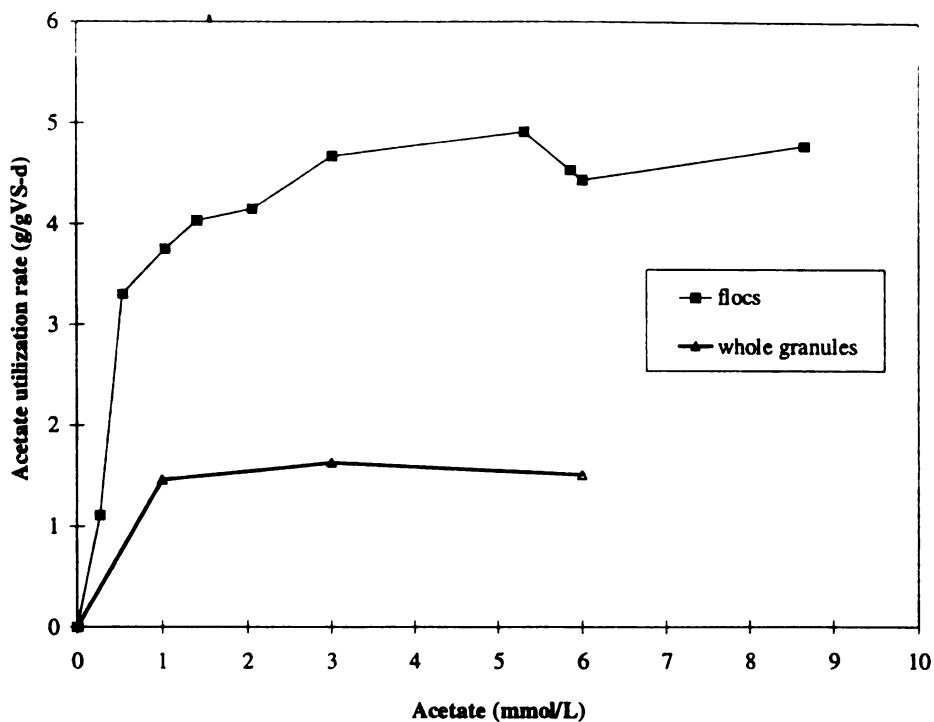


Figure VIC-4. Acetate utilization rate at different acetate concentrations and granule sizes. temperature=37°C. granule diameter: flocs=33 μ m, whole granules=1.85mm.

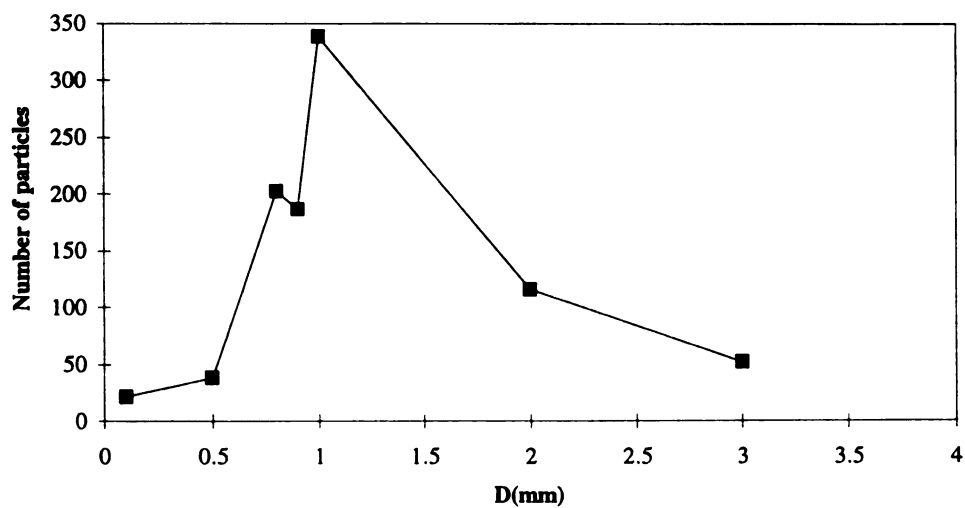


Figure VIC-5. Size distribution of disrupted granules.

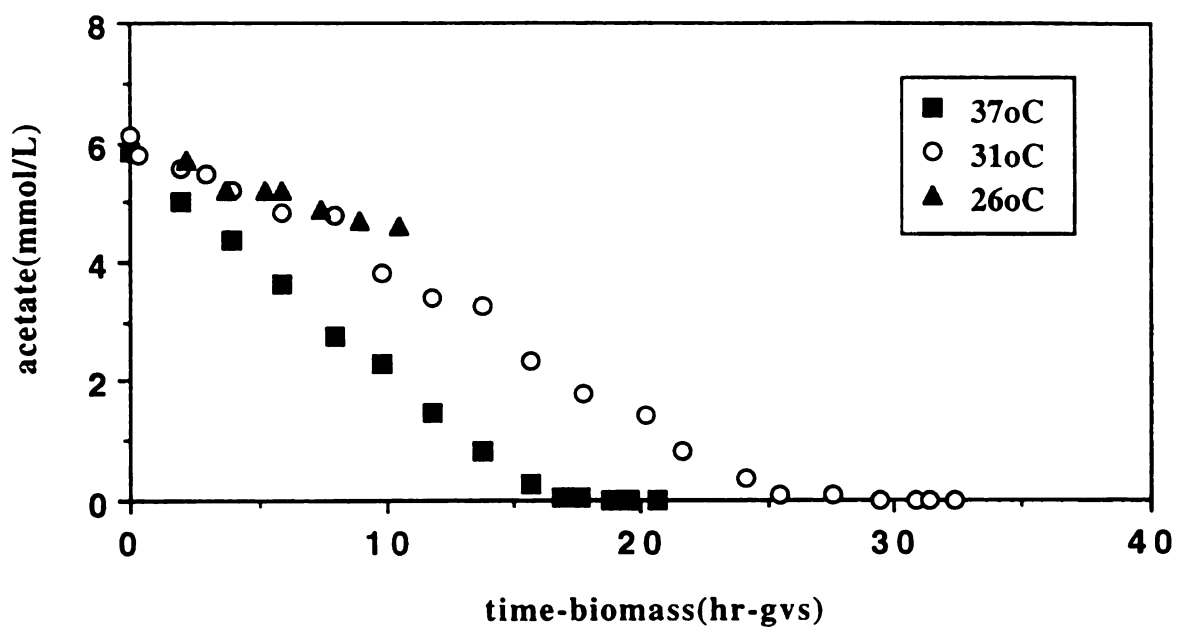


Figure VID-1. Acetate utilization at 37°C, 31°C, 26°C by whole granules. Time scale was adjusted by biomass (VS, g). The slope represents utilization rate in mM acetate/g VS-h.

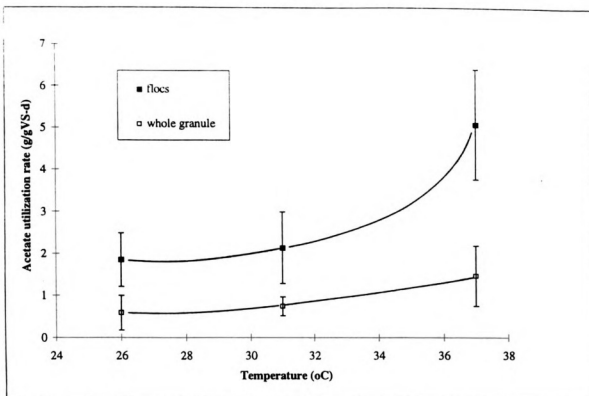


Figure VID-2. Acetate consumption rate of flocs and whole granules at 37°C, 31°C and 26°C. bars represent +/- SD of two repeated assays.

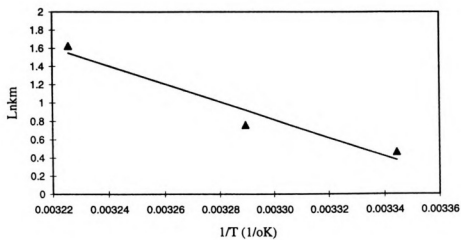


Figure VID-3. Linearization of km and temperature effects for acetate utilization by flocs. $y = 33.44793 - 9888.54 X$ $R^2 = 0.95$

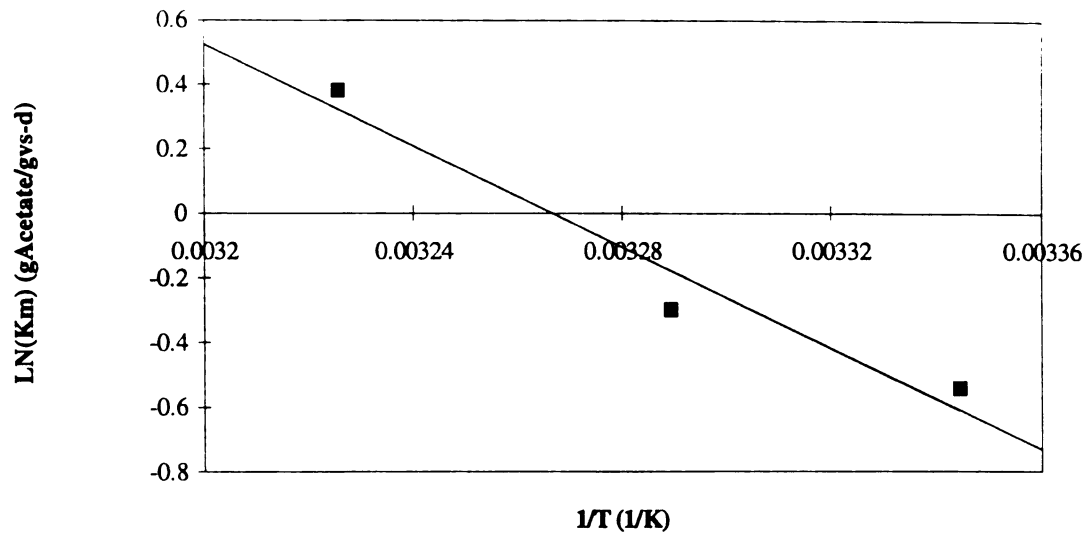


Figure VID-4. Linearization of k_m and temperature effects for acetate utilization by whole granules. $y=25.658-7854.31 x$, $R^2=0.95$.

Table VIB-1. Environmental and operational conditions
used for the bench-top reactor

Operation mode	batch CSTR
Temperature	37°C
pH	7.00±0.01
Working volume	1.4 - 1.5L
Gas space volume	0.5 - 0.6L
Inoculum	0.5 - 2g

Table VIB-2. Sampling frequency for the acetate utilization assays

Acetate (mmol/L)	Sampling frequency	Experiment period (hr)
0 - 1	2 min	0.5
1 - 2	3 min	1
2 - 3	5 min	1
3 - 5	5 min	1
> 5	10 min	2

Table VIB-3. Sampling frequency for the propionate utilization assays

Propionate (mM)	Sampling frequency	Experiment period (min)
0 - 1	1 min	20
1 - 2	2 min	30
> 2	3 min	60

Table VI B-4. Summary of literature values of acetate and propionate utilization kinetics compare to results from this study

Acetate		Propionate		Temp.	Culture	References
<i>K_s</i> (mM)	<i>km</i> (g/g-d)	<i>K_s</i> (mM)	<i>km</i> (g/g-d)	(°C)		
2.6	8.1	0.43	9.6	35	sludge	Lawrence&McCarty, 1969
3.0	8.56			35	sludge	Kugelman&Chin, 1970
1.2	18.8	0.29	37	35	sludge	Lin,et al. 1989
		0.52		35	sludge	Gujerw&Zehnder, 1983
0.88	5.03	0.13	6.46	35	sludge	Chang et al. 1983
3.8				35	Methanosarcina	Smith&Mah, 1978
0.47				35	<i>Methanothrix soehngenii</i>	Zehnder et al. 1980
1.72	7.6	0.186	2.3	35	granule	Wu, 1991a
	0.48		0.3	35	brewery granule	Wu&Hickey, 1991b
100	7.5	100	5.28	35	sludge	Smith, 1987
1.17 ^a				35	disintegrated granule	Hamelars&Koster, 1986
2.1 ^a				30	disintegrated granule	Debeer, et al., 1992
0.7				35	<i>Methanothrix soehngenii</i>	Huser, et al., 1981
		0.044-0.191		35	sludge	Kaspar&Wuhrmann, 1978
		0.15-0.45		35	sludge	Heyes&Hall, 1983
0.004				37	sludge	Fukuzaki, 1990a
0.104				37	<i>M.barkeri</i>	Fukuzaki, 1990a
1.2				35	<i>Methanothrix concilli</i>	Patel, 1984
2.8-5.3 ^a				30	crushed granule	Alphenaar,et al.,1993
2.3-7.9				30	granule	Alphenaar,et al.,1993
		0.016	0.16	37	sludge	Fukuzaki, 1990b
0.45 ^a	5.11 ^a	0.4 ^a	6.25 ^a	37	brewery granule (flocs)	this work

a mass transfer was not limiting

Table VIB-5. Kinetics of ethanol and hydrogen utilization by the brewery granules compared to reported values in the literature

<i>K_s</i>		<i>km</i>	Temp. (°C)	Culture	Reference
H ₂ (μM)	Ethanol (mM)	Ethanol (g/g-d)			
4.3			32	sludge	Mosey, 1989
6.0 ^a			30	sludge	Robinson&Tiedje, 1982
0.3	100	3.83	35	sludge	Smith, 1987
		0.19	35	granule	Wu, 1991a
		2.98	35	granule	Wu, 1991a
8.5				triculture	Ahring&Westermann, 1987 dissolved H ₂
5.9 ^{a,b}	3.37 ^a	5.49 ^a	37	brewery granule	this work

a mass transfer was not limiting

b derived from ethanol degradation, in gas phase concentration

Table VIC-1. Experimental design of liquid film resistance experiment for the brewery granules

Acetate (mM)	Impeller speed (rpm)	Biomass (gVS)
7	200	2
7	300	2
7	500	2
7	600	2
7	700	2
7	800	2

Table VIC-2. Estimated unsteady state effectiveness factor for substrate utilization using brewery granules at 37°C and pH=7.0

Substrate	k_m , intrinsic* (g/gVS-d)	k_m , apparent** (g/gVS-d)	η (%)
Acetate	5.11	1.66	32
Propionate	6.25	2.62	41
Ethanol	5.49	4.16	75

* flocs

** whole granules

Table VID-1. Estimated km of whole granule and flocs at 37°C, 31°C and 26°C, in g/gvs-d.

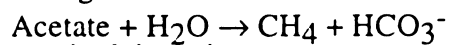
Inoculum source	Temperature		
	37°C	31°C	26°C
Flocs	5.08±1.322	2.13±0.852	1.85±0.641
Whole granules	1.66±0.720	0.74±0.223	0.58±0.410

* acetate as substrate

Table VIE-1. Acetate threshold and calculated minimum available Gibb's free energy during acetate metabolism

Acetate threshold range(μM)	$\Delta G'$ -(kcal/mol)	Temp. (°C)	Culture ^c
10-70	2.80±0.49 ^b	31	flocs
10-20	2.20±0.05	31	Whole granule
10-60	1.97±0.95	37	flocs
4-20	2.17±1.14	37	Whole granule

a. average acetate threshold 16.6mM, ΔG -2.53Kcal/mol (-10.55KJ/mol) reaction:



b. standard deviation

c. methanogenic brewery granules

Table VIE-2. Reported acetate threshold values

Temperature (°C)	Acetate (μ M/mM)	Culture	Resources
60	25-75 μ M	TAM	Ahring&Westermann, 1987
58	12-21 μ M	Methanothrix	Hang&Zinder, 1989
58	0.3-1.5 μ M	Methanothrix	Zinder&Koch, 1984
58	0.8-2.5 mM	Methanosarcina	Hang&Zinder, 1989
37	69 μ M	Methanothrix	Westermann, 1989
37	0.4-1.1 mM (dissociated) 4.43 mM (undissociated)	<i>M.barkeri</i>	Fukuzaki, 1990a
37	1.18 mM	<i>M. barkeri</i>	Westermann, 1989
37	0.396 mM	<i>M.mazei</i> s-6	Westermann, 1989

Table VIE-3. Reported hydrogen threshold values for different hydrogenotrophic anaerobes

Culture	H ₂ (pa)	Resources
Hydrogenotrophic Methanogen(mesophile)	2-10	Cord-Ruwisch,1988, Zinder,1990
Hydrogenotrophic Methanogen(mesophile)	6.5	Lovely,1985
Hydrogenotrophic acetogens	40-90	Cord-Ruwisch,1988, Zinder,1990
Hydrogenotrophic Methanogen(thermophile)	14	Lee&Zinder,1988
Hydrogenotrophic Methanogen(thermophile)	2.6-75	Zinder&Koch,1984
Sulfate reducer	1	Cord-Ruwisch,1988,
Methanogenic brewery granule ^a	0.5-2.6	this study

a. from six independent assays

CHAPTER 7. IDENTIFICATION OF GRANULE STRUCTURE, MAJOR MICROBIAL GROUPS AND PATHWAYS

A. Introduction

Anaerobic oxidation of ethanol to corresponding fatty acids is accomplished in cocultures of ethanol-fermenting, H₂-producing bacteria. The reduction of protons to form hydrogen as a reduced fermentation product is an endergonic reaction under standard conditions. The syntrophic degradation of ethanol, therefore, can only occur if the reducing equivalents derived can be transferred to suitable electron acceptors keeping the hydrogen partial pressure low [Thauer et al.1977]. The energy available from ethanol degradation depends on the type of H₂-oxidizing species and on the terminal electron acceptor used. Sulfate reducing bacteria can reduce sulfate, as an electron acceptor, to sulfide during ethanol oxidation [Postgate and Campbell,1966]. In the absence of sulfate, ethanol oxidation can be coupled with hydrogen transfer to methanogens [Wolin,1976] [Bryant et al.1977]. In this case, ethanol is oxidized with a concurrent reduction of carbon dioxide to form acetate or propionate [Schink, 1984] [Eichler and Schink, 1984] [Braun et al., 1981] [Samain et al.,1982], or condensed with acetate to form butyrate [Bornstein and Barker,1948]. Bacteria able to oxidize ethanol to form acetate and propionate were isolated from sewage sludge and sediments [Eichler and Schink,1984] [Schink,1984]. Formation of acetate and propionate was also observed in another study using an ethanol-fermenting bacterium [Samain et al.1982]. Labeled acetate and propionate were found to be the intermediates of ¹⁴C labeled ethanol degradation. Addition of hydrogen inhibited ethanol degradation and resulted in an accumulation of labeled butyrate [Schink et

al.1985]. Fermentation of ethanol to acetate and propionate by *Desulfobulbus* was strongly inhibited by hydrogen [Schink, et al.1987]. Propionate-forming bacteria were believed to contribute significantly to ethanol degradation. The pathway of propionate formation from ethanol by *Pelobacter propionicus* and its energetics were extensively discussed [Laanbroek et al.1982] [Schink, et al.1987]. Working with defined chemostat cocultures, the potential available energy during ethanol oxidation was captured more efficiently by homoacetogens than methanogens or sulfate reducers [Seitz et al.1990]. A hydrogen partial pressure less than 10^{-4} atm is necessary for anaerobic oxidation of propionate to be energetically favorable [Thauer et al. 1977] [Gujer and Zehnder,1982]. This low concentration of hydrogen is maintained by interspecies transfer of hydrogen from H_2 -producing bacteria to H_2 -consuming bacteria. Formate transfer has been proposed as an alternative route during ethanol degradation. The evidence and significance of interspecies hydrogen and formate transfer has been exclusively reviewed [Bryant et al.,1967] [Phelps et al.,1985] [Thiele and Zeikus,1988a] [Boone et al.,1989]. Experiments show chloroform did not inhibit ethanol-oxidizing acetogens and formate was synthesized from bicarbonate and ethanol during syntrophic ethanol oxidation in flocs isolated from a whey digester [Thiele and Zeikus,1988c]. Recent work indicated that interspecies formate transfer was not important for propionate and butyrate degradation, using thermophilic granules from a UASB reactor [Schmidt and Ahring,1993].

Little effort has been towards propanol production and consumption during ethanol fermentation. Schink [1984] described a new strain Ott Bd 1, which was isolated

from freshwater sediments and sewage sludge that was able to oxidize propanol to propionate with concomitant reduction of acetate and bicarbonate. This pathway resulted in a low cell growth yield. It has been demonstrated that hydrogen utilizing methanogens can oxidize ethanol and iso-propanol to produce acetate and acetone. The reducing equivalents generated were used for methane production [Widdel and Wolfe, 1986]. Propanol was observed during ethanol, propionate and formate perturbation on a CSTR with ethanol and propionate enrichments [Smith, 1987]. Hydrogen was not believed to be associated with propanol production. Possible pathways for propanol production under the experimental conditions used were proposed to be concurrent ethanol oxidation and propionate reduction to form acetate and propanol [Smith, 1987].

Anaerobic granules isolated from sludge digester or UASB reactors have been studied extensively. The interior structure, composition and population distributions of the anaerobic granules are closely related to metabolic performances and mass transfer phenomena within the granules. Physicochemical and biological studies on the characteristics of granules revealed a tightly packed structure with low internal porosity and a negatively charged surface [Alibhai, 1986]. Silicon, phosphorous, and sulfur were common elements observed within the granules. Granule shape, ash content, and surface area were dependent on the feed composition of the wastewater that the granules were used to treat. Both stratified and homogeneous structures have been observed [Alibhai, 1986]. Extracellular polymer (ECP) in granules is primarily composed of protein. In activated sludge systems, carbohydrates are the predominant component of extracellular polymers [Morgan, 1990]. Phosphorous and calcium were the major

elements found in ashed ECP extracts from granules [Morgan,1990]. A model of a lattice type cellular compartmentalization within granules (homogeneous network between syntrophs acetogens and CO₂-reduction methanogens) was suggested after analyzing interspecies H₂ transfer during anaerobic ethanol metabolism [Thiele and Zeikus,1988a]. This arrangement was supported by thin-section electron and phase-contrast fluorescence microscopy [Thiele, et al.1988b]. Granules fed with sucrose had a three layered ultrastructure [MacLeod,1990]. The exterior layer contained a heterogeneous population. The internal core consisted of large number of *Methanothrix*-like cells. Micro-colonies were observed inside granules from a UASB treating brewery waste [Wu, et al.1991b]. A *Methanothrix sp.* was observed to be the predominant methanogen in these brewery granules. *Methanobacterium sp.* and sulfate reducing bacteria were also identified. The differences in population distribution within different granules could reflect the variation in carbon sources the granules are acclimated to [Wu,et al.1991b]. Immunological methods were employed to study the population diversity in granules [Visser, et al.1991]. Microbial diversity was greater for mesophilic (38°C) granules compared to thermophilic (55°C) granules. Different catabolic pathways were found dominated in different regions of the granules from a UASB fed with acetate [Ahring et al., 1993]. Solids concentration, activity, porosity and density of granules were different for each “layer” of the granule radius. Only the outer layer of the granules were observed to be highly active. Large empty spaces were observed with the granules in one study [Alphenaar,et al.,1993].

The present study was undertaken to examine ethanol degradation by brewery granules from a UASB reactor fed with a synthetic brewery waste(Appendix A), to

examine propanol formation and consumption during ethanol oxidation, and investigate the physical structure of brewery granules and its microbial population. Energetics, carbon and electron balances were performed for the major biochemical reactions occurring during anaerobic oxidation of ethanol to methane. An attempt was made to ascertain possible reactions that lead to formation of propanol, using isotopic technique and thermodynamic studies. The interactions of ethanol, propanol, propionate, and hydrogen during ethanol degradation are discussed.

B. Ethanol degradation

The self-immobilized anaerobic consortia (brewery granules) described in previous chapter were acclimated to a mixed substrate in which 70% of the COD was ethanol (Appendix A). A study was initiated to examine the intermediate products, degradation energetics, and carbon and electron flow during anaerobic ethanol oxidation by these brewery granules. The ethanol assay was conducted at 37°C and pH of 7.0, in a two-liter bench-top Multigen reactor (Figure VIB-1; Chapter VI B). The Multigen reactor was operated as a batch CSTR with an impeller speed of 600 rpm. The ethanol degradation assay were conducted using both whole granules and flocs derived from the granules (Chapter VI). Inocula transfer was conducted under a nitrogen atmosphere. Background concentrations of acetate and propionate were 6.9 mM and 0.19 mM for the assay using flocs, and less than the method detection limits when using whole granules (the assay using whole granules are discussed separately, in section VII C). A detailed description of media and inocula preparation is presented in Appendix B. All possible

intermediates and products, ie: acetate, propionate, n-propanol, formate, H₂, CO, CO₂ and methane, were measured. Biomass concentration was determined at the conclusion of the assay to be 0.94gVS. Analytical techniques for determining above compounds and the QA/QC are presented in Appendix C. The bicarbonate concentration was calculated based on the initial bicarbonate concentration and concentration of CO₂ and acetate measured at various times during the course of experiment, based on the equation below:

$$[\text{HCO}_3^-]_i = [\text{HCO}_3^-]_o + K_{a1} \times P_{\text{CO}_2i} \times \frac{K_h}{[H^+]_i} - [\text{Acetate}]_i \quad \dots(\text{VII-1})$$

Where the subscript o denotes initial concentration; K_{a1} is dissociate constant in bicarbonate-carbonate system, 5.012x 10⁻⁷; P_{CO_{2i}} is partial pressure of carbon dioxide at time *i*; K_h is Henry's constant, 0.0246 mol/L-atm; [Acetate]_{*i*} is acetate concentration at time *i*. It is assumed that the gas phase and liquid phase of CO₂ are in equilibrium.

Starting with an initial concentration of 20.7 mM of ethanol, substrate, intermediates and end products were measured over time. Ethanol was completely oxidized within 10 hours (Figure VIIB–1). Acetate, the major intermediate product accumulated up to a concentration of 24 mM and then declined. Methane was produced rapidly until acetate was depleted, reaching a final value of 36mM. As shown in Figure VIIB–1 the headspace CO increased 12 fold from 4 ppm and to a plateau value of 50 ppm by 5 hours. The CO concentration then decreased rapidly to 1-2 ppm and remained at that level after 6 hours. The peak concentration of CO was observed three hours earlier than the peak concentration of acetate and two and a half hours after the peak concentration of hydrogen was observed.

From Figure VIIB-2, it can be readily seen that formate and hydrogen were produced almost immediately and simultaneously. Both electron sink products increased and decreased quickly during initial 10 hours of the assay. The aqueous concentration of formate reached a peak of 430 μM after one hour. The peak concentration of hydrogen in the gaseous phase was observed one hour later. Gas phase hydrogen had a dramatic change in concentration. A peak hydrogen concentration of 1120 ppm was observed two hours after the beginning of the assay; hydrogen decreased to 4 ppm when ethanol was depleted (at 11 hours).

As shown in Figure VIIB-3, the propionate concentration decreased slightly during the initial two hours of the assay and then increased rapidly up to 0.7 mM by 12 hours when ethanol was depleted. This initial decrease in propionate concentration suggested there might be another reaction mechanism responsible for propionate removal in addition to it being oxidized to acetate.

The production of n-propanol was observed immediately after the assay was initiated. The concentration of n-propanol reached a peak of 0.4 mM at the four hour mark, two hours after propionate concentration decreased to its initial lowest point. Starting at the six hour mark, the concentration of propanol began to decrease. Formation of propanol, possible interactions between propionate, propanol and ethanol are discussed in Chapter VII C.

The mass of carbon dioxide present more than tripled during the initial ten hours of the assay and then declined slightly. Production of CO_2 from acetate conversion to methane and bicarbonate equilibrium in the medium both contributed to variations in the

CO₂ concentration. The rapid increase in CO₂ seen during the early points of the assay is the result of ethanol oxidation.

B-1. Carbon and electron balance

Carbon and electron balances were performed using the data collected (Figure VIIB-4 and 7). All carbon in the medium, including carbon monoxide, carbon dioxide, bicarbonate, acetate, ethanol, propionate and n-propanol were calculated as mM of carbon, using the following equation:

$$C_{ij} = \text{carbons of compound } j \times S_i \quad \dots(\text{VII-2})$$

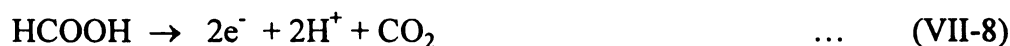
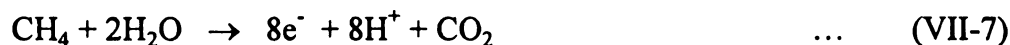
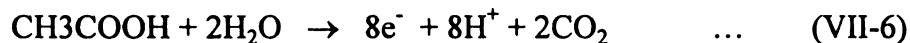
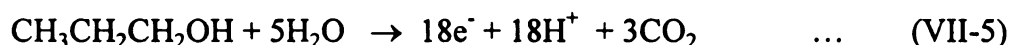
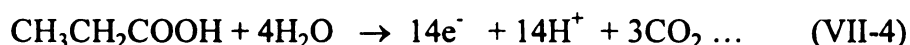
where i is the time (in hours) ($i = 0, 1, 2, \dots, 36.5$); j is the compound; C is the concentration of carbon (mM); S is the concentration of the compound (mM); C_{ij} is the carbon concentration of compound j at time i .

From Figure VIIB-7, it can be seen that total carbon in the medium could be accounted for quite well; a 94.7% of recovery of carbon was obtained at the conclusion of the assay. Ethanol, acetate, CO₂ and CH₄ were the major sources of carbon during ethanol degradation as expected. The main flow of carbon was from ethanol → acetate → CO₂ and CH₄. Methane and carbon dioxide accounted for 75.8% and 24.2% of carbon in the end products (theoretically 75% and 25%, respectively, from ethanol degradation; ethanol → 1.5CH₄ + 0.5CO₂). Assuming all of the acetate in the medium was converted to CH₄, 66.4% of methane came from acetate and 33.6% from CO₂ reduction (calculated based on the carbon balance), This is close to stoichiometric relationship of 2/3 CH₄ from acetate (reaction 1 and 6). The 5.3% of the carbon that was not recovered probably went to cells.

The change in biomass during the course of the experiment was not assayed for.

Bicarbonate accounted for more than 50% of the carbon in the medium throughout the assay. The carbon in CO₂ was equilibrated with bicarbonate which can be seen from increased bicarbonate concentration (mM carbons) and slightly decreased concentration in carbon dioxide at the end of the assay. The concentration of n-propanol, propionate and CO ranged from 0 to 3 mM of carbon.

Electron equivalents that are derived from the complete conversion to carbon dioxide for each compound were determined by writing the following half-cell reactions:



The electrons generated from ethanol oxidation flow through acetate, propionate, propanol and end up in methane as shown in Figure VIIB-4. Electron equivalents in hydrogen, formate, carbon monoxide and sampling losses were negligible, indicating these are intermediates and electrons were quickly transferred to products. Approximately 93.5% of the total electron equivalents were recovered at the conclusion of the assay. A total of 6.5% of the electron equivalents were lost from medium, some of these which

could have been used for cell synthesis. A peak of electron equivalents from acetate occurred at the 8 hour mark, this may be the result of a sampling error. The main flow of electrons was from ethanol \rightarrow acetate \rightarrow methane. Propionate and n-propanol accounted for only a minor portion of electron flow.

B-2. Energetics of ethanol degradation

Gibb's free energy changes for reactions in Table VIIB-1 were calculated. The calculations and the heat of formation for each element were after Thauer's work [Thauer et al.1977]. Temperature was adjusted for 37°C. A pH of 7.0 was used because little variation was observed (7.0-7.3) during the assay. The acetate splitting reaction (acetate \rightarrow CO₂ + CH₄) was rewritten as reactions 3 and 15 so that the influence of CO could be analyzed. Presented in Figures VII B-5 and 6 is the free energy change profile during anaerobic ethanol oxidation for reactions involving ethanol, acetate, formate, CO, H₂, HCO₃⁻ and CH₄. Ethanol oxidation to acetate and hydrogen (reaction 1) was stable at -6 to -10kcal/mol throughout the entire course of ethanol oxidation (Figure VIIB-5). The energy available for the reduction of CO₂ to methane (reaction 6) varied significantly from -1kcal/mol to -15kcal/mol. Acetate conversion to methane and CO using hydrogen as the electron donor (reaction 3) proceeded until last hour of the assay. The second half of acetate splitting reaction (reaction 15, CO \rightarrow CO₂) had a relatively constant negative value, between -4 to -7kcal/mol, throughout the assay.

Gibb's free energies for ethanol oxidation to form acetate and formate (reaction 2) was stable at -6kcal/mol (Figure VIIB-6). Hydrogen and formate were close to

equilibrium (reaction 4). Methane production through formate reduction was favorable (reaction 7, -19kcal/mol) and relatively stable.

C. Pathway of n-propanol formation

During the ethanol conversion assays using the brewery granules (see section B, Chapter VII), n-propanol production was observed during the initial time period (Figure VIIB-3). The appearance of n-propanol in the medium was virtually immediate, reaching a peak value when propionate was still accumulating. N-propanol decreased to below the detection limit (0.05mM) when propionate reached its highest concentration. There are several reaction mechanisms which could contribute to n-propanol formation during ethanol fermentation. A list of possible reactions and their standard Gibb's free energy were presented in Table VIIC-1. N-propanol could be produced from ethanol and carbon dioxide (reactions 11 and 12), from ethanol and propionate (reaction 14), from propionate (reaction 9), or from ethanol alone (reaction 10). The purpose of this study was to examine possible pathways for propanol formation, to identify the involvement, if any, of CO₂ in the formation of n-propanol (reactions 11 and 12) as the source of an additional carbon, and to confirm the reproducibility of n-propanol production from previous experiments. The study was accomplished using reaction energetic analyses and an isotopic assay using ¹³C labelled ethanol and bicarbonate.

C-1. Reaction thermodynamics of n-propanol formation

Reaction energetics were studied for ethanol degradation as well as n-propanol formation and consumption, and interactions with propionate. Gibbs' free energy ΔG under the experimental conditions of each reaction in Table VIIC-1 for ethanol assay in flocs were determined (see Chapter VII B for calculation). The calculations were based on a pH of 7.0. Bicarbonate concentration was determined based on medium bicarbonate concentration and the reactor CO_2 , pH and acetate concentration (refer to Chapter VII B for calculation). Propionate oxidation to acetate (reaction 8) and propanol oxidation to propionate (reaction 9) were written in both directions to analyze the role of propionate. The Gibbs' free energy variations during ethanol degradation for reactions involving ethanol, n-propanol and propionate are presented in Figure VIIC-1 to 4. Ethanol oxidation reactions to form propionate and acetate were not included.

Results presented in Figure VIIC-1 and 2 indicate that all five reactions (reaction 9', 10, 11, 12, 14) could be involved in n-propanol formation. Ethanol oxidation coupling propionate reduction to form propanol and acetate (reaction 14; Figure VIIC-1) is energetically favored during the initial six hours of the assay. N-propanol production from ethanol (reaction 10) and from ethanol and bicarbonate (reaction 11) had highest available free energy levels (-12 to -15.3 kcal/mol). The energy available for ethanol oxidation with a reduction of carbon dioxide to form propanol and propionate (reaction 12) varied significantly from -10 kcal/mol to near zero (Figure VIIC-1). Propanol could be produced from ethanol (reaction 10, 11, 12 and 14), or from propionate (reaction 9' and 14). N-propanol could be converted to form propionate (reaction 13). Hydrogen was

involved in most of the reactions studied (reactions 1, 8, 9, 10, 11, 12) with two exceptions: production of propanol from ethanol oxidation and propionate reduction (reaction 14) and propanol oxidation with a reduction of acetate and bicarbonate (reaction 13). Formation of propionate is possible from ethanol, acetate and propanol (Figure VIIC-3). Reaction 9 (propionate formation from propanol oxidation) was favored during the later hours (9-11 hrs) of the assay. Gibb's free energy for reactions of propionate and propanol formation and consumption appeared to be time dependent (Figure VIIC-2, 3 and 4). Available energy variations for reaction 1, 8, 8', 9, 9', 10, 11, 12, 13 and 14 during the initial 11 hours (until ethanol and n-propanol concentrations approached zero) are presented in Table VIIC-4.

A graphic presentation of possible reactions between ethanol, propanol and propionate within initial 11 hours and the available free energy, from Table VIIC-4, is shown in Figure VIIC-7a to c. Hydrogenotrophic methanogenesis occurred during the entire time course of the assay (Figure VIIB-5). This is not shown in the figures.

During initial five hours, complex reactions could have occurred (Figure VIIC-7a). Ethanol could have been converted to acetate, propionate and n-propanol through reactions 1, 10, 11, 12 and 14. Significant amounts of hydrogen gas was generated by reactions 1 and 10. The H_2 content in the gas phase accumulated up to 1120ppm. Reactions 8', 9', 11', 12 and hydrogenotrophic methanogenesis were sinks for hydrogen, serving to keep the hydrogen partial pressure low and thus ensuring the continuation of hydrogen yielding reactions. N-propanol formation was favored almost immediately via propionate reduction (reaction 9' and 14), ethanol oxidation (reaction 11, 12, 14) and

ethanol conversion alone (reaction 10). The concentration of n-propanol accumulated reaching a plateau value of 0.4mM (Figure VIIB-3). Energetically, consumption of propanol could proceed via reaction 13. Propionate could also be reduced to form propanol during this time, because of the high concentration of hydrogen. For this same reason, propionate oxidation to acetate (reaction 8) was not energetically favorable for the initial eight hours of the assay. The reverse reaction, acetate reduction to form propionate (reaction 8'), however, could occur. Propionate could be formed from ethanol through reaction 12 and probably other reactions [Schink et al.1985], from propanol (reaction 13) and acetate (reaction 8'). From Figure VIIB-3, it can be seen that the propionate concentration decreased during the initial three hours when propanol accumulated at a linear rate, and then increased while propanol production slowed. Propionate consumption via reaction 9' and 14 were energetically favorable during this period. Measurements showed that acetate and propionate accumulated continuously during this time period.

Between six to eight hours, reduced concentration of ethanol and high acetate concentration caused reaction 14 became unfavorable. The whole reaction scheme of ethanol, propanol and propionate is described in Figure VIIC-7b. Ethanol could still be oxidized to form propanol, propionate and acetate. During this time period, n-propanol accumulation slowed down because of fewer reactions involved in n-propanol production (reaction 14 became energetically unfavorable). As a result, actual concentration of n-propanol begin to decrease (Figure VIIB-3).

Beginning at the nine hour mark, a major change occurred as shown in Figure VIIC-1c. The energy available for two reduction reactions (reaction 8' and 9') changed in favor of formation of more oxidized products. N-propanol oxidation to form propionate (reaction 9), and propionate oxidation to form acetate (reaction 8) became energetically favorable, as a result of a dramatic decrease in the hydrogen concentration to ≤ 20 ppm (Figure VIIB-2). At this point, hydrogen could be produced by more reactions (8 and 9 join the pool) and consumed by two less reactions (8' and 9'). Formation of propanol could be from ethanol only, reaction 10, 11 and 12 until ethanol became depleted at 11 hours. Formation of propionate appears to be related to propanol oxidation (reactions 9 and 13) and ethanol oxidation (reaction 12).

C-2. ^{13}C experiment on n-propanol formation

An isotopic assay to assess the pathway of n-propanol formation during ethanol degradation was performed. Ethanol was the sole carbon and energy source. A screening test was first initiated to determine the maximum concentration of ethanol that could be used, without any significant impact on degradation of ethanol or propanol production, while obtaining as high a level of n-propanol as possible. The second purpose of this assay was to compare the results with those of previous experiments obtained using granule flocs and whole granules (Chapter VII B). Three sets of isotopic assays were performed; one with $[1-^{13}\text{C}]$ ethanol (Cambridge Isotope, 99%) and ^{12}C bicarbonate (Baker Analyzed, sodium bicarbonate), the second using $[1-^{13}\text{C}]$ bicarbonate (Isotech, 99%) and ^{12}C ethanol (Quantum, 200 proof). The third set of batch used the same carbon

source as the first one but the ethanol concentration was 30% higher. Each set had two replicates. The assays were performed at 37°C in serum bottles using PBBM medium (Appendix A). The inocula was brewery granules (whole granules) from a bench-scale UASB reactor(see description in Chapter VI B). The pH was adjusted to 7.0 at the beginning of each assay. Assays were conducted under strict anaerobic conditions. Duplicates of samples were collected for GC and GC/MS analyses. The screening test was conducted using the same method as the isotope assay except labeled compounds were not used. Concentrations of ethanol, n-propanol, propionate and acetate were measured by GC. For the isotopic assays ^{13}C propanol was quantitated using GC/MS. Detailed descriptions of the protocol of isotopic assay are presented in Appendix B–6. Analytical techniques for ethanol, propanol, propionate, acetate and ^{13}C propanol and QA/QC are described in Appendix C.

Ethanol concentrations of 30, 50 and 65 mM were used in the screening tests. Ethanol, n-propanol, propionate and acetate were tracked with time until propanol decreased below detection limits. Substrate and products variation during n-propanol appearance, from the screen test and previous assay, are shown in Table VIIC–2. Results indicated that n-propanol and propionate peak concentrations increased with initial ethanol concentration. With one exception, n-propanol was observed when the ethanol concentration was at 20-25mM and the ratio of acetate to initial ethanol concentration (in mM) ranged from 0.29-0.37 (Table VIIC–2). When an acetate/ethanol(initial concentration) ratio of 0.76-0.81 was observed, n-propanol decreased to below detection limits in all cases. N-propanol either appeared at approximately the same time as

propionate, or formed when propionate was present in the medium. The peak n-propanol concentration observed was greater when using flocs than whole granules.

Ethanol concentrations of 50 and 65 mM were selected as the initial substrate concentrations for the ^{13}C [C-1] isotopic assays. The assays were concluded when the n-propanol peak disappeared. Peak ^{13}C mass intensities of major fragments of n-propanol were determined by gas chromatography and mass spectra. The ratio of the mass intensity

for n-propanol, $\frac{^{13}\text{M}^+}{^{12}\text{M}^+ + ^{13}\text{M}^+ - \text{H}^+}$ (or 61/60)(where M is mass fraction of n-propanol)

and $\frac{^{13}\text{M}^+}{^{12}\text{M} - \text{H}^+}$ (or 61/59) were then calculated (Table VIIC-3). The control was

unlabeled ethanol (0.5mM). Sample groups A represents 1-C labeled ethanol (65mM) and bicarbonate (65mM), group B represents unlabeled ethanol (50mM) and 1-C labeled bicarbonate (50mM), group C represents 1-C labeled ethanol (50mM) and bicarbonate (50mM), respectively. The natural abundance of ^{13}C to ^{12}C (for n-propanol 61/60) is 3.3% as shown in the control (0.032). N-propanol from group C2 could not be assessed. This is because more biomass was used than intended. The reaction proceeded too quickly such that the n-propanol peak was not picked up. The labeled n-propanol mass in group A was 1.3 and 1.4 (average) times that of group C for mass ratio 61/60 and 61/59, respectively. This is consistent with the ratio of initial ethanol concentration (1.3:1 as group A:C).

There were similar patterns of reaction intermediates (acetate, propionate and n-propanol) from all three sets of serum bottle assays compared to screen tests (3 batches) and previous assays (see section B, Chapter VII). Typical progress curves of ethanol, n-

propanol, propionate and acetate are shown in Figure VIIC–5 and 6. During ethanol oxidation, acetate began to accumulate immediately, followed by n-propanol and propionate. Propanol reached a peak value and then decreased rapidly while acetate and propionate increased continuously. Ethanol and n-propanol disappeared at approximately the same time for all assays conducted.

D. Identification granule structure and major microbial groups

An attempt to ascertain granule structure and the major microbial groups was performed. Granule structure was analyzed using a Olympus microscope (BH–2) and a Confocal laser beam microscope. Thin section granule samples were prepared for granule structure observation (Appendix B). During the activity assays, prevailing population of sheathed filamentous rods were also observed to be a *Methanothrix*–like species in the brewery granules as shown in Figure VIID–2 to 5. *Methanobacterium*–like short thin fluorescence rods was observed. Different populations were distributed randomly on the surface and within the granules (Figure VID–2). The major species was *methanothrix*–like species. Clusters of *Desulfobulbus*–like big fat rods and *Desulfovibrio*–like short curved rods were also observed (Figures VIID–5 and 6).

The granules had a layered structure (Figure VIID–1a,b,c), similar to that reported by Macleod et al.[1991]. The outer layer, or "crust" had a 100µm thickness, within this region there was a high density, mixed population (Figure VIID–2a, b). Different groups of cells appeared mixed and contained in "finger-like" clusters in this layer. These "fingers" were separated from each other by channels that appeared to lead out to the surface of the granule (ie. for gas vents). A separate transparent layer connected this out layer to the central core of the granule (Figure VIID–3). At the center of the granule, the density of cells was low (Figure VIID–4) although population distribution was not much

different from that observed in the outer layer. Empty spaces were also observed (Figure VIID-1a).

E. Discussion

Analyses of carbon and electron flow during ethanol degradation showed good recovery. The fraction of carbon in the end products (76% CH₄ and 24% CO₂) were very near the theoretical values (1% difference). Most electrons ended up in methane. Two thirds of the methane was produced from acetate, as expected.

Acetate disproportionation to methane and CO₂ can be described as a two-step reaction with CO as a intermediate product: 1) acetate splitted to CO and CH₄ (reaction 3), 2) CO oxidized to CO₂ (reaction 15) [Zeikus et al.,1985, Hickey and Switzenbaum,1990]. Thermodynamic data from granule flocs showed both reactions occur during ethanol oxidation (Figure VIIB-6). Combined reaction of acetoclastic methanogenesis (reaction 3 plus reaction 15), in which CO does not appear, was energetically favorable throughout the entire time course.

Results from several separate assays have shown a consistent trend of ethanol conversion to n-propanol, propionate and acetate. Progress curves of these compounds were not significantly different when using flocs or whole granules as the inocula. The formation and disappearance of n-propanol during ethanol degradation using anaerobic granules were reproducible. Immediate production of n-propanol was observed when propionate and acetate were present (Table VIIC-2, Figure VIIB-3). Propanol appeared in the medium after a short lag in assays conducted where there were no propionate and

acetate (Figure VIIC-5 and 6), indicating it is possible that propionate is a precursor in propanol formation. This was further supported by an observed initial decrease in propionate concurrent with a linear increase in propanol (Figure VIIB-3). Two n-propanol oxidation reactions to form propionate (reaction 9 and 13), had a negative stable free energy level (13) or were favored energetically during the initial eight hours (9). Reaction 13 has been identified [Schink, 1984].

Analyses of Gibb's free energy available for ethanol degradation under the experimental conditions indicated a number of complex interactions were possible (Table VIIC-4). Hydrogen appeared to play a strong role as a driving force governing reactions involving propionate. Propionate degraders are sensitive to hydrogen concentration in the medium. A low hydrogen partial pressure (10^{-6} - 10^{-4} atm, or 1 - 100 ppm) is required to maintain a negative Gibb's free energy and allow propionate degradation to proceed. This hydrogen level was maintained between hydrogen-producers and hydrogen-utilizers. During the initial eight hours of the assay, the hydrogen (and formate) concentrations were sufficiently high (up to 1100 ppm for H_2), to make propionate oxidation to acetate energetically unfavorable, and the reverse reactions: acetate reduction to propionate and subsequent propionate reduction to propanol possible. Any reaction observed in the propionate concentration during this period was likely due to conversion to more reduced products. Four reactions potentially serve as hydrogen sinks (reactions 8', 9', 11, 12) during the initial eight hours. After the hydrogen concentration decreased, propionate was oxidized. More hydrogen producing reactions became favorable (reactions 8, 9, 1, and 10); and a hydrogen level of 3-12 ppm was subsequently maintained.

Isotopic assays using whole granules revealed that labeled n-propanol was formed as an intermediate of labeled ethanol degradation. ^{13}C n-propanol was high from labeled ethanol (group A and C) and only at trace levels when labeled bicarbonate was used (group B; Table VIIC-3). Ratio of mass intensities or the ratio of ^{13}C n-propanol to ^{12}C n-propanol, of 0.26, 0.21, 0.18, and 0.20, 0.15, 0.13 for molecular weight/charges 61/60 and 61/59, respectively, were observed from labeled ethanol group. This was about nine times the control (0.032 and 0.028, respectively). These values for group B appeared in trace amount (0.05 for 61/60 and 0.04 for 61/59, respectively) which was near the natural abundance level. These results suggested that bicarbonate was not a significant contributor as an additional carbon source for n-propanol formation. Thus reaction 11 and 12 (Table VIIC-1) are unlikely to be the major pathways responsible for n-propanol production.

Results suggested that ethanol-degraders and propionate-utilizers are responsible for the formation of propanol. Since there is no evidence that n-propanol was formed via ethanol and bicarbonate (reactions 11 and 12) from the isotopic assay results, these reactions are ruled out as the source of propanol. The reactions that satisfy both assay and free energy levels in propanol formation are reduced to reaction 9' (propionate to propanol), 10 (ethanol to propanol), and 14 (ethanol and propionate to propanol and acetate). In this study, Gibb's free energy available for reaction 14 was negative during the initial six hours. Propanol concentration peaked at approximately 4 hours and then decreased (Figure VIIB-3). Propionate was always present when n-propanol formation was observed for all assays conducted. It is apparent that reaction 9' was energetically

favorable during the initial eight hours of the assay. The reverse reaction, propanol oxidation to propionate, could proceed only after the initial eight hours. From our measurements, propanol concentration was depleted faster beginning at nine hours and soon disappeared from the medium. Propionate is involved in both reactions 14 and 9' and, therefore likely played an important role as a possible precursor for propanol. Reaction 9' and 14 are both likely candidates involved in propanol formation during ethanol degradation. Smith [1987] reported that reaction 14, formation of propanol and acetate from ethanol and propionate was the most likely reaction that occurred during a perturbation of ethanol, propionate and formate for a propionate and ethanol enrichment in a CSTR. This was based on a free energy analyses. Our results showed excellent agreement with Smith. The mechanism and species carry out these two reactions were unknown. The amount of reducing power available had a strong impact on propionate consumption and propanol formation. Hydrogen was not believed to be associated with propanol production during the experiments of Smith [1987]. Propionate or ethanol enrichment mixed culture and CSTR in previous study, versus ethanol, propionate and acetate enrichment mixed culture and batch experiment in this study, could contribute to this discrepancy.

However, the question left is the source of the additional carbon molecule of propionate from ethanol degradation. This carbon molecule could not come from bicarbonate, derived from ^{13}C experiment. Thus reaction 10, condensation of ethanol to release a carbon dioxide and form n-propanol, is more likely a candidate for n-propanol production.

Microscopic observations of the brewery granules revealed a predominant group of *Methanothrix*-like acetate utilizing methanogen (Figure VIID–2 and 5). Other major groups observed were *Desulfobulbus*-like rods and *Desulfovibrio*-like rods (Figure VIID–5 and 6). *Methanobacterium*-like rods were also observed under epifluorescence microscopy. These observations are in agreement with results reported by Wu [1991a]. A layered structure for anaerobic granules has been reported by MacLeod et al.[1990] and Alphenaar et al. [1993]. It has been demonstrated that *Desulfor vulgaris* was the prevalent ethanol-oxidizing organism in the whey digester flocs [Thiele, et al,1988c, Thiele, et al,1988b]. Lens and co-workers observed that glucose utilization was located exclusively in the outer layer of 200-300mm of granules fed with glucose and mixed sugars. Viable bacteria was observed only in the peripheral zone of large granules (diameter 5mm)[Alphenaar et al.1993]. Similarly, the brewery granules investigated in this study (diameter 3mm) had a high density outer layer of ca.100mm (Figure VIID–1). This outer layer was heterogeneous in population. Ethanol and propionate degraders, acetoclastic and hydrogenotrophic methanogens were all present in this layer in a network. Thiele and co-workers [1988a, 1988b] presented a syntrophic acetogenic and methanogenic cell model–lattice type arrangement in granule flocs. Our results have shown similar arrangement in brewery granules. Spaces between “fingers” (Figure VIID–2) indicated vigorous gas production. Methanogenesis occurred at the surface of the granule. Compared to other studies, glucose or sucrose fed granules had methanogenic activity only in the center core of the granules [Lens et al.1993] [MacLeod et al.1990]. This difference may primarily be due to the nature of the substrate. The granules in this study

were acclimated to a mixed carbon source of compound of ethanol, acetate and propionate. Cell density decreased from the outer regions towards the center of the granules (Figure VIID–3 and 4). A high cell density outer layer and a low cell density central core were separated by a transparent layer in these granules, suggesting a substrate gradient from the outer layer toward the center as a consequence of substrate utilization and diffusion. Higher substrate fluxes are maintained in the outer layer. Using Monod kinetics, therefore, this resulted in higher biomass growth. Lower cells density in the central core of the granule could be the result of reduced supply of carbon source to the interior of the granules. Empty spaces were observed within the brewery granules (Figure VIID–1a) which also agreed with previous reports [Alphenaar et al.1993]. The reason is unclear.

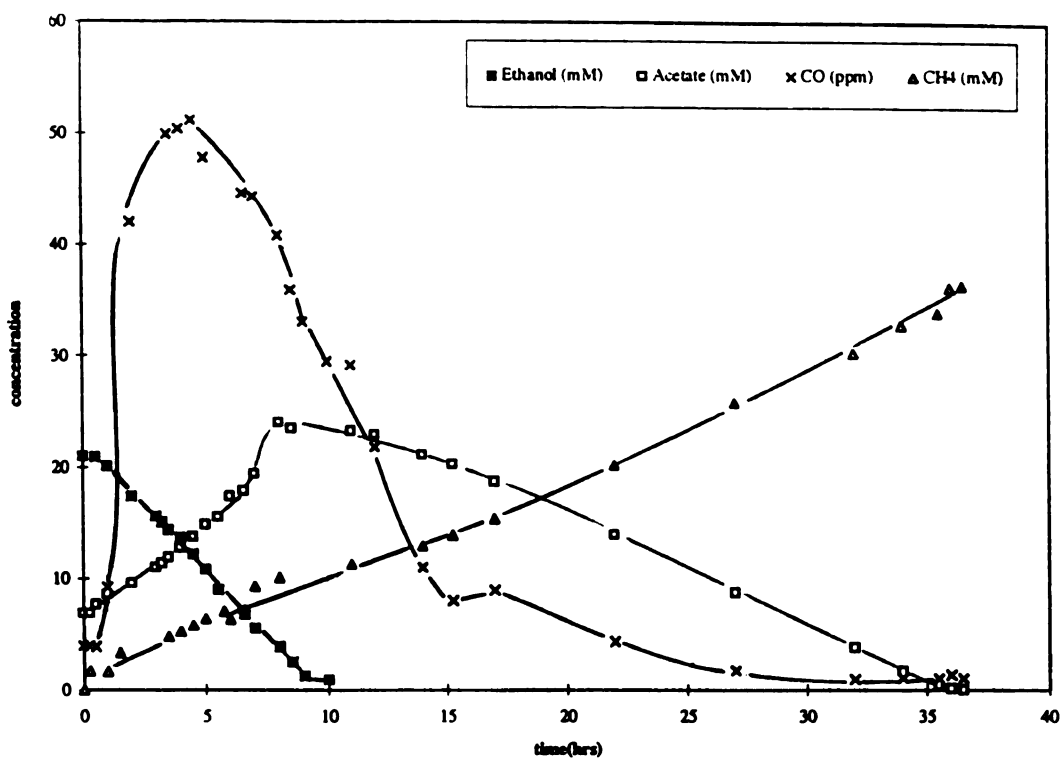


Figure VIIB-1. Substrate and products concentration profile (ethanol, acetate, methane and carbon monoxide) during ethanol fermentation

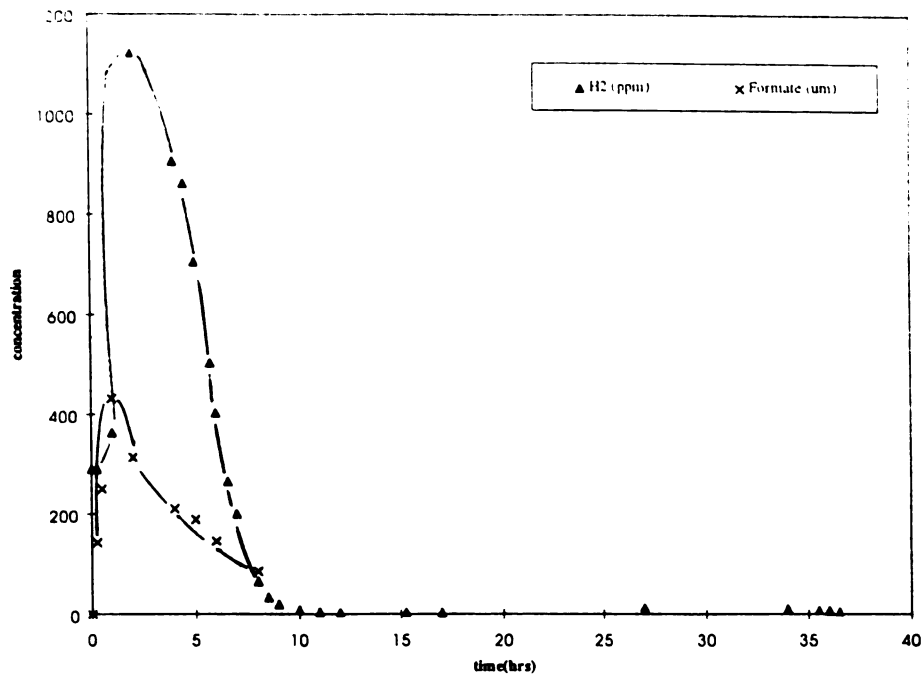


Figure VIIB - 2. Substrate and products concentration profile (hydrogen and formate) during ethanol fermentation

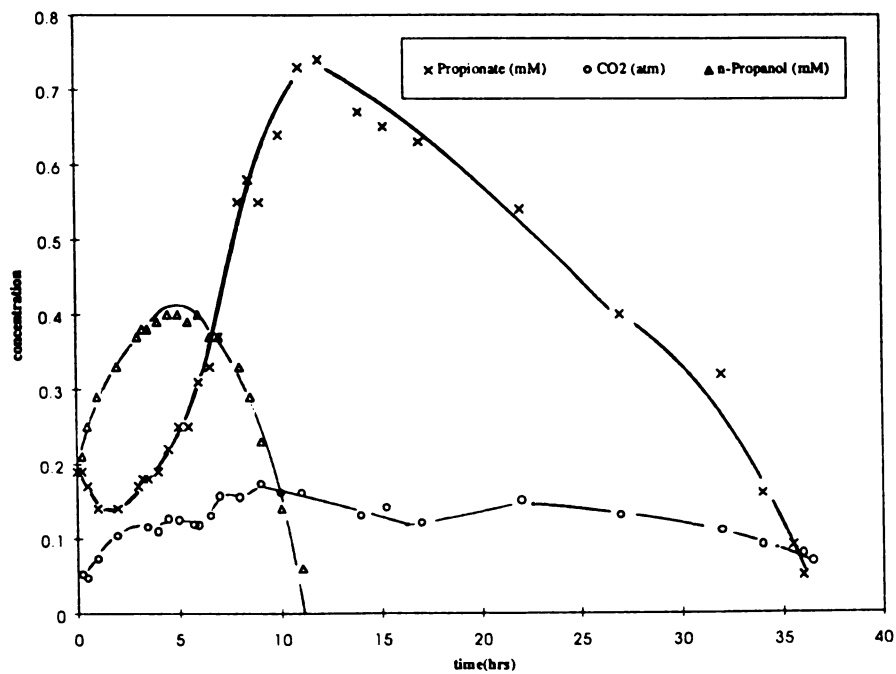


Figure VIIB - 3. Substrate and products concentration profile (propionate, n-propanol and carbon dioxide) during ethanol fermentation

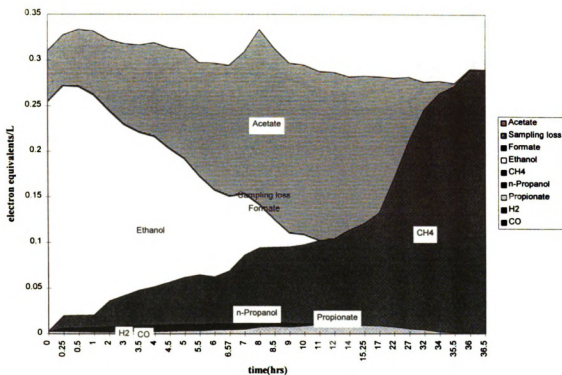


Figure VIIB-4. Electron balance of substrate and products during ethanol degradation in batch CSTR study using brewery granules (flocs).

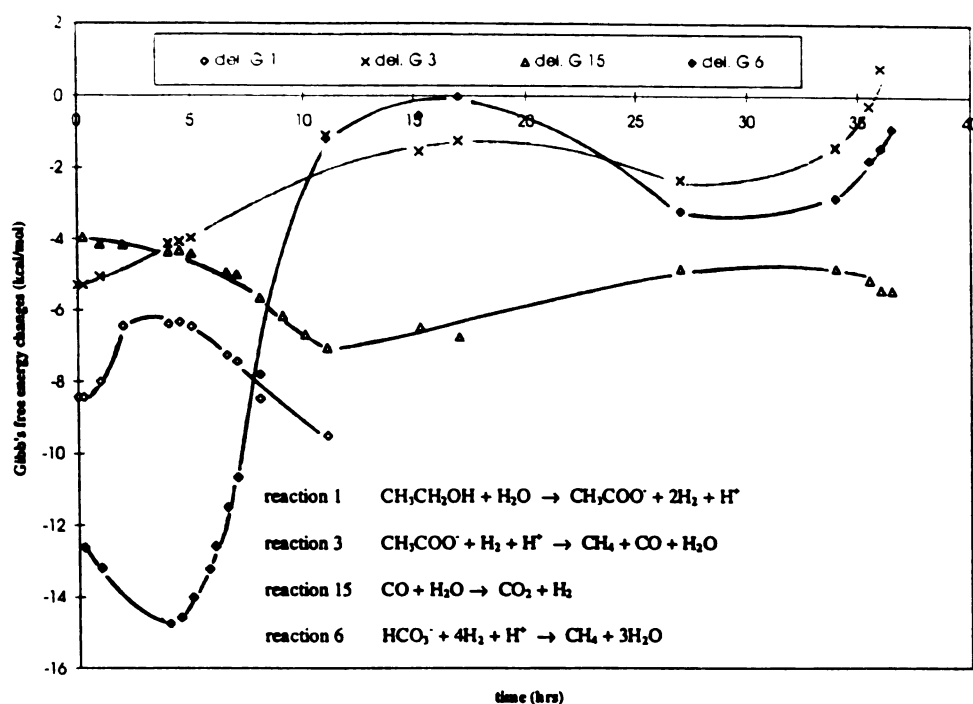


Figure VIIB-5. Gibb's free energy changes during ethanol degradation: reaction 1, 3, 6 and 15.

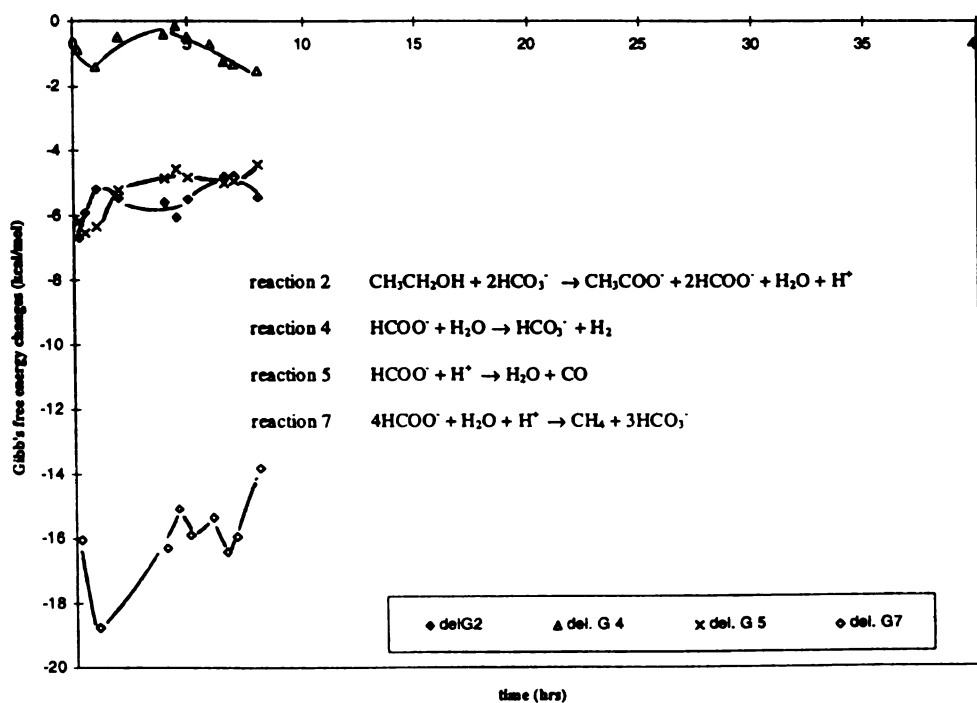


Figure VIIB-6. Gibb's free energy changes during ethanol degradation: reaction 2, 4, 5 and 7.

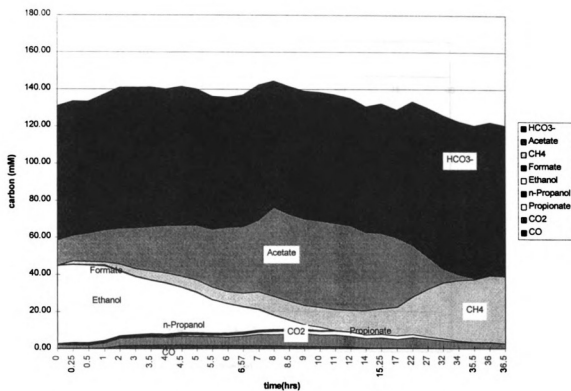


Figure VIIB-7. Carbon balance of substrate and products during ethanol assay using brewery granules (flocs) in batch CSTR.

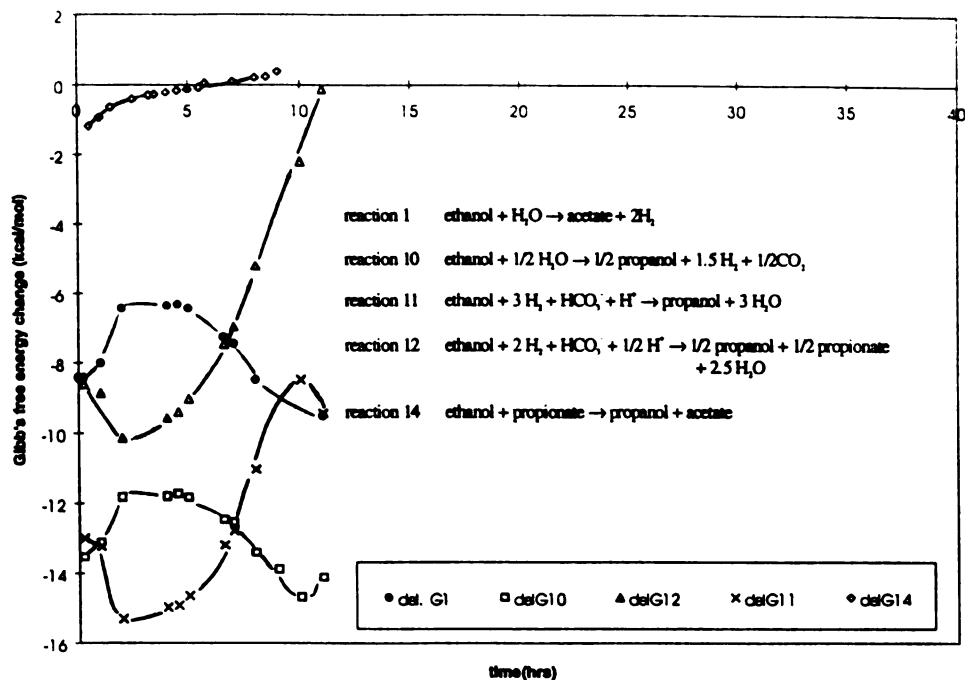


Figure VIIC-1. Gibb's free energy variations of ethanol oxidation reactions.

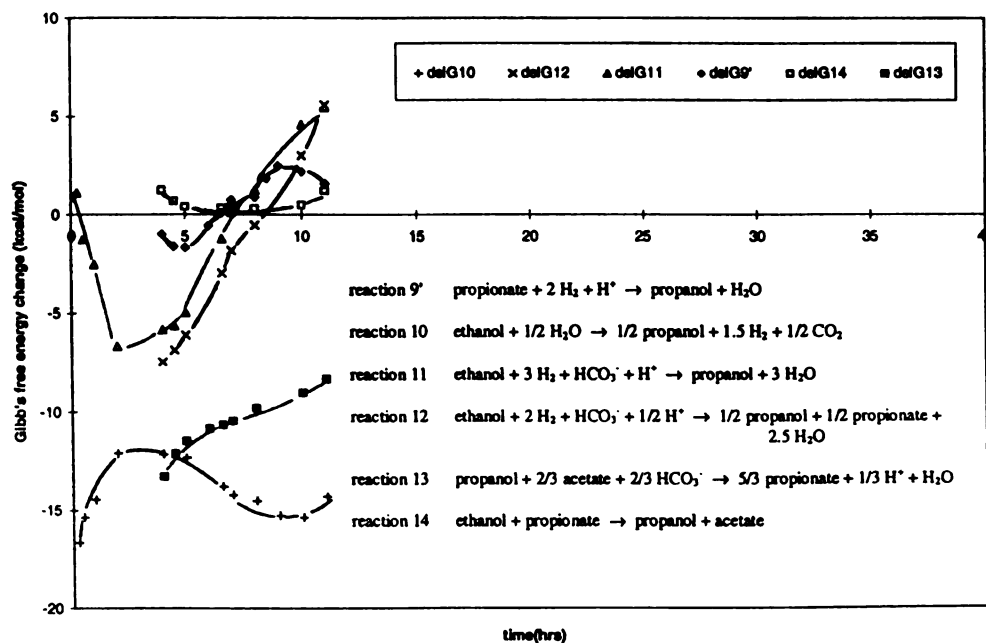


Figure VIIC-2. Gibb's free energy variations of propanol formation and consumption reactions during ethanol degradation by brewery granules.

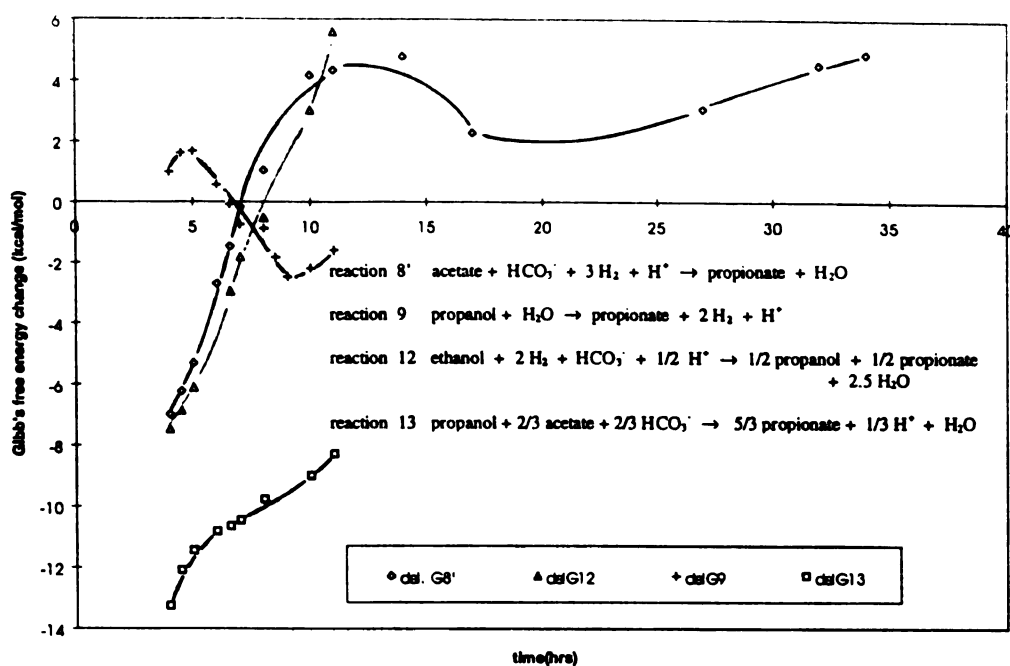


Figure VIIC-3. Gibb's free energy variations of propionate formation reactions during ethanol degradation by brewery granules.

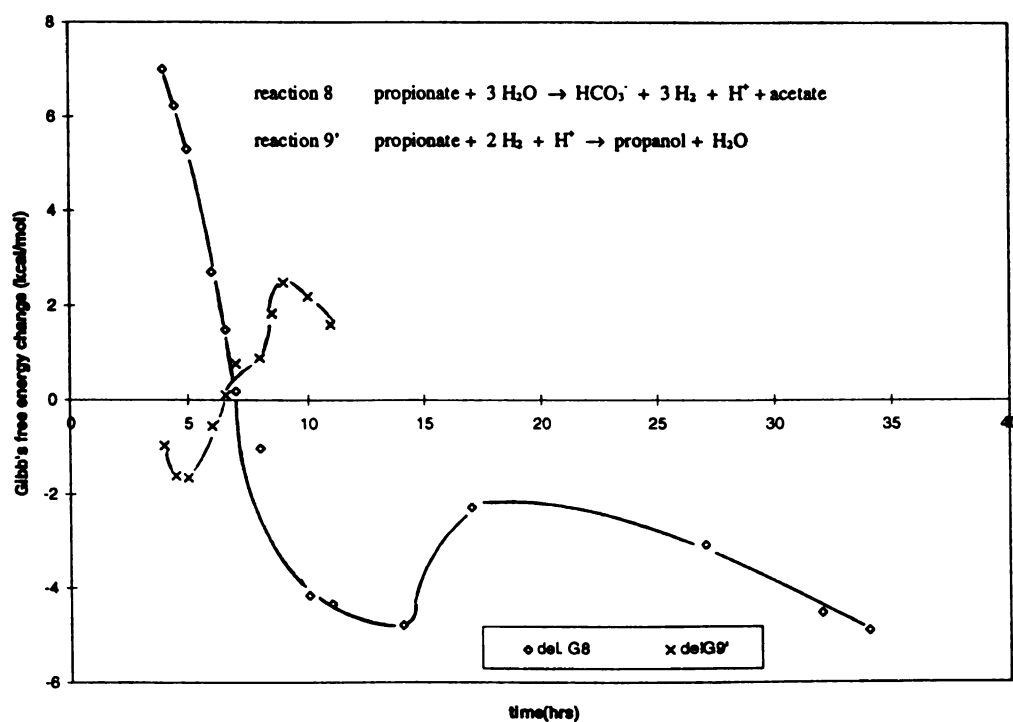


Figure VIIC-4. Gibb's free energy variations of propionate consumption during ethanol degradation by brewery granules.

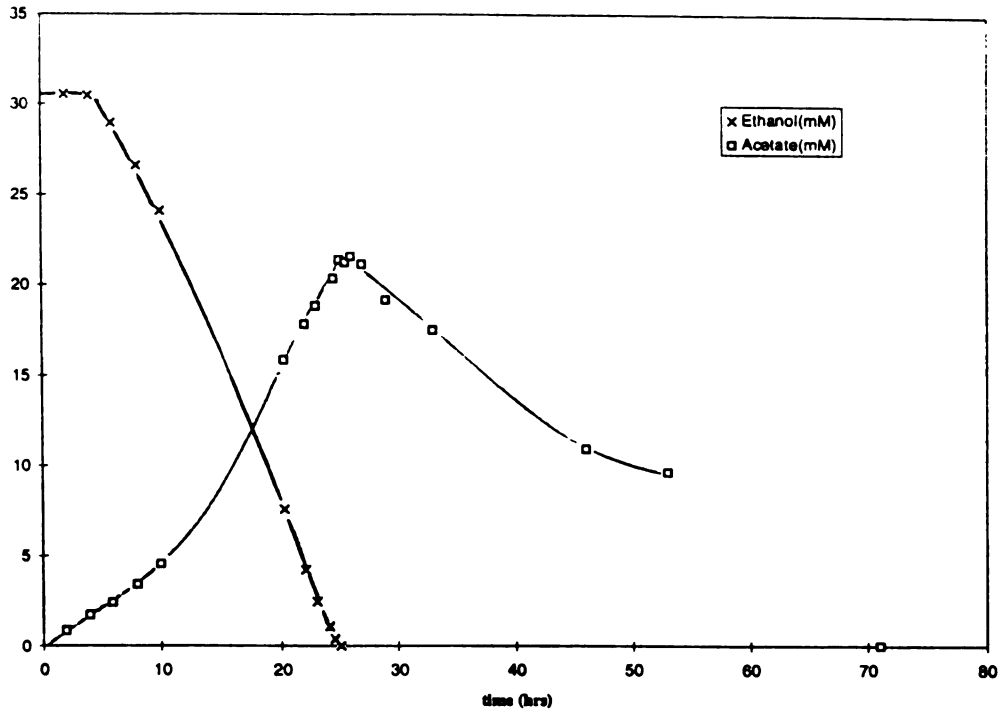


Figure VIIC-5. Typical progress curves of ethanol and acetate during ethanol degradation using whole granules (experiment was stopped after 71 hrs).

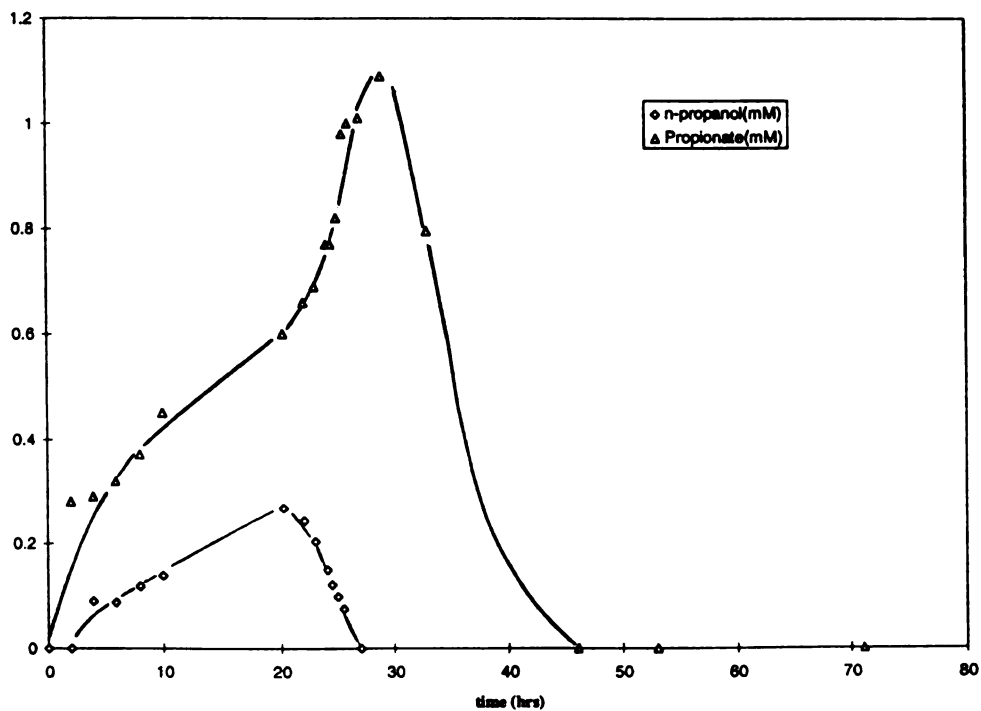
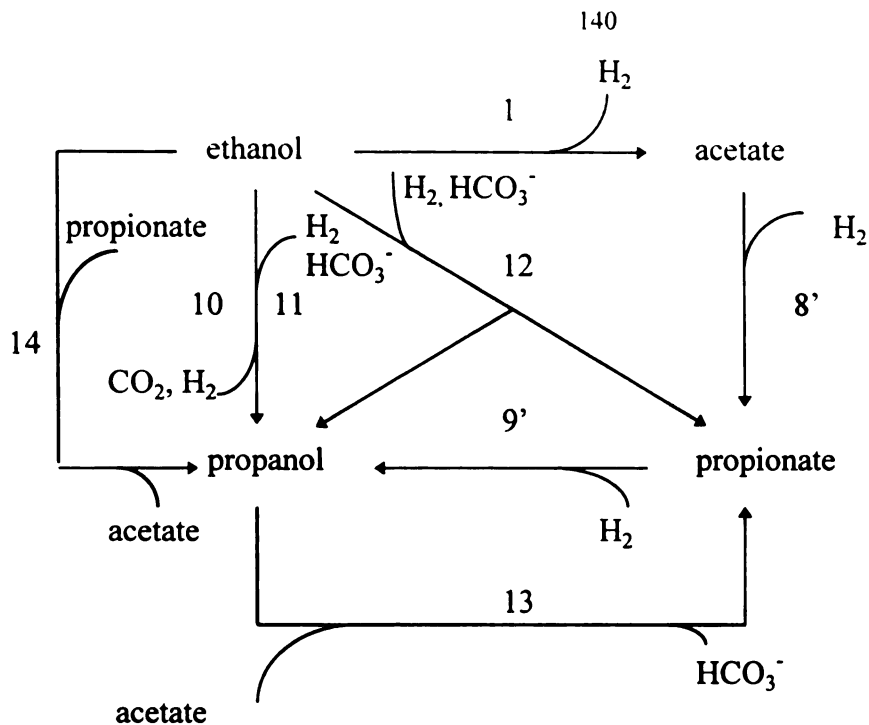
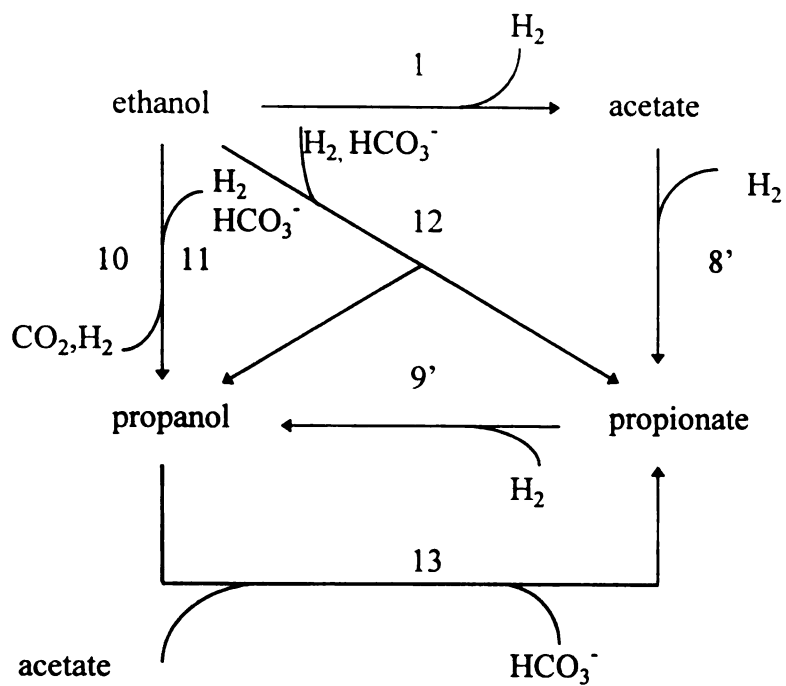


Figure VIIC-6. Typical progress curves of propionate and n-propanol during ethanol degradation using whole granules (experiment was stopped after 71 hrs).

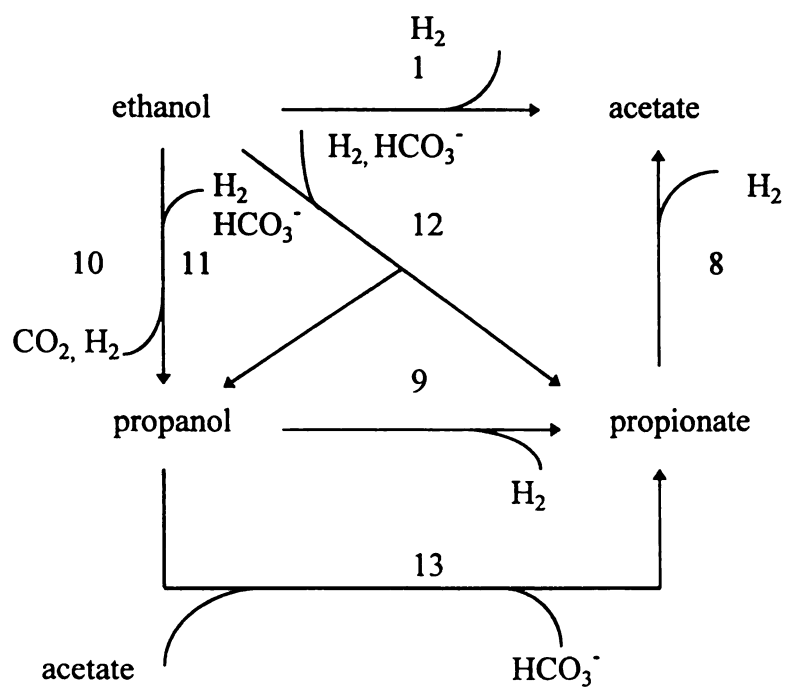


a) $t = 0.5 - 5$ hrs

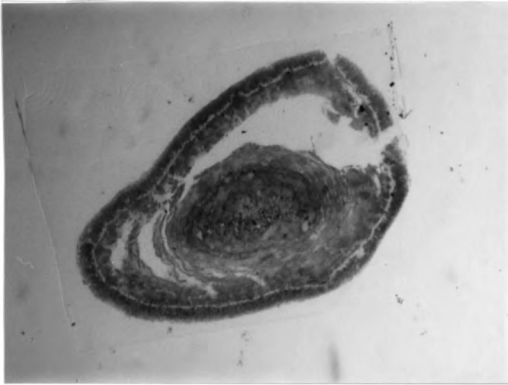
Figure VIIC-7. Possible reactions occurred during initial 11 hours in ethanol assay based on available free energy analyses using brewery granule floccs. a) $t=0.5-5$ hrs b) $t=6-8$ hrs c) $t=9-11$ hrs.



b) $t = 6 - 8$ hrs

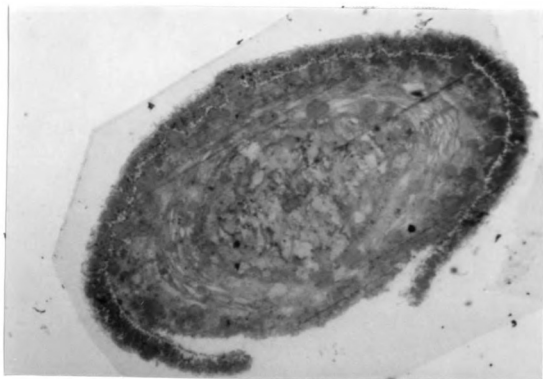


c) $t = 9 - 11$ hrs.

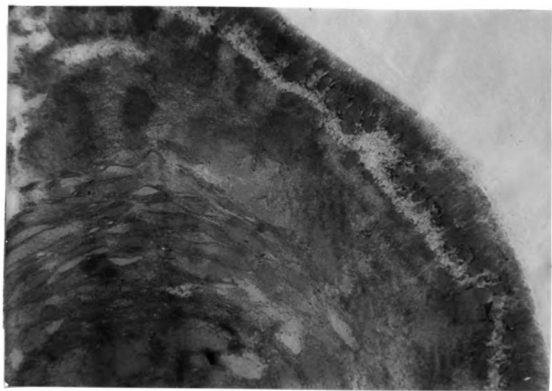


a)

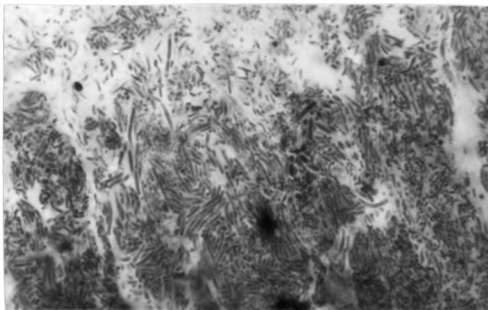
Figure VIID-1. Low magnification thin section microscopy of granules from bench UASB reactor-layered structures: a) cross section view of granule A. magnification 44, b) cross section view of granule B. magnification 65, c) a section of a granule, higher cell density in the outer-layer. magnification 167.



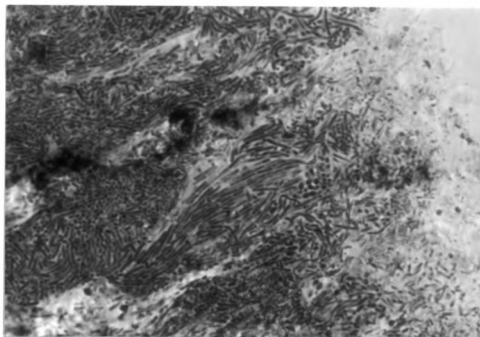
b)



c)



a)



b)

Figure VIID-2. Heterogeneous microbial distributions in outer-layer of a granule. (Olympus BH-2 epifluorescence microscope) magnification 1790. a) finger looking structure, spaces in between serve as gas vent. Clusters of different rods distributed through out the entire layer. b) another section of the outer-layer

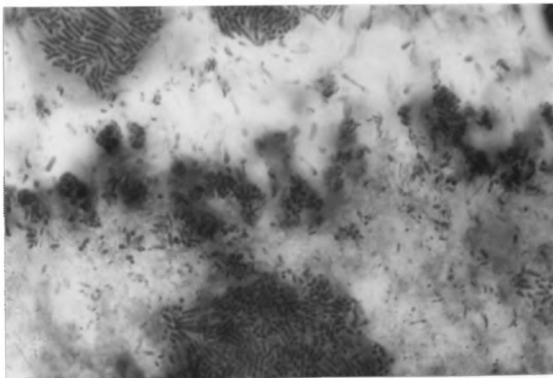


Figure VIID-3. Transparent layer: spaces between outer layer and central core of a granule. (Olympus BH-2 epifluorescence microscope, magnification 1790)

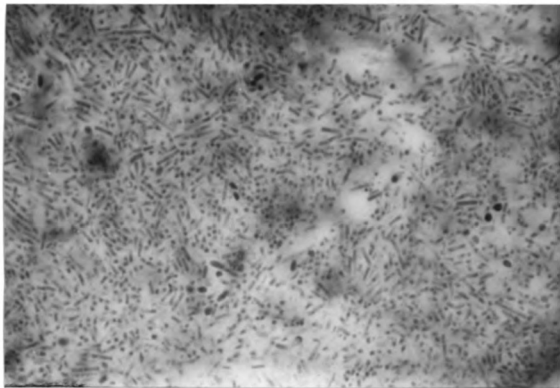


Figure VIID-4. Decreased cell density in the central core of a granule. (Olympus BH-2 epifluorescence microscope, magnification 1790)

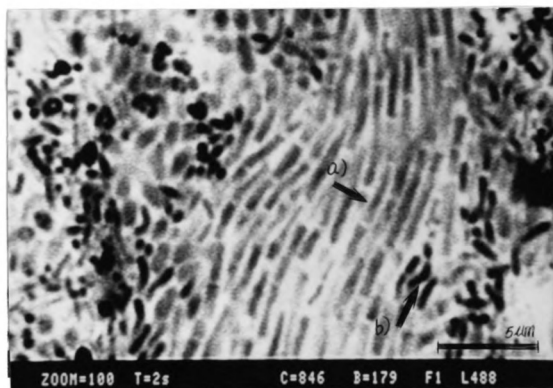


Figure VIID-5. Confocal laser beam microscopy of predominant species in brewery granules a) *Methanothrix*-like rods, b) *Desulfovibrio*-like rods

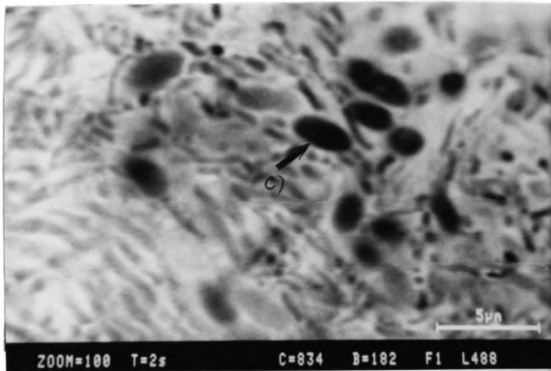


Figure VIID-6. Confocal laser beam microscopy of predominant species in brewery granules c) *Desulfobulbus*-like big rods

Table VIIB-1. Possible reactions involving ethanol, acetate, methane, carbon monoxide, hydrogen, formate and carbondioxide during ethanol fermentation and their standard Gibb's free energy

	Reactions	ΔG° (kcal/mol)
reaction 1	$\text{CH}_3\text{CH}_2\text{OH} + \text{H}_2\text{O} \rightarrow \text{CH}_3\text{COO}^- + 2\text{H}_2 + \text{H}^+$	2.3
reaction 2	$\text{CH}_3\text{CH}_2\text{OH} + 2\text{HCO}_3^- \rightarrow \text{CH}_3\text{COO}^- + 2\text{HCOO}^- + \text{H}_2\text{O} + \text{H}^+$	1.67
reaction 3	$\text{CH}_3\text{COO}^- + \text{H}_2 + \text{H}^+ \rightarrow \text{CH}_4 + \text{CO} + \text{H}_2\text{O}$	-3.78
reaction 4	$\text{HCOO}^- + \text{H}_2\text{O} \rightarrow \text{HCO}_3^- + \text{H}_2$	0.3
reaction 5	$\text{HCOO}^- + \text{H}^+ \rightarrow \text{H}_2\text{O} + \text{CO}$	-3.97
reaction 6	$\text{HCO}_3^- + 4\text{H}_2 + \text{H}^+ \rightarrow \text{CH}_4 + 3\text{H}_2\text{O}$	-32.4
reaction 7	$4\text{HCOO}^- + \text{H}_2\text{O} + \text{H}^+ \rightarrow \text{CH}_4 + 3\text{HCO}_3^-$	-31.1
reaction 15	$\text{CO} + \text{H}_2\text{O} \rightarrow \text{CO}_2 + \text{H}_2$	-4.78

Table VIIC-1. Possible reactions involving n-propanol, propionate and ethanol during ethanol degradation and their standard Gibb's free energy

	Reactions	ΔG° (kcal/mol)
reaction 1	$\text{CH}_3\text{CH}_2\text{OH} + \text{H}_2\text{O} \rightarrow \text{CH}_3\text{COO}^- + 2\text{H}_2 + \text{H}^+$	2.30
reaction 10	$\text{CH}_3\text{CH}_2\text{OH} + 1/2\text{H}_2\text{O} \rightarrow 1/2\text{CH}_3\text{CH}_2\text{CH}_2\text{OH} + 1.5\text{H}_2 + 1/2\text{CO}_2$	3.65
reaction 11	$\text{CH}_3\text{CH}_2\text{OH} + 3\text{H}_2 + \text{HCO}_3^- + \text{H}^+ \rightarrow \text{CH}_3\text{CH}_2\text{CH}_2\text{OH} + 3\text{H}_2\text{O}$	-18.85
reaction 12	$\text{CH}_3\text{CH}_2\text{OH} + \text{HCO}_3^- + 2\text{H}_2 \rightarrow 1/2\text{CH}_3\text{CH}_2\text{CH}_2\text{OH} + 1/2\text{H}^+ + 1/2\text{CH}_3\text{CH}_2\text{COO}^- + 2.5\text{H}_2\text{O}$	-17.41
reaction 14	$\text{CH}_3\text{CH}_2\text{OH} + \text{CH}_3\text{CH}_2\text{COO}^- \rightarrow \text{CH}_3\text{CH}_2\text{CH}_2\text{OH} + \text{CH}_3\text{COO}^-$	-0.57
reaction 13	$\text{CH}_3\text{CH}_2\text{CH}_2\text{OH} + 2/3\text{CH}_3\text{COO}^- \rightarrow 5/3\text{CH}_3\text{CH}_2\text{COO}^- + 1/3\text{H}^+ + 2/3\text{HCO}_3^- + \text{H}_2\text{O}$	-9.31
reaction 9'	$\text{CH}_3\text{CH}_2\text{COO}^- + 2\text{H}_2 + \text{H}^+ \rightarrow \text{CH}_3\text{CH}_2\text{CH}_2\text{OH} + \text{H}_2\text{O}$	-12.4
reaction 8	$\text{CH}_3\text{CH}_2\text{COO}^- + 3\text{H}_2\text{O} \rightarrow \text{HCO}_3^- + 3\text{H}_2 + \text{H}^+ + \text{CH}_3\text{COO}^-$	18.2

Table VIIC-2. Substrate and major products acetate and propionate concentration varied with propanol during ethanol assay

Initial ethanol concentration (mM)	time (h)	products ^a			Ethanol concentration (mM)	Ratio ^c acetate initial ethanol
		acetate (mM)	propionate (mM)	propanol (mM)		
32 ^b	15	3.20	0.13	0.05	23.70	0.1
	37	12.90	0.23	0.08	13.00	
	61	26.00	0.39	0.01	0.90	0.81
50 ^b	47.2	16.60	0.26	0.04	24.96	0.33
	69	29.66	0.41	0.16	10.30	
	100	38.04	0.62	0.01	0.24	0.76
67 ^b	56.5	19.32	0.31	0.13	34.90	0.29
	73	40.26	0.37	0.18	20.70	
	131	52.91	0.67	0.03	1.20	0.79

a. concentrations of acetate, propionate and propanol for the beginning, peak, and end of the propanol accumulation curve are presented.

b. assay using whole granules; background acetate and propionate were undetectable.

c. the ratio of acetate/initial ethanol when propanol began accumulating and disappearing were 0.37 and 0.78 during ethanol degradation assays using flocs.

Table VIIC-3. GC/MS results from ^{13}C labeled ethanol assay

	^{13}C Mass of intensity			Ratio of intensity		Note
	$M/Z=61^b$	$M/Z=60^c$	$M/Z=59^d$	61/60	61/59	
Control	2.5	78.04	100	0.032	0.025	0.5 μM n-propanol (unlabeled) ^e
A1	3.37	12.94	17.06	0.260	0.198	^{13}C labeled ethanol, unlabeled bicarbonate
A2	2.61	12.61	17.23	0.207	0.151	^{13}C labeled ethanol, unlabeled bicarbonate
B1	0.59	12.53	14.8	0.047	0.040	^{13}C labeled bicarbonate, unlabeled ethanol
B2	ND	10.55	8.8	ND	ND	^{13}C labeled bicarbonate, unlabeled ethanol
C1	2.28	12.4	18.23	0.184	0.125	^{13}C labeled ethanol, unlabeled bicarbonate

a. M-molecular weight of n-propanol fragment, Z-charge

b. 61 - $^{13}\text{M}^+$

c. 60 - $^{12}\text{M}^+ + ^{13}\text{M-H}^+$

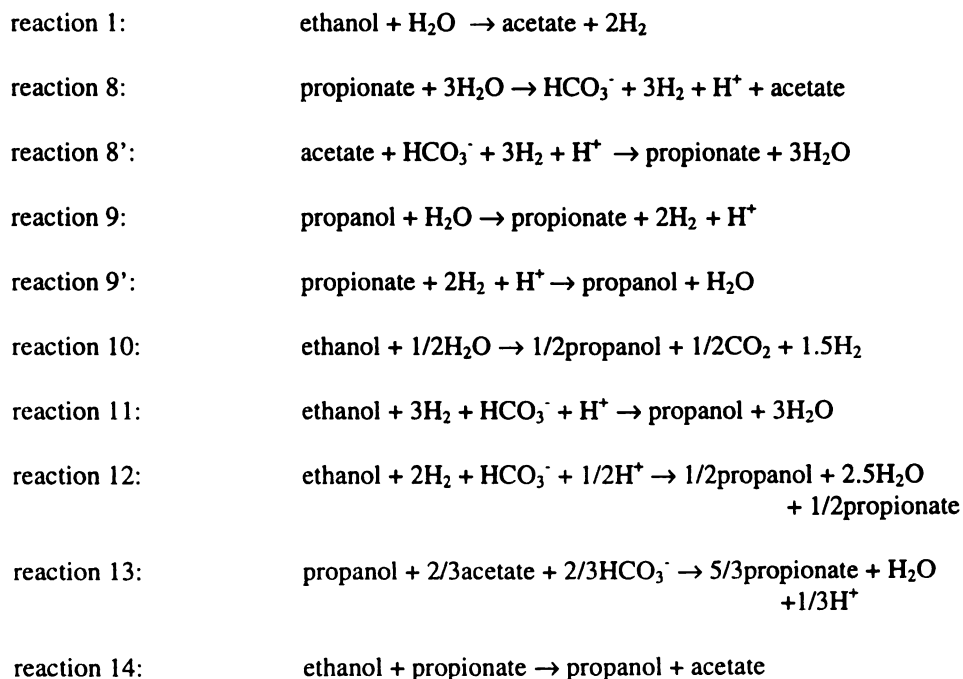
d. 59 - $^{12}\text{M-H}^+$

e. natural abundance of $\frac{^{13}\text{M}^+}{^{12}\text{M}^+ + ^{13}\text{M-H}^+}$ for 1 carbon is 1.1%, for n-propanol is 3.3%

Table VIIC-4. Gibb's free energy profile of major reactions during initial hours of ethanol degradation

Time (hr)	$\Delta G'$ for each reactions (kcal/mol) ^a									
	1 ^d	8	8'	9	9'	10	11	12	13	14
0.5	-8.44	+ ^b	-3.72	+	-2.29	-13.55	-13.00	-8.61	-9.77	-1.19
1	-8.00	+	-4.47	+	-2.18	-13.12	-13.24	-8.86	-10.38	-0.95
2	-6.45	+	-6.65	+	-3.50	-11.83	-15.31	-10.15	-10.52	NA
4	-6.39	+	-6.22	+	-3.32	-11.81	-14.98	-9.57	-10.41	-0.23
5	-6.46	+	-5.30	+	-3.16	-11.85	-14.65	-9.03	-10.21	-0.13
6	NA ^c	+	-4.57	+	-2.60	NA	NA	NA	-10.03	+
6.5	-7.26	+	-3.79	+	-2.17	-12.48	-13.19	-7.45	-9.94	+
7	-7.44	+	-3.27	+	-1.90	-12.56	-12.79	-6.96	-9.86	+
8	-8.47	+	-1.03	+	-0.83	-13.42	-11.03	-5.22	-9.44	+
9	NA	NA	NA	-0.40	+	-13.89	NA	NA	NA	+
10	NA	NA	NA	-1.08	+	-14.68	-8.47	-2.21	NA	+
11	-9.51	-4.06	+	-1.22	+	-14.13	-9.42	-0.14	-8.10	+

a. negative values are listed. b. "+" represents positive $\Delta G'$ value. c. NA, not available. d. reaction number.



MICHIGAN STATE UNIV. LIBRARIES



31293014110617

THESIS

4

MICHIGAN STATE UNIVERSITY LIBRARIES



3 1293 01411 0591

LIBRARY
Michigan State
University

PLACE IN RETURN BOX to remove this checkout from your record.
TO AVOID FINES return on or before date due.

DATE DUE	DATE DUE	DATE DUE
_____	_____	_____
_____	_____	_____
_____	_____	_____
_____	_____	_____
_____	_____	_____
_____	_____	_____
_____	_____	_____

MSU Is An Affirmative Action/Equal Opportunity Institution

c:\circ\datedue.pm3-p.1

**CHARACTERIZATION OF PERFORMANCE AND MONITORING
OF THE UPFLOW ANAEROBIC SLUDGE BLANKET REACTOR**

Volume II

By

May Meiliang Wu

A DISSERTATION

Submitted to
Michigan State University
in partial fulfillment of the requirements
for the degree of

DOCTOR OF PHILOSOPHY

Department of Civil and Environmental Engineering

1995

CHAPTER 8. MONITORING AN UASB REACTOR TREATING A SYNTHETIC BREWERY WASTE

A. Introduction

The complex degradation sequence in anaerobic treatment of organic matter in wastewater and coupled with the sensitivity of the different microbial populations requires a strong monitoring and control strategy, to adequately detect instability of a process or any change in system responses from a target level. Improved monitoring and control should lead to improved system performance and avoidance of gross process failure. Numerous attempts have been made to reveal the causes of instability and to better control anaerobic process using control charts, pattern recognition, fuzzy control and expert systems [Olsson et al.,1989] [Berthouex,1989] [Locher et al.,1990] [Boscolo et al.1993] [Barnett and Andrews,1992]. Recent developments in anaerobic microbiology and available instrumentation has expanded monitoring of the anaerobic treatment process to a variety of system parameters. Successful process monitoring can be accomplished by using several process indicators which characterize current process status. In the near future, these indicators may be used to help identify the causes when poor operation exists. Ideal process indicators have the features of being: 1) sensitive with low noise 2) easy to measure 3) have intrinsic meaning 4) be a sign of early warning 5) on-line measurement available.

Early process indicators used for anaerobic digestion systems included pH [Clark and Speece, 1970] [Zoetemayer et al.,1982], VFA [Asinari di San Marzano,1981] [Powell and Archer, 1989], bicarbonate [Colin 1984] [Rozzi et al,1985], redox potential

these parameters pH, VFA and gas production are good process indicators for detecting slow to develop system failures such as those experienced for sludge digestion. In high rate anaerobic system such as UASB reactors, however, process parameters that provide a fast response under shock loading and other perturbations is required to avoid serious system failure. Automation of pH monitoring is available. A reduction in pH, which could lead to inhibition of methanogenesis, is caused by accumulation of acids when the buffering capacity is exhausted. Therefore, it is the result of a system imbalance rather than an early warning sign. The measurement for bicarbonate is usually performed via a titration technique which is not easily automated. VFA accumulation is a sign of lack of balance between acetogens and methanogens. The determination of VFA at present is off-line and observed to be a less sensitive indicator than gas production. Variation of the composition of the major gases, CH₄ and CO₂, is sensitive and reflects intrinsic imbalances in the digestion of sludge. The response of the gas composition is observed, however, only when system failure is well developed. Gas production and methane production have rapid responses to changes in organic loading rate and on-line automation is available. However, the variation of methane production and gas production can be either a sign of inhibition of methanogen, or a result of background influent organic loading rate fluctuations.

Another class of methods tested focus on the microbial populations in the digesters. These methods using enzymatic, immunological means, gene probe and lipid composition analysis to detect enzyme activity [Agardy et al.,1963] [Thiel and Hattingh, 1967] [Lenhard, 1968], fatty acids variation [Henson et al.,1988a,1988b], antibodies [Strayer and Tiedje,1978] [Macario and Conway de Macario, 1983] and F₄₂₀ [Schulze et

al.,1988], a co-factor specific to methanogens. DNA and ATP monitoring [Agardy and Shepherd,1965] [Chung and Neethling, 1988] have also been investigated. Immunological method has been successfully used in UASB for studying long-term population shifts [van Lier et al.1991]. These methods, however, are slow and off-line. A detailed review of monitoring technologies in anaerobic wastewater treatment is provided by Switzenbaum et al. [1990].

Hydrogen and CO are intermediates of methane fermentation of organics. Accumulation of H_2 is inhibitory to hydrogen producing microorganisms. As a result of this inhibition, more reduced products can build-up as alternative electron sinks [Chung,1976] [Kaspar and Wuhrmann,1978]. CO is a metabolic intermediate involved in synthesis of carboxyl group of acetyl-CoA and decarboxylation of acetate via carbon monoxide dehydrogenase (CODH) [Krzycki et al.,1982] [Stupperich et al.,1983] [Zeikus et al.,1985] [Eikmanns and Thauer,1984] [Nelson and Ferry,1984] [Krzycki and Zeikus,1984]. Monitoring trace gases H_2 and CO has attracted attention for anaerobic process monitoring due to the fact that they are relatively easy to measure, slightly soluble in water, sensitive, can be measured on-line and have the potential of measuring metabolic status. H_2 and CO were observed to have fast responses to organic overloading before VFA accumulation or build-up, pH and methane decrease [Hickey and Swizrnbaum,1988] [Hickey et al.,1987a] [Hickey et al.,1989] [McCarty and Smith,1986]. Mosey [1983] developed a mathematic model based on H_2 variations in sludge digesters. Carbon monoxide had a characteristic responses under heavy metal inhibition of digester [Hickey et al.,1987b]. A thermodynamic relationship between H_2 , CO, methane content, CO_2 and

effluent acetate concentration has been postulated to predict acetate concentrations during organic overload of sludge digesters [Hickey and Switzenbaum,1990]. However, controversies still exist on whether CO and H₂ are useful monitoring parameters for the control of anaerobic process. The H₂ level in a fixed bed reactor was observed to be affected by differences in reactor configuration [Harper and Pohland,1987]. Pauss et al.[1990,1993] using a hydrogen probe to measure liquid phase H₂ on-line and observed no correlation between OLR and the ratio of $H_{2(L)}/H_{2*}(L)$ because of variations in the liquid-gas mass transfer limitations of H₂ within the reactor they used. CO production in a CSTR during glucose, formate and acetate perturbations were reported to be inconsistent [Bae and McCarty,1993].

This portion of study focused on examining responses of H₂ and CO and reactor performance during various hydraulic loading rates, organic loading rates and variation in feed composition at pseudo-steady state, and examining the potential of using H₂ and CO as indicators for monitoring UASB reactor system, to detect onset of unstable conditions (organic overloading) and system failure. The experiments were conducted during pseudo-steady state and unsteady state perturbations on a UASB reactor treating a synthetic brewery waste. Data were analyzed using statistical methods to detect any recognizable patterns of H₂ and CO, including mean and variance analysis, correlation between trace gases and performance variables, trend of CO and H₂ during pseudo-steady state and perturbations and spectra analysis.

B. Monitoring CO and H₂ during pseudo-steady state operation

B-1. On-line monitoring system of the bench-scale UASB reactor

Monitoring experiments were performed using a bench-scale UASB reactor (described in Chapter V) equipped with an on-line data acquisition and control system PARAGON (Intec) through an analog/digital (A/D) interface (OPTO-22) and a personal computer (386). The reactor set-up used for gas, liquid and data acquisition is presented in Figure VIIIB-1.

Gas phase CO, H₂, CH₄ and gas production from the UASB were sampled and analyzed on-line. Head space samples were collected from a gas loop connected to reactor head space. Gas stream generated from reactor first passed through a condenser to remove moisture in gas stream, then entered the gas loop. The gas stream was pumped continuously into an infrared Methane Analyzer (ADC SB100) for on-line quantitation of methane. Analog signals from Methane Analyzer were transmitted to the host computer. The gas stream then exited the Methane Analyzer where the flow was split into two streams: the majority of the gas stream went back to the reactor head space while the other branch was passed through the sample loop of a Trace Gas Analyzer (RGA3). CO and H₂ were collected via automated actuated gas sampling valves and analyzed in the Trace Gas Analyzer. The components remained in the column were back flushed to vent with carrier gas. Data analysis of H₂ and CO was performed automatically by the integrator/controller module (ICM) in the RGA3. The ICM was programmed for complete operation, which was monitored by the PARAGON program in the host computer. Gas produced from the reactor passed through a three-way valve which was connected to a

gas meter and an exhaust pipe. Gas production was measured by means of a liquid displacement technique. Each gas count (ca.3-5ml) was recorded and cumulative gas production totaled using the PARAGON system.

The inlet liquid flow rate to the UASB reactor was controlled via an automated pump (Watson–Marlow 503U) connected to the PARAGON system to ensure the desired OLR was attained. A mixture of inlet and recycled flow was continuously passed upward through sludge bed/blanket and clarifier. Effluent was collected at the top of the reactor. The majority of the reactor effluent from the clarifier zone was recirculated (Watson–Marlow 503S). Liquid samples were collected manually from the reactor recirculation line for VFAs, pH and alcohols analysis. Biomass was collected through sampling ports in the sludge bed. Detailed descriptions of the data acquisition system, analytical methods and QA/QC procedures for gas, liquid and solid phase sample analysis are presented in Appendix C.

B-2. Pseudo-steady state experiments

A synthetic brewery waste (11.4 kgCOD/m^3 , Appendix A) was used as feed to the UASB reactor. Anaerobic granules were cultivated in the UASB reactor, operated at 37°C . Liquid pH was maintained at 6.8-7.0. Operational conditions of the UASB reactor during pseudo-steady state are shown in Table VIIIB-1. Pseudo-steady state was assumed to have been attained when all effluent parameters stabilized after a change in OLR and more than three HRT. Experiments began about three weeks after start-up. The OLR was varied from 4 to $23 \text{ kgCOD/m}^3\text{bed-d}$, HRT from 0.5 to 2.5 days, and feed concentration

from 6-14 kgCOD/m³. This experiment was designed to examine each parameter individually, by operating the UASB reactor at different combinations of OLR, HRT and feed concentration. First, OLR was varied at two levels (15 and 23 kgCOD/m³bed-d) while HRT (0.5 days) and feed concentration (14 kgCOD/m³) were held constant. Then, HRT was varied at two levels (0.5, 1.5 days) while OLR (15 kgCOD/m³bed-d) and feed concentration (14 kgCOD/m³) remained unchanged. Feed concentration effects were examined at two levels (9 and 11 kgCOD/m³) while keeping OLR at 10 kgCOD/m³bed-d and HRT at 1.5-1.8 days. The effect of increasing the OLR through changing feed pumping rate (HRT varies, feed concentration fixed) or changing both feed and mineral pumping rates (fixed HRT, feed concentration varies) were examined at three levels (4, 10, 14 and 6, 10, 15 kgCOD/m³bed-d respectively). A total of eight runs of different combinations were conducted (Table VIIIB-2). Reactor gas, liquid and solid phases were monitored for nine months during this experimental period. Gas phase H₂, CO, CH₄ content and gas production rate were measured hourly. Reactor effluent VFA and pH were measured daily. Biomass in the effluent (TSS and VSS) were measured weekly. Sludge bed solids concentration (TS and VS) were measured monthly. The pseudo-steady state data files were combined on a semiweekly basis and then transferred as a SAS data series. Computations were made for gas production rate based on cumulative hourly monitoring data. Minor disturbances of the system which happened during operation were corrected for (ie. methane analyzer failure and trace gas analyzer error signals).

Typical profiles of acetate, propionate, CO, H₂, CH₄ and gas production rate during pseudo-steady state operation are shown in Figure VIIIB-2. The largest in variation

was observed for H_2 concentration: methane was the least in variation parameters. CO fluctuated at ± 0.2 ppm. During the entire operational period, acetate and propionate concentrations remained below 2mM and 1mM, respectively. At an $OLR < 14$ $kgCOD/m^3bed-d$ the acetate and propionate concentrations were near or below detection limits (0.1mM). During the entire pseudo-steady state operations, COD removal efficiency, determined based on a mass balance of gas production, ranged from 71 to 94%, the averaged being 85%. Methane production, based on COD removed, ranged from 0.28 to 0.37 $LCH_4/gCOD$ removed, with an average of 0.34 $LCH_4/gCOD$ removed.

B-3. Statistics of H_2 , CO and other process variables

B-3.1 General statistics

Statistical analysis of the pseudo-steady state operational data was performed. For mean, variance, standard error, coefficient of variance (CV, the ratio of variance to mean), correlation, Student t statistics, confidence interval and population distribution for acetate, propionate, CH_4 , gas production, pH, CO and H_2 , at each pseudo-steady state operational condition. The CVs were then averaged to obtain a mean of CV for overall steady state operation. The mean, CV and standard error for each variable during the overall pseudo-steady state is presented in Table VIIB-6.

B-3.11 Mean, coefficient of variance, population distribution and standard error

Population distribution tests indicated all variables followed normal distribution. Methane content had the narrowest range (74.2%-85.6%) for the mean while H_2 the

widest (19-173 ppm). The variation of each variables was estimated by the value of the coefficient of variation (CV). The higher the CV, the greater the fluctuation or higher the sensitivity. H_2 had the highest CV (75.2), CH_4 the lowest (2.6). The variation of CO (36.9) was moderate as was acetate (49.1). These variables, grouped according to their variation were: $H_2 > > \text{acetate} > \text{CO} > \text{propionate} > \text{gas production} > CH_4$. The standard error was highest for H_2 than for CH_4 , indicating high background noise of H_2 .

B-3.12 Confidence level and mean as a function of OLR

Confidence levels of each monitoring variable were calculated using a Student t test at the $\alpha=0.05$ level. Acetate, propionate, CO, H_2 , CH_4 and gas production were computed using standard error. The mean and confidence intervals (CI) of each variable were then plotted against OLR (Figure VIIIB-5, 6 and 9). The means of acetate, propionate, CO and gas production all increased with increased applied OLR. This increase was clearly linear for gas production and non-linear for acetate, propionate and CO. The CH_4 concentration decreased with increased OLR, also in a non-linear fashion. There is no discernible pattern to the mean of H_2 concentration. The CIs of Gas production, CH_4 and CO were small and consistent throughout the entire OLR range tested. The CI of CO increased slightly at high OLR (23 kgCOD/m³bed-d). In contrast to the other variables, the CIs of H_2 was high. The CIs of H_2 overlapped between OLRs of 10 and 23 kgCOD/m³bed-d, indicating there was no statistical differences in H_2 concentrations between these two OLRs. Acetate and propionate had considerably higher CIs, which increased at the highest OLR (23 kgCOD/m³bed-d).

B-3.13 Correlation

Correlation analysis showed acetate, propionate and methane content were most closely correlated with other variables (at $\alpha=0.01$; Figure VIIB-10). Gas production and CO concentration were related to three other variables. There was no correlation between H₂ and any other variables.

Bivariate plots of CO and H₂ with acetate for eight pseudo-steady state operations were used to examine the correlation between acetate and trace gases. The results (Figure VIIB-3 and 4) indicate that CO concentration was scattered in some individual runs although it correlated with acetate based on whole data.

B-3.14 Analysis of variances and multiple comparison tests

Analysis of variances (ANOVA) was performed on the six monitoring variables to test the significance in variation among the OLRs tested. Result of significance tests, presented in Table VIIB-9, indicated high F values for all of the variables. The values of Fs were significant at $\alpha=0.001$ level (indicated by three '+' signs), which provided strong evidence of real differences among the means of each variables for the eight OLRs tested. Thus it can be concluded that every individual monitoring variable does not belong to a population within a common mean μ at different OLRs.

To further examine at which two OLRs variables are different from each other, multiple comparison tests, Duncan's multiple range test and LSD (least significant differences) tests, were conducted on the population means of each variable ($\alpha=0.05$). The variables were then grouped based on OLR (Table VIIB-10). Acetate and propionate

were grouped similarly. The grouping of gas production and CH_4 , CH_4 and CO were close, respectively. All of the variables at OLR 23 $\text{kgCOD/m}^3\text{bed-d}$ were different from others except H_2 . Most variables had little differences at low OLRs.

B-3.2 OLR, HRT and feed concentration effects

Sample means of the 8 pseudo-steady state operational data sets were shaped into five groups according to different control variables (Table VIIIB-2). The mean of acetate, propionate, H_2 , CO, CH_4 and gas production at different combinations of OLR, HRT and feed concentration are listed in Table VIIIB-7. Within each group, means were compared to detect any trend. The monitoring variables followed OLR variations. Acetate, propionate, gas production and CO generally varied in parallel with OLR. CH_4 varied in the opposite direction.

When HRT and feed concentration were both held constant at 0.5 days and 14 kgCOD/m^3 , means of all variables with the exception of methane, increased with an increase in the OLR from 14.5 to 23 $\text{kgCOD/m}^3\text{bed-d}$ (I). When the HRT was decrease while OLR and feed concentration remained about same (II), CO, H_2 , propionate and gas production changed slightly. CH_4 decreased and acetate increased. At a fixed OLR of 10 $\text{kgCOD/m}^3\text{bed-d}$ and HRT varying at 1.5-1.8 days (III), the responses were weak. When the OLR was increased by increasing the pumping rate (HRT decreased;IV), acetate, propionate, CO, H_2 and gas production increased and CH_4 decreased as OLR increased in response to increased OLR. When the OLR was increased by increasing the feed concentration (HRT remained constant;V), the same phenomena was again observed; all

the variables increased or decreased (CH_4) with increased OLR. HRT reduction caused an increase in CO , H_2 concentrations and gas production and a decrease in CH_4 in one case (group IV, Table VIIIB-7), and the opposite in another case (group II, Table VIIIB-7). This implies that HRT does not have a strong influence on the gas monitoring variables at the OLR and HRT ranges studied. This was also the case when feed concentration was varied.

B-3.3 Spectra analysis

Spectra analysis was conducted on pseudo-steady state operational data for six monitoring variables (acetate, propionate, H_2 , CO , CH_4 and gas production) in order to detect any cyclical patterns. The spectra technique uses finite Fourier transformation to reduce data into a sum of sine and cosine waves of different amplitudes and wavelengths [Brockwell and Davis, 1987]. The periodogram represents a sum of the squares. The periodogram is smoothed by a weighted moving average to produce an estimate for the spectral density of the series. Frequencies of each series are plotted against the periodogram. The maximum frequency calculated from the periodogram indicates any hidden periodicity.

The data was further examined by Fisher's test at each OLR, to differentiate any hidden periodicities from white noise. The hypothesis (H_0) that the data is generated by a Gaussian white noise sequence, was tested against the alternative hypothesis (H_1) that the data is generated by a Gaussian white noise sequence with a superimposed deterministic periodic component. The test was computed using the following equation:

$$P(E_q \geq x) = 1 - \sum_{j=0}^q (-1)^j \binom{q}{j} \left(1 - \frac{jx}{q}\right)_+^{q-1} \quad \dots \quad (\text{VIII-1})$$

where P is probability; E_q is a realized value of x ; q is $\frac{n-1}{2}$, n is data size; x is Kappa test statistics. $\alpha=0.05$ was used in the test.

Thirdly, cross-correlation of monitoring variables under the pseudo-steady state operation was analyzed, to examine the time phase between the spectra (delay in response) of different variables. Phase spectrum periodograms were computed for each pair of variables at each OLR.

Spectra analysis were conducted by writing several SAS programs and plotting results for each variable. The maximum frequencies determined are presented in Table VIIIB-3. Acetate and CH_4 concentration have the same maximum frequency throughout the operation. In three out of seven cases propionate had the same common frequency as acetate and CH_4 . For two out of seven cases CO had the same common frequency as acetate. The maximum frequencies of acetate and CH_4 ranged from 0.26-2.62; five out of seven data sets had values that were within the range of 0.26-0.57. Similarly, propionate had maximum level between 0.26 to 0.63 for five out of seven OLRs. CO , H_2 and gas production ranged from 0.11-0.84 for most of the experimental conditions tested. The maximum frequency of each monitoring variable appears to be independent of the OLR imposed onto the system. CH_4 and acetate were related to some degree in frequency. The variation of gas production and H_2 did not appear to be periodical in nature.

White noise tests were performed using SAS for Kappa's test (x) and q . Fisher's test was then calculated manually using equation VIII-1 for each variable at each OLR.

The probability was compared at the $\alpha=0.05$ level, and the decision made to either reject or accept the hypothesis H_0 . Rejection of H_0 means the data series has a hidden periodicity. Accepting H_0 means that the data is described by random noise. The probability levels for each variable are listed in Table VIIB-5. In three out of seven cases propionate and CO had periodicity (H_0 was rejected). At lower than two cases each variable showed some degree of periodicity, however, white noise was normally observed for all the variables tested. The periodicities were weak for most variables.

Results of cross-correlation analysis using SAS are presented in Table VIIB-4. For each pair of variables, real periodogram was plotted with time-phase ranging from $-\pi$ to π . CH_4 had a delay from CO ranging from -0.1 to -0.25 in most cases. Acetate and propionate had the same time phase when OLR was high. Time phase between the rest pair of monitoring variables was unclear.

B-4. Reaction energetics

Acetogenesis and methanogenesis are the two major processes involved in the biodegradation of the synthetic brewery waste. During biodegradation, ethanol degraded quickly. During pseudo-steady state operations, ethanol was never detected in the reactor effluent (detection limit 0.1 mM). Thus the reaction thermodynamics were performed primarily using propionate and acetate degradation. Values of the mean of each monitoring variable derived from statistical analysis (Chapter VIII B-3) were used in the energy calculations. The major biochemical reaction equations and their Gibb's free energy under standard conditions (after Thauer et al.,1977) are shown in Table VIIB-8. In order

to track the influence of CO and H₂, reactions 2 and 3 were split from the reaction Acetate → CH₄ + CO₂.

At standard conditions, the Gibb's free energy for propionate degradation is positive. From a thermodynamic point of view, the reaction could therefore not proceed to the right. To reach a negative value of ΔG , H₂ must be low. ΔG for each OLR was calculated using the actual concentrations during pseudo-steady state operations and the reactor operational conditions (37°C, pH=7) (Figure VIIIB-7). CO and H₂ were analyzed using the head-space concentration. The values of the first 2 points of each of the four reactions were different from the values of the rest of the points of these reactions. This may be caused by the low concentration of acetate and propionate (near detection limits) at an OLR of 4.2 and 5.8 kgCOD/m³bed-d. This also affected the level of the other variable. The calculated $\Delta G'$ of propionate degradation (reaction 1) was positive. The reaction was therefore not likely to occur. However, the propionate concentration in the feed (15mM) decreased down to less than 1mM during the operation. The discrepancy between the calculated free energy values was probably due to the lack of equilibrium between the gas present in the head space and the gas dissolved in the aqueous phase.

H₂ and CO present in the head space did not necessarily represent the concentration in the liquid phase that microorganism actually experienced. Pauss et al. [1990a] reported a 70 times difference between dissolved H₂ and head space H₂. This could be due to 1) limiting mass transfer from liquid to gas phase [Pauss et al. 1990a,1990b], 2) hydrogen's rapid turnover rate and its perhaps widely varying concentration in solution. An attempt was made to measure dissolved H₂ and CO in the

UASB reactor in a separate experiment at various head-space concentrations (for method see Appendix C). The value of the pseudo-steady state gas phase H_2 and CO concentrations were adjusted using the results obtained from dissolved gas analysis from the same UASB reactor, in a separate test. The ratio of measured gas concentration to gas concentration at equilibrium with liquid phase concentration ($H_2^*(g)$ and $CO^*(g)$), calculated based on the measurements of dissolved gas concentrations, were presented in Table VIIIB-11. A ratio of less than one, or the gas phase concentration is smaller than equilibrium gas concentration ($H_2^*(g)$ or $CO^*(g)$), indicates that mass transfer of the compound from liquid phase to gas phase is limited. This ratio for H_2 was greater than one, however, was smaller than one for CO. Thus the results suggested that mass transfer from liquid phase to gas phase was limiting for CO and was not limiting for H_2 . Dissolved gas concentrations of H_2 and CO during pseudo-steady state operations were then estimated (Figure VIIIB-8). The free energy of the propionate degradation was negative at pseudo-steady state. For each reaction within the OLR range studied, the $\Delta G'$ values were quite stable. Reaction 2 (acetate \rightarrow CO) had three positive points. However, $\Delta G'$'s for the whole reaction of acetoclastic methanogenesis (reactions 2 +3) were negative. The average free energy level of propionate oxidation (reaction 1) was -20 kJ/mol; of acetate decarboxylation (reaction 2+3) -20 kJ/mol; of H_2 oxidation (reaction 4) -5 kJ/mol.

C. Unsteady state OLR perturbations and system responses

Unsteady-state OLR variation experiments were performed by imposing step OLR increases and decreases as well as imposing impulse loads on the bench-scale UASB reactor treating a synthetic brewery waste. OLR was varied by changing the feed rate. Perturbation of different OLR strengths and durations were tested. The effect of fixed duration of steps (regular variation) and a combinations of impulse and step increases (random variation) were also examined. The OLR was increased high enough to cause a system failure. Trace gases, H_2 and CO , and performance variables acetate, propionate, gas production rate, methane content, pH and suspended solids were monitored. Reactor granule volume was maintained at 1.5-1.7 L (unexpanded bed volume).

C-1. OLR variation at 5, 8, 12, 15 kgCOD/m³ bed-d

A regular perturbation experiment performed by varying OLR at a fixed frequency (24 hrs) and duration of each step (3 hrs) was conducted (Figure VIII-11). Three perturbations were imposed on the UASB reactor. The background OLR was 5 kgCOD/m³bed-d. The OLR was increased stepwise from 5 to 8, 12 and 15 kgCOD/m³bed-d, and then back by increasing and then decreasing the forward flow rate to the reactor (decreasing HRT from 2.6 to 1.3 days). Results of the experiment are graphically presented in Figures VIII-11 to 13. The UASB responded quickly to changes in OLR. Gas production rate followed the changing in OLR extremely well. CO also appeared track the changes in OLR with little delay. No discernable trend was observed for H_2 . Acetate and propionate levels rose only slightly at each new step OLR (0.1-0.3

mM). Methane content decreased by 3-4% as the OLR was increased. After the OLR was decreased, methane concentration increased rapidly, reached a peak value and then returned to the normal steady-state range (Figure VIII-11). Reactor pH also decreased slightly (0.2 pH unit) during the step OLR increases. Since the responses were relatively low, a high level of OLR perturbation was desired.

C-2. OLR variation at 5, 10, 15, 20, 25 kgCOD/m³bed-d

A second experiment for examining responses to a regular variation of OLR with the same frequency and duration of each step but at a higher amplitude in the OLR increase was conducted. The OLR was varied from 5 kgCOD/m³bed-d to 25 kgCOD/m³bed-d. The HRT was concurrently varied from 2.6 days to 22 hrs. Three perturbations were imposed upon the laboratory UASB reactor (Figure VIII-14). The gas production rate followed increases and decreases in OLR quite well. The CO concentration also increased and decreased in concert with OLR. The response of H₂ was low. A decrease in system performance was observed when the OLR was increased to 25 kgCOD/m³bed-d during the second and third perturbations. Gas production rate decreased from 1120ml/h at the peak rate of the second day (29-31 hrs) to 800 ml/h at the peak of the third perturbation (53-56 hrs). Maximum CO concentrations increased from 0.4 ppm (first and second perturbation) to 0.6 ppm (third perturbation; Figure VIII-15). A lag was observed in the response of CO to the perturbation. Effluent VFAs accumulated when the OLR was at its peak (Figure VIII-16). During the third day, acetate and propionate concentrations peaked at 0.5 mM compared to 0.28 mM and 0.12 mM, respectively, for the second day.

Butyrate and iso-butyrate were also observed in the effluent at this time (Figure VIII-16). Methane varied in a same pattern as for the previous experiment. It decreased gradually when the OLR was high and increased quickly when the OLR was decreased (Figure VIII-14). Reactor pH decreased slowly from 7.0 when VFAs were observed to accumulate, reaching 6.7 at the end of the experiment. There was no significant change in effluent VSS concentration during the initial two days. VSS concentration increased slightly during the third day (120 mg/L) from a level of 20 ppm and did not immediately return back to previous level once the experiment was discontinued and the OLRr maintained at the starting level of 5 kgCOD/m³bed-d (Figure VIII-17).

C-3. OLR variation at 10, 30, 40, 50, 60 and 104 kgCOD/m³bed-d

To examine the responses of random versus regular OLR variations, a four-consecutive-day experiment was conducted. Two types of variations: random and regular were applied, each for 24 hours. Random OLR variations were accomplished by a combination of steps (variable duration of 1 to 3 hrs) and impulses. The OLR ranged from 10-60 kgCOD/m³bed-d (at 104 kgCOD/m³bed-d during an impulse). The HRT was varied from 6 to 12.6 hours (with exception of impulse). The applied OLR and HRT during this experiment are presented in Figure VIII-18. A regular variation of OLR at 10 and 25 kgCOD/m³bed-d, with a fixed duration of 2 hours for each step increases, was first imposed on the system. This was followed by a random variation up to 30 kgCOD/m³bed-d in steps and an impulse of 104 kgCOD/m³bed-d. On the 3rd day, a high strength random variation was imposed on the reactor to push the system to its limit. The peak applied

OLR was increased up to 60 kgCOD/m³bed-d. Duration of each step increase at 30, 60 and 50 kgCOD/m³bed-d, respectively, was 3 hours. Immediately after this perturbation, a random variation similar to the one performed on day 2 was repeated to study the impact of the day 3 perturbation on the system.

The gas production rate had a distinct response pattern to OLR variations. It was one of the most sensitive variables tested (Figure VIII-19). Gas production rate closely followed the input pattern of OLR, although a 1 to 2 hours lag was observed. The total gas production was 11.9 liter on day 2 (20-34 hr) and 12.1 liter on day 4 (68-91 hrs). Under the strong perturbation conditions during day 3 (44-68 hrs) the gas production rate decreased to 68% of the theoretical potential production (growth was not included). This indicates the methanogens were probably overloaded. The methane production was estimated to be 0.28 m³CH₄/kgCOD removed for the third perturbation. Background methane production was 0.38 m³CH₄/kgCOD removed.

During this perturbation, H₂ responded to the changes in OLR (Figure VIII-18). A ca. 1 hour delay in response was observed. After the system had been significantly disturbed on day 3, H₂ had a slightly higher response to the random perturbation performed on day 4, compared to the same experiment performed on day 2 (Figure VIII-18).

CO appeared sensitive to both step and impulse of OLR perturbations (Figure VIII-19). Once CO accumulated it took an average of 10 hours to return to the initial level. On day 4 (68-91 hrs), during the repeated random perturbation, the CO concentration remained relatively stable at a level of 400 ppb. This could be the result of

stimulated CO dehydrogenase (CODH) activity during the heavy perturbation of day 3. The initial CO concentration was 500 ppb, higher than the expected level of 200 ppb. This may be the result of the system being exposed to air when a gas reservoir was installed and a gas valve replaced prior to initiating the experiment.

The effluent VFA did not have any strong response to the OLR during the low strength perturbations of days 1,2 and 4 (0-44 hrs and 68-91 hrs.; Figure VIII-20). On day 3, however, the high level OLR variation resulted in significant accumulation of acetate, propionate, COD and higher molecular weight VFAs including iso-valerate, n-valerate, iso-butyrate, n-butyrate and 2-methyl-butyrate (Figure VIII-20 and 22). A mass balance performed on the system showed that the majority of effluent soluble COD came from acetate and propionate. Since the reactor effluent suspended solids were very low during this experiment (Figure VIII-21), soluble COD was due primarily to the effluent VFAs. VFAs began to accumulate significantly when the OLR was increased from 30 kgCOD/m³bed-d to 60 kgCOD/m³bed-d, during the third perturbation. The VFA concentration continued to increase even when the OLR was decreased down to 50 kgCOD/m³bed-d, indicating that the acetoclastic methanogens were unable to keep pace with acetate production. Acetate and propionate reached peak concentrations of 14 mM and 5 mM (COD of 1450 mg/L), respectively, by 54 hrs. VFAs with 4-5 carbons such as butyrate, iso-butyrate, 2-methyl-butyrate, valerate, iso-valerate were detected when acetate and propionate concentrations were high (Figure VIII-22). Once the perturbation was stopped (OLR decreased back to 10 kgCOD/m³bed-d), the concentrations of VFAs decreased.

Methane content, pH and suspended solids exhibited weak response during the first and second OLR perturbations (0-44 hrs; Figures VIII-19 and 21). Under the high strength OLR perturbation of day 3 (44-68 hrs), methane content decreased continuously from 75% to 65% over 10 hours until the perturbation was stopped. The pH declined from 7.0 to 6.2, during this period. Methane content and pH recovered after 10 and 5 hours, respectively. The random variation repeated on day 4 (68-91 hrs) had a stronger impact on these variables. Methane concentration decreased by 5% during this period compared to during the identical random variation of day 2 (20-44 hrs) when methane remained quite stable at 75%. The pH decreased to a lower level and remained at that level longer than for the first random variation.

The response observed for suspended solids was again the slowest and the most insensitive to OLR variation. A slight increase in both total suspended solids (TSS) and volatile suspended solids (VSS), both below 100 mg/L level, was observed during the experiment. The VSS/TSS ratio was 0.8 indicating the TSS was essentially all biological in nature. The granular sludge bed was stable throughout the four day period. Breakdown of the granules and appearance of flocs within the bench-scale UASB was observed ca. two weeks after the experiment. Whether this was related to the experiment is not clear.

The perturbations due to regular and random variations at low OLR levels during the initial two days were insufficient to significantly perturb system performance as judged by accumulation of effluent VFAs. The strong random variation performed during day 3 (44-68 hrs) did result in a significant response, reflected by the accumulation of effluent acetate and propionate (>10 mM and 5mM, respectively ;Figure VIII-20). Effluent COD

accumulation (1450 mg/L; Figure VIII-20) as well as the appearance of 4 and 5 carbon compounds (Figure VIII-22) was also observed. Gas production, methane concentration and pH all decreased (Figures VIII-18, 19 and 21). These results demonstrated that a high strength OLR (i.e. 50-60 kgCOD/m³bed-d) perturbation applied to a UASB reactor for more than 6 hours had a pronounced effect on the system. If continued this loading rate could lead to system failure.

The random variation performed on day 4 after the strong disturbance on the system had a greater effect on methane, pH, CO and H₂ than the same variation performed on day 2 (Figures VIII-18 and 19). Gas production, effluent VFA and COD didn't significantly differ between days 2 and 4. Results suggested impulse, random and regular variation at low OLR had relatively weak impact on system performance while step increases at high strength and longer duration could perturb the system significantly. Such a perturbation experiment was desirable to study the behavior of trace gases and reactor performance at extreme conditions.

C-4. OLR variation at 10, 30, 40, 50, 60 kgCOD/m³ bed-d

An unsteady state OLR regular variation experiment (a repeat of the perturbation three in previous experiment, but with an increased duration of each step) was performed. This was done to examine the maximum OLR level that the system can stand, system recovery and the response of system variables. The OLR was increased from 10 to 30, 40, 50 and 60 kgCOD/m³ bed-d (Figure VIII-23). The HRT was varied from 11 to 5.3 hours

(Figure VIII-23). The duration of each step was 24 hours increased from 3 hours used for the prior experiment (see C-3).

Initial results are shown in Figure VIII-23 to 27. Performance of the bench-scale UASB reactor was markedly affected by the increased duration and strength of the OLR step increases used in this experiment. The H_2 concentration increased to over 1000 ppm from a starting value of 200 ppm; the pH decreased to 5.2 from 7.0, VFAs accumulated, and gas production rate decreased at an OLR of $60 \text{ kgCOD/m}^3 \text{ bed-d}$. The methane content decreased from 83% to 75% during this period. The presence of 3, 4, 5, carbon and higher molecular weight compounds, such as butyrate, valerate, 2-methyl-butyrates, propanol and ethanol, was observed. The step down from 60 to $50 \text{ kgCOD/m}^3 \text{ bed-d}$ was not completed because of imminent reactor failure. Two hours after the step down to $50 \text{ kgCOD/m}^3 \text{ bed-d}$ ($t=72-74 \text{ hrs.}$), gas production rate continued decreasing while VFAs continued accumulating; H_2 (g) remained at $>1000 \text{ ppm}$ and the pH continued to decline. To observe the system recovery, the shock loading was terminated by reducing the OLR to the initial $10 \text{ kgCOD/m}^3 \text{ bed-d}$ level (at $t=75 \text{ hrs.}$). Most monitoring variables, including H_2 , CO , gas production rate, pH, VFAs, returned to near steady state levels within 10-20 hrs.

The pattern of gas production rate followed the OLR during the first and second OLR steps (30 and $40 \text{ kgCOD/m}^3 \text{ bed-d}$) and remained at 1.0 L/h and 1.18 L/h , respectively (Figure VIII-24). When the OLR was set to $60 \text{ kgCOD/m}^3 \text{ bed-d}$, the gas production rate increased to 1.4 L/h then began to decline. This decrease in gas production even continued 3 hours after the OLR was stepped down to the original OLR

(10 kgCOD/m³ bed-d). Gas production peaked again at t=81 hours due to the consumption of accumulated VFAs, ethanol and propanol. It took 20 hours for the gas production rate return to the background level.

H₂ essentially tracked OLR (Figure VIII-24). H₂ concentration reached 1000 ppm level at an OLR of 60 kgCOD/m³ bed-d. Two hours after the OLR was reduced to 10 kgCOD/m³ bed-d, the H₂ concentration started to decrease. It took 12 hours for the H₂ (g) concentration to return to its background level. The response pattern of H₂ was different from that of gas production rate during the period from 65 to 95 hours, when the system was near failure and the subsequent decrease in OLR and recovery.

It appeared that CO increased in responding to each OLR step and then stabilized at a certain level. Headspace CO increased initially and then stabilized at 200 ppb for the first and second steps (30 and 40 kgCOD/m³ bed-d; Figure VIII-24). The CO concentration reached 300 ppb when the OLR was increased to 60 kgCOD/m³ bed-d. During the system recovery, CO peaked between 79 and 90 hours, similar to gas production rate. This peak may be caused by the degradation of high concentration of acetate accumulated during shock loading. CO had more fluctuation during the recovery than during the OLR step increase period compared to H₂. It took 20 hours for CO to return to background levels.

Methane was the slowest of the gaseous components measured in responding to the perturbation. The OLR step increases to 30 and 40 kgCOD/m³ bed-d did not cause any change in methane content. Methane content was reduced by 3% by the end of 60 kgCOD/m³ bed-shock loading. A significant decrease and then rapid increase of methane content to 70% and 78% were observed after the step down in OLR (77 -81 hrs). A new

level of 76% in methane content was established $t=95$ hours. Return of methane content to the original (pre-shock) level did not occur until 2 weeks later.

Ethanol and n-propanol were the major alcohol components found in the effluent (Figure VIII-26). Both ethanol and n-propanol had identical response curves. Their concentrations reached peak values (1.5 mM and 1.2 mM, respectively) at the 73 hour mark when the reactor system approached failure. The concentration of these alcohols decreased immediately after the OLR was decreased.

Most high molecular weight acids (with the exception of iso-butyrate and iso-valerate) exhibited similar response patterns during the second and third steps of OLR increase and during recovery. All VFAs measured appeared in the effluent during the second step OLR increase and disappeared at the 81-82 hour mark. Acetate concentration increased in accordance with OLR (Figure VIII-25) except the first step. After an initial increase at the second step in OLR, acetate concentration stabilized at 4 mM (from 30-48 hrs). The third step in OLR resulted in acetate reaching a concentration of 20 mM.

Fourteen hours after operation at this step (62 hrs), $60 \text{ kgCOD/m}^3 \text{ bed-d}$, a rapid increase in acetate concentration was observed. When the OLR was reduced to the background level, acetate decreased from 55 mM to 0.1 mM in a period of 10 hours. The response of propionate was similar to that of acetate except concentrations were lower (Figure VIII-25). OLR steps to 40 and $60 \text{ kgCOD/m}^3 \text{ bed-d}$ resulted in an increase in propionate concentration to 3 mM and 8 mM, respectively. A peak of 10 mM was observed at 72 hours. The reduction in propionate concentration was also rapid after the OLR was decreased. Propionate concentration decreased to its background level in less than 10

hours. Butyrate had the same pattern of variation as acetate (Figure VIII-25) during the perturbation. An initial increase followed by a stable concentration during the second step OLR of $40 \text{ kgCOD/m}^3 \text{ bed-d}$. Butyrate reached 1.5 mM at about 71 hours as system failure proceeded and it returned to background level in 7 hours once the perturbation was lifted. Iso-butyrate was not present at equal concentrations with butyrate when butyrate concentration exceeded 0.2 mM (Figure VIII-25). The variation in the five carbon fatty acids, i.e., valerate, iso-valerate and 2-methyl-valerate, is presented in Figure VIII-26. Both valerate and 2-methyl-butyrate varied in an identical pattern. A peak of 0.2 mM and 0.17 mM (2-methyl-butyrate and valerate, respectively) was observed at 72 hours.

Little variation in pH was observed during the first and second steps of OLR (Figure VIII-27). During the $60 \text{ kgCOD/m}^3 \text{ bed-d}$ OLR operational period, pH gradually decreased from 7.0 to 5.9 by 71 hrs. A significant decrease of pH to 5.2 within three hours (71-74 hrs) occurred which signaled a system failure. Immediately after the shock loading was lifted, pH increased back to 7.0 in 10 hrs.

D. Discussions

The behavior of H_2 and CO were quite different during the pseudo-steady state experiments. At a low OLR (4-6 kgCOD/m³bed-d) the mean response level of H_2 did not exceed 30 ppm (Table VIII-7). When the reactor was operated at higher OLRs (≥ 10 kgCOD/m³bed-d) and longer HRTs (>1 d) the mean of H_2 concentration surpassed 100 ppm. Although the mean of the H_2 concentration increased with increased OLR to some degree, and acetate followed OLR well, the bivariate plot of H_2 and acetate appeared scattered (Figure VIII-4). H_2 had no correlation with any other variables monitored (Figure VIII-10). Sensitive but high background noise of H_2 during pseudo-steady state indicated from its CV and standard error value (Table VIIB-6) could contribute to this phenomena.

By contrast, CO had moderate variations and low background noise (Table VIII-6). The mean of CO concentration remained at 0.1 ppm at low OLR (4-6 kgCOD/m³bed-d), and reached a high value of 0.59 ppm at a high OLR (23 kgCOD/m³bed-d). The mean of CO increased in response to increased OLR (Figure VIII-6). CO correlated with other monitoring variables except H_2 (Figure VIII-10). Although correlated with acetate, CO did not show a particular pattern when varied with acetate (Figure VIII-3). This could be caused by the mass transfer limitation of dissolved CO gas to the head space, the variation of degree of the limitation which has wide range (Table VIIB-11) and the variation of methanogenic activity.

During OLR perturbations, when repeat the same type and level of OLR variation following a strong perturbation (i.e. 60 kgCOD/m³bed-d), responses of H_2 increased while

the response of CO decreased. H₂ was very sensitive to high OLR but had no observable pattern at low OLRs. CO tended to stabilize at a new slightly higher level after an initial increase in OLR step. When system failure occurred, H₂ reached a high level of 10x of its pseudo-steady state concentration. CO, however, did not show significant increase until 24 hours later.

Mean analysis of pseudo-steady state data from the bench UASB reactor indicated all monitoring variables, acetate, propionate, gas production rate, methane content, pH, hydrogen and carbon monoxide varied with OLR (Table VIII-6). This was confirmed by analysis of variance (Table VIII-9). Results from both analysis show that gas production rate, CO, methane content, acetate and propionate, in general, were different between low and high OLRs (Figure VIII-5,6,9, Table VIII-10), suggesting a possible threshold could exist at certain OLRs for acetate, propionate, CO and CH₄. For gas production, however, due to its close coupled behavior to OLR(Figure VIII-5), the threshold concept is not applicable. Acetate, propionate, gas production and CO generally increased with increased OLR. CH₄ varied in the opposite direction.

Results demonstrate that OLR variation using either feed concentration (at constant HRT) or feed rate (at constant feed concentration) did not have a great impact on system response and trace gases CO and H₂. Feed concentrations or HRT influenced the responses of monitoring variables to a much small extent. The feed concentration did not have any significant effect on the observed system responses (OLR 10 kgCOD/m³bed-d, Table VIII-7). The impact of HRT was not consistent.

Acetate, propionate and methane content, CO and gas production rate were closely correlated. The correlation was positive for most monitoring variables except with methane content (Figure VIII-10). These variables varied with OLR; the negative correlation of methane content in response to OLR can also be seen in Figure VIII-5.

The maximum frequency of each monitoring variable seems to be independent of the OLR imposed onto the system (Table VIII-3). Based on results from frequency analysis, no cyclic pattern was detected for gas production, H₂, CO, methane, acetate and propionate. The variations of all monitoring variables were primarily caused by random noise or background fluctuations in the system, concluded from white noise test. Similar results were obtained from a separate cross-correlation test; there was no clear cross-correlation between pairs of monitoring variables due to lack of periodicity.

Results demonstrated that the pseudo-steady state brewery waste biodegradation can be described using Gibb's free energy. The free energy levels were relatively stable throughout the operation despite the OLR variation. H₂ and CO present in the headspace did not necessarily represent the concentration in the liquid phase that the microorganisms actually experienced. Gibb's free energies based on dissolved gas concentration varied significantly from calculations based on head space concentration, suggesting energetical analysis is not a means of a good tool for monitoring. For both H₂ and CO, liquid phase and head space are not at equilibrium (Table VIIIB-11). It is not surprising, therefore, that no clear cut correlation between head space H₂ and CO and OLR was observed.

Results from four sets of OLR perturbation experiments indicated that the strength, and duration of each step increase in OLR had a strong impact on the bench

UASB reactor. The reactor was able to accept OLR's up to 40 kgCOD/m³bed-d without any significant deterioration in process performance. An OLR of 60 kgCOD/m³bed-d can perturb the system performance significantly. The system can withstand this OLR and maintain a pseudo-steady state level for the maximum of fourteen hours before becoming instable. During this time period, system variables, such as VFAs, exhibited relatively steady concentration levels with little fluctuation. Once the reactor buffering capacity was exhausted, or microbial populations were over stressed, the dynamic balance no longer held and intermediates started to accumulate linearly.

During the time period when reactor performance began to fail, gas production, VFAs and H₂ were among the most sensitive variables to show changes. Methane content was the least sensitive. Gas production rate decreased from its steady state level; acetate and propionate concentration rapidly accumulated. During this period higher molecular weight VFAs appeared and the major substrate, ethanol, was not completely degraded. As a result, pH decreased significantly (5.2) and a high H₂ (1000 ppm) environment developed. These unfavorable conditions prevented both methanogenesis and acetogenesis from proceeding, finally leading to system failure.

During system recovery, a high peak of CO (15.7 ppm) appeared followed by a peak of gas production (Figure VIII-24), suggesting rapid increase of acetate oxidation and methanogenic activity. Alcohols and VFA concentration were immediately decreased which resulted in the pH increasing. Gas phase components recovered slowly compared to that of aqueous phase components. VFAs and pH were back to their original levels within 5 and 10 hours, for OLRs of 10-104 and 10-60 (24 hours steps), respectively. Gas

production rate, CO , H_2 and CH_4 returned to background concentrations in 10 and 20 hours, for OLRs of 10-104 and 10-60 (24 hours steps), respectively. The sequence of recovery after an OLR of $60 \text{ kgCOD/m}^3\text{bed-d}$ perturbation, for each component was: alcohols and long chain VFAs > acetate and propionate > pH > H_2 > gas production rate and CO > methane. This correlates to the sequential reactions expected.

CO is an intermediate in methanogenesis from acetate (Figure VIIC-18).

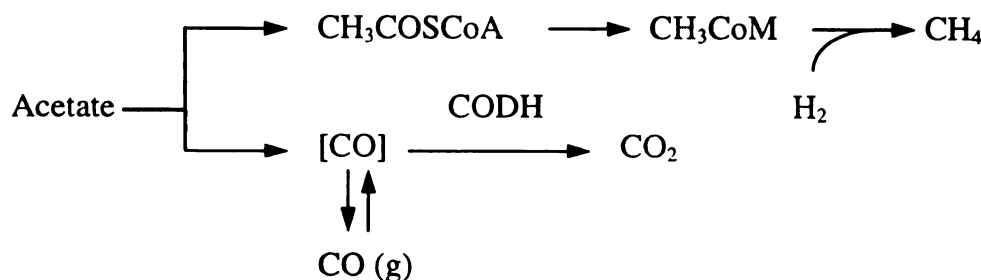


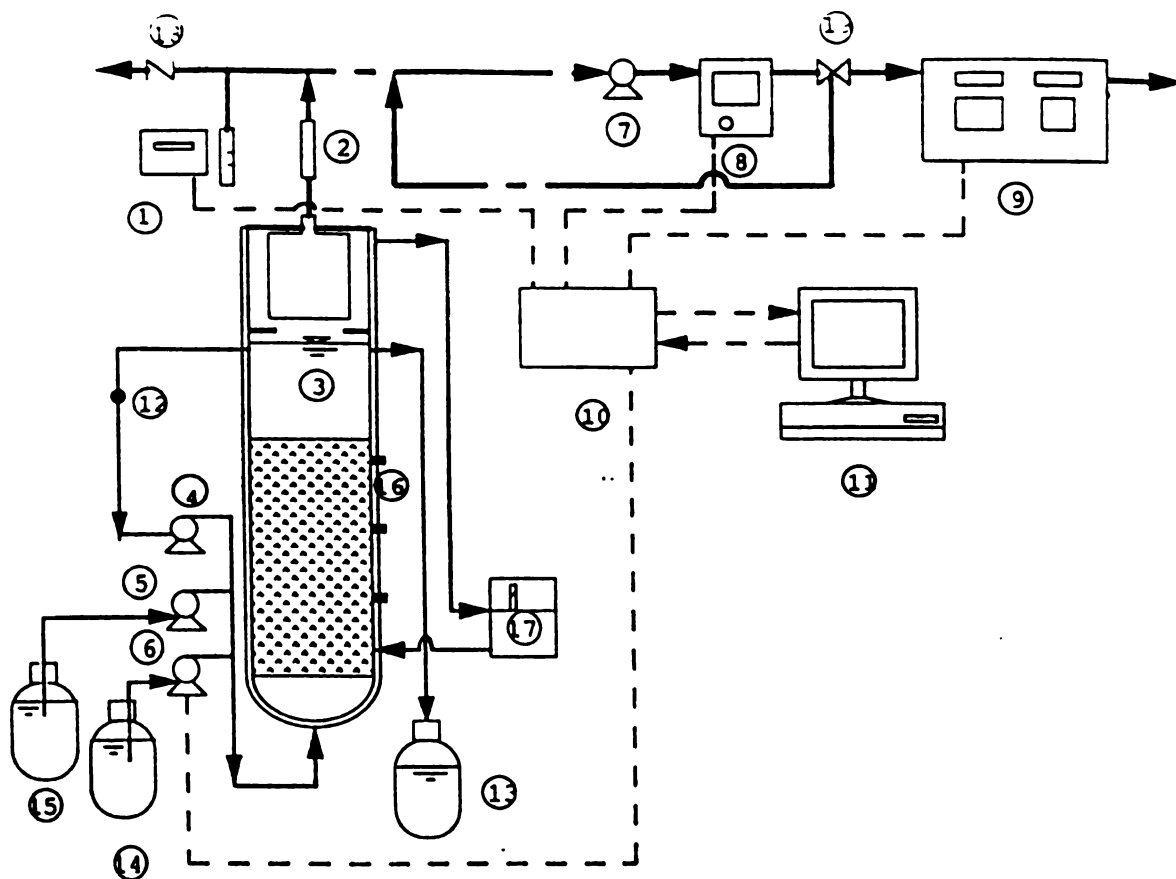
Figure VIIC-18. Carbon monoxide gas production from acetoclastic methanogenesis

CO accumulation took much longer than H_2 to return to its initial level, suggesting that the reaction $\text{CO(g)} \rightarrow [\text{CO}]$ does not readily occur. The reduction of CO(g) concentration is likely due to dilution of the reactor headspace with the gases being produced rather than consumption, as occurred with H_2 .

A low level impulse and an impulse of $104 \text{ kgCOD/m}^3\text{bed-d}$ did not have a major impact on system performance, except gas production and CO (Figure VIII-19). There

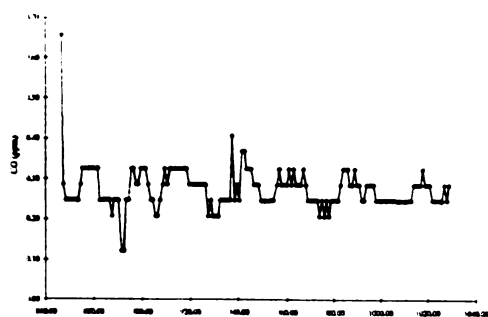
was no clear difference between the influence of regular and random variations of OLR on the UASB reactor performance.

Both pseudo-steady state and unsteady state experiments showed a consistent trend of monitoring variables with OLR. At low strength OLR variations (5-25 kgCOD/m³bed-d), responses were small. When OLR was increased to 60 kgCOD/m³bed-d, responses of VFAs, H₂, CH₄, pH and gas production increased dramatically. Acetate, propionate, CO and gas production rate followed OLR. CH₄ decreased when OLR increased. pH gradually decreased as the experiment was proceeded. Suspended solids and CH₄ varied slightly.

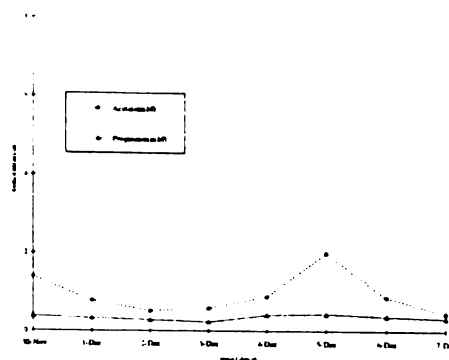


- | | | |
|---------------------------|------------------------|---------------------------------------|
| ① gas counter | ⑨ trace gas analyzer | ⑰ water bath |
| ② moisture condensor | ⑩ D/A interface. | ⑱ gas vent valve |
| ③ laboratory UASB reactor | ⑪ PC control | ⑲ gas split valve |
| ④ recycle pump | ⑫ liquid sampling port | |
| ⑤ media pump | ⑬ effluent | — liquid line |
| ⑥ feed pump | ⑭ feed | — gas line |
| ⑦ gas pump | ⑮ media | - - - data acquisition & control line |
| ⑧ methane analyzer | ⑯ sludge waste | |

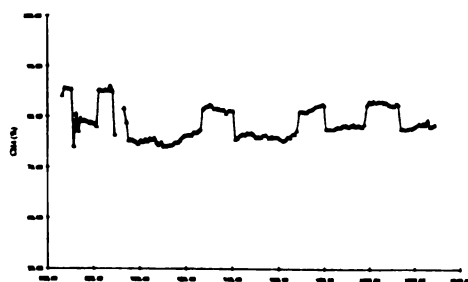
Figure VIIIB-1. Schematic representation of the bench-scale UASB reactor with on-line data acquisition system.



(a)



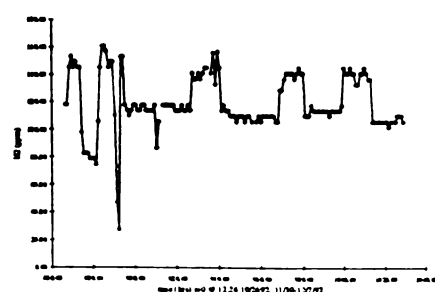
(d)



(b)



(e)



(c)

Figure VIIIB-2.

Typical profiles of (a)CO, (b)methane (c)H₂ (d)acetate and propionate, and (e)gas production rate at pseudo-steady state. (OLR 15 kgCOD/m³bed-d, HRT 1.5d, feed concentration 13.7 kgCOD/m³). Time scale: (a)-(d) in hrs; (e) in days. Data collected from Nov.30 to Dec.7,1992.

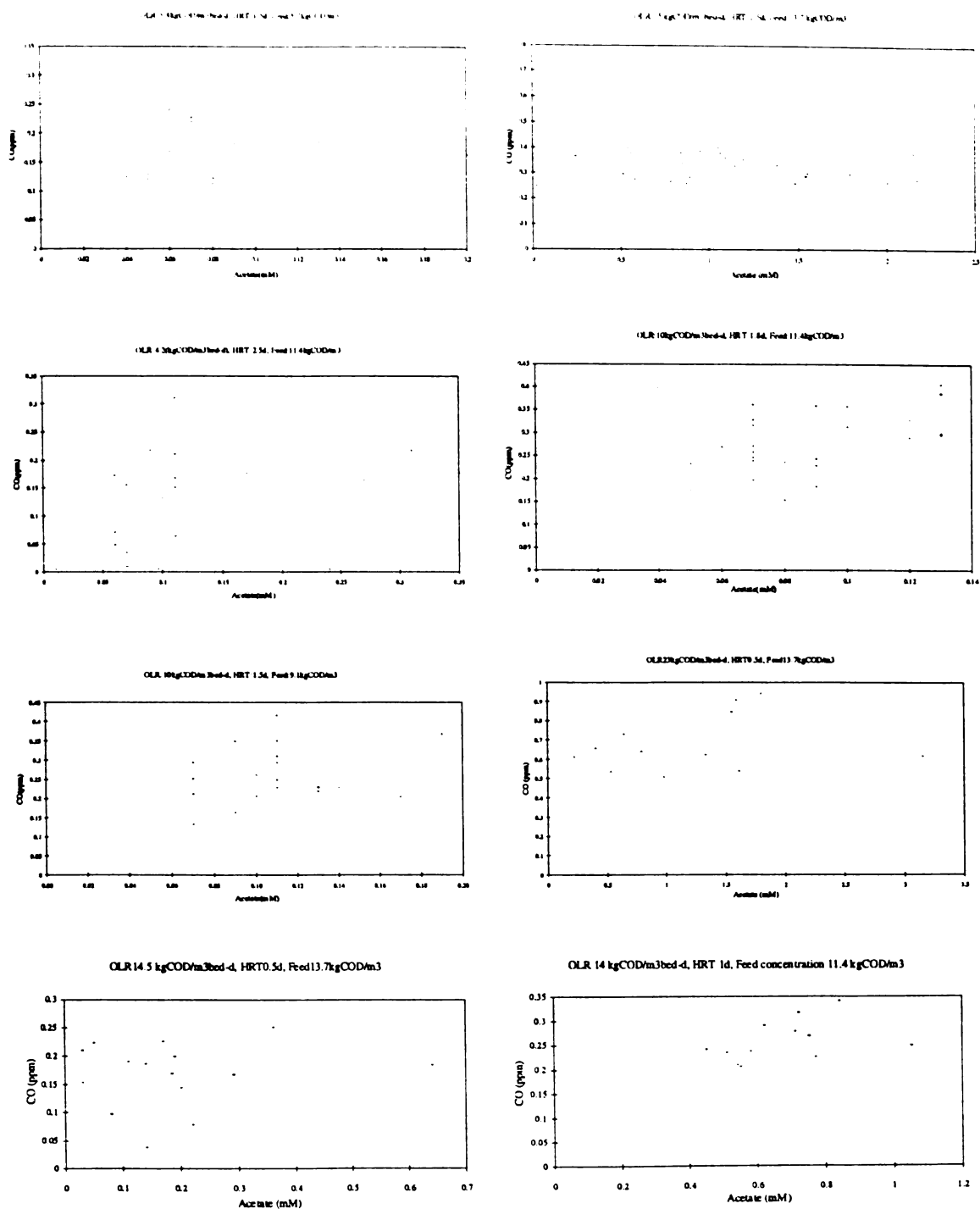


Figure VIIB-3. Bivariant plot of CO versus acetate at each pseudo-steady state

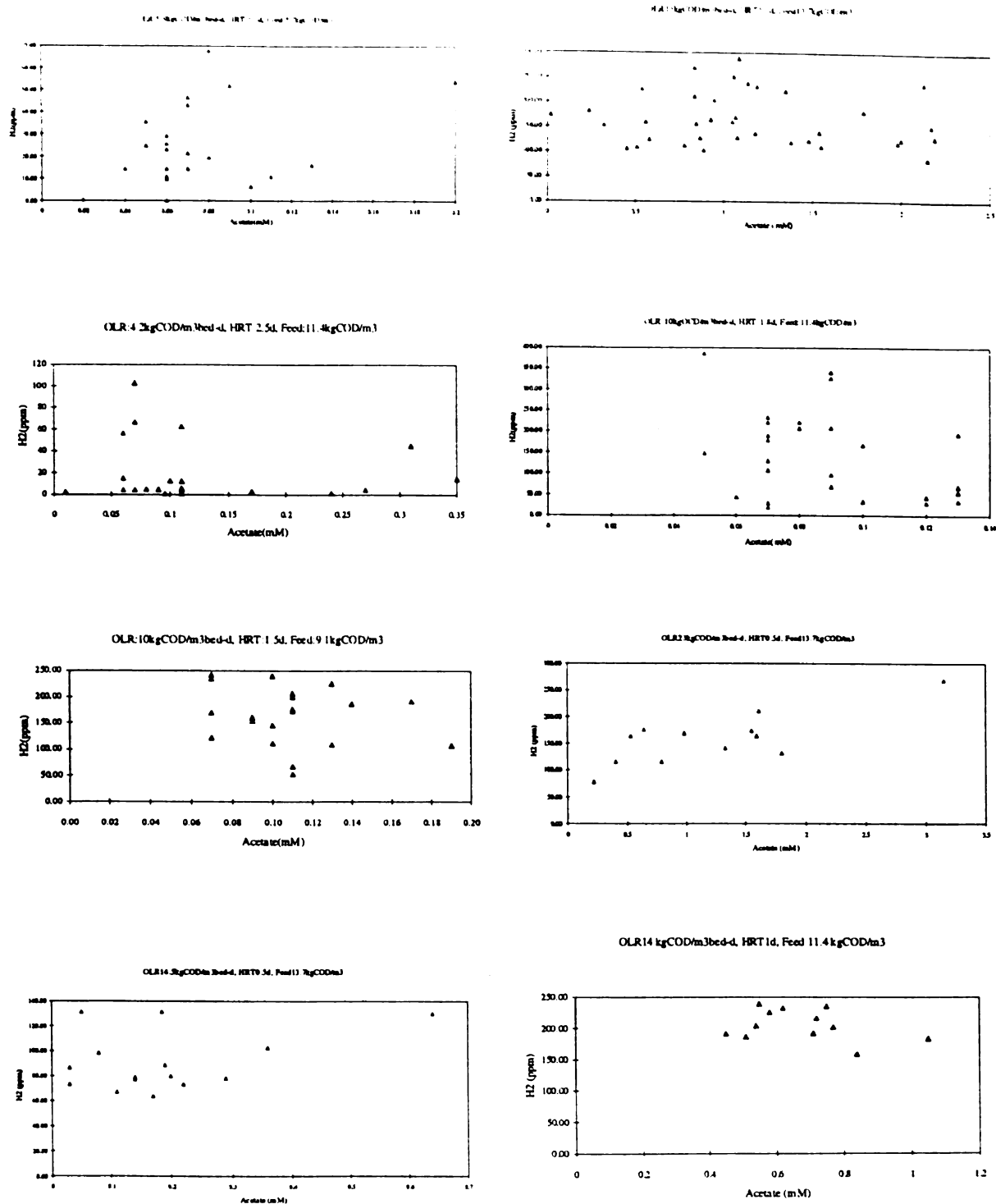


Figure VIIB-4.

Bivariant plot of H_2 versus acetate at each pseudo-steady state

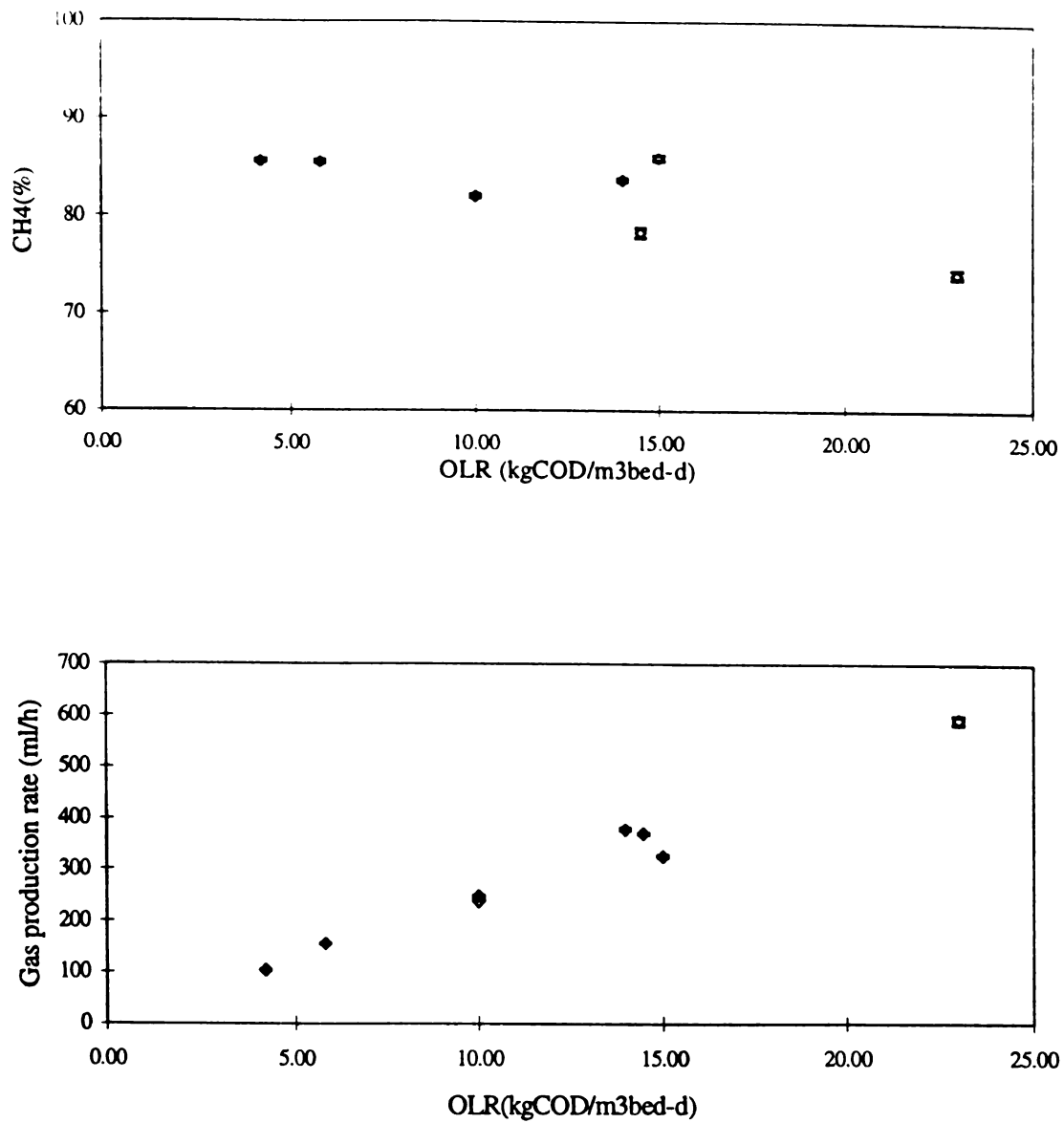


Figure VIIB-5. Mean and confidence intervals of methane and gas production during pseudo-steady state operation. bars represent 95% confidence intervals.

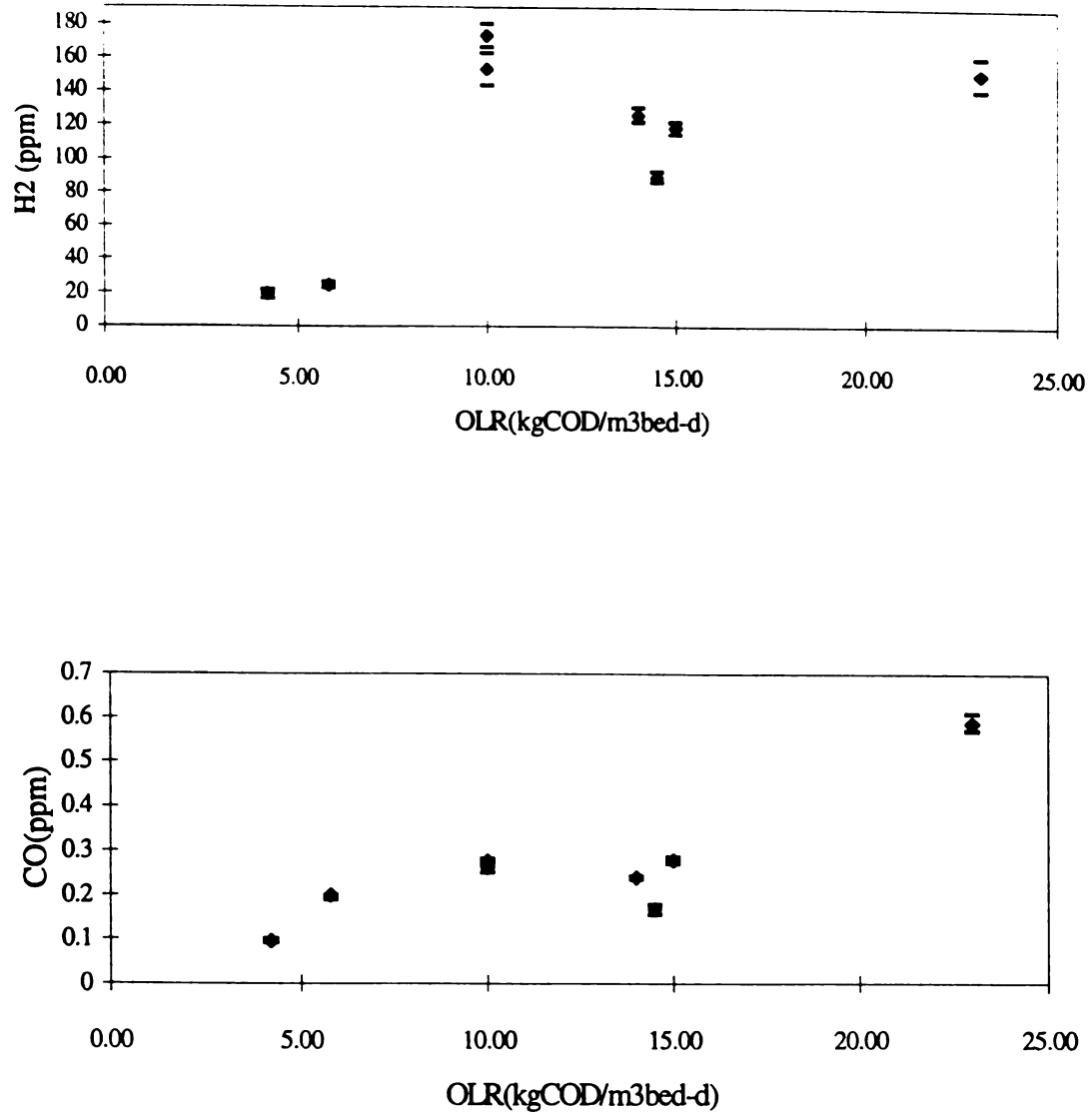
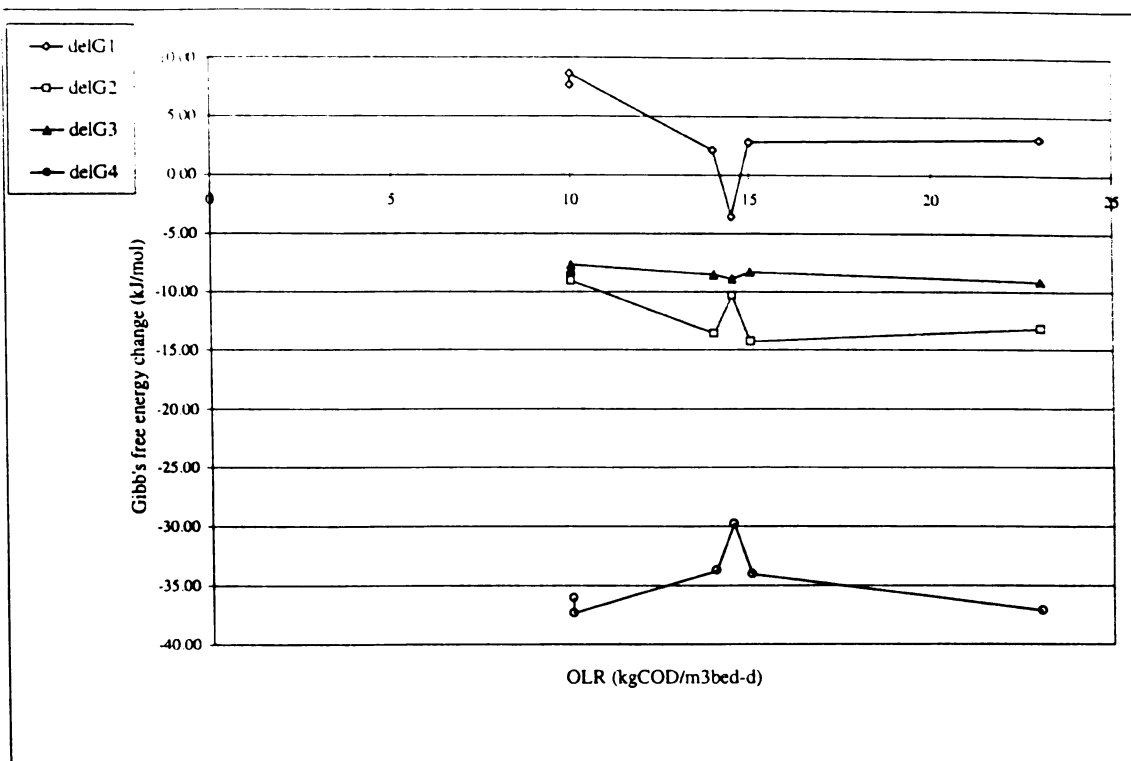
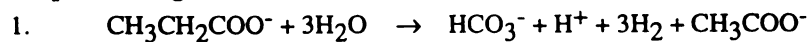


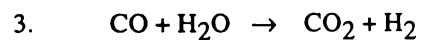
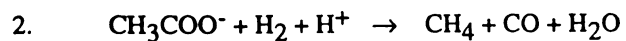
Figure VIIB-6. Mean and confidence intervals of H_2 and CO during pseudo-steady state operation. bars represent 95% confidence intervals.



Propionate degradation



Acetate degradation



CO₂ reduction

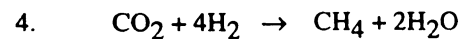
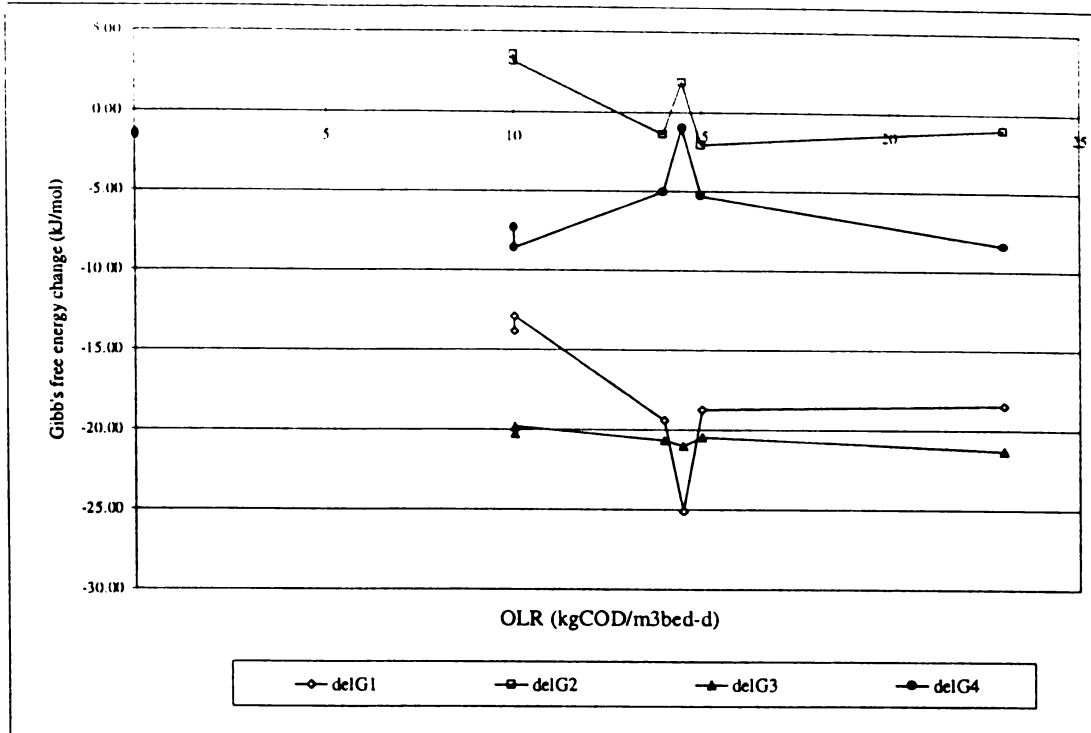
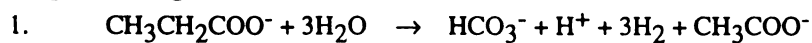


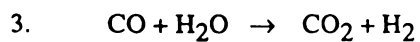
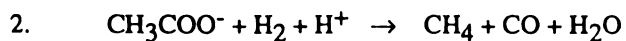
Figure VIII B-7. Free energy change of propionate oxidation and methanogenesis during pseudo-steady state operation. (head space CO and H₂ used for calculation)



Propionate degradation



Acetate degradation



CO₂ reduction

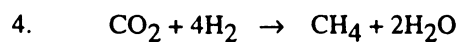


Figure VIIB-8.

Free energy change of propionate oxidation and methanogenesis during pseudo-steady state operation. (dissolved CO and H₂ used for calculation. CO and H₂ were head space concentrations in equilibrium with measured dissolved gas concentrations)

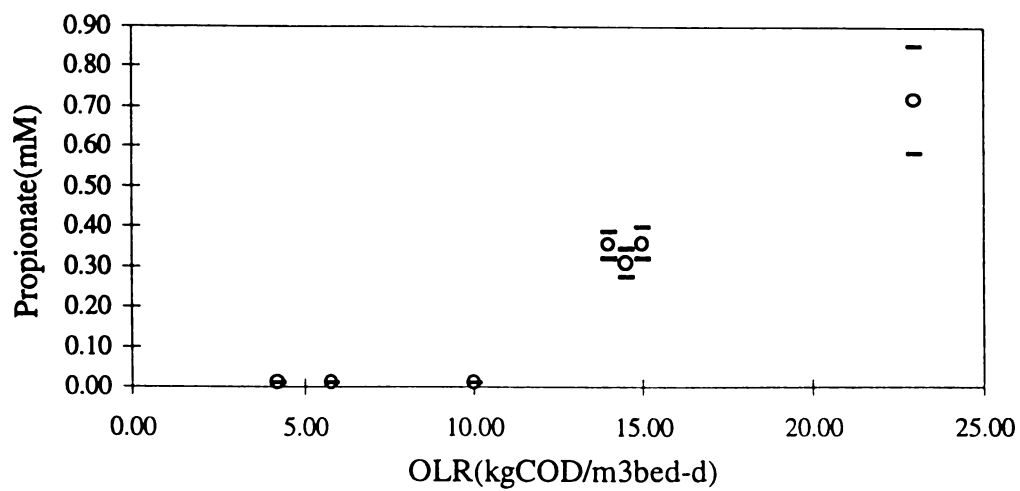
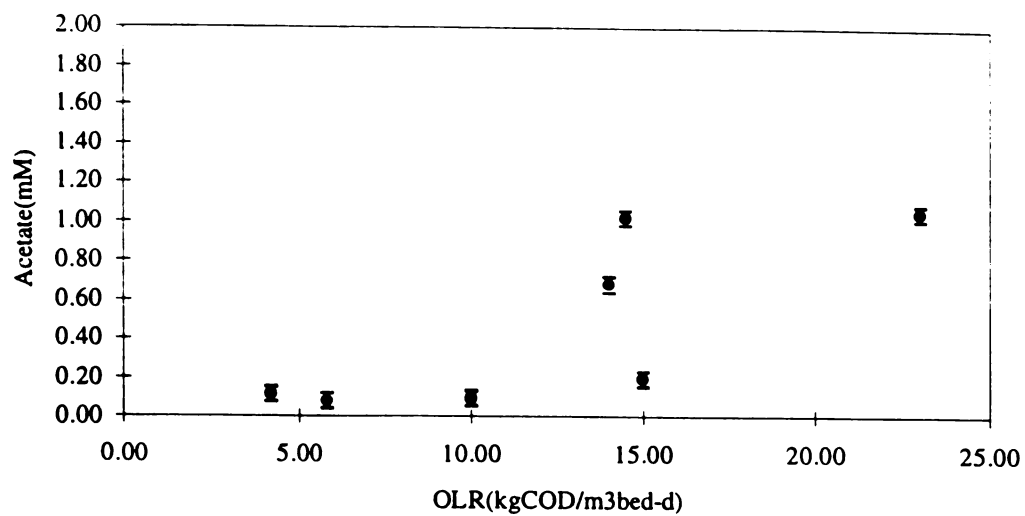


Figure VIIB-9. Mean and confidence intervals of acetate and propionate during pseudo-steady state operation. bars represent 95% confidence intervals.

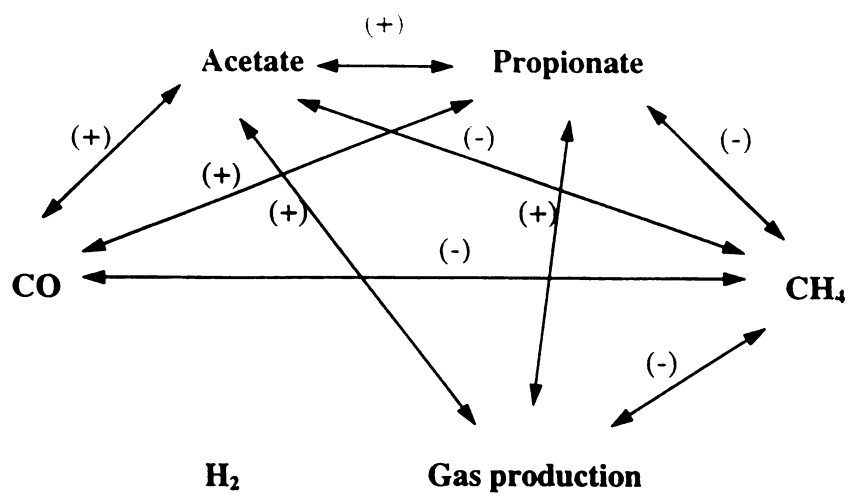


Figure VIIB-10. Schematic diagram of correlations among monitoring variables at pseudo-steady state operations (based on results from correlation analysis; (+) – positive correlation; (-) – negative correlation; correlation test at $\alpha=0.01$)

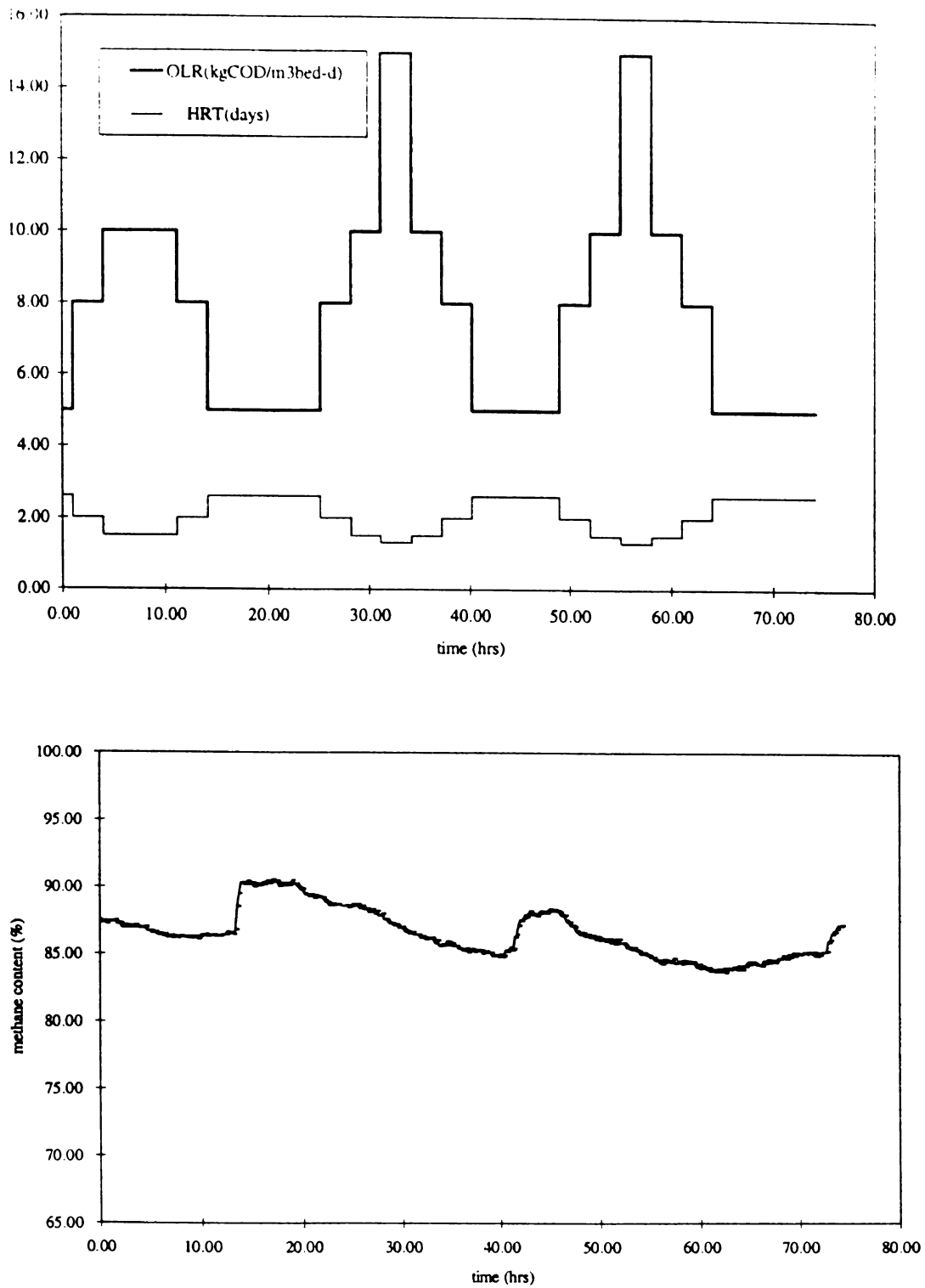


Figure VIII-1. Applied OLR and HRT and reactor methane content variation during OLR loading variation experiments (OLR: 5-15kgCOD/m³bed-d)

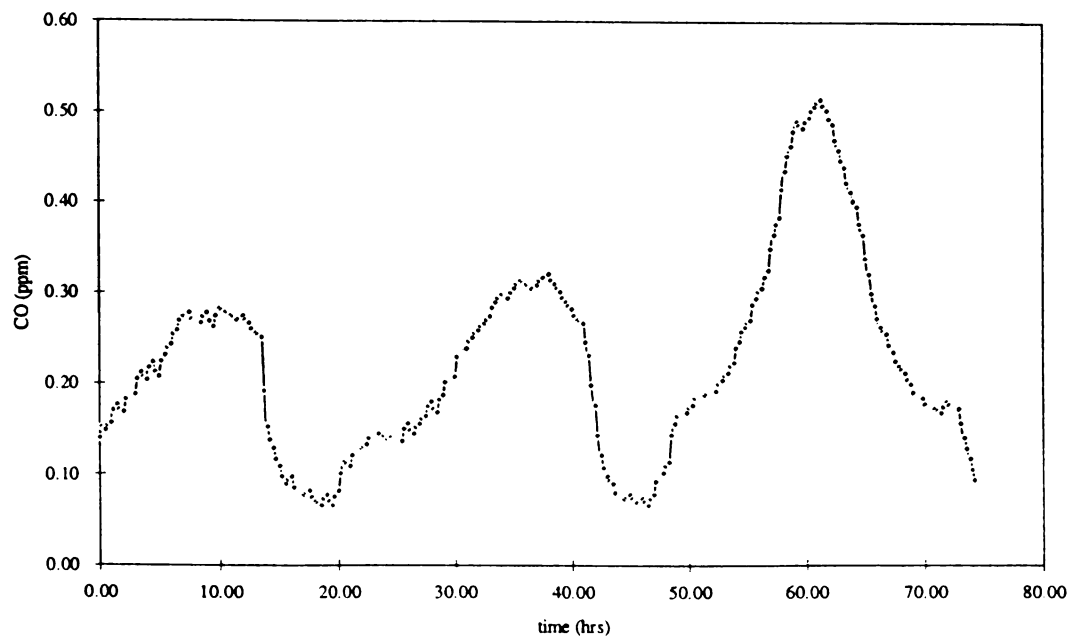
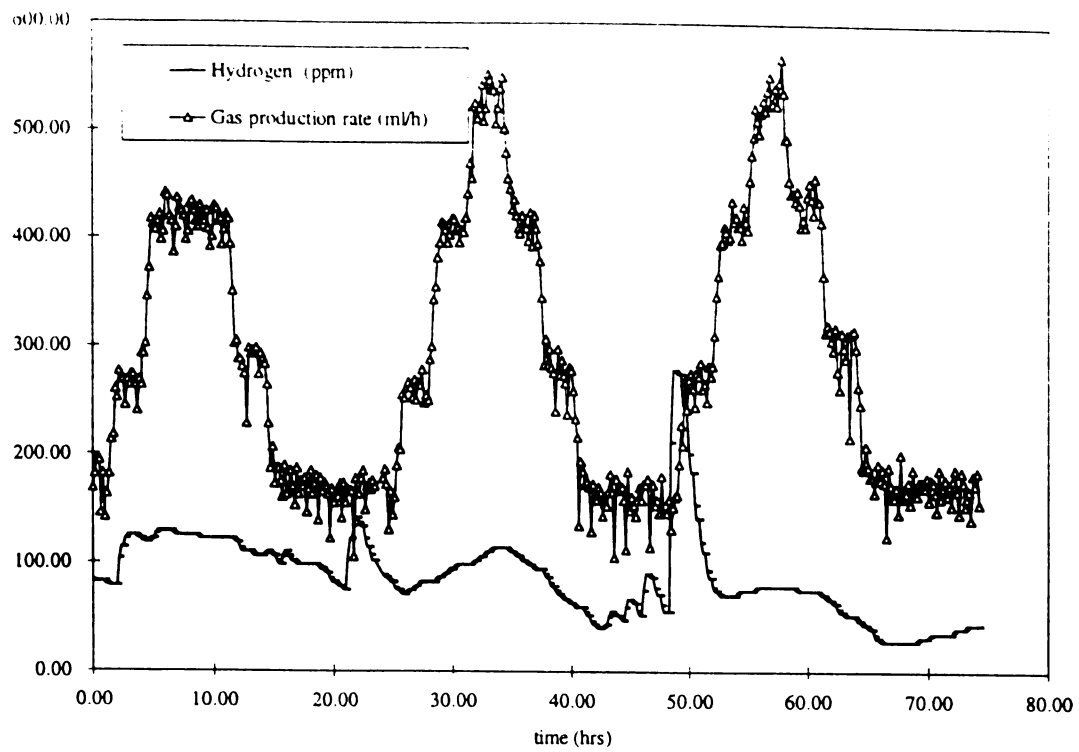


Figure VIIC-2. Hydrogen, carbon monoxide and gas production rate during loading variation experiments (OLR: 5-15 kgCOD/m³bed-d)

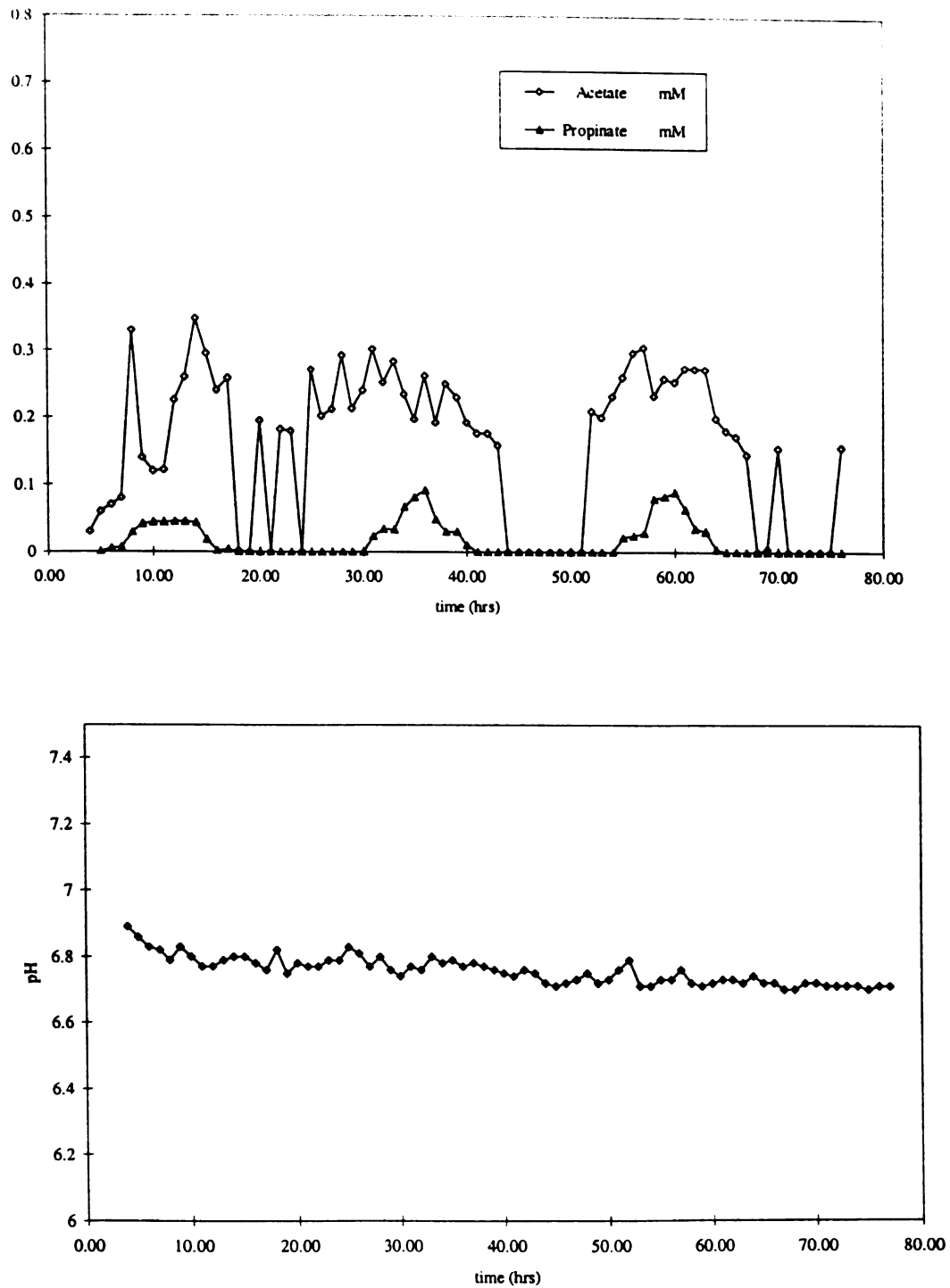


Figure VIIC-3. Acetate, propionate and pH during variation experiments (OLR: 5-15 kgCOD/m³bed-d)

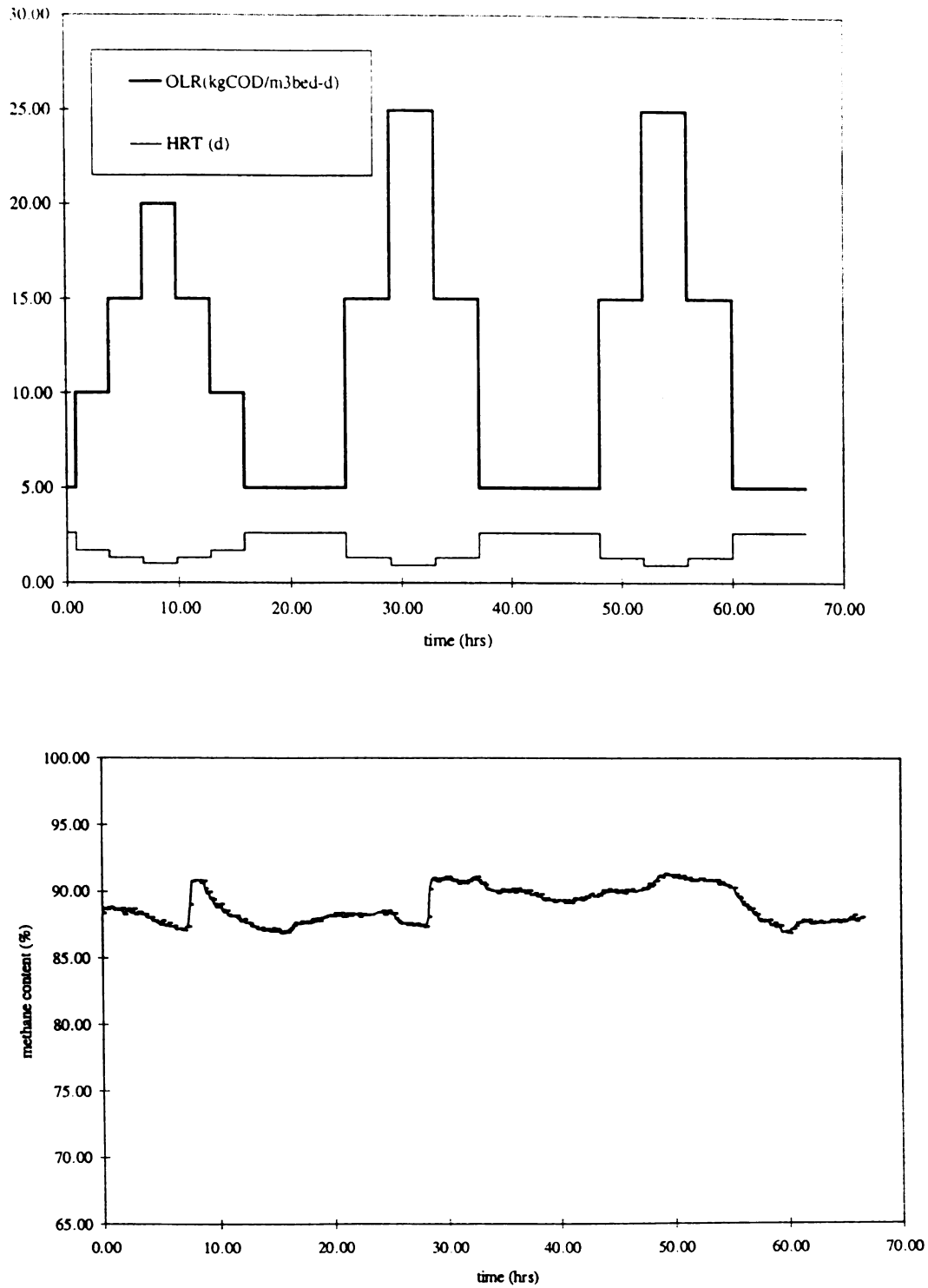


Figure VIIC-4. Applied OLR and HRT and reactor methane content variation during OLR loading variation experiments (OLR: 5-25 kgCOD/m³bed-d)

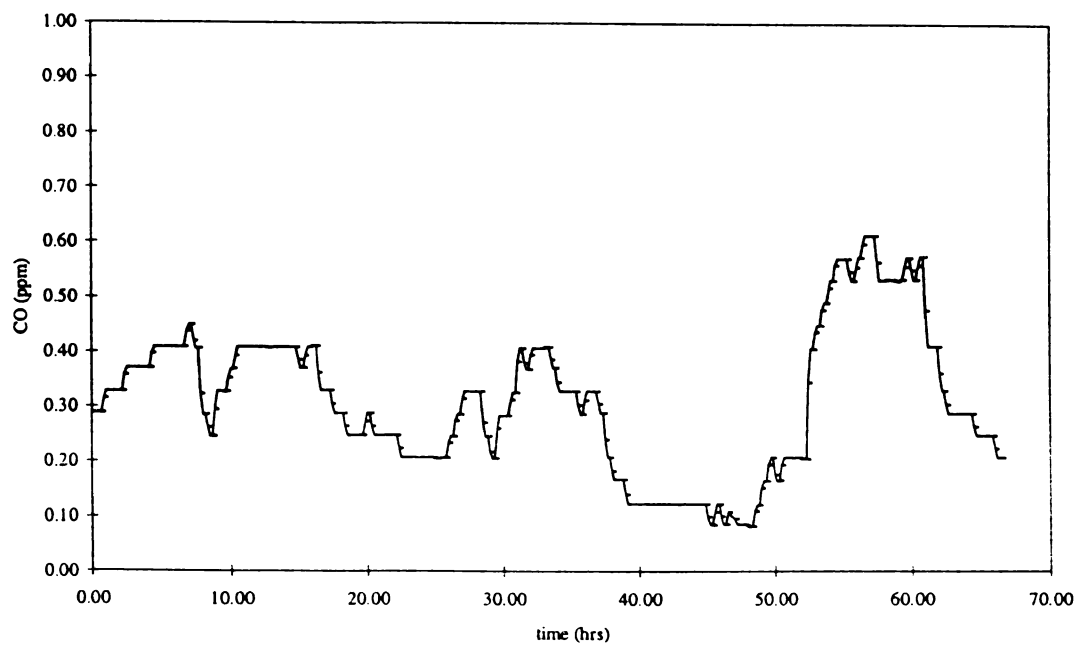
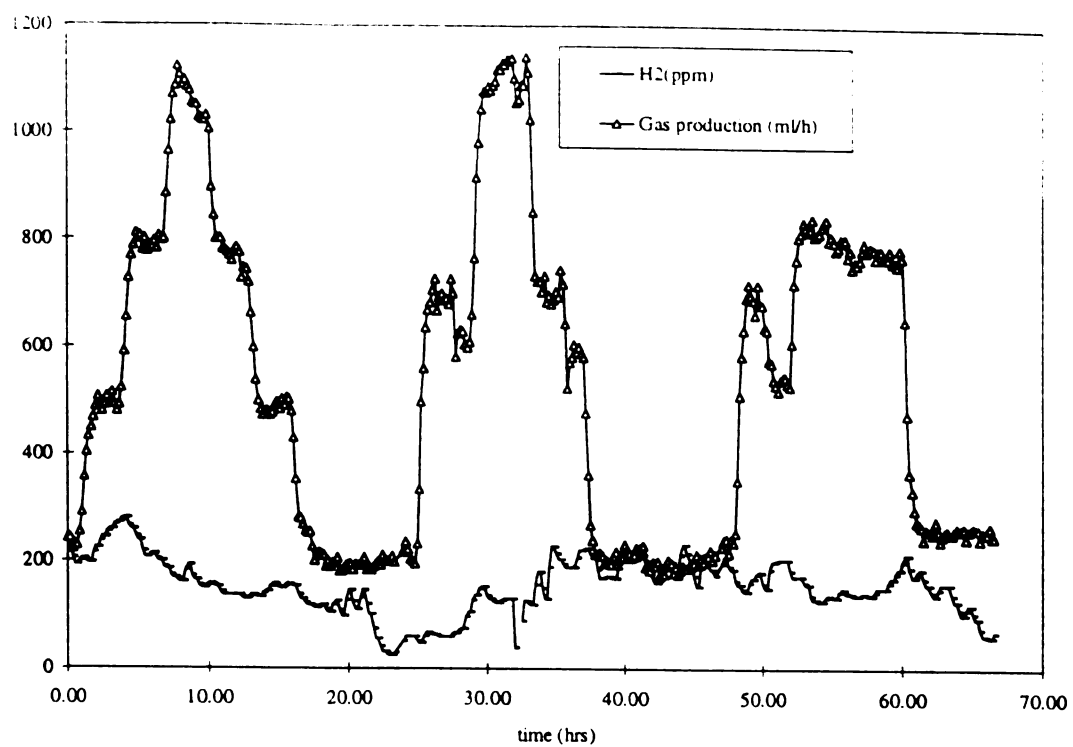


Figure VIIC-5. Hydrogen, carbon monoxide and gas production rate during OLR variation experiments (OLR: 5-25 kgCOD/m³bed-d)

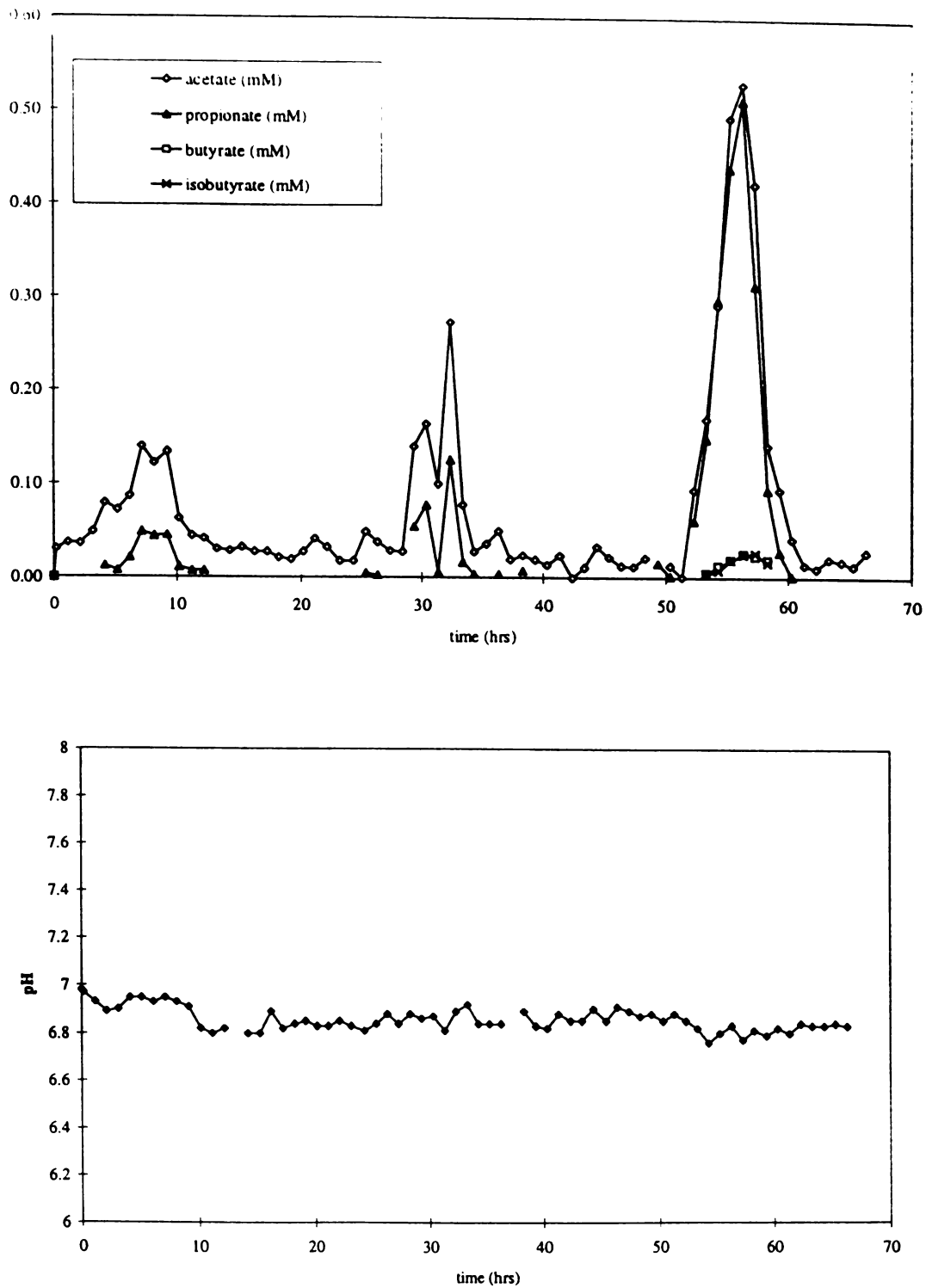


Figure VIIC-6. Acetate, propionate, butyrate, isobutyrate and pH during OLR variation experiments (OLR: 5-25 kgCOD/m³bed-d)

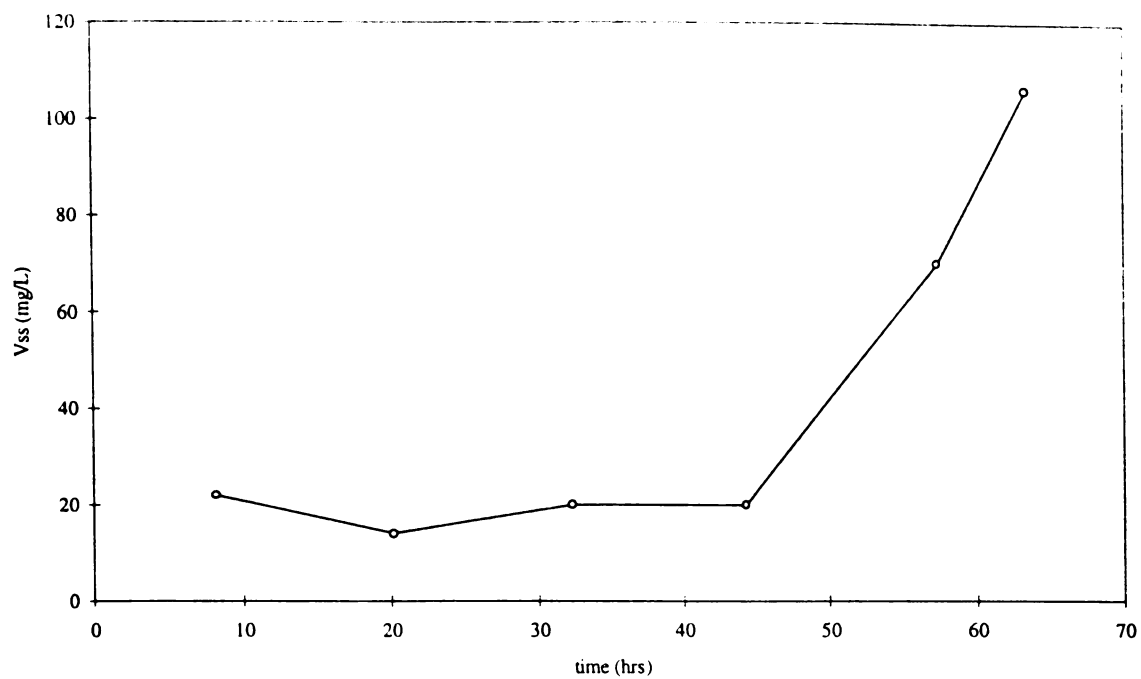


Figure VIIC-7. Volatile suspended solids (Vss) during OLR variation experiment (OLR: 5-25 kgCOD/m³bed-d).

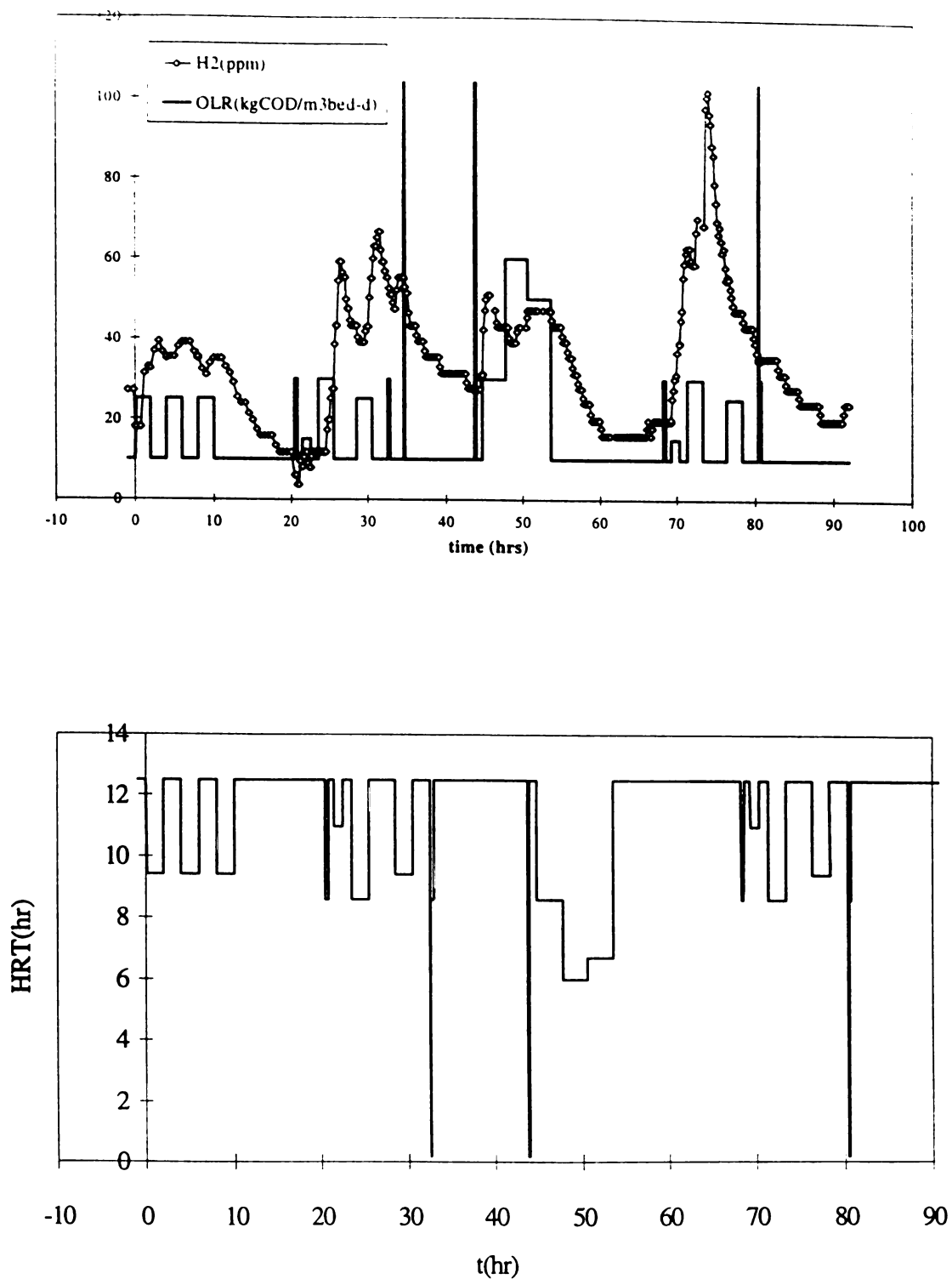


Figure VIIC-8. Applied OLR and HRT and reactor H₂ responses during OLR variation experiments (OLR:10-104 kgCOD/m³bed-d)

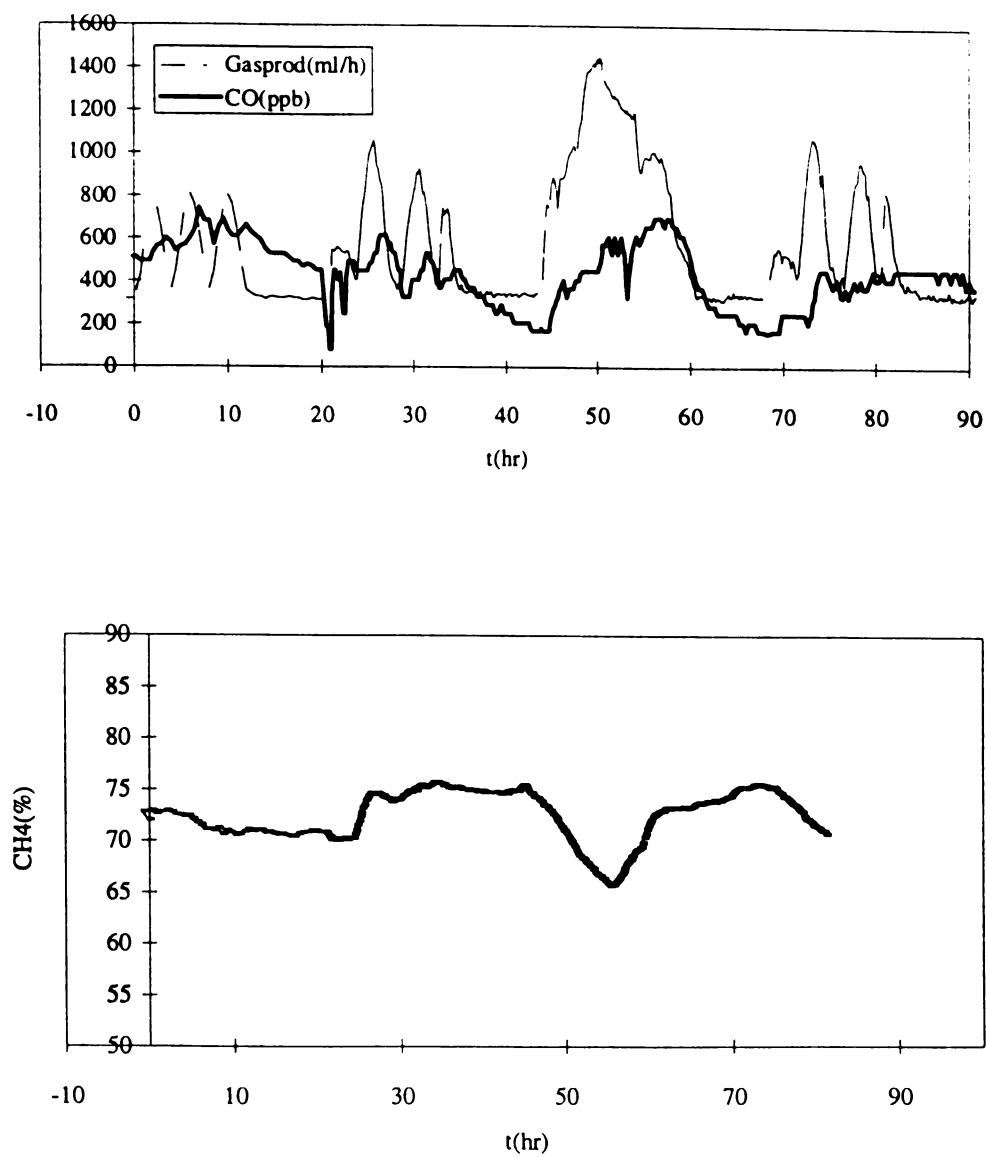


Figure VIIC-9. Gas production rate, CO and methane content during OLR variation experiments (OLR: 10-104 kgCOD/m³bed-d).

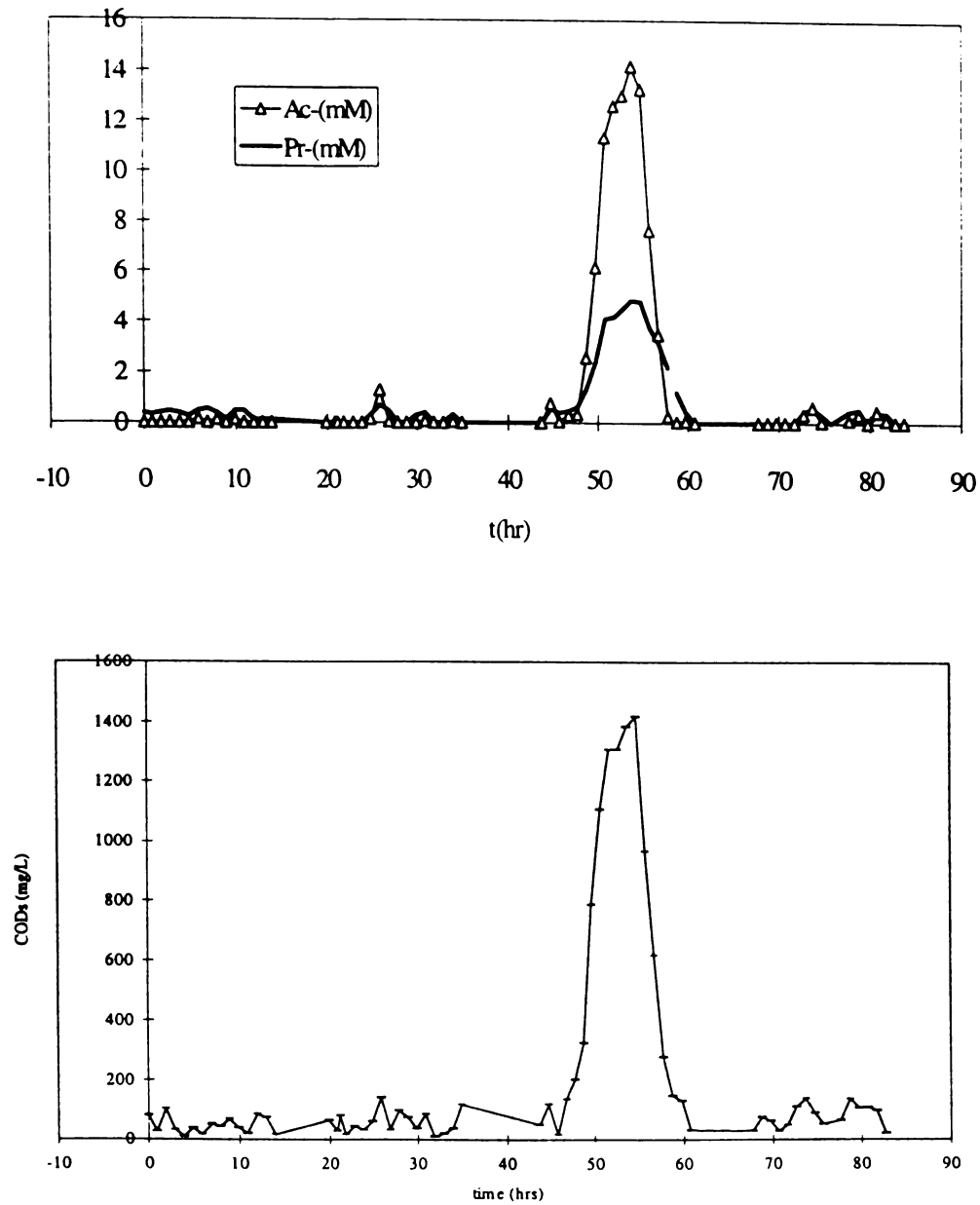


Figure VIII C-10. Acetate, propionate and soluble COD during OLR variation experiment (OLR: 10-104 kgCOD/m³bed-d).

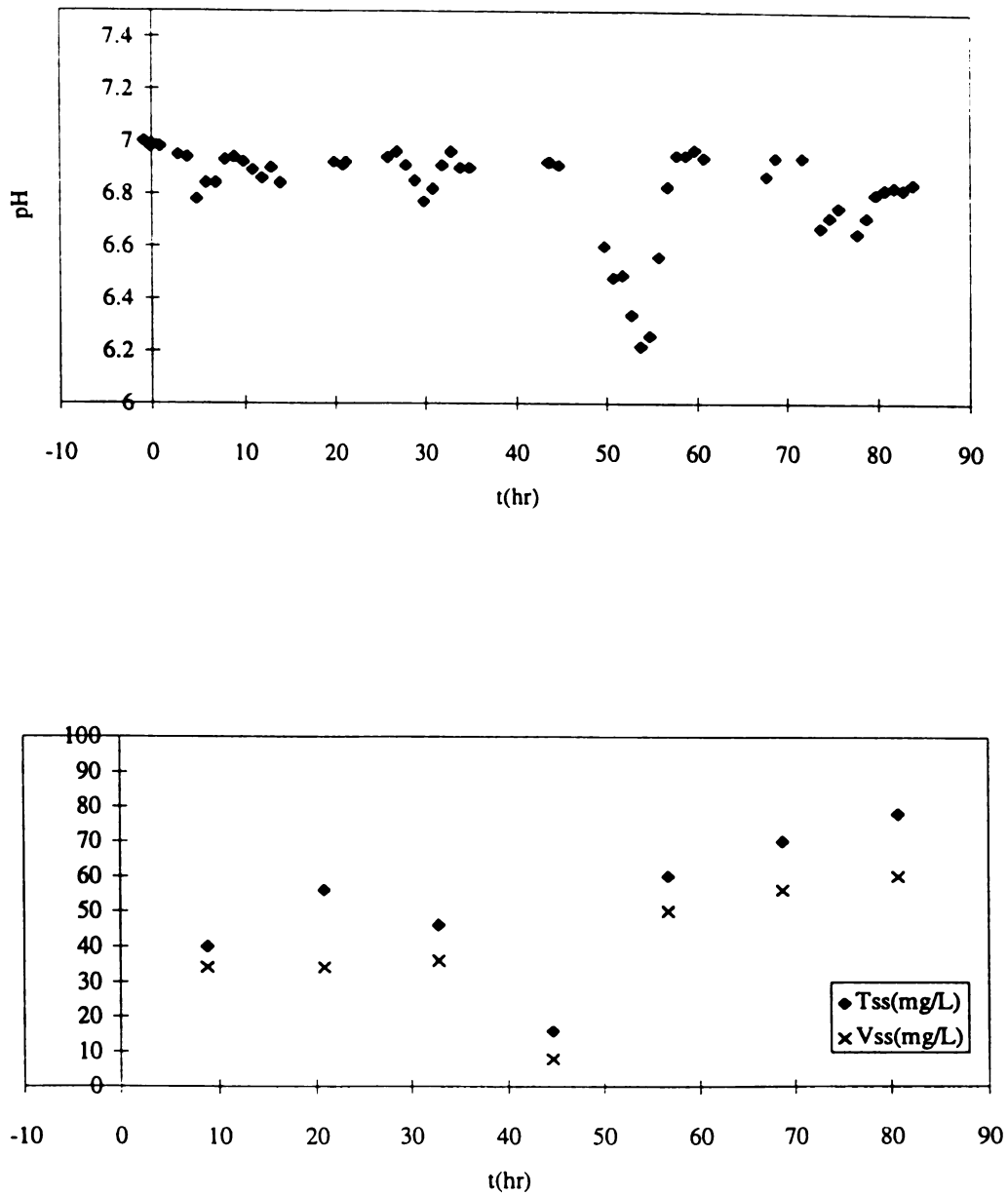


Figure VIII C-11. pH, total suspended solids (TSS) and volatile suspended solids (VSS) during OLR variation experiments (OLR: 10-104 kgCOD/m³bed-d).

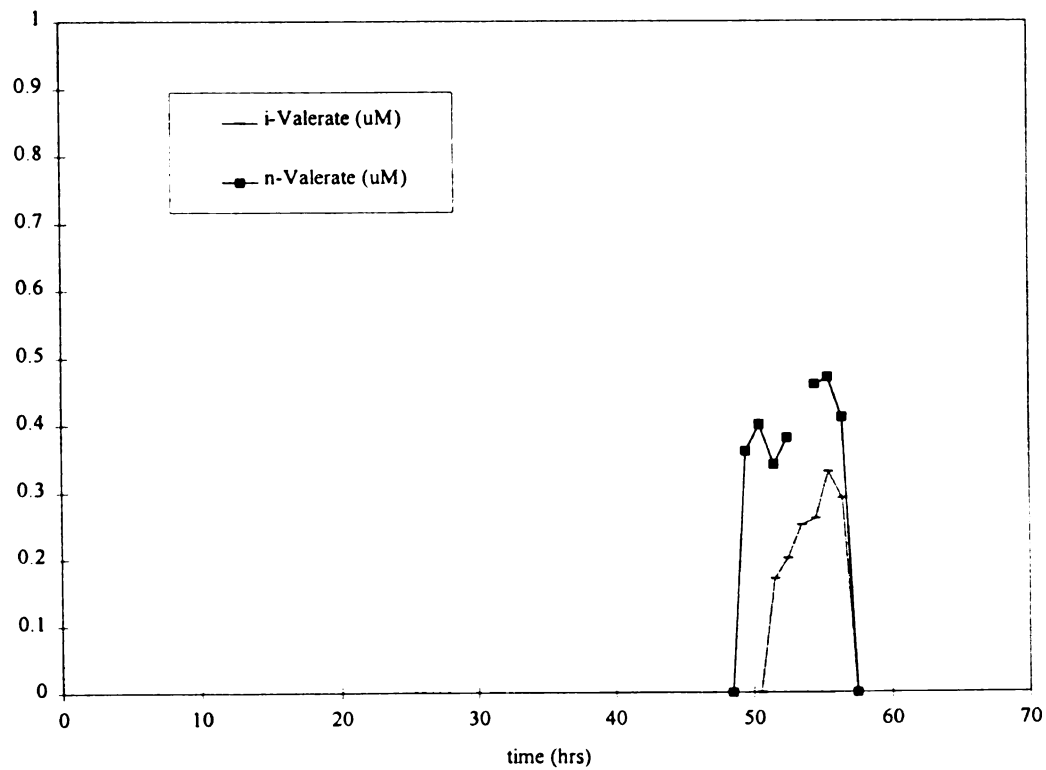
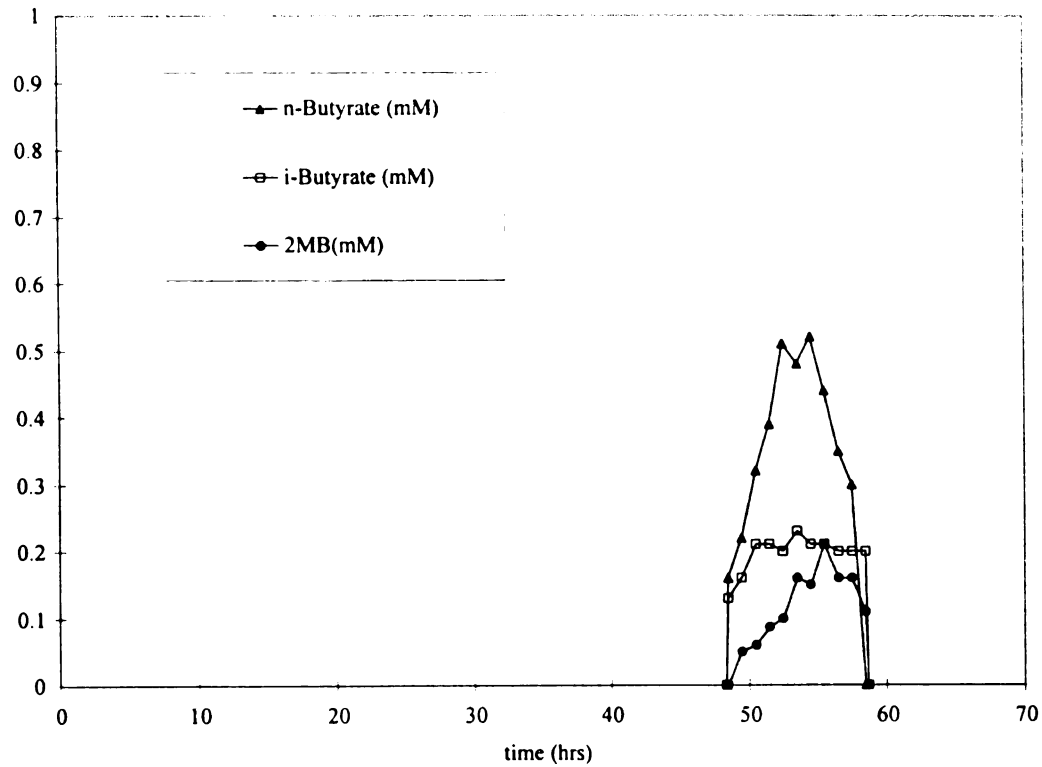


Figure VIIC-12. Four and five carbon compounds measured during OLR variation experiment (OLR:10-104 kgCOD/m³bed-d).

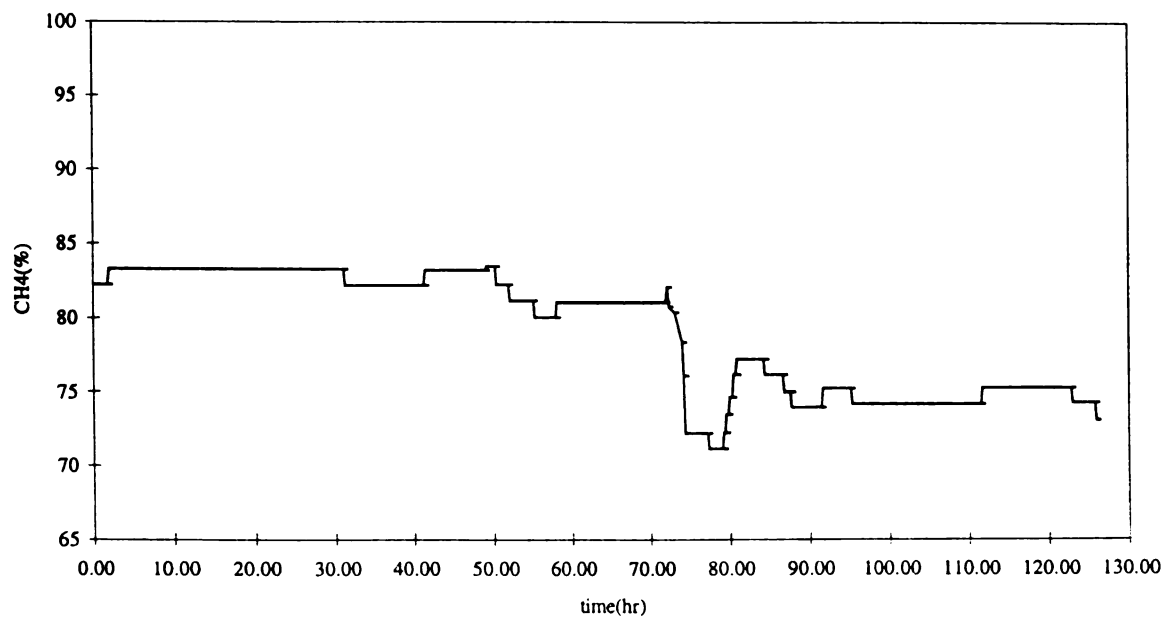
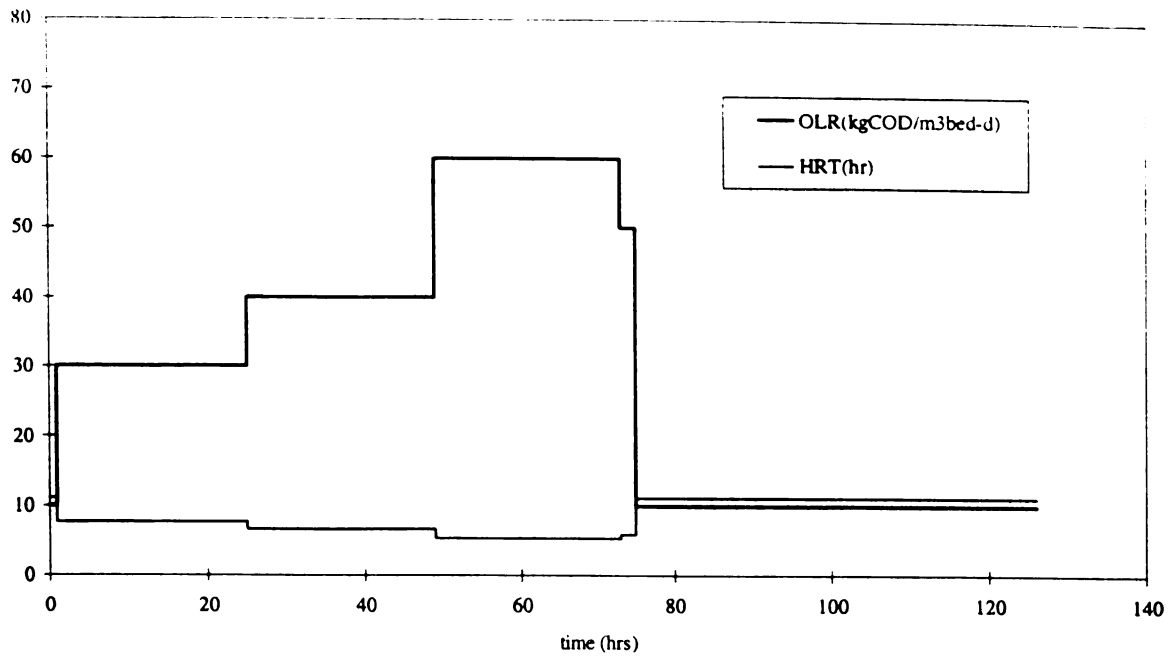


Figure VIIC-13. Applied OLR and HRT and reactor methane content variation during loading experiment (OLR: 10-60 kgCOD/m³bed-d).

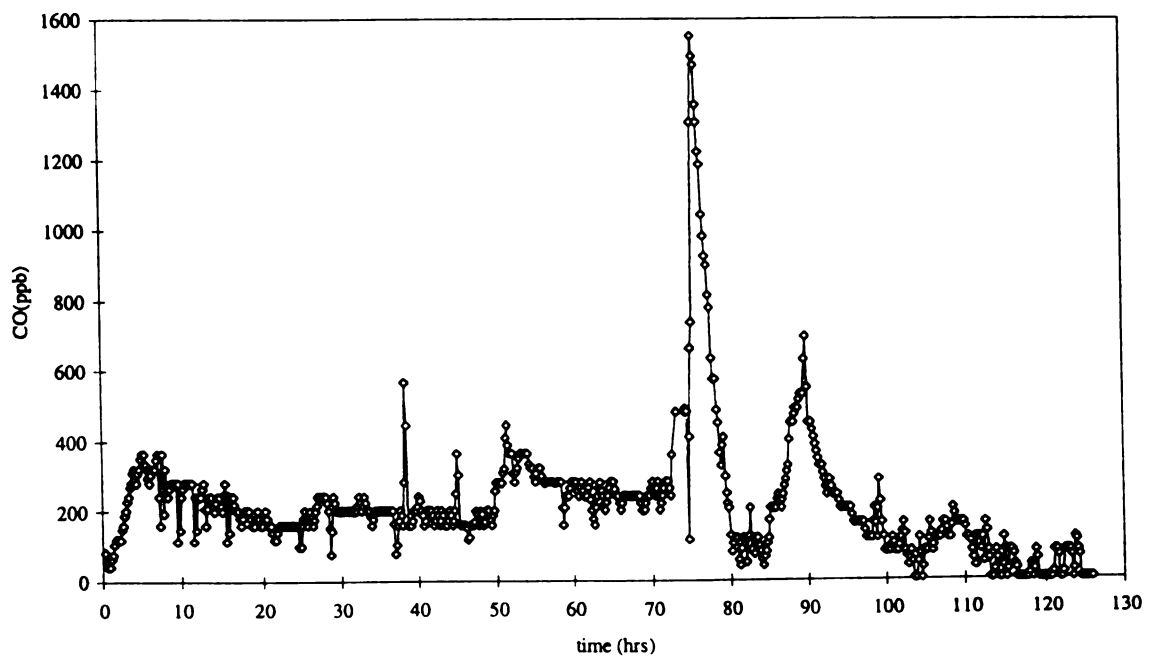
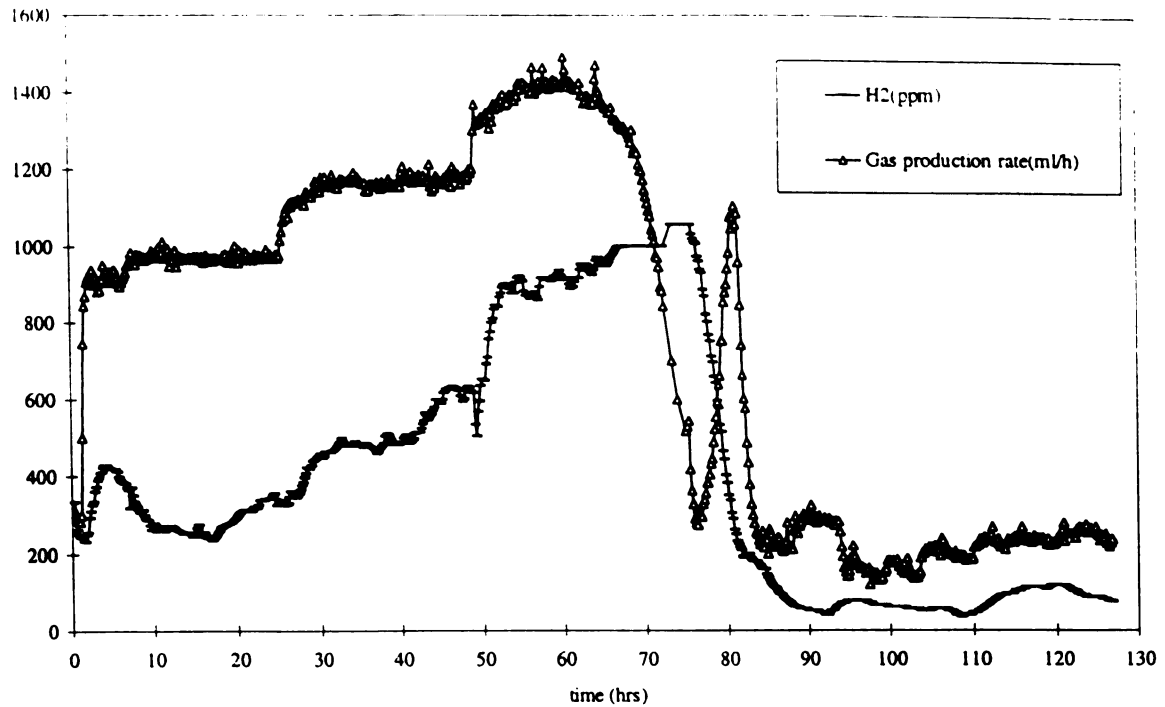


Figure VIIC-14. Gas production rate, H_2 and CO responses during OLR variation experiments (OLR: 10-60 kgCOD/m³bed-d)

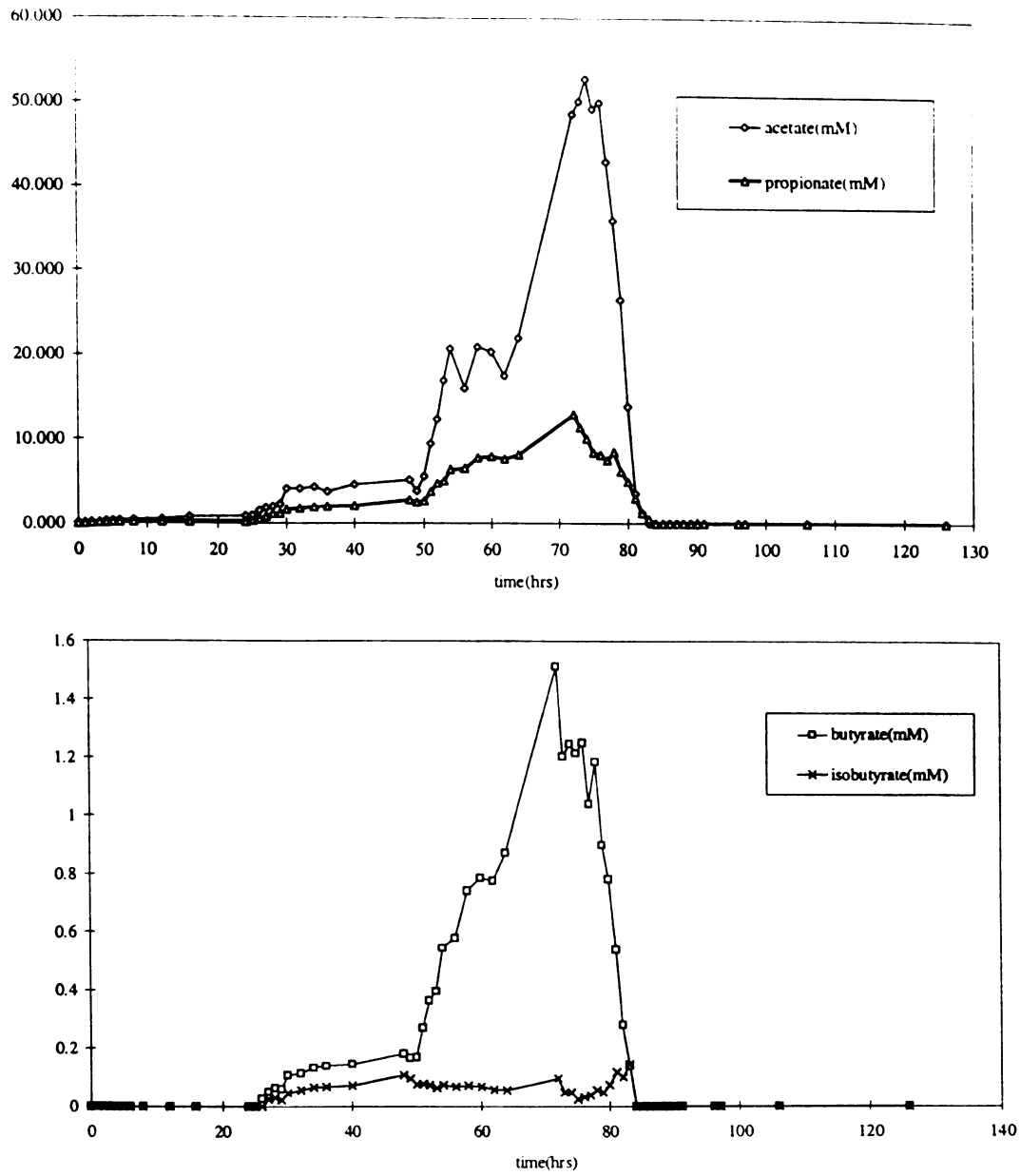


Figure VIIC-15. Acetate, propionate, butyrate and isobutyrate during OLR variation experiment (OLR: 10-60 kgCOD/m³bed-d).

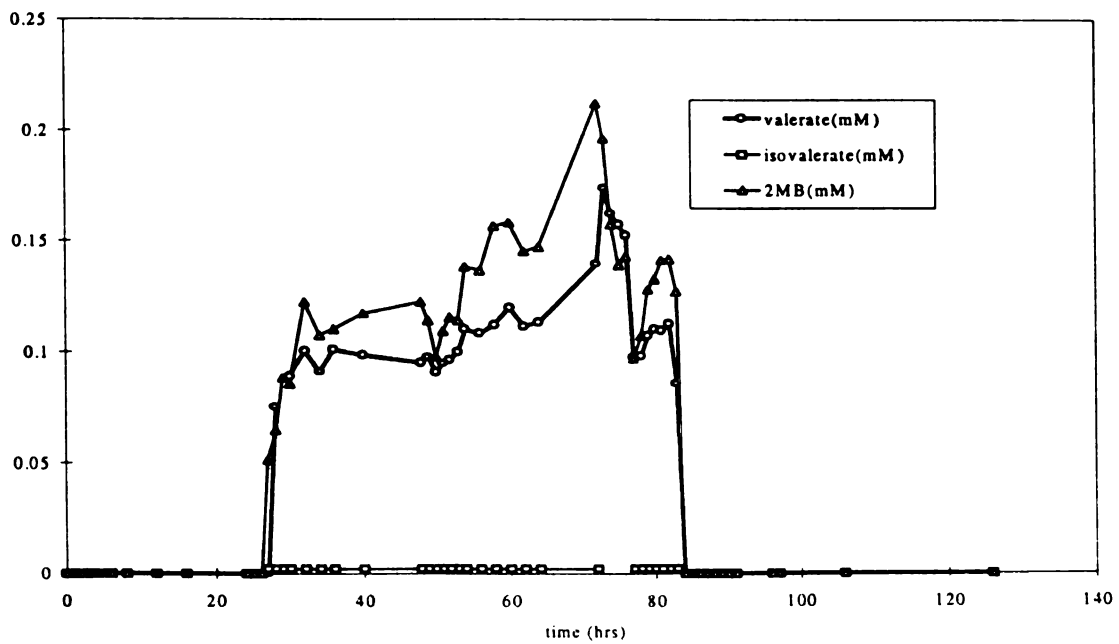
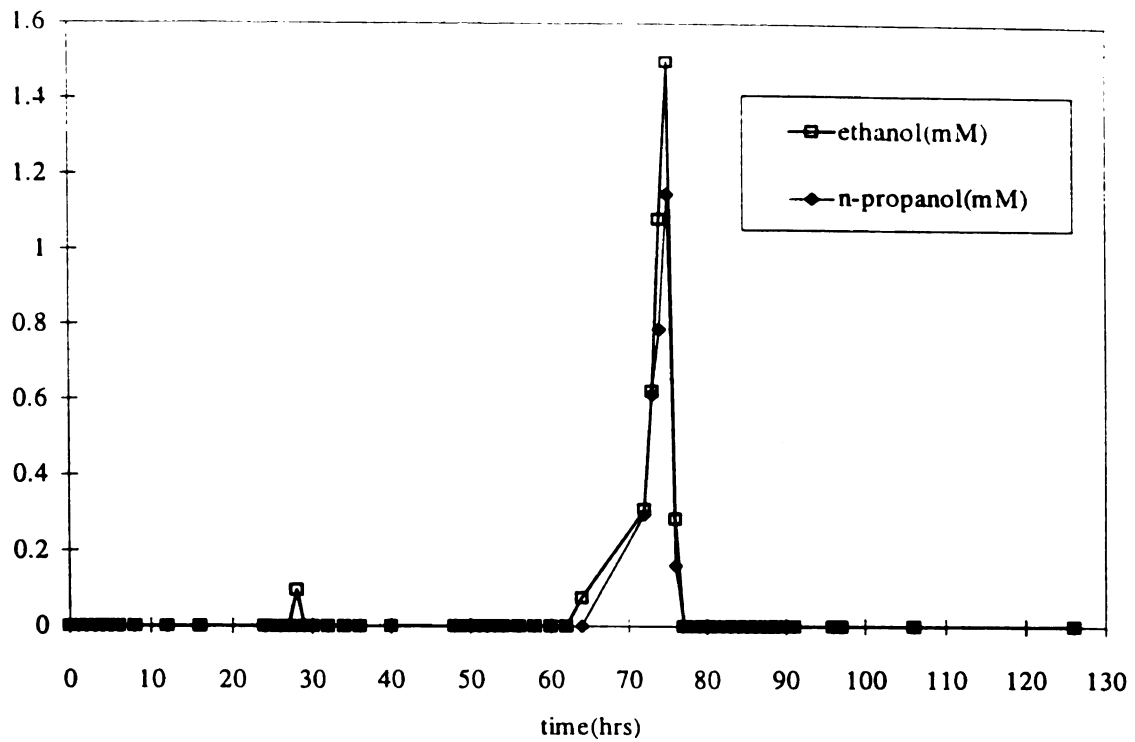


Figure VIIC-16. Ethanol, n-propanol, valerate, isovalerate and 2-methyl-butyrate during OLR variation experiments (OLR: 10-60 kgCOD/m³bed-d). 2MB: 2-methyl-butyrate.

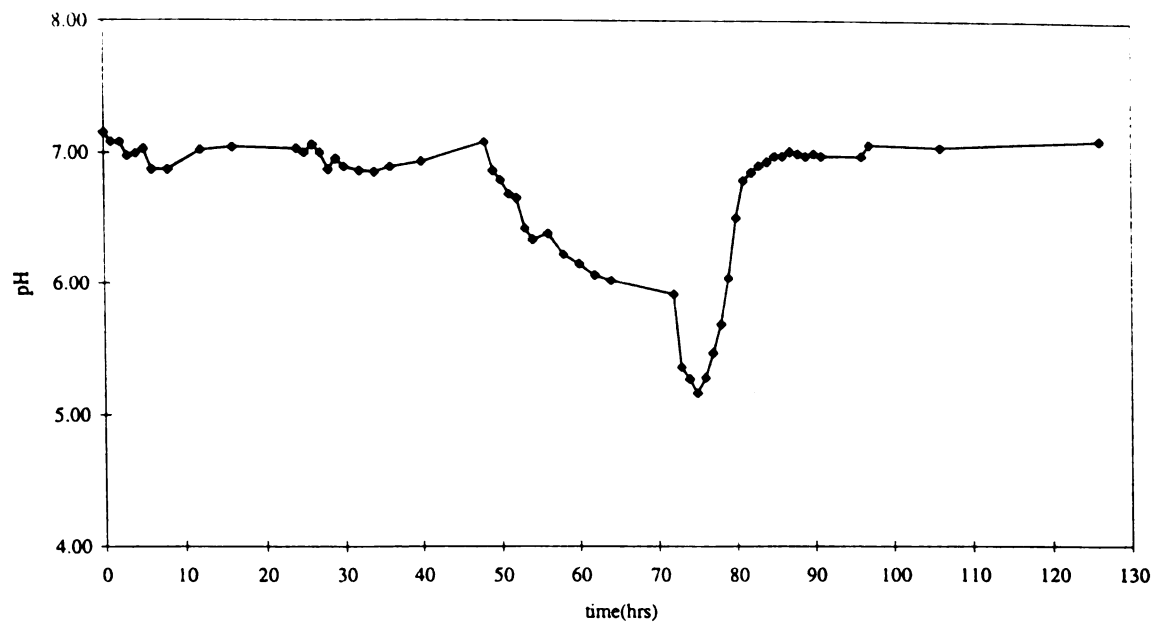


Figure VIIC-17. pH variation during OLR experiment (OLR:10-60 kgCOD/m³bed-d).

Table VIIIB-1. Operational conditions of the bench-scale UASB reactor during pseudo-steady state experiment

Organic Loading Rate (kgCOD/m ³ bed-d)	4.2, 5.8, 10, 15, 23
Hydraulic Retention Time (d)	0.5, 1, 1.5, 2.5
Feed Concentration (kgCOD/m ³)	5.7, 9.1, 11.4, 13.7
Temperature (°C)	37
pH	6.8 - 7.0
Reactor Liquid Volume (L)	3.1
Head Space Volume (L)	0.2
Granular Bed Volume (L)	1.5
Bed Expansion (%) of total liquid volume	65
Up Flow Velocity (ml/min)	165
Gas Recirculation Rate (L/min)	0.5

Table VIIIB-2. OLR, HRT and feed concentration at pseudo-steady state experiments

Experiment group	OLR (kgCOD/m ³ bed-d)	HRT (day)	Feed concentration (kgCOD/m ³)	Effects examined
I	23	0.5	13.7	OLR
I	14.5	0.5	13.7	
II	14.5	0.5	13.7	HRT
II	15	1.5	13.7	
III	10	1.5	9.1	Feed concn.
III	10	1.8	11.4	
IV	4.2	2.5	11.4	OLR (vary HRT)
IV	10	1.8	11.4	
IV	14	1.0	11.4	
V	5.8	1.5	5.7	OLR (vary feed)
V	10	1.5	9.1	
V	15	1.5	13.7	

Table VIIIB-3. Maximum frequency of acetate, propionate, CO₂, gas production and methane at different OLR. (calculated from periodogram)

Table VIIIB-4. Time phase between each pair of monitoring variables in frequency.

OLR	A/P	A/CO	A/H ₂	A/CH ₄	A/GP	P/CO	P/H ₂	P/CH ₄	P/GP	CO/H ₂	CO/CH ₄	CO/GP	H ₂ /CH ₄	H ₂ /GP
4.2	-0.4	-0.4	1.0	1.8	0.1	-0.18	-1.6	-0.75	NA	NA	-0.25	1.1	-0.3	NA
5.8	-1.2	-0.6	-0.5	0.0	0.6	-3.1	-0.25	0.55	1.3	0.1	-2.5	-0.45	0.25	3.1
10	-0.6	0.3	3.0	-2.8	NA	0.3	1.4	1.1	-1.1	NA	-0.8	0.9	0.28	3.0
14	0.22	0.13	-0.8	-2.8	1.1	-0.35	0.0	-0.9	NA	NA	-0.1	2.45	0.0	-0.1
15	0.0	-1.5	0.75	1.2	-1.5	0.0	-3.1	1.0	-0.32	0.2	-1.8	-2	-1.1	0.0
14.5	0.0	-2.9	1.4	0.7	0.1	0.0	-0.45	1.7	2.0	-1.8	1.1	NA	1.15	0.11
23	0.0	0.53	-0.1	-2.17	NA	0.5	0.0	-3.1	NA	0.0	-1.5	-1.1	0.0	0.0

frequency range : - π to π (-3.14 to 3.14).

A/P=-0.4 means A delayed from P by 0.4 (1/d).

A-acetate, P-propionate, GP-gas production. OLR as kgCOD/m³bed-d

Table VIIIB-5. Fisher's white noise test results for each variable at different organic loading rate.

OLR		H ₂	Acetate	Propionate	CO	GP	CH ₄
4.2	x	3.0844	3.5025	—	9.1413	2.9224	5.4822
	P	0.3949	0.2358	—	0.0000	0.4734	0.011
	decision			—	reject		reject
5.8	x	2.8720	3.1138	2.3035	2.2290	2.9039	4.4020
	P	0.4544	0.3412	0.7770	0.8170	0.4382	0.095
	decision						
10	x	5.7867	9.9356	18.2281	3.0882	5.3868	6.6225
	P	0.057	0.0002	0.0000	0.8147	0.091	0.012
	decision	reject	reject	reject			reject
14	x	2.6043	1.8017	3.6702	4.0904	3.9884	2.1916
	P	0.3478	0.7762	0.025	0.02	0.0254	0.5969
	decision			reject	reject	reject	
15	x	1.6320	2.4110	2.1149	1.7557	1.8587	1.8135
	P	0.8841	0.3594	0.5487	0.8077	0.7357	0.6485
	decision						
14.5	x	1.9294	2.2639	3.9867	2.1697	2.1430	2.7841
	P	>0.05	0.6307	0.0445	>0.05	0.7098	0.2653
	decision			reject			
23	x	1.7940	2.0822	2.2368	3.4731	1.8986	1.7150
	P	>0.05	>0.05	0.4652	0.0435	0.7067	0.8344
	decision				reject		

Hypothesis: Ho: data series is generated from white noise; H1: data series is generated from periodic component. $\alpha=0.05$.

P —probability of ξ (the realized value of x) is greater than x ; x —Kappa's test statistics.

Table VIIIB-6. Range of mean, coefficient of variances and standard error of monitoring variables during pseudo-steady state experiment

Component	Mean range	Coefficient of Variance (mean of 8 operations)	Standard error range
H ₂	19 -173 ppm	75.2	0.936-4.999
Acetate	0.08 - 1.04 mM	49.1	0.005-0.168
CO	0.10 - 0.58 ppm	36.9	0.002-0.010
Propionate	0.10 - 0.72 mM	9.9	0.015-0.061
Gas production	104 - 592 ml/h	6.0	0.334-4.174
CH ₄	74.2 - 85.6 %	2.6	0.064-0.234

Ranged among eight pseudo-steady state operations
 $\alpha = 0.05$

Table VIIIB-7. OLR, HRT and feed concentration effect on H₂, CO and performance variables

OLR	HRT	Feed	Acetate	Propionate	CH ₄	CO	H ₂	Gas production
(kgCOD/m ³ bed-d)	(d)	(kgCOD/m ³)	(mM)	(mM)	(%)	(ppm)	(ppm)	(ml/h)
14.5	0.5	13.7	0.2	0.3	85.4	0.17	89.2	326
23	0.5	13.7	1.0	0.7	74.2	0.59	150.9	592
14.5	0.5	13.7	0.2	0.3	85.4	0.17	89.2	326
15	1.5	13.7	1.0	0.4	78.3	0.28	118.4	370
10	1.8	11.4	0.1	ND ^a	82.0	0.28	153.1	248
10	1.5	9.1	0.1	ND	82.0	0.26	173.0	239
4.2	2.5	11.4	0.1	ND	85.6	0.10	19.0	104
10	1.8	11.4	0.1	ND	82.0	0.28	153.2	248
14	1.0	11.4	0.7	0.4	83.7	0.24	126.1	378
5.8	1.5	5.7	0.1	ND	85.5	0.20	24.3	155
10	1.5	9.1	0.1	ND	82.0	0.26	173.0	239
15	1.5	13.7	1.0	0.4	78.3	0.28	118.4	370

a. ND<0.1mM

Table VIIIB-8. Gibb's free energy change for propionate oxidation and methanogenesis at standard conditions

Propionate degradation		$\Delta G_o'$ (kcal/mol)
1.	$\text{CH}_3\text{CH}_2\text{COO}^- + 3\text{H}_2\text{O} \rightarrow \text{HCO}_3^- + \text{H}^+ + 3\text{H}_2 + \text{CH}_3\text{COO}^-$	18.2
Acetate degradation		
2.	$\text{CH}_3\text{COO}^- + \text{H}_2 + \text{H}^+ \rightarrow \text{CH}_4 + \text{CO} + \text{H}_2\text{O}$	-3.78
3.	$\text{CO} + \text{H}_2\text{O} \rightarrow \text{CO}_2 + \text{H}_2$	-4.78
CO₂ reduction		
4.	$\text{CO}_2 + 4\text{H}_2 \rightarrow \text{CH}_4 + 2\text{H}_2\text{O}$	-31.25

Table VIII B-9. Analysis of variance of each monitoring variables among OLRs operated at pseudo-steady state ($\alpha=0.05$)

Variables	Observations	OLR levels ^a	F value	Significance test
Acetate	157	7	52.98	+++
Propionate	157	7	260.28	+++
CO	157	7	70.9	+++
H ₂	157	7	15.79	+++
CH ₄	157	7	71.94	+++
Gas production	157	7	1297.91	+++

a. OLR at 4.2, 5.8, 10, 14, 14.5, 15, and 23 kgCOD/m³bed-d.

Table VIIIB-10. Results from Duncan's multiple range test and LSD test on means of monitoring variables (grouped by OLR)^a

Variables	Group					
Gas production	23	<u>14</u>	<u>15</u>	10	5.8	4.2
CH ₄	23	<u>14</u>	<u>15</u>	<u>10</u>	<u>5.8</u>	4.2
CO	23	<u>15</u>	<u>14</u>	<u>10</u>	5.8	4.2
Acetate	23	15	14	<u>10</u>	<u>5.8</u>	<u>4.2</u>
Propionate	23	<u>15</u>	<u>14</u>	<u>10</u>	<u>5.8</u>	<u>4.2</u>
H ₂	<u>23</u>	<u>15</u>	<u>10</u>	<u>14</u>	<u>5.8</u>	<u>4.2</u>

a. variables have same underline are not different

Table VIIIB-11. Head space and dissolved H₂ and CO in the bench-scale UASB reactor

	H ₂ (l) nM	CO(l) nM	H ₂ (g) (ppm)	CO(g) (ppm)	$\frac{H_{2(g)}}{H_{2(g)}^*}$ ^b	$\frac{CO_{(g)}}{CO_{(g)}^*}$ ^b
mean	4.83	9.25	53.71	0.158	16.3	0.145
SD	5.59	17.94	34.53	0.058	17.3	0.129
Range	1.36-18.50	0.71-51.45	9.6-94.5	0.11-0.26	2-50	0.02-0.34

a. Total eight observations. three replicates each sample for dissolved gas analysis.

b. H₂* (g) and CO* (g) are gas phase H₂ and CO concentrations that are in equilibrium with liquid phase concentrations, calculated from dissolved gas measurements.

CHAPTER 9. MODELING UASB REACTOR USING A DYNAMIC MODEL INCLUDING REACTOR HYDRAULICS, REACTION AND DIFFUSION

A. Introduction

Dynamic modeling of anaerobic processes helps utilize our current knowledge of the process dynamics kinetics, mass transfer and hydraulics, to explore techniques for predicting and preventing process failure. A dynamic model can also reflect the dynamic responses of the process variables to external disturbances and its inherent dynamic character. The dynamics of a wastewater treatment plant cover a very wide spectrum. A model summarizes the current understanding of the dynamics and may at least qualitatively verify observations of the process response to different disturbances. Thus, the model can be a valuable tool in exploring the consequences of different unscheduled disturbances or key operating parameters.

The output or prediction of a model can be at several levels: 1) predict the existence of a phenomena, 2) predict the phenomena quantitatively, 3) make predictions which are in the appropriate direction and of right order of magnitude. Models need to be calibrated and verified using pilot- or full-scale testing and simulation with other independent sets of operational data.

Models can take many forms. Mechanistic models are most useful to the researcher seeking to understand the events occurring in a system. Such models are deterministic and incorporate direct links between inputs and outputs through rate equations that seek to mimic reaction mechanisms. Some models, however, can be highly empirical. These are most useful to the operator because they can be stochastic and can reflect real world

responses. Empirical models are highly system specific and thus are not easily transportable to new situations. Many other alternatives lie between these extremes. This chapter will focus on mechanistic models for anaerobic waste water treatment process.

Considerable effort has been expended on developing a dynamic model for the anaerobic waste treatment process [Andrews, 1969] [Andrews and Graef, 1971] [Graef and Andrews, 1974] [Carr and O'Donnell, 1977], [Mosey, 1983] and [Rozzi, et al., 1985]. Andrews [1969] presented a dynamic model describing a single culture (methanogens) substrate utilization, pH, bacterial growth (with inhibition by non-ionized acetic acid), alkalinity and gas production. The interactions between gas, liquid and biological phases within the anaerobic digester were considered in this model [Andrews and Graef, 1971]. A temperature variable was added in to this model to express growth rate as a function of temperature [Buhr and Andrews, 1977]. Hill and Barth [1977] expanded this model to include hydrolytic and acetogenic phases and ammonia inhibitory effects for continuous suspended growth fermentors treating animal manure. Various dynamic models have been developed using a similar approach to describe anaerobic sludge digestion and wastewater treatment reactors with multiple substrates and multiple stages (hydrolysis, acetogenesis, and methanogenesis). The involvement of additional microbial species with up to five microbial populations and associated reactions were included in these models [Rozzi et al., 1985] [Costello et al., 1991]. Conversion of formate, hydrogen and carbon dioxide to acetate by homoacetogenic bacteria has also been considered in modeling [Hill, 1982] [Bryers, 1985]. With new discoveries in anaerobic microbiology, the central role of hydrogen gas as an intermediate product was considered during dynamic modeling [Heyes

and Hall, 1981] [Mosey,1983]. Mosey [1983] proposed a four population model using H_2 utilizing methanogen as the key organisms. Metabolism of glucose is regulated by H_2 partial pressure through its effect on the NAD/NADH redox couple. This model was later extended to include accumulation of lactic acid [Costello et al.,1991a].

For all biofilm situations, substrate utilization and diffusion occur simultaneously within the biofilm [Harremoës, 1976] [Atkinson and Davies, 1974] [Kissel et al.,1984]. Two characteristic types of biofilm were described during the modeling of substrate utilization [Williamson and McCarty,1976a]. Rittmann and McCarty [1980] extended this model to include biofilm growth, and predicted steady state biofilm thickness and substrate flux. Subsequent work [Rittmann, 1982] addressed the growth and loss of the biofilm and the establishment of a steady-state biofilm. Rittmann [1985] provided a modeling analysis of the substrate-loading fluctuations on fixed-bed biofilm reactors.

Much less work has been focused on the transient state conditions for biofilms not at steady state. Unsteady state is the most critical situation for modeling associated with real-time control strategies. Dynamic diffusion-reaction biofilm models have been presented for aerobic processes considering both flat and spherical geometry, for the biofilm [Benefield and Molz, 1984,1985]. Bolte and Hill [1993] described attached growth anaerobic fermenters using a reaction-diffusion dynamic model. This model described four microbial population interactions and six metabolic pathways during anaerobic degradation of a model animal waste ($C_6H_{13}NO_3$).

Model verification showed that a multiple substrate and pathway reaction model was able to predict the production and consumption of lactic acid and, to a lesser degree,

hydrogen inhibition and regulation of butyrate and propionate utilization [Costello et al., 1991b]. Model evaluations have shown that most models are unable to predict VFA and gas production during unsteady state [Jones and Hall, 1989]. An excellent paper by Jones et al. [1992] provided a process identification procedure using an extended Kalman filter state estimation algorithm to estimate unmeasured process states and parameters for a pilot fluidized bed reactor. A four population dynamic model structure was then postulated.

All of these models were based on CSTR (complete mixed flow) assumptions. There are only a few dynamic models developed for UASB reactors, in which biofilm exists in the form of granules. Bolle et al. [1985] attempted to describe UASB reactor using a flow model combined with sludge transport and kinetics. Unfortunately, the description of kinetics did not include substrate diffusion within the granules. Most reaction-diffusion biofilm dynamic models developed to date were either analyze the problem using flat geometry or with spherical geometry biofilms, but at steady-state [Bolte and Hill, 1993] [De Beer, et al., 1992] [Lens, et al., 1993].

The primary goal of this portion of the study was to develop a dynamic model for UASB reactors with granular sludge. This model will combine reactor hydraulics, substrate utilization kinetics developed in earlier chapters and diffusional information within anaerobic granules, in order to predict UASB reactor system responses during organic loading rate perturbations. General approaches used in development of models were: 1) define the problem 2) characterize the reactor hydraulics 3) identify major reactions 4) determine the kinetics 5) identify mass transport within the granules 6) apply

mass balances on the substrates of interest for each element in reactor 7) integration of a hydraulic flow model and diffusional effects into the dynamic model 8) numerical method used for obtaining a solution 9) model calibration 10) model evaluation using an independent data set gathered from the UASB reactor. The bench UASB reactor (Chapter V) was used as the model reactor. Acetate was the model substrate.

B. Development of a dynamic model

A dynamic model has been developed to describe UASB reactors from several aspects including reactor hydraulics, biological reaction kinetics and mass transfer within the anaerobic granules. This model integrates the UASB hydraulic model (Model 2; Chapter V), reaction kinetics km , Ks (Chapter VI) and granule structural information (Chapter VII) to a structured model, in order to examine different factors that influence UASB reactor performance. The model was evaluated using a data set of when an acetate impulse was applied to the reactor. Verification was obtained using data from a two-step OLR increase in acetate experiment using the bench-scale UASB reactor. During hydraulic modeling using Lithium Chloride impulse, this model was simplified to Model 2 (Chapter V). Results obtained from the hydraulic modeling was then compared with the data from the acetate OLR step change experiment.

B-1. Model development, solution technique, and parameters

The dynamic model is comprised of three parts: substrate utilization within the biofilm (granules), mass transfer and transport in the granular bed, and mass transport within clarifier (zone above the bed). Several assumptions were made: 1) granules were spherical with a radius of R ; 2) substrate diffuses into the granules, penetrating a layer with a thickness of δ from the outer surface of granules. At the inner edge of this layer, the substrate gradient is zero; 3) central core of the granules was impermeable to the substrate and no biological activity; 4) the degradation of acetate can be described using Monod kinetics; 5) acetate utilizers are evenly distributed throughout the entire granule layer δ ; 6)

growth of acetate utilizing methanogen is neglected due to the slow growth rate and relatively short period of the perturbation (i.e. four hours) to the system; 7) mass continuity holds at the interfaces between bulk liquid and the liquid boundary layer, and between the liquid boundary layer and granule surface; 8) the granular bed can be described as a CSTR (substrate concentration in the liquid volume of the bed is uniform); 9) By-pass flow and dead space are present; 10) The clarification zone can be described as a dispersion PFR and 11) there is no substrate diffusion into the reactor dead volume.

Substrate utilization within the granules was described as a diffusion-reaction process. In granular sludge bed, substrate is transport through advection in the bulk liquid and transferred to the liquid boundary layer of granules. Mass transport in the clarification zone is described by advection and dispersion processes. By applying mass balances on the anaerobic granules, the granular bed, and the clarifier, following fourteen model equations were obtained

$$\frac{\partial S}{\partial t} = D \left(\frac{\partial^2 S}{\partial x^2} - \frac{2}{R-x} \frac{\partial S}{\partial x} \right) - \frac{k_m X_m S}{K_s + S} \quad \dots \quad (\text{IV-35})$$

$$\text{BCs: (i) } -D \frac{\partial S}{\partial x} + K_l S = K_l S_b, \quad x=0 \quad \dots \quad (\text{IV-36})$$

$$\text{(ii) } \frac{\partial S}{\partial x} = 0, \quad x=\delta \quad \dots \quad (\text{IV-37})$$

$$\text{IC: (i) } S(x, 0) = S_s(x) \quad x \in (0, \delta) \quad \dots \quad (\text{IV-38})$$

At steady state

$$D \left(\frac{\partial^2 S_s}{\partial x^2} - \frac{2}{R-x} \frac{\partial S_s}{\partial x} \right) = \frac{k_m X_m S_s}{K_s + S_s} \quad \dots \quad (\text{IV-39})$$

$$\text{BCs: (i) } -D \frac{\partial S_s}{\partial x} + K_L S_s = K_L S_{bo} \text{ , } x=0 \quad \dots \quad (\text{IV-40})$$

$$\text{(ii) } \frac{\partial S_s}{\partial x} = 0, \quad x=R \quad \dots \quad (\text{IV-41})$$

where D is the effective substrate diffusion coefficient (m^2/s); S_s is substrate concentration within biofilm at steady state (mM); k_m is specific substrate utilization rate (g acetate/gVS-d); X_m is biomass density within the active layer of the granules (gVS/cm^3); K_s is half velocity constant (mM); K_L is mass transfer coefficient (mm/s); S_{bo} is steady state substrate concentration in bulk liquid (mmol/L); x is an axis originating from the surface of granules towards the central core; R is granule radius (mm).

$$V_b \frac{dS_b}{dt} = V_b E(t) - QfS_b(t) - K_L A_r (S_b - S(0,t)) \quad \dots \quad (\text{IV-42})$$

$$\text{IC: } S_b(0) = S_{bo} \quad \dots \quad (\text{IV-43})$$

$$E(t) = \begin{cases} \frac{Mf}{VbT_{in}}, & \text{if } 0 \leq t \leq T_{in} \\ 0, & \text{if } T_{in} \leq t \end{cases} \quad \text{For impulse} \quad \dots \quad (\text{IV-44})$$

$$E(t) = \begin{cases} QfS_{bkgd}, & \text{if } 0 < t < T_{stp1} \\ QfS_{stp1}, & \text{if } T_{stp1} \leq t < T_{stp2} \\ QfS_{stp2}, & \text{if } T_{stp2} \leq t \end{cases} \quad \text{For step increase...} \quad (\text{IV-45})$$

where V_b is working volume of CSTR (L); $E(t)$ is an input function; A_r is total granule surface area (mm^2); S_b is bulk substrate concentration (mmol/L); S is substrate concentration within granules at unsteady state; Qf is the flow fraction that enters the main stream (L/d); Mf is fraction of mass input that go through reactor working volume (g); S_{bkgd} is feed concentration before step increase; S_{stp1} is feed concentration at first step

increase; S_{sp2} is feed concentration during the second step increase. T_{sp1} is the time that the first step is initiated; T_{sp2} is the time that the second step is initiated. T_{in} is substrate injection time for the acetate impulse.

$$\frac{\partial S_d}{\partial t} = \frac{D_p}{L^2} \frac{\partial^2 S_d}{\partial Z^2} - \frac{u}{L} \frac{\partial S_d}{\partial Z}, \quad t > 0, \quad 0 < Z < l \quad \dots \quad (IV-46)$$

$$\text{BC: } S_d(0, t) = S_b(t) \quad \dots \quad (IV-47)$$

$$\text{IC: } S_d(Z, 0) = S_{b0} \quad \dots \quad (IV-48)$$

where S_d is concentration in clarification zone; D_p is dispersion coefficient of the liquid in the PFR (mm^2/s); u is flow velocity in PFR (mm/s); L is the length of the PFR. Detailed derivations of above second order, partial differential equation (PDE) and ordinary differential equations (ODEs) are presented in Chapter IV.

The above equations were solved numerically, using a FORTRAN program. The ODEs were solved by IMSL (international math subroutines library). The PDE was solved using a finite-difference method [Ames, 1977]. Unit transformations were performed on the model equations which were then scaled to simplify computations. The granule active layer, δ , in X axis was divided into 100 steps. The time scale was divided into 120 steps. Solution was obtained by stepwise search for each parameter until convergence was obtained.

Model parameters were estimated through separated experiments (km , Ks , Chapter VI), measured for the UASB reactor bed and granules (δ , ϵ , R), using literature values (D) as the initial guess, or determined directly by the simulation. Presented in Table IXB-2 are the model parameters. Major parameters that were estimated during simulation were: the acetate diffusion coefficient within the granules D , the mass transfer coefficient through

the liquid boundary layer K_L , biomass density within granules X_m , CSTR dead volume V_d , fraction of flow through working volume f , dispersion factor $\frac{D_p}{L^2}$, and inverse HRT within dispersion PFR, $\frac{u}{L}$. The last two parameters were observed to vary with gas production rate. Dead volume, V_d , and by pass flow, $(1-f)Q$, varied with operation and performance of the UASB reactor. Thus a converged range of these parameters were estimated. The volume of the dispersion PFR was obtained by multiplying reactor total flow rate Q with hydraulic retention time in the dispersion PFR, $\frac{L}{u}$ (min). Dead volume is determined by subtracting CSTR working volume and dispersion PFR volume from reactor total volume.

B-2. Simulation of UASB response during acetate impulse loading

An OLR of 9-10 kgCOD/m³bed-d and a HRT of 11 hrs were maintained during the acetate impulse experiments. The granular bed was fluidized to obtain a total bed volume of 1.7-2.1L. Reactor gas production rate and head space methane content varied from 5.3-6.7L/d and 75-80%, respectively. Effluent acetate concentrations were below detection limit during the pseudo steady state operations prior to the start of the acetate pulse addition. Presented in Table IXB-1 are operational conditions of the bench-scale UASB reactor during the acetate impulse. A concentrated solution of sodium acetate was injected into the UASB reactor recirculation line close to the reactor inlet, to produce an impulse. The effluent acetate concentrations were then tracked with time. Gas production rates were also monitored. Acetate accumulated rapidly up to 10 mM and then decreased

U
r
U
P
d
c
H
h
h
N
e
di
se
di
m
ob
IXE

below detection limits in 90 minutes. Gas production responded in a similar pattern. A peak gas production value of 33 L/d was reached. This is 5 - 6 times of that observed during normal operation (Table IXB-1). The computer program was run using measured data to estimate model parameters (D , K_L , X_m , V_d , f , $\frac{D_p}{L^2}$, $\frac{u}{L}$). The simulated acetate response curve is presented in Figure IXB-1. Results show that the model describes the UASB responses during acetate impulse very well. Under the experimental conditions, bypass flow was 8% of total flow. Dead volume was 6% of total reactor volume. CSTR and dispersion PFR occupied 92% and 2% of reactor total volume, respectively. Diffusion coefficient of acetate within granules was 33% of that in water ($D_{\text{water}} = 13.3 \times 10^{-10} \text{ m}^2/\text{s}$, [Bennett and Myers, 1982]). Dispersion factor $\frac{D_p}{L^2}$ was 0.005 min^{-1} which was five times higher than that estimated during the hydraulic modeling (0.001 min^{-1} ; LiCL impulse). A list of parameters estimated from the acetate impulse experiments are shown in Table IXB-3.

Effects of hydraulic and diffusion-mass transfer in UASB reactor modeling were examined. A comparison was made among reaction models involving hydraulics or diffusions-mass transfer, including one CSTR with reaction–diffusion model, two CSTR in series with reaction–diffusion model, hydraulic model (using Model 2) with reaction (no diffusion), and the hydraulic–reaction–diffusion model. The computer program was modified for each of above models. These models were run with the experiment data to obtain a best fit. Results were then plotted with the measured data as shown in Figure IXB-3 and 4. CSTR dilution out curve (no reaction and diffusion) and a simple hydraulic

model (using Model 2) were also presented. The hydraulic–reaction–diffusion model appeared most satisfactory to describe the observed response. The hydraulic-reaction model fit closely to the measured data only when the active biomass concentration in bed was reduced to 5 gVS/Lbed from 7.85 gVS/Lbed (measured; accounted for the active layer δ biomass). Neither a single CSTR nor a two CSTR reactor in series represented the UASB reactor (Figure IXB-4). Both hydraulic and diffusional factors affect UASB responses. Hydraulics had a more pronounced effect (Figure IXB-3).

B-3. Model prediction during acetate step increases

To verify the hydraulic–reaction–diffusion model developed, data from a two–step acetate increase applied to the bench UASB reactor was used. Using the parameters estimated from the acetate impulse experiment, model predictions were made and compared with the experimental data. Acetate step OLR increases were performed by increasing the acetate concentration from 25 mM to 125 mM for the first step, and from 125 mM to 225 mM for the second step. Other components of the synthetic brewery waste feed was not changed during the experiment. The inlet flow rate was held constant. The bench–scale UASB reactor was operated at conditions similar to that used during the acetate impulse, as shown in Table IXB-1. Acetate concentration as well as gas production rate were monitored during the entire time course of the experiment. Background acetate concentration was below the detection limit. The second step increase was initiated 105 minutes after the start of the first step. The experiment was concluded after 4 hours. A 100 mM increase in inlet acetate concentration did not produce a

significant response in effluent acetate concentration, as shown in Figure IXB-2. The effluent acetate concentration increased only slightly, up to 1 mM during the second acetate step increase. A delay in the acetate response was observed during both steps. The observed response of the UASB reactor to the acetate step increases were predicted using the model (Figure IXB-2). Gas production rate increased with each step, reaching 12 L/d for the first step and 17.7 L/d during the second step. The reactor had only a small by-pass flow of equal to 1% of the total flow. There was no dead volume. The CSTR working volume was 90% of total reactor volume. The dispersion PFR occupied 10% of total volume, higher than during the acetate impulse (2% of total volume). Hydraulic

parameters $\frac{D_p}{L^2}$ and $\frac{u}{L}$ were observed to be 0.0035 min^{-1} and 0.0125 min^{-1} (Table IXB-

3). Two days prior to the experiment, the UASB reactor had a disturbance because the gas collector became clogged by granule clusters which formed within the bed. The granule clusters were removed. Some granules were lost as a consequence of the cleaning procedure. This incident could affect the uniformity of the sludge bed and the bed volume, as observed in the reduction in dead volume and increase in dispersion PFR volume.

C. Sensitivity analysis

A sensitivity analyses was performed on the model parameters using acetate impulse data, to examine the extent of effects of hydraulic, biological and mass transfer on overall degradation within UASB reactors. Parameters analyzed were: specific substrate utilization rate km , half-velocity constant Ks , acetate diffusion coefficient within granules D , granule diameter R , mass transfer coefficient K_L , CSTR dead volume Vd , by-pass flow $(1-f)Q$, and dispersion factor $\frac{D_p}{L^2}$. Results from parameter sensitivity analyses are

presented in Figures IXC-1 to 9. The UASB reactor responses appear to be very sensitive to the specific substrate utilization rate, km (Figure IXC-1). Large km tends to lower the response curve due to an increased reaction rate. The change in the curves with respect to changes in km becomes more pronounced when km is small. A decrease in km of 25% has more effect than an increase in the same amount. The acetate concentration curve decreases with a decrease in the half-velocity constant, Ks (Figure IXC-2). This is caused by an increased substrate affinity or greater slope in the Monod curve and subsequent increased reaction rate. The magnitude of change in acetate response for a 25% variations in Ks is not significant. Both km and Ks primarily affect the second half of the response curve, that is the portion when concentration begins to decrease or after 20 minutes time course. Variation of granule radius R has the greatest effect on the concentration curve among all parameters examined (Figure IXC-3). When the granule radius is reduced by 1/3 ($R=0.5\text{mm}$ from 1.5mm), total surface area increases 2.6 times if granule bed volume and the active biomass layer δ remain unchanged. More mass flux can diffuse into each granule. As a result, overall substrate utilization rate increases and the concentration curve

decreases. This influence becomes stronger when the magnitude of the impulse acetate mass (S_0) is higher. The variation in the diffusion coefficient D and its effect on acetate utilization during impulse is shown in Figure IXC-4 and 5. Acetate concentration increases with a decrease in the diffusion coefficient because of increased diffusional limitations. This change becomes small when the diffusion coefficient is high (ie.36x;Figure IXC-4). An 80-fold change in the diffusion coefficient produces greater variation in concentration curve at $S_0=5\text{mM}$ than that at $S_0=17\text{mM}$. The estimated diffusion coefficient for acetate is $4.42 \times 10^{-10} \text{ m}^2/\text{s}$, which is about 33% of its diffusion coefficient in H_2O (37°C). It can be seen from Figure IXC-4 that a three-fold change in the diffusion coefficient makes only a slight change in acetate concentration. Thus the effects of the diffusion coefficient on overall substrate utilization rate is not significant under the experiment conditions used. The mass transfer coefficient through liquid boundary layer K_L appeared to be the least sensitive parameter tested (Figure IXC-6). Variations in K_L from 1.67×10^{-4} to 0.05 mm/s (300 times) did not result in any change in reactor acetate concentration. Analyses revealed significant influences of hydraulic parameters on reactor acetate concentration. The acetate response curve decreased when dead volume in the granular bed increased from zero to $0.33V$ (V -reactor total volume; Figure IXC-7). The larger the dead volume in the reactor bed, the lesser the working volume will be. With the same acetate mass input, the initial reactor bulk concentration will increase. As a result of this higher flux, transfer into the granules is enhanced which subsequently increases substrate utilization rate. Thus response curve becomes smaller. The effect of by-pass flow on UASB reactor responses is shown in Figure IXC-8. Increasing the by-pass flow increases the amount of

mass lost through by-pass stream, which appears in the effluent for a short time period at the beginning of the experiment. Therefore, the main concentration curve is reduced.

When there is no by-pass flow, all the mass of acetate in the impulse goes through the reactor working volume, and the concentration curve increases. Reactor dispersion was

analyzed using a dispersion factor $\frac{D_p}{L^2}$. When dispersion increased, the reactor

concentration decreased (Figure IXC-9). As expected, the curve becomes wide and smooth, approaching the response of a completely mixed flow reactor. A decrease in the dispersion factor tends to increase the peak acetate concentration curve with concurrent narrowing of the curve. In an extreme case, dispersion equal to zero. A zero dispersion factor means no dispersion or the reactor is plug flow (PFR). Results of the hydraulic-

reaction-diffusion model (CSTR+dispersion PFR) and a CSTR+PFR model (when $\frac{D_p}{L^2}=0$)

are presented in Figure IXC-10. The CSTR+PFR model did not describe the UASB reactor. All three hydraulic parameters (dead volume, by-pass flow and dispersion factor) affect the whole range of the concentration curve.

D. Discussion

Data from an acetate impulse experiment were simulated using the hydraulic-reaction-diffusion model with a good fit. The acetate step increase experiments were also predicted by the model using same set of parameters (reaction and diffusion), with a slight variation in the hydraulic parameters. In general, the hydraulic-reaction-diffusion model was adequate to describe performance of the laboratory-bench scale UASB reactors.

One CSTR has often been assumed sufficient to describe UASB reactors. Results presented in Figure IXB-4 demonstrate that neither one ideal CSTR with or without diffusion, nor two CSTRs in series with diffusion, could provide adequate description of the UASB reactor.

Results indicated all three terms in the model: reaction kinetics, diffusion and hydraulics are important to properly characterize the performance of UASB reactors (Figure IXB-3). Each term contributes significantly to the model. Reaction kinetics is the part of major importance and is often the only term emphasized. There are a great differences between dispersed cell systems (hydraulics–reaction model) and biofilm systems (hydraulic–reaction–diffusion model) when they were applied to describe UASB reactors (Figure IXB-3). Hydraulics and mass transfer have different impacts on UASB response curves. Reactor hydraulics produced a delay in the peak acetate concentration due to non-ideal flow. The response of ideal CSTRs to an impulse is a peak concentration point at the beginning of the time course. Existence of a dispersion PFR reduced the volume of CSTR. The delay time observed is the HRT in the dispersion PFR. Mass transfer within the granules affects the peak height of acetate response curves. In a

dispersed cell system, the mass input to a sludge bed will be utilized immediately following Monod-type kinetics. The bulk substrate concentration will then decrease rapidly (Figure IXB-3) and the concentration curve decreases. The best fit of a dispersed cell system could only be obtained when active biomass concentration in bed (X) used in the simulation was reduced to 5 gVS/Lbed, which is 64% of the measured value (7.85 gVS/Lbed; Table IXB-2). Even with this value, the curve was still lower than all of the measured data. This is expected because of the effect of mass transfer limitations within the granules. Substrate can be utilized only after it has diffused to granule surface and then inside. The mass transfer process reduces the overall observed reaction rate when mass transfer is limiting. As a consequences the concentration curve increases. The model could not describe UASB reactors well without taking into account hydraulic and diffusional considerations. The importance of these two factors, therefore, should not be ignored.

The major objective of modeling a process is to make predictions and help understand what factor most affect performance. The model developed was able to describe UASB reactor performance in a systematic way, identifying major factors that influence reactor overall degradation. Thus predictions can be made for different experimental conditions not tested.

The values of model parameters that were estimated, were within a reasonable range. Effective diffusion coefficient of acetate within granules, D , was observed to be 33% of that in pure water. Reported literature values varying between 22-34% [Nilsson and Karlsson, 1989; Speece, 1988] and 40-80% [Alphenaar et al., 1993]. A D of 34% of that in pure water has been used in a pH profile model and appeared adequate [Debeer et

al.,1992]. The mass transfer coefficient, K_L , was 0.013 mm/s which is close to the reported value 0.009 mm/s [Inoue and Koyama,1989]. K_L appeared to be insensitive to overall substrate utilization. This does not exclude the limitation of mass transfer within the liquid boundary layer because the thickness of this layer may play a role. Results of the mass transfer experiment indicated reduction of the liquid boundary layer could increase the overall acetate utilization rate (Chapter VI). Comparing results for the impulse and step OLR, kinetic parameters (k_m , K_s), biomass parameters X_m , and mass transfer parameters D and K_L , remain unchanged. The reaction-diffusion part of the model were consistent.

In a system such as granular sludge blanket reactors, where diffusion and reaction both exist, the overall observed reaction rate depends on coupled substrate transport and substrate utilization kinetics. Parameters affecting substrate degradation could include granule radius (R), diffusion coefficient (D), the thickness of active layer from granule surface (δ) and kinetic constants (K_m, K_s). When the thickness of the active layer was constant, as observed in the brewery granules tested herein (Chapter VII), and kinetic parameters do not vary at the experiment conditions; overall substrate utilization rate is sensitive to interactions of the diffusion coefficient and granule diameter. Granule size appeared to be one of the most influential factors affecting substrate utilization in the UASB reactor (Figures IXC-3 and 4). A reduction of granule radius from 1.5mm to 0.5mm resulted in a one third reduction in the peak acetate concentration for an impulse concentration of 30mM. This decrease was approximately 40% when the initial impulse concentration was 17mM (Figure IXC-3). These results of granule size effects confirmed

experimental data obtained from mass transfer study on anaerobic granules (Chapter VI). Bailey & Ollis [Chapter 4, 1986] discussed the reaction-diffusion problem within immobilized enzyme catalytic systems using a dimensionless approach. From the analyses, effectiveness factor (ratio of observed reaction rate to intrinsic reaction rate) was a function of particle size, diffusion coefficient, particle geometry, reaction orders, bulk liquid concentration and reaction kinetic parameters. Particle sizes play a significant role in determining effectiveness factors. At small initial impulse concentrations, the diffusion coefficient D tends to have more influence on observed responses (Figure IXC-5) than when initial acetate concentration is high, suggesting that mass transfer becomes less limiting when the substrate flux increased greatly.

Variation of hydraulic parameters change the whole response curve, while kinetic parameters primarily influenced the second portion of the response curve. Kinetic parameters had little impact on first portion of the response curve. The distribution of acetate within the reactor depended largely on reactor hydraulics (by-pass, CSTR, PFR, etc.). Substrate must go through mass transfer and diffusion process before reaction can occur. Immediately after introduction of an impulse, mass transfer and diffusion processes were the predominant mechanisms.

Comparing the results of the three experimental runs (Table IXB-3), one can observe that hydraulic parameters did not vary significantly. Reactor working volume predicted by the model, from LiCl impulse and acetate experiments, were in a close agreement, 90 to 92% of reactor total volume (Table IXB-3). Dead volume and dispersion PFR volume were also within several percent.

During the acetate step OLR increases, an incident occurred prior to the experiment. Compact clusters of granules clogged the reactor. These granules were likely a portion of the dead volume within the bed. During a cleaning procedure to reducing clogging, some granules were lost from the reactor. This reduced both the dead volume and total sludge bed volume. As a result, the reactor dead volume decreased from ca. 6-7% to zero. Concurrent with this, the dispersion PFR volume increased from 2% to 10%, the majority of which was due to the decrease in bed volume. The increase in the dispersion PFR also resulted in a greater delay in system response (Figure IXB-2).

Granule flocs were often observed in the UASB reactor. These flocs tend to form a loose layer above the bed. This layer of flocs occupies a certain volume in the clarification zone. Flocs are small particles that are formed from the break-down of larger granules and thus have some microbial activity. These flocs produce biogas and, increase the mixing volume in the reactor. This may contribute to the small dispersion PFR volume (LiCl and acetate impulse).

Dispersion in the UASB varied with operational or experimental conditions. The dispersion factor $\frac{D_p}{L^2}$ was observed to increase with applied OLR and therefore, reactor gas production rate (Table IXB-4). For the LiCl impulse experiment the OLR (9 kgCOD/m³bed-d) and gas production (5.3L/d) were lower than for the other experimental runs. During the acetate OLR step increases, an increase in the acetate concentration by 100 mM in the feed for each step resulted in a gas production more than double for the first step increase (12 L/d), and more than triple for the second OLR step increase (17.7 L/d). An impulse of acetate resulted in 17 mM acetate concentration in the reactor,

produced much higher gas production. A peak value of 33.6L/d was observed. The dispersion factor during these experiments increased from 0.001 to 0.005 for the LiCl impulse and acetate impulse experiments, respectively. In this model, dispersion is a measure of mass transport in the clarification zone in addition to advection. Gas bubbles raise from the bed through clarification zone resulted in increased dispersion in this layer. It is reasonable that with a high OLR, the large amount of gas bubbles produced from reaction bed would result in increased dispersion in the clarification zone.

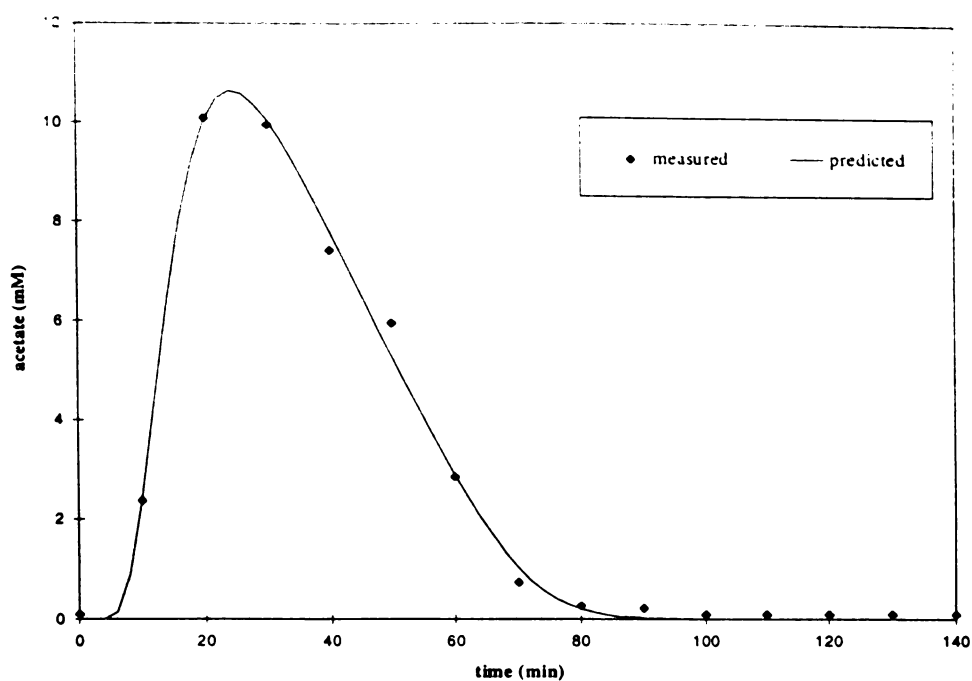


Figure IXB-1. Model simulation of acetate concentration during an acetate impulse and measured data from a bench-scale UASB reactor.

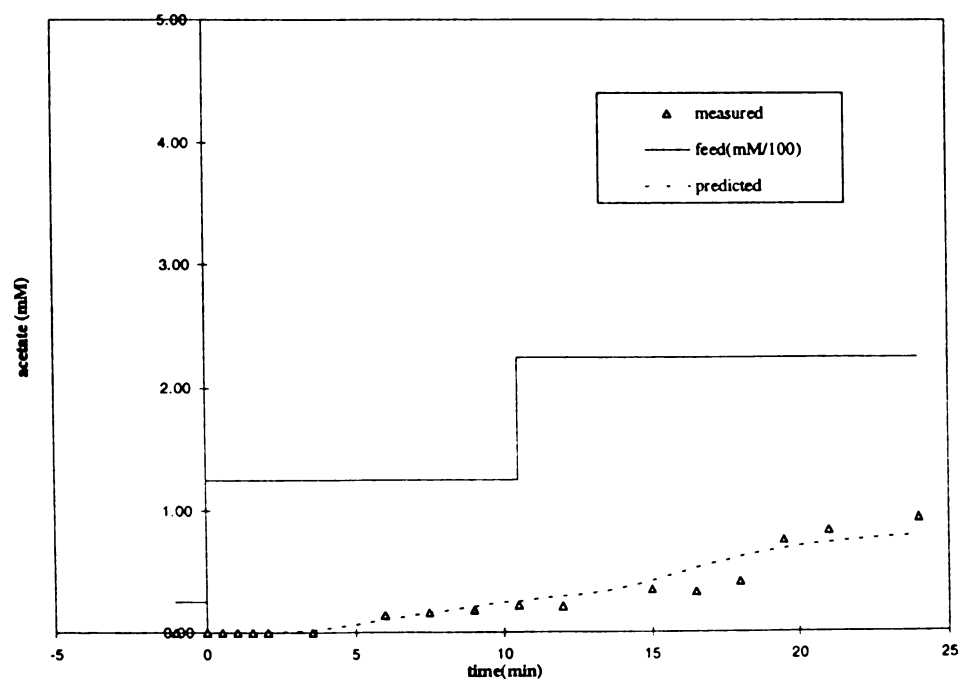


Figure IXB-2. Model simulation results of effluent acetate concentration during a step increase in acetate inlet concentration compared to measured data from the bench UASB reactor.

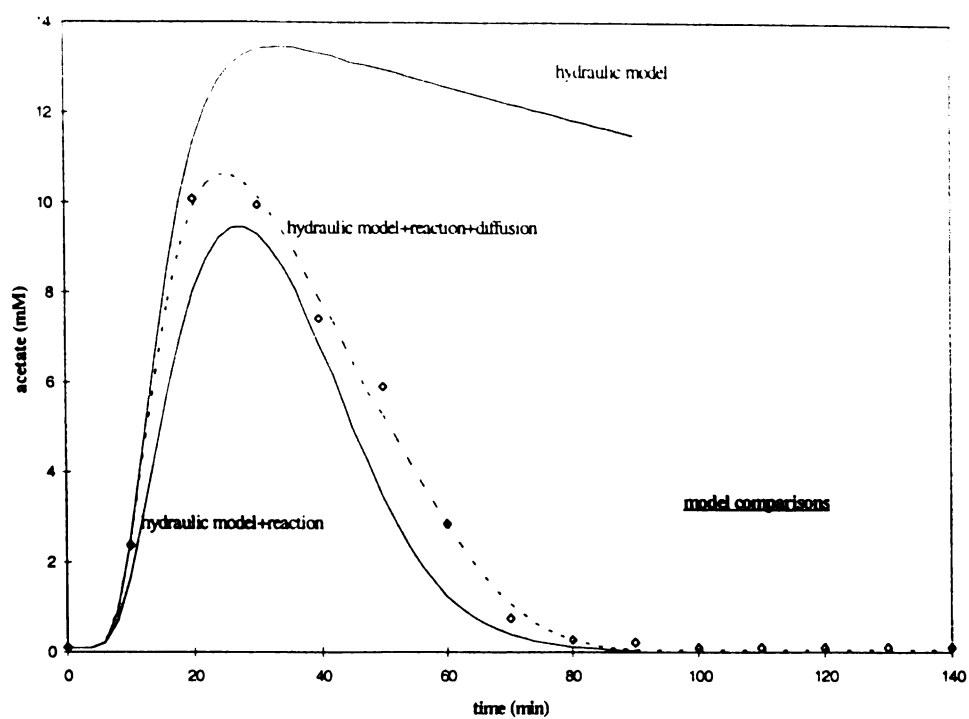


Figure IXB-3. Effect of reaction and diffusion in modeling data from the acetate impulse experiment.

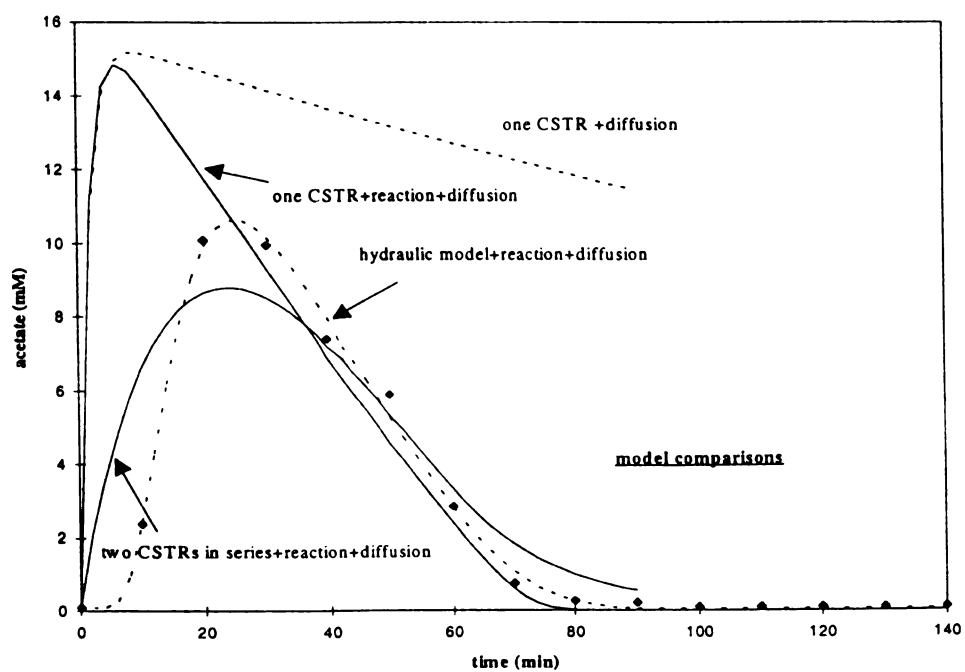


Figure IXB-4. Model comparisons: one or two CSTRs and the newly developed hydraulic model with reaction and diffusion.

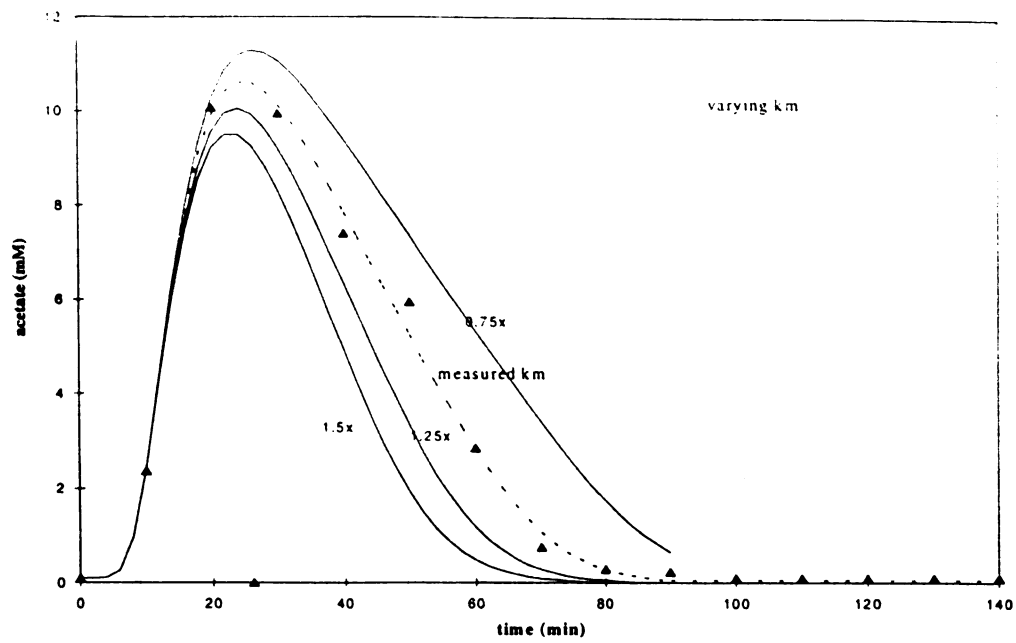


Figure IXC-1. Effect of maximum substrate utilization rate, k_m , on UASB reactor response during the acetate impulse experiment.

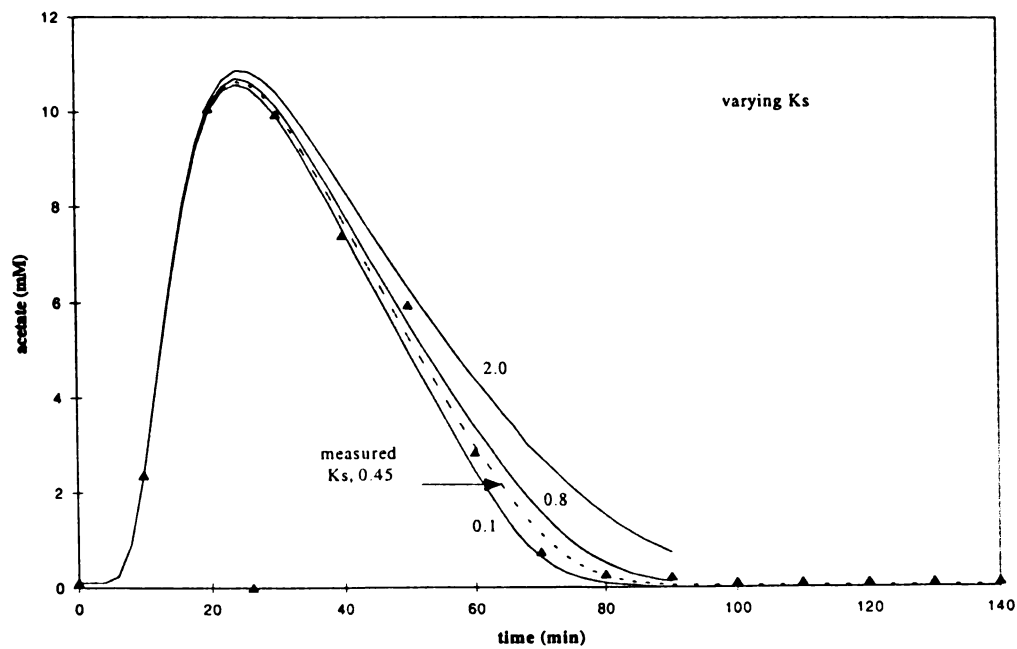


Figure IXC-2. Effect of half velocity constant, K_s , on UASB reactor response during the acetate impulse experiment.

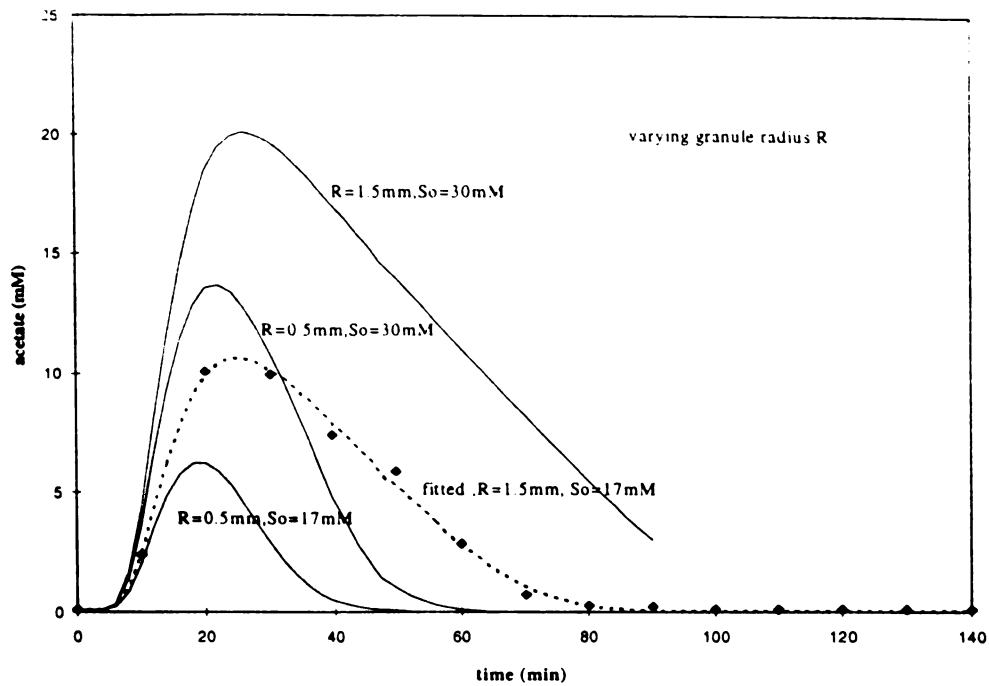


Figure IXC-3. Effect of variation in granule radius R on UASB response during acetate impulse at different initial substrate concentrations (S_o).

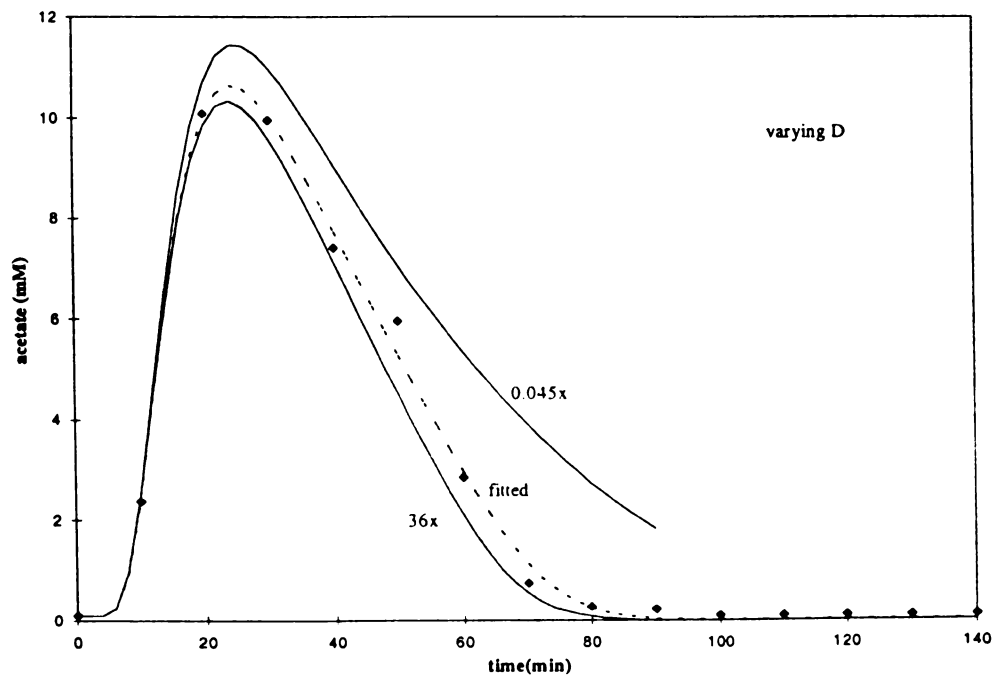


Figure IXC-4. Effect of diffusion coefficient, D , on acetate concentration curve during acetate impulse.

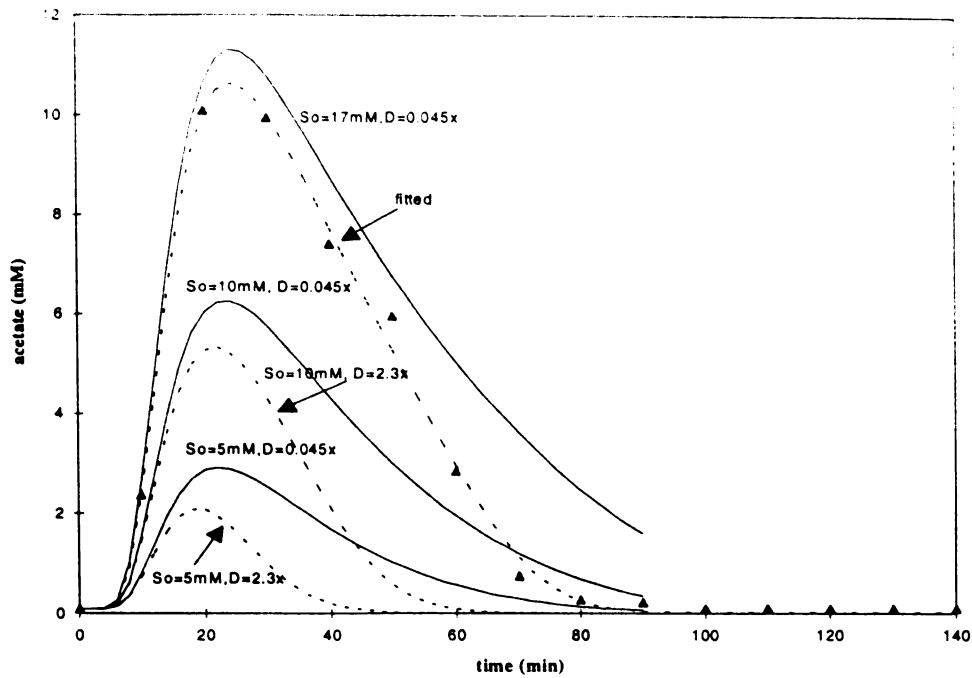


Figure IXC-5. Effect of variations in diffusion coefficient D on UASB response during acetate impulse at different initial substrate concentration (S_o).

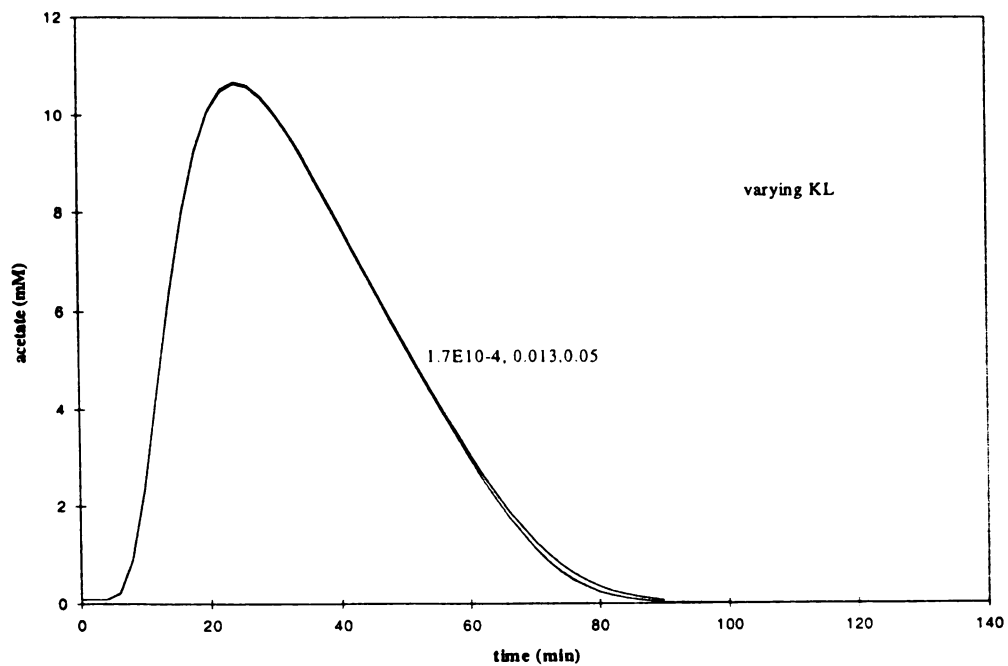


Figure IXC-6. Effect of mass transfer coefficient, K_L , on UASB response during acetate impulse

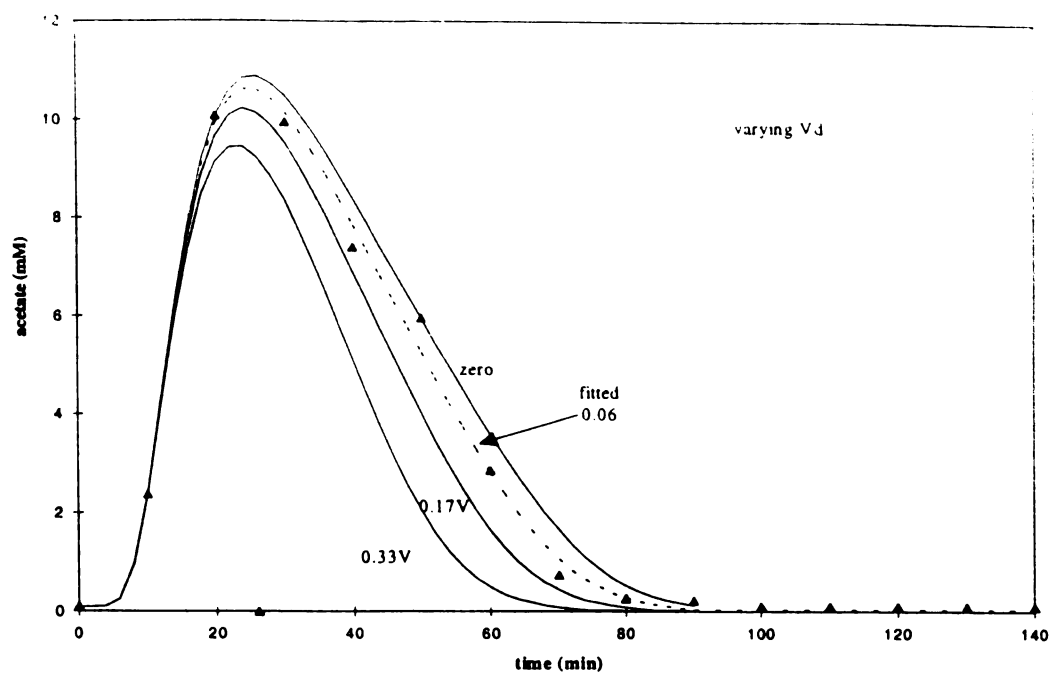


Figure IXC-7. Effect of dead volume, V_d , on acetate impulse modeling.

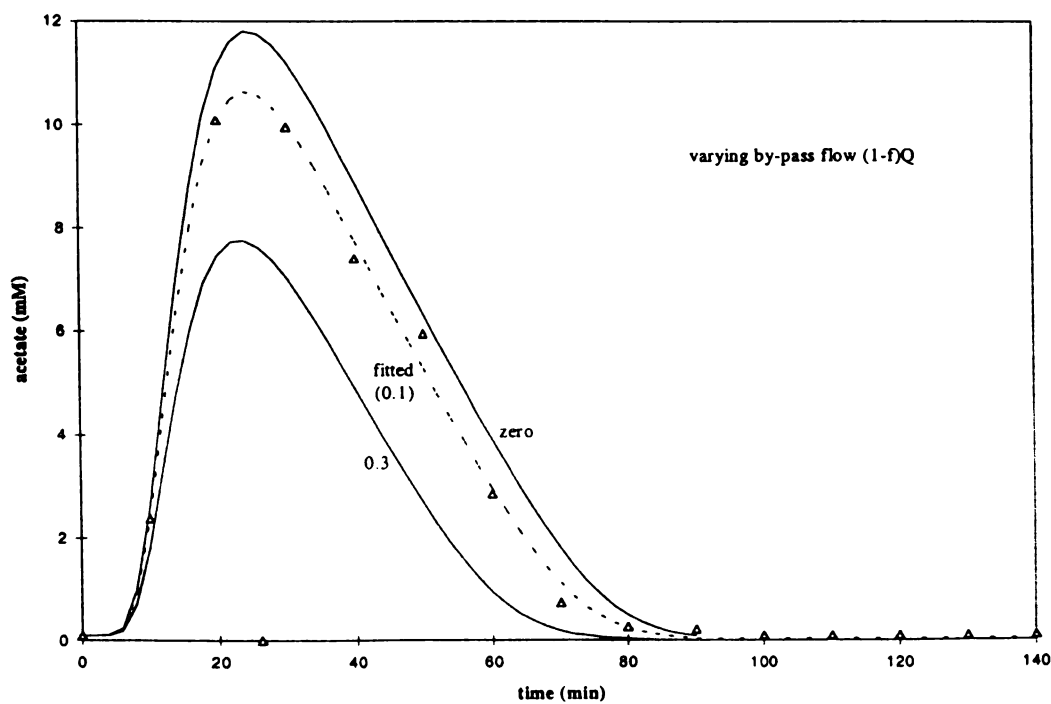


Figure IXC-8. Effect of by-pass flow $(1-f)Q$ on UASB response curve during acetate impulse

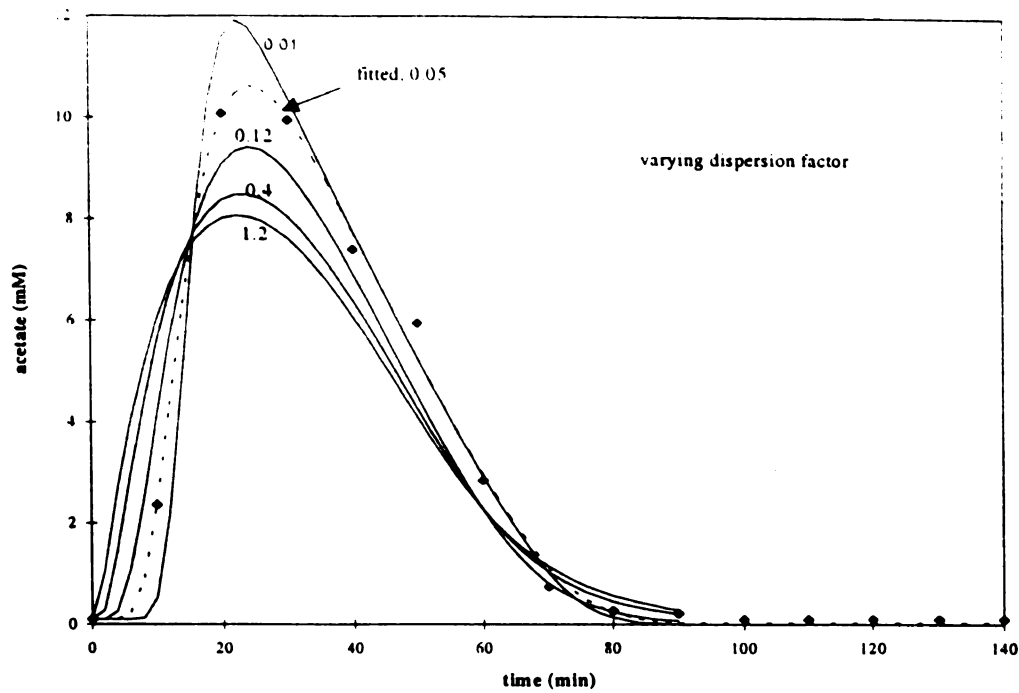


Figure IXC-9. Effect of dispersion factor, $\frac{D_p}{L^2} (\times 10)$, on UASB response during an acetate impulse

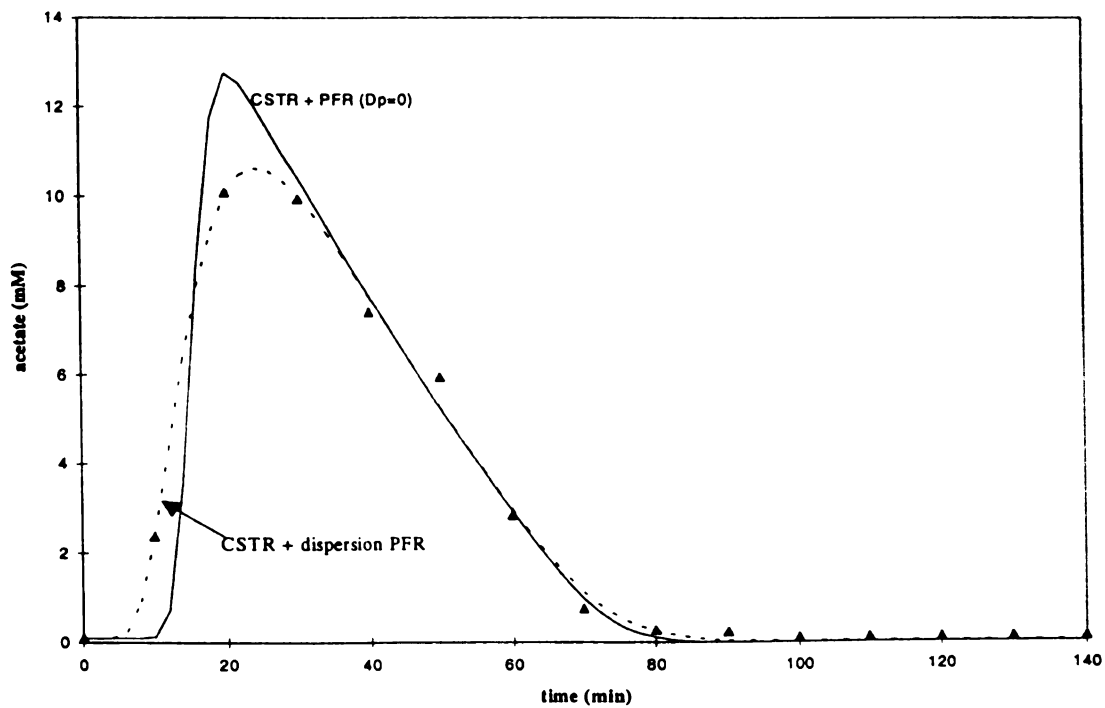


Figure IXC-10. Comparison of dispersion PFR and PFR (dispersion factor is zero) during acetate impulse modeling

Table LXB-1. Experimental conditions of the bench-scale UASB reactor during the acetate impulse and step OLR increase experiments.

OLR (kgCOD/m ³ bed-d)	9 - 10	Reactor total volume (L)	3.1
HRT (hrs)	11	Reactor gas volume (L)	1.1
Temperature (°C)	37	granular bed volume (solids and liquid) (L)	1.6 - 1.7
pH	6.8-7.1	Gas production rate (L/d)	5.3 - 6.7
Total flow rate (L/d)	6.6 - 6.7	Methane content (%)	75 - 80
Feed COD^a (kg/L)	11.4		

a. the feed is a synthetic brewery waste which contains 25mM of acetate (Appendix A)

Table IXB-2. Model parameters used in simulation

k_m^a	(gAc/gX-d)	5.11
K_s^a	(mmol/L)	0.45
D_g	(m ² /s)	4.42×10^{-10}
R^a	(mm)	1.5
ϵ^b		0.69
δ^c	(μ m)	100
A_r^b	(mm ²)	1.05×10^{-6}
$X^{b,g}$	(gVS/L)	42
X_m	(gVS/cm ³)	0.135
K_L	(mm/s)	1.3×10^{-2}
f^c		0.8 - 1.0
$\frac{D_p}{L^2}^d$	(1/min)	0.001 - 0.005
$\frac{u}{L}^d$	(1/min)	0.01 - 0.065

a. measured from separate kinetic studies

b. measured from the granular bed of the UASB reactor

c. obtained from previous hydraulics study (Chapter V)

d. final converged range

e. granule active layer from the surface toward central core.

f. D_g is diffusion coefficient of acetate within granules; ϵ is granular sludge bed

porosity = $\frac{\text{voidspace}}{\text{totalvolume}}$; R is granule radius; A_r is total granule surface area in the

bed; X is biomass concentration within the bed; X_m is biomass (acetate utilizers) density within the granules; f is the fraction of flow entering the working volume.

g. measured as volatile solids. when account for the active portion within the granule(δ), which is 18.7% of a granule total volume, the active acetate utilizer biomass concentration in the bed will be 7.85 gVS/Lbed.

Table IXB-3. Results obtained from acetate impulse and step OLR increase and Lithium Chloride impulse.

	LiCl impulse	Acetate step increase	Acetate impulse
K_L (mm/s)	NA	0.013	0.013
D (m ² /s)	NA	4.42×10^{-10}	4.42×10^{-10}
f	0.76	0.99	0.90
$\frac{D_p}{L^2}$ (1/min)	0.001	0.0035	0.005
$\frac{u}{L}$ (1/min)	0.064	0.0125	0.0625
$V_{\text{disp.PFR}}^b$	0.02V ^a	0.1V	0.02V
Gas production rate (L/d)	5.3	1st step: 12.0 2nd step: 17.7	peak: 33.6
V_b (CSTR working volume)	0.91V	0.90V	0.92V
V_d (dead volume)	0.07V	0 V	0.06V

a. V is reactor total volume

b. calculated from $\frac{u}{L}$.

Table IXB-4. Comparison of UASB reactor hydraulics and mass transfer during Lithium Chloride and acetate impulse and acetate step OLR increase

	LiCl impulse	Acetate step increase	Acetate impulse
$\frac{D_p}{L^2}$ (1/min)	0.001	0.0035	0.005
Gas production rate (L/d)	5.3	1st step: 12.0 2nd step: 17.7	peak: 33.6
Background OLR (kgCOD/m ³ bed-d)	9.0	9.0	9.4

CHAPTER 10. SUMMARY AND CONCLUSIONS

The study performed on the UASB reactor and the brewery granules are summarized and conclusions drawn presented below:

A. UASB reactor hydraulics

1. UASB reactors represented non-ideal flow reactors for the experimental conditions tested (ranging from 4-10 kgCOD/m³bed-d OLR and 12 hrs-2days HRT). Reactor flow regimes were different at low and high OLR due to the differences in gas production. Hydraulic flux had strong influences on the mixing.
2. The granular sludge bed in the UASB reactor was non-uniform with respect to expansion at the same flux rate. Granule particle sizes varied along the height of the bed. The extent of mixing varied throughout the bed. Hydraulic regime in the bed could be described as a combination of mixed flow, dead volume and by-pass flow. The structure and proportion of these non-ideal flow elements varied with the operational conditions and reactor status.
3. The flow models developed (Models 1 and 2) described the hydraulics of the UASB reactor very well, for low and high OLR, respectively.

B. Kinetics of substrate utilization within the brewery granules

4. Mass transfer and diffusional limitations had a significant influence on overall substrate utilization when using whole granules (up to 3.0mm in diameter) and disrupted granules (1.1mm). Substrate utilization through both liquid film and granules

were mass transfer limited. The order of diffusional limitation for substrate, in terms of effectiveness factor, was acetate > propionate > ethanol.

5. UASB reactor system performance can be improved by minimizing mass transfer resistance. This can be accomplished by reducing granule size and increasing reactor liquid recirculation rate.

6. Acetate utilization using granule flocs followed Monod kinetics and Van't Hoff-Arrhenius relationship very well, indicating mass transfer limitation was minimized. These kinetic parameters can be used to represent the intrinsic kinetics of the biomass in the granular sludge.

7. Temperature impact on substrate utilization within the granules was more pronounced when $T \geq 31^\circ\text{C}$ for flocs, disrupted granules and whole granules. The magnitude of the impact on substrate utilization rates correlated with granule size. No exponential relationship between temperature and reaction rate was observed for the large granules (whole granules and disrupted granules). This indicates the overall degradation rate is mass transfer limited. Temperature effects were predominant when using small flocs ($33\mu\text{m}$) produced by physically disrupting the granules.

8. Ethanol degradation to methane followed a stoichiometric relationship. Major electron flow can be described as ethanol \rightarrow acetate \rightarrow methane. N-propanol observed was an intermediate from ethanol degradation.

9. Propanol pathway study proved no evidence of CO_2 involvement in propanol formation during ethanol degradation.

10. The reaction of ethanol condensation to form propanol is likely a candidate for propanol formation during ethanol degradation. Hydrogen plays a strong role as a driving force governing reactions involving propionate, based on reaction energetic analyses.

C. Microbial populations and granule structure

11. The brewery granules tested have a complex internal structure, including an active layer at the peripheral of granules with finger like cell clusters, and a central core. The active layer was high in cell density, heterogeneous in microbial population. Ethanol and propionate degraders, acetoclastic and hydrogenotrophic methanogens were present in the active layer in a mixed network rather than in layered arrangement. *Methanothrix* sp. were the prevailing population of acetoclastic methanogens in the anaerobic granules.

D. Monitoring UASB reactor

12. UASB reactor performance variables VFAs, gas production rate, methane content and responses of H₂ and CO were influenced primarily by OLR. The impact of feed concentration was not significant.

13. The degree of variation of the monitoring variables, based on their CV (ordered from low to high), was: CH₄ > gas production > propionate > CO > acetate >> H₂, indicating H₂ had highest variation and thus most sensitive while CH₄ was the least sensitive. Standard errors of monitoring variables suggested H₂ had the highest

background noise while CH_4 had the lowest noise. There is no cyclic pattern within the monitoring variables.

14. UASB reactor performance at unsteady state was affected by OLR strength, step increase and the duration of the each step. An OLR of $60 \text{ kgCOD/m}^3\text{bed-d}$ applied to the UASB reactor for more than 14 hours can lead to system failure. Gas production, VFAs and H_2 were among the most sensitive variables in responding to high OLR perturbations. Methane content and suspended solids were the least.

15. Liquid phase components recovered faster than that of gas phase components, after a high strength OLR ($60 \text{ kgCOD/m}^3\text{bed-d}$) perturbation. The sequence of the recovery for each component was: alcohols and long chain VFAs > acetate and propionate > pH > H_2 > gas production rate and CO > methane.

16. H_2 was very sensitive to high strength OLR (i.e. $60 \text{ kgCOD/m}^3\text{bed-d}$) and displayed an increased response to repeated perturbations and the system failure. However, H_2 concentration exhibited high background noise. CO correlated with performance variables well. The response of CO was high to the first OLR perturbation but response decreased during repeated OLR perturbations that occurred within 24-48 hours. Response of CO to system failure was slow. Both H_2 and CO may not be used alone as anaerobic system indicators. Successful monitoring can be accomplished by using gas and liquid phase controlling variables together.

E. Dynamic modeling of UASB reactor

17. The dynamic hydraulic-reaction-diffusion model (Model 2) developed in this study adequately described the transient behavior of the UASB reactor under acetate OLR perturbations. The kinetic parameters measured using the granules in separate experiments were successfully applied to the model. The model has the feature of being comprehensive, structured and mechanistic. Most UASB reactors used in the U.S. are operated at conditions similar to the bench-scale UASB reactor tested (OLR of 10 kgCOD/m³-d and HRT of ≤ 12 hrs). The model developed therefore has the potential to be a tool for understanding and examining the inherent properties of the system and predicting system behavior during organic perturbations.

18. Neither a CSTR reaction model alone without mass transfer, nor a reaction-diffusion model with a CSTR, could adequately describe UASB response during an acetate OLR perturbation. This confirms that an ideal CSTR does not describe the UASB well.

19. Simulation results indicated the UASB reactor system was sensitive to hydraulic parameters, granule sizes and kinetic parameters and not sensitive to mass transfer coefficient, K_L . Granule radius (R) was among the most sensitive parameters in governing overall substrate utilization rate. This agrees with the experimental results from kinetic and mass transfer studies.

CHAPTER 11. RECOMMENDATIONS FOR FUTURE RESEARCH

1. Due to structural differences in the microbial population within anaerobic granules, such as layered or heterogeneous outer structure, which may influence the diffusion of substrate and reaction intermediates, a study of mass transfer within the granules of layered structure is needed.
2. Multiple substrates and multiple pathways should be included in the hydraulic-reaction-diffusion model developed (Model 2), to describe the anaerobic degradation of complex organic waste. The effect of the thickness of the active layer (δ) needs to be tested.
3. The response of the UASB system to toxicity and inhibition should be included in the model and studied in detail.
4. Pilot- and/or full-scale testing and further field verification of the hydraulic-reaction-diffusion model (Model 2) needs to be performed.
5. Finally, based on the information gathered from studying UASB reactor systems, a monitoring and control strategy needs to be developed to reach the ultimate goal of characterization of the system – process control. The application of this transient model for process control requires advances in development of expert systems, fuzzy control, time series model combining with knowledge based control.
6. Further research on n-propanol production during ethanol degradation is needed, including identifying the involvement propionate, the reaction mechanism, reaction kinetics, and the key microbial species involved in the pathway and their growth and substrate utilization kinetics.

APPENDIX A

Appendix A

Medium and feed composition

In order to prevent precipitation and growth in the feed to the UASB reactor, two separate media feeds were made: one to supply the minerals and trace nutrients required (mineral medium) and the second to supply the organics (synthetic brewery waste feed). Trace minerals were prepared separately and added as a solution to the mineral medium. The composition of the mineral media solution and trace minerals used are presented in Tables A-1 and A-2, respectively. All chemicals were of reagent grade.

Table A-1. Mineral medium composition
(prepared in 16 liter batches)

Chemical	Amount	Supplier
NaCl	3.2g	Baker Analytical
NH ₄ Cl	3.2g	Baker Analytical
MgCl ₂ ·6H ₂ O	3.2g	Mallinckrodt
CaCl ₂ ·2H ₂ O	1.6g	Sigma Chemical
K ₂ HPO ₄	0.1g	Columbus
KH ₂ PO ₄	0.05g	Baker Analytical
NaHCO ₃	30.24g	Mallinckrodt
Trace mineral*	32ml	_____

* prepared separately

A total of four different organic concentrations for the synthetic brewery waste feed were used to feed the laboratory-pilot UASB reactor. Feed I was

11.4kgCOD/m³, feed II was 5.7kgCOD/m³, feed III was 9.1kgCOD/m³ and feed IV was 13.7kgCOD/m³. The feeds were adjusted using sodium hydroxide to obtain a final pH of 5.0±0.1. Feed I was used during steady state operation(Chapter VIII). The composition of Feeds I-IV are are presented in Tables A-3 and A-4.

Table A-2. Composition of trace mineral solution
(prepared in 1 liter batches)

Chemical	Amount	Supplier
Nitrilotriacetic acid	12.8g	Sigma Chemical
FeSO ₄ ·7H ₂ O	0.1g	Sigma Chemical
MnCl ₂ ·4H ₂ O	0.1g	Sigma Chemical
CoCl ₂ ·6H ₂ O	0.17g	Columbus
CaCl ₂ ·2H ₂ O	0.1g	Sigma Chemical
ZnCl ₂	0.1g	Fisher Scientific
CuCl ₂ ·2H ₂ O	0.02g	Fisher Scientific
H ₃ BO ₃	0.01g	Aldrich
Na molybdate	0.01g	Sigma Chemical
NaCl	1.00g	Baker Analytical
Na ₂ SeO ₃	0.017g	Sigma Chemical
NiSO ₄ ·6H ₂ O	0.026g	Fisher Scientific

Table A-3. Synthetic brewery waste feed composition
(prepared in 8 liter batches)

Feed I

Chemical	Amount	Supplier
NaOH	9.6g	Mallincrodt
Resazurin (0.2%)	10ml	Sigma Chemical
Acetic acid	12ml	Fisher seientific
Propionic acid	8.88ml	Mallincrodt
Glucose	7.2g	Sigma Chemical
FeSO ₄ .7H ₂ O	1.335g	Sigma Chemical
Ethanol(190proof)	36.8ml	Quantum

Table A-4. Synthetic brewery waste feed composition
(prepared in 8 liter batches)

Feeds II, III, IV *

Chemical	Feed II	Feed III	Feed IV
NaOH	4.80g	7.68g	11.52g
Resazurin (0.2%)	10ml	10ml	10ml
Acetic acid	6.0ml	9.6ml	14.4ml
Propionic acid	4.4ml	7.1ml	10.7ml
Glucose	3.60g	5.76g	8.64g
FeSO ₄ .7H ₂ O	0.6675g	1.068g	1.6g
Ethanol(190proof)	18.4ml	29.4ml	66.2ml

* for chemical supplier see Table A-3.

Phosphate buffered basal medium (PBBM) was used during n-propanol assay. Medium pH was brought to 7.2-7.4, boiled and flushed with N₂. After autoclaving, Phosphate buffer (15% KH₂PO₄ and 29% K₂HPO₄), reducing agent (2.5%Na₂S), and sterilized vitamins were then added. Table A-5 presents the composition of PBBM.

Table A-5 Phosphate Buffered Basal Medium
(prepared in 1 Litter batch)

Chemicals	Quantity
Double Distilled Water	945 ml
NaCL	0.9 g
MgCL ₂ .6H ₂ O	0.2 g
CaCL ₂ .2H ₂ O	0.1 g
NH ₄ CL	1.0 g
Trace Mineral II*	10 ml
Resazurin Solution, 2%	1 ml

* see Table A-2

APPENDIX B

Appendix B

Materials and Methods

B-1. Activity assays for acetate, propionate and ethanol using brewery granules

B-1.1. Inoculum and media

B-1.1.1. Inoculum preparation and biomass estimation

Granules were obtained from a laboratory bench-scale UASB reactor(Figure VIII-1) which was acclimated to the synthetic brewery waste(Table A-3) for 6 months. Granules taken from the bench-scale UASB were stored at room temperature in an 8 L carboy equipped with a water seal. Before the start of this experiment, the inocula were incubated overnight at 37°C with a trace amount(ca. 1-2 mg/l) of ethanol to stimulate the activity of different populations and reduce any lag phase in the assay. At the conclusion of the assays, the granules were subjected to microscopic examination for particle size measurements and population observations. Granule size was estimated by geometric averaging. Several fields under the microscope were randomly selected for the particle size distribution measurement. The geometric mean for each field was determined and particle size was estimated using the following equation:

$$\text{Mean size} = \Sigma[P_i Q_i / Q_i] / n \quad \dots \quad (\text{B-1})$$

where P_i is particle size in each field($i=1,2,3..m$), Q_i is the number of that particle in size i within that field(ranging 1-80), j is the number of field($j=1,2,3...n$).

Biomass concentrations were analyzed for total solids and volatile solids(TS and VS) for experiments conducted using the Multigen reactor contents(Appendix C).

B-1.12. Medium preparation and inoculum transfer technique

Between 1.2 and 1.4 L of medium (composition in Table A-1) in a 2 L glass flask was flushed with nitrogen gas(AGA Inc.) for 20 minutes. The solution pH was adjusted to 7.00 ± 0.01 using 3N HCL or 3N NaOH(under nitrogen). After transferring the medium to a Multigen reactor, a known amount(80–100ml) of inocula(granules or flocs) was transferred promptly to the multigen reactor(New Brunswick Scientific, model F1000) (Figure VI-1). The reactor was then sealed, heated and stirred(for detail description of the multigen system refer to Chapter VI). To reduce any oxygen brought into the reactor during transfer, 0.25 ml of 2.5% Na₂S (Fisher Scientific) was injected into the reactor from the sampling port. The experiment was initiated immediately after the desired temperature was attained in the reactor.

B-1.2. Assays for intrinsic kinetic parameters for acetate, propionate and ethanol degradation

Brewery granules, obtained from the laboratory bench-scale UASB reactor were first disrupted using a mortar and pestle. This was sufficient to disrupt the granules to an average size of 1.1 mm in diameter. These small granules were then further fractionated in a Multigen reactor(impeller speed 600rpm) for several hours and examined under microscope until flocs of about 33 μ m in diameter were

formed. During this process, 3-4 mmole/L of acetate was maintained in the reactor to avoid endogenous metabolism. The Flocs were then transferred to a water sealed flask. The flask was then amended with 0.2 ml of 2.5% Na_2S , and stored at room temperature. Analytical methods for VFA, ethanol, n-propanol, formate, H_2 , CO , and CH_4 are described in Appendix C. Protocols for the intrinsic kinetic assays were described in Chapter VI. Typical sampling frequency for these assays are presented in Tables VI-2 and VI-3.

B-2. Residence time distribution(RTD) experiments for the laboratory bench-scale UASB reactor

A concentrated tracer, lithium chloride(Sigma Chemical) or acetate solution was injected into the inlet of the reactor using a 50 ml syringe equipped with a 21-gauge needle. Liquid samples(1.0 ml) were collected from the sampling port at recirculation line(Figure VIII-1). Samples were directly transferred into 1.5 ml polypropylene eppendorf micro test tubes(Brinkmann) using a 3 ml syringe and a 21-gauge needle. Samples were then centrifuged in an eppendorf centrifuge(Brinkmann, model 5415) at 12000rpm for 2 minutes. The supernatant was collected for analysis. Analytical methods for determining Lithium chloride and acetate concentration is described in C2 and C6, Appendix C. A sampling frequency of 2 minutes was used for the organic and hydraulic flux assays. A sampling frequency of 10% of the hydraulic retention time(HRT) was used during flow modeling experiments using lithium and 10 to 15 minutes using acetate.

B-3. Tracer recovery test for adsorption on granular sludge

The extent of lithium chloride adsorption on the granular sludge was determined to examine any influence of adsorption during the tracer study. The tracer recovery test was conducted in 58 ml serum bottles sealed with rubber stopper and aluminum crimps. The step by step procedure is described below:

- (1) 58 ml serum bottles with 5 ml nutrient media(pH=7.0) were vacuum flushed with N₂ for 0.5 hr, and sealed. A 3 ml volume of synthetic brewery waste was added to the bottles using a 3 ml syringe with a 21-gauge needle. These media had the same composition as the reactor feed and mineral media(Appendix A).
- (2) 0.1 ml of 2.5% Na₂S was added into the serum bottles to scavenge any O₂.
- (3) the serum bottles were flushed with 20% CO₂/80% H₂ for 5 minutes to adjust the pH range to between 6.8-7.0.
- (4) 5.0 ml of anaerobic granules were added into the serum bottles, using a 5 ml syringe with a 18-gauge needle.
- (5) 0.5 ml of 3.2 g/l LiCl solution was added into the bottle to obtain a final liquid volume of 13 ml and LiCl concentration of 120 mg/l.
- (6) The serum bottles were incubated at 37°C (same as the reactor temperature) in an Incubator Shaker(New Brunswick, model G25) at 170 rpm for 24 hours to reach equilibrium.
- (7) A 1.2 ml of liquid sample was withdrawn from each of the serum bottles into 1.5 ml eppendorf test tubes. The tubes were then centrifuged at 12000 rpm for 2 minutes in an eppendorf centrifuge. The supernatant was then collected for analysis.
- (8) Lithum concentration was determined by a Ion Chromatography(Dionex model 2000)

B-4. Unsteady state perturbation experiment using the laboratory bench-scale UASB reactor

An organic loading rate(OLR) perturbation was introduced using the on-line monitoring and control syetem PARAGON(Intec) through an analog/digital(A/D) interface (OPTO-22) and a Watson-Marlow pump(503 U)(Figure VIII-1, Appendix C-4). A Typical feed control program for step OLR variation is presented below:

Table B-1. Typical sequency preogram during unsteadystate perturbation experiment
(block SEQ INFLUENT in PARAGON)

Step	Slope/min	End Value	Hold Time(min)	Next Step
1	0	3.0	60	y
2	0	4.75	180	y
3	0	7.0	420	y
4	0	4.75	180	y
5	0	3.0	600	y

Impulse OLR were performed manually by injecting the desired mass of organic carbon directly into the reactor inlet. Trace gas (H₂ and CO) monitoring settings for PARAGON program and Integrater/controller module(ICM) of trace gas analyzer are presented in Table B-2.

**Table B-2. Unsteady state monitoring parameters setting
for Paragon and ICM**

PARAGON blocks	RGA3 ICM
Traux H₂ range:0.04-1000ppm	Span: H ₂ =0.04-1000ppm
Traux CO range:0.004-10.4ppm	CO =0.004- 10.4ppm
SEQ tracegas: hold time=16.9667min	Sense: 500
or 26.9667min	
Hist: data collect=10min	

Other portions of the PARAGON program and the ICM program remained same as these presented in Appendix C–2 and Appendix C–4, respectively.

B-5. Dissolved H₂ and CO measurements

B-5.1. RGA3 trace gas analyzer ICM module program

sense=100

for other settings see Appendix C–2.

B-5.2. Procedure for dissolved H₂ and CO measurements

A serum bottle technique was used for the dissolved gas analyses. To prevent any biological activity(uptake or production of CO and H₂) during the measurements of dissolved gases, which could interfere with the results, a strong alkali(NaOH) solution was added into the serum bottle prior to adding the sample. After the aqueous sample reached equilibrium with gas phase in the serum bottle, the gas phase H₂ and CO concentration were measured. Dissolved gas concentration in the sample was estimated according to Henry's law. For

calculations of the dissolved H_2 and CO refer to Chapter VIII-F. A detailed description of the serum bottle procedure used is presented below:

Initially, 25 ml serum bottles were vacuum flushed and pressurized with N_2 (AGA, Inc) for 12 minutes and sealed with a rubber stopper and aluminum crimp. The bottles were then autoclaved to ensure sterility. 2 ml of a 3N NaOH solution was added under N_2 atmosphere. The following steps were then executed:

- * warm up serum bottles in a 37°C shaking water bath(American Scientific YB-521)
- * flush a 5 ml glass gas syringe(SGE) with a mininert valve(SVLLMA) and a 21gauge needle in an anaerobic sterile bottle
- * flush the syringe with the head space of the serum bottles twice, slowly take 1 ml gas sample, inject to RGD2 trace gas analyzer, checking for the background
- * flush a 10 ml syringe with reactor effluent twice from the reactor sampling port
- * slowly take 10 ml liquid sample to ensure no bubble formation due to a vacuum forming using the syringe.
- * inject the sample immediately into the anaerobic serum bottles using a 21-gauge needle. The concentration of NaOH in the serum bottles was ca. 0.5N.
- * shake serum bottles for 5 minutes in 37°C water bath(American Scientific YB-521) to reach equilibrium

- * flush a 5.0 ml glass gas syringe with a mininert valve and a 21-gauge needle in an anaerobic sterile bottle filled with N₂ gas
- * take a 1.0 ml gas sample from the serum bottle head space
- * inject into trace gas analyzer(RGD2) for analysis

B-6. Isotopic assay for determining n-propanol pathway

n-propanol assay was performed on serum vials (158 ml). ¹³C(1-C) ethanol (Cambridge Isotope, 95%) was used as substrate. Serum vials were vacuum flushed with N₂ for 0.5 hr. 50ml PBBM medium (Table A-5) was transferred into serum vials and the content pH was adjusted to 7.0 using 80%CO/20%H₂ gas. 0.3ml of granule was injected in to serum vials using a 1ml syringe with a 18-gauge needle. ¹³C(1-C)ethanol was then added in to the solution using a 3ml syringe with a 21-gauge needle. Above procedure was conducted under N₂ atmosphere. Aqueous samples were withdrawn from serum vials using a 1ml syringe with a 21-gauge needle and were filtered through a 0.2 μm syringe filter. Samples were then extracted with ethyl-acetate(see following section). ¹³C n-propanol was determined using gas chromatography/mass spectra, at a scan wavelength of 471-485nm.

B-6.1 Protocol for extraction of n-propanol

- * in a 4ml glass vial, add 1ml sample mixed with 1ml ethyl-acetate(Aldrich, 99.5%), shake well
- * pipet 0.5ml top layer of the solution into a 1.2ml auto sampler crimp vial(toflon lined)

- * add 0.5ml ethyl-acetate, seal the vial with aluminum crimp, mix well
- * store sample in refrigerator for analyses

B-7. Microscopy

Granule and flocs size distributions were estimated using an Olympus DF plan bright field microscope. Microbial population observations were performed on an Olympus phase contrast microscope(model BH-2) equipped with a mercury lamp, and a Confoco laser beam microscope. The autofluorescence of methanogens was observed with a B(IF-490) excitation filter. Transmission electron microscopy(TEM) was performed with a Philips CM-10 electron microscope.

Thin section granule samples were immersed into a 2.5% Glutaraldehyde solution containing a 0.1 M phosphate buffer(pH=7.2). The ratio of fixative to sample was approximately 10:1(v/v). Samples were left submerged for a week at 4°C to ensure complete penetration of fixative. The fixed samples were rinsed three times at room temperature using a 0.1 mM phosphate buffer(pH 7.2), and then postfixed with 1% OsO₄ in the same buffer. The samples were then dehydrated through a graded series of ethanol solutions and propylene oxide. Finally, the samples were embedded in polybed 812 plastics. Thin sections were cut with a LKB ultratome and stained with 0.5% toluidine blue.

APPENDIX C

Appendix C

Quality Assurance and Quality Control

This section details the monitoring, sampling, storage, analyses and calibration procedures established to assure and control the quality of analytical measurements. These procedures were used for the batch kinetics experiments and the laboratory bench-scale UASB reactors. Unless specified here, the QA/QC plan follows the recommendations given in the Radian Corporation document: "*Guidelines for the Preparation of GRI Quality Assurance Project Plans*" (August 1990).

C-1. Monitoring and sample recording during laboratory bench-scale UASB reactor operation

Critical reactor components and parameters were monitored and recorded daily. The Daily Monitoring Sheet was filled out during each monitoring check. A Daily Monitoring Sheet used for the laboratory bench-scale UASB reactor is attached (Appendix C4). During unsteady state perturbation experiments, a separate monitoring sheet was used (Appendix C4). Gas phase sample data were available through an on-line data acquisition system equipped with a personal computer (386). Separate files were created twice a week. Data was in general monitored hourly. The Daily Monitoring Sheet along with the gas monitoring file served as the official record of the conditions in a reactor on any given day of an experiment. The sheet also served as the official record of some directly measured parameters, mineral media and feed preparation, changes made in reactor parameters, problems encountered and samples collected. A generic list of the information recorded on Daily Monitoring Sheet is presented in Table C-1.

Table C-1. List of information recorded on Daily Monitoring Sheets

Direct measurements	
gas composition	liquid pH
gas production	effluent VFA/ethanol
gas and liquid phase CO/H ₂	influent VFA/ethanol
reactor temperature	TSS/VSS
feed temperature	bed height
flow rate(feed/media/recycle)	
Pump and tubing checks	
feed pump and tubing	
medium pump and tubing	
effluent tubing	
Feed and mineral preparation	
feed supply	
medium supply	
Troubleshooting	
gas collector pressure/floating granule	
effluent tubing precipitation	
pH variation	
Samples taken for analysis	
Acetate, propionate, ethanol	
CO, H ₂ , CH ₄ , gas production rate	
TSS, VSS	

Gas phase monitoring and analysis records were stored in the "History File" of Paragon data acquisition package. Data in the file was transferred and rearranged bi-weekly into a "Lotus 1-2-3" working file via a W00 file. The records were stored on a hard disk and backup copies were maintained on floppy disks. The bi-weekly data files were combined through the Excel spread sheet weekly. Gas production rate computation was conducted and gas phase monitoring variables(H_2 CO, CH_4 and gas production) plotted with time for further analysis.

C-2. Sampling, storage, analysis and calibration

A summary of the various analyses performed and the methods employed are presented in Table C-2.

C-2.1 VFAs, ethanol and n-propanol

C-2.11 Sampling and storage

The laboratory bench-scale UASB reactor and Multigen bench top reactor samples were taken with a 5 ml polyethylene syringe which has been flushed with reactor fluid prior to sampling. The samples were slowly withdrawn into the syringe to avoid any gas bubbles from forming in the solution. Samples were collected, transferred into 1.5 ml eppendorf tubes and centrifuged at 12000 rpm in an eppendorf centrifuge(Brinkmann model 5415) for 2 minutes. A 0.8 ml aliquot of supernatant was then collected using a pipette and acidified with 0.3 M oxalic acid at a ratio of 1/10 (acid/sample) in a 1.2 ml auto sampler crimp vial.

Table C-2. Analytical methods for samples from laboratory bench-scale UASB and batch experiments

Parameter	Method
VFAs/ethanol,propanol	Gas Chromatography with packed column/FID
CO/H ₂	Reduction Gas Detection using a Hg reaction bed and photo diode detector
CH ₄	Infra red gas analyzer
Gas production	liquid displacement/ conductivity
TSS	dry at 105°C *
TS	evaporate at 60°C,dry at 105°C *
VSS	ignition at 550°C *
VS	ignition at 550°C *

* in accordance with *Standard Methods*[16th ed.]

Finally, the samples were sealed with a Teflon liner and aluminum crimp. The sample vials were either immediately analyzed or stored at 0°C. Stored samples were all analyzed within one week.

C-2.12 Analysis and calibration

Liquid samples were analyzed for VFA with a HP 5890 Gas Chromatograph, equipped with a packed column, FID, and HP7673A automator injector. Separation was accomplished using a 4% Carbowax organic phase on a 80/120 carbopac P column, ID 2mm, 2m in length(Supelco). N₂ was used as the carrier gas(16-20 ml/min). Column

temperature was programmed for better peak separation. Three different programs(working files 5, 7, 8) were used for sample analysis according to the concentration range and species of interest. Analysis conditions are listed in Table C-3. Standard calibration curves were made using an internal standard method. Propionate was selected as an internal standard for acetate calibration.

Eight levels of acetate standard concentrations, ranging from 0.1 to 20 mM, were used for calibration using both work file 7 and 8, and were compared for linearity at low range and high range(Figure C-1 and C-2). Standard concentrations of acetate at 0.01-0.05 mM were used for calibration with work file 5. Linearity did not exist for work file 7 at concentrations lower than 1 mM (Figure C-1). It was determined that the conditions in work file 8 were better for accurately quantifying low concentrations (0.1-1 mM) of acetate, work file 7 was best for the high concentration range(>1 mM) and work file 5

Table C-3. GC operational conditions for VFAs analysis

Parameters	work file 7	work file 8	work file 5
Gas flow rate N ₂	16-20ml/min	16-20ml/min	16-20ml/min
H ₂	30ml/min	30ml/min	30ml/min
air	300ml/min	300ml/min	300ml/min
column head pressure	50psi	50psi	50psi
Temperature			
injection port	200°C	190°C	190°C
column	175°C	140-220°C, ramp 5°C/min	140°C
detector	200°C	220°C	220°C

for micromolar level quantitation. Since the response of propionate, butyrate and iso-butyrate were proportional to acetate under the conditions used, butyrate and propionate standards were made together with acetate, at 5 mM for each component. The acetate, propionate, and butyrate standard was analyzed along with samples to check any change in response scale. Adjustment was made as required. Sample concentration was calculated based on the standard curve. The detection limit for acetate was 4 mM, 0.1 mM and 1 mM using work files 5, 8 and 7, respectively. Propionate, iso-butyrate and butyrate detection limits were 0.1 mM, 0.1 mM and 0.1 mM with work file 8. Standard curves for 2-methyl-butyrate, n-valerate, iso-valerate were made separately, as external standards. These acids were analyzed using work file 8. Detection limits were 0.04 mM, 0.3 mM and 0.1 mM for 2-methyl-butyrate, n-valerate and iso-valerate, respectively. The VFA standard was fixed with 0.3 M oxalic acid at 1/10 (acid/standard), prepared once a month and stored at 0°C when not in use.

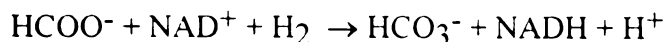
Ethanol and n-propanol standards(external standards), were prepared without acidification. The ethanol standard was made once a month and stored at 0°C. Ethanol and n-propanol were analyzed using work file 8. The detection limit for ethanol was 0.01 mM and for n-propanol it was 0.05 mM.

C-2.2 Formate

C-2.2.1 Sampling, analysis and calibration

Formate was analyzed for enzymatically using formate dehydrogenase. Formate dehydrogenase have the following reaction when NAD is present using formate as

substrate:



The amount of NADH, as measured by the extinction change at 365 nm, is proportional to the amount of formate present. The extinction change was measured using a spectrophotometer(UV160,Shimadzu). The proportionality factor was determined by standardization of the assay with formate standards. The maximum value of the extinction-time curve was recorded. Both standard and samples were adjusted with blanks(without NAD). Sample formate concentration was determined using the standard curve. Samples were first adjusted to pH of 7.0-7.5 using 1N NaOH. Details of the procedure were conducted according to "*Methods of enzymatic analysis*"[Bergmeyer,H.R.].

C-2.3 Gas phase analysis

C-2.31 Gas sampling loop and instrumentation

Gas phase CO, H₂, CH₄ and gas production from bench-scale UASB were sampled and analyzed on-line. Gas samples were collected from a gas loop connected to reactor head space(200 ml). To remove moisture in gas stream, a condenser was placed at the top of the reactor prior to where the gas entered the gas loop, to dry the gas and prevent condensation in the gas loop itself. The reactor gas loop set-up is presented in Figure VIII-1.

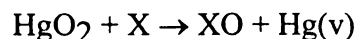
The gas stream was pumped at a flow rate of 0.5 L/min continuously into an infrared Methane Analyzer(ADC SB100) for on-line quantitation. Gas produced was

collected into a three-way valve. The valve also connected to a gas meter(house made by MBI) and a exhaust pipe. Gas produced was continuously forwarded through the gas meter and then vented out of the system.

Gas samples were introduced into a trace gas analyzer(RGA3) for CO and H₂ analysis from reactor head space via automated actuated gas sampling valves. A 10-port, in-line gas sampling valve was connected to a trace gas loop (250 ml, within the instrument) that reactor headspace was continuously pumped through. During load position, trace gas loop is separated from column. Carrier gas N₂ flow in column is reversed. The components remaining in column are back flushed to vent with the carrier gas. In the inject position, trace gas sample loop and column are connected in series. CO and H₂ are allowed to elute from column to detector. Sample inlet and outlet lines were shorted in order to provide continuity of sample flow.

C-2.32 CO and H₂ analysis and calibration

Sample components of interest(H₂ and CO)were separated chromatographically within an isothermal mandrel-heated column oven in a Reduced Gas Analyzer(RGA3, Trace Analytical) and quantitated by a reduced gas detection method. Species eluting from the chromatographic column pass immediately into the detector which contains a heated bed of mercuric oxide. The following reduction reaction occurs:



where X is the reduced gas species. The mercury vapor produced by the reaction is quantitated by a ultraviolet photo diode. The detection limits for H₂ and CO were 40 ppb and 4.0 ppb, respectively. A spherocarb 60/80 packed column was used in Reduced Gas Analyzer(RGA3, and RGA2). Operational conditions are presented in Table C-4.

Data analysis was performed automatically by the integrator/controller module(ICM) in the RGA3. The ICM consisted of a single board computer. It was programmed for complete operation, including sample collection(timed events), zeroing, detector signal noise filtering, peak detection and integration, components identification, calibration and self-testing. The operation of ICM was monitored by the program in the host computer through the Opto-22 analog/digital interface board. ICM program set-up for CO and H₂ used in the study is shown in Table C-5.

Table C-4. Reduced Gas Analyzer operating conditions

Column temperature	90°C
Detector temperature	265°C
Carrier gas flow rate	16±0.5ml/min
Sample volume	250mL
Injection time	70s
Backflush time	19min-55min
N ₂ gas pressure	30psig
Air pressure	25psig

Trace gas H₂ and CO calibration was conducted using the ICM with 10.4 ppm CO(in N₂, Specialty Gas) and 50.3 and 95.2 ppm H₂(in N₂, Specialty Gas).

For kinetic assays, H₂ and CO were determined on a RGA2 gas chromatograph with a RGD2 reduced gas detector. The operation conditions were 90°C for the column and 265°C for the detector. Backflush time was set at four minutes using a timer(Eagle Signal). Carrier gas (N₂) flow conditions were same as RGA3. Calibration was made by inject 1ml aliquots of 101ppm and 50.3ppm H₂ standard(in N₂, Specialty Gas), and 1ml aliquots of 10.2ppm and 5.37ppm CO standard(in N₂, Specialty Gas). All sample H₂ and

CO concentrations were calculated from a standard response (peak heights) factor calculated from the standard injections. Standards were injected with every batch of samples. The detection limit of RGD2 were 3.8 ppm and 0.5 ppm, for H₂ and CO, respectively.

Table C-5. ICM parameters programming

Detector test:	x8 25mv
range:	x1
ICM	
Table-peak-gate:	pk01 on 0012s off 0025s
	pk02 on 0038s off 0052s
Event-integrator-1:	on 0010s off 0090s
Test-detector-raw:	span 32mv
-smooth:	filter x8
-slope:	pk01 014s → 20s
	pk02 040s → 70s
Table-filter-sense:	200 mV
-slice:	0.125s
Table-peak-STD:	pk01 100ppm Tol 100%
	pk02 10.4ppm Tol 100%
unit:	ppm
method:	external
name:	pk01 H2 pk02 CO
Table-valve-auto:	0.004s
Table-stream-SEQ:	01-00-000-000
Table-ext.start-active:	on
alarm:	low
Table-trend-Tr01	strm 01 comp 01 zero 0.04 span 1000
	Tr02 strm 01 comp 02 zero 0.004 span 1.0
Event-1-01(cycle time):	0180s

Table 5-C. (Cont'd)

1-02(step time):	0001s
1-03(process data):	0170s
1-04(integrator on):	0014s
1-05(integrator off):	0090s
1--10(zero):	0001s
1-13(filter on):	0001s

C-2.33 Dissolved H₂ and CO**C-2.331 Sampling and storage**

Liquid samples(10ml) were taken from bench UASB reactor using a 10ml syringe. The samples were injected into 58ml anaerobic sterilized serum bottle sealed with a rubber stopper and aluminum crimp. Bottles were then brought into equilibrium in a water shaker(American Scientific YB-521)at 37°C at setting 8 for 5 minutes. NaOH was placed in the bottle to obtain a final concentration of 0.5N. Dissolved H₂ and CO were analyzed immediately.

C-2.332 Analyses and Calibration

Dissolved H₂ and CO were measured by injecting 1ml serum bottle headspace sample into a reduced gas analyzer(RGA2 and RGD2). GC conditions were exactly same as described in sectionC2-3.2. Background sample of the serum bottles were taken.

Replicate injections were made for each sample. All sample H₂ and CO concentrations were calculated from a standard response(peak heights) factor calculated from the standard injections. Standards were injected with every batch of samples. Detailed protocol for dissolved H₂ and CO analyses refer to Appendix B5-2.

C-2.34 CH₄

C-2.341 Sampling, Storage, Analyses and Calibration

The gaseous sample in the bench UASB reactor flowed continuously through the analysis cell of the instrument(ADC), which is situated between a hot wire source and the infra red(IR) detector. Methane absorbs energy from the IR source and reduces the amount reaching the detector. Output signal from the detector was collected, and stored in the Paragon program of the host computer. Calibration and zeroing were performed weekly. The zero was adjusted separately at power off(mechanical adjustment) and power on using air. The span was adjusted with 99.9% CH₄ standard gas at flow rate of 0.5L/min for 15 minutes after warming up the instrument.

For kinetic assays, methane was determined by a gas chromatograph using manual injection. Gas sample was collected from the Multigen reactor headspace and injected 0.1ml aliquots into the GC immediately. Two aliquots were injected and averaged. The GC used was a Hewlett-Packard 5890 with a flame ionization detector. Separation was accomplished with a Supelco Inc. VOCAL capillary column(30m, 0.53mmID, 3.0mmfilm). GC conditions were: Oven 45°C, Detector 200°C, Injector 150°C. Calibration was made by injecting 0.1ml aliquots of 99.99% methane standard gas(AGA, specialty). All sample methane concentrations were determined based on standard response(peak area) factor calculated from the standard injections. Standards were injected with every batch of samples.

C-2.35 Gas production

Gas volume produced in the reactor was measured by means of liquid displacement and change of conductivity. A three-way valve was connected to the reactor head space, the gas meter, and an exhaust part. The gas produced depressed the liquid level in the gas meter(Figure C-3, position1) from first to second electrode until the volume between the two electrodes was completely displaced replaced by the gas (position2). The change of conductivity(from water to gas) was then transmitted into a digital signal to a counter. The gas count was recorded and stored in the Paragon. The three-way valve was then actuated and the "packet" of gas vented(position2). The valve was immediately placed back to the original position while the liquid level in the gas meter returned to the first electrode level(position1).

The gas meter was calibrated by injecting air through the gas meter using a 15ml syringe. The gas counts and volume injected were recorded. Five to ten injections were made to obtain an averaged gas volume per count for calculation of gas production. The calibration was made every six months. Liquid level of gas meter reservoir was filled every 2 months. Gas meter electrodes were cleaned with 0.3 M oxalic acid solution every 2 months to remove any biofilm build .

C-2.36 CO₂**C-2.361 Sampling and storage**

Gas samples(0.6ml) were taken in 1.0ml gas tight syringe from the Multigen reactor headspace. Samples were taken directly to the gas chromatograph for immediate analyses.

C-2.362 Analyses and Calibration

Carbon dioxide were measured by injecting Multigen reactor headspace samples into the gas chromatograph. The GC used was a GOW-MAC series 580 with a TCD. Separation was accomplished with a Supelco, Inc. carbosphere 80/100 packed column(1/8 in S.S., 6 ft). GC conditions were: Injector 100°C, Detector 150°C, Oven 150°C.

Calibration was made by injecting 0.6ml aliquots of 20%CO₂/80%N₂(AGA, specialty). The calculated response(peak area) factor was used to calculate all concentrations. Standards were injected with every batch of samples.

**C-2.4. Total Suspended Solids(TSS) and Volatile
Suspended Solids(VSS)****C-2.41 Sampling and storage**

Effluent samples from the laboratory bench-scale UASB reactor were withdrawn from the effluent port continuously over 20-24 hours to provide a time-integrated sample. The effluent flow was collected in a 2 L cylinder. Since occasionally some floating granules escaped from the reactor bed into the effluent (which may interfere with the

suspended solids measurement).any granules settled in the bottom of the cylinder were removed. For analyses, 50 ml mixed aliquots were filtered in a vacuum filter through 4.5 cm Whatman 934 AH glass fiber filter paper.

C-2.42 Analysis

Filters were dried at 105°C overnight for TSS, ignited at 550°C for VSS, using an aluminum dish, and weighed as described in section 209C&D of *Standard Methods*[1985]. All weights and volumes were recorded on a Solids Data Sheet(attached Appendix C4.)

Blank filters were prepared prior to sample analysis. For blanks, 50 ml deionized distilled water was filtered, dried, ignited according to the same procedure as for the samples. The blanks were stored in a vacuum dessicator. Blanks were weighed prior to sample filtering.

C-2.5. Total Solids(TS) and Volatile Solids(VS) for granules

C-2.51 Sampling and storage

Granular sludge samples were collected from the laboratory bench-scale UASB reactor through the bed discharge port. The granule samples from the Multigen reactor was collected using a 3 ml syringe connected to a piece of 1.6 mm ID Teflon tubing. Samples were settled in a 25 ml glass cylinder covered with parafilm for 20-30 minutes. Solids volume was then recorded. Samples were transferred into preweighed porcelain crucibles for analysis.

C-2.52 Analysis

The samples were evaporated in a 60°C oven overnight and dried at 105°C for one hour and then weighed for total solids analysis. Volatile Solids(VS) were determined after ignition at 550°C for one hour, as described in *Standard Method*, section 209C&D[1985]. All weights and volumes were recorded.

Blanks were prepared in the same way as described for samples. After drying, ignition and cooling, blank crucibles were stored in a vacuum dessicator. Blanks were weighed prior to sample collection.

C-2.6 Lithium

C-2.61 Sampling and storage

Lithium samples of 5ml were collected from the sampling port of the bench UASB reactor, filtered through a 0.2µm syringe filter, and transferred into a 10ml glass tube. The samples were stored at 0°C. Stored samples were all analyzed within one week.

C-2.62 Analysis and calibration

Lithium concentration was determined by Flame Emission Spectroscopy. The FES used was a Spectra AA-20 Plus using air-acetylene. Analyses conditions were: wavelength 670.8nm, slit width 1.0nm. A series dilutions of five standards were made. Triplets were injected into the FE for each standard concentration. Results were averaged to obtain a standard curve. Samples were injected into the FES and the concentrations were calculated according to the standard curve. Standards were injected with every batch

of samples. Ion Chromatography was also used in determining Lithium concentration during the organic and hydraulic flux effect experiment(Chapter V B). The IC used was a Dionex, model 2000) equipped with a conductivity detector. Calibration was performed using the same method described above.

C-3. Data sheets

The data sheets for steady state daily monitoring and unsteady state monitoring are presented as Table C-6 to 7, respectively.

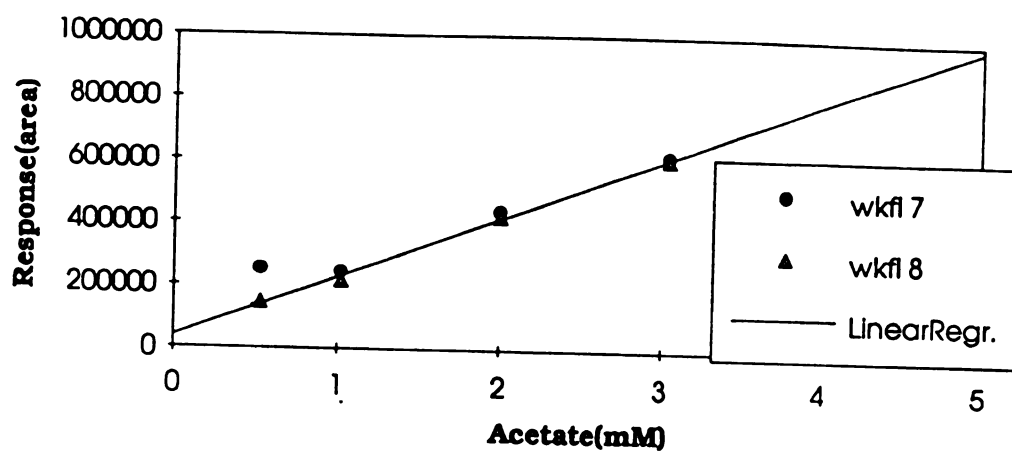


Figure C-1. Response of work file 7 and 8 to low concentration of acetate

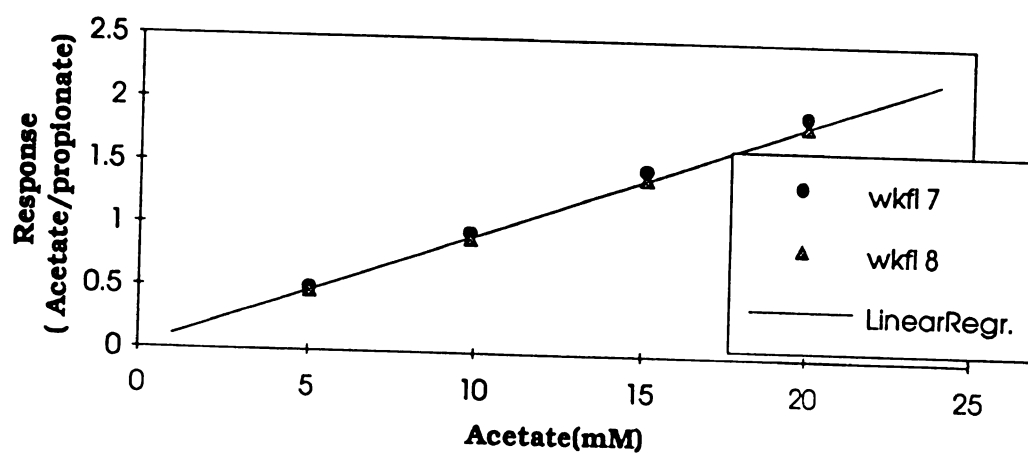


Figure C-2. Response of work file 7 and 8 to high concentration of acetate

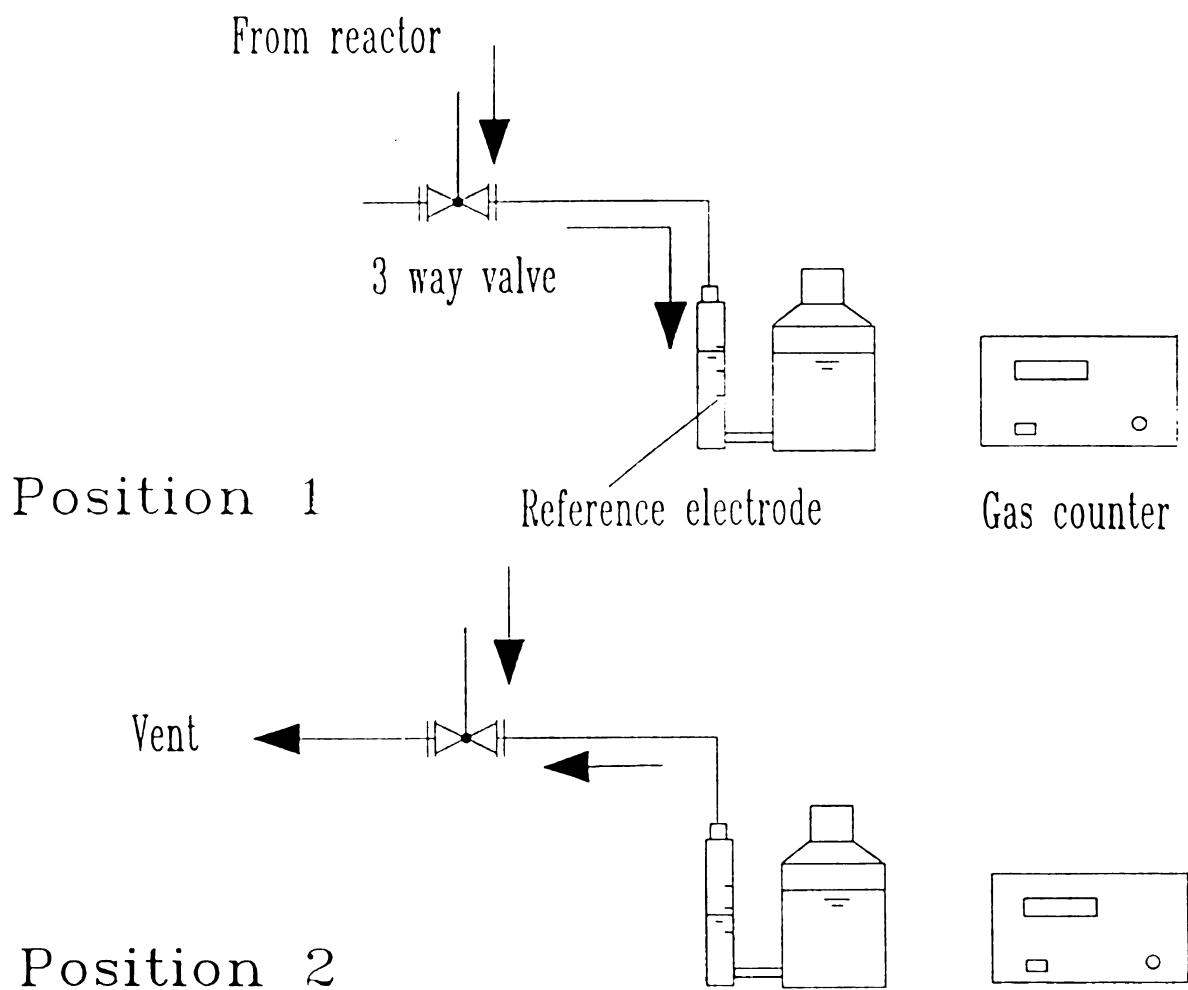


Figure C-3. Schematic diagram of on-line gas volume measurement

Table C-6. pseudo-steady state daily monitoring sheet

PARAMETER	FREQUENCY OF MEASUR- MENT	MON	TUE	WED	THUR	FRI	SAT	SUN
Date								
Time								
pH (M.L.)	daily							
Eff. (ml)	daily							
Bed (ml)	daily							
Flow rate (ml/d)	daily							
Change carbouy(M/F)								
Inf. Act. (mM)								
Prop. (mM)								
Ethanol (mM)								
Gluc. (mM)								
Eff. Tss (mg/l)								
Vss (mg/l)								
CODs (mg/l)	weekly							
Eff. Act. (mM)	daily							
Prop. (mM)	daily							
H ₂ (mM)								
CO (mM)								
Feed level(L)								
Gas meter reading	daily							
Total gas (ct/h)	daily							
CH ₄ (%)	daily							
H ₂ (ppm)	daily							
CO (ppm)	daily							
Recyc. pump reading	daily							
Feed pump reading	daily							
Feed tubing check	daily							
Med.pump reading	daily							
Med.tubing check	daily							
Temp. heater (oC)	daily							
Temp. cooler (oC)	daily							
Effluent tubing	daily							
Note								

Table C-7. Unsteady state monitoring sheet

[illegible]

APPENDIX D

Appendix D

Determination of Monod Kinetic Constants k_m and K_s by Nonlinear Least Square Method

D-1. Differential form.

The differential form of Monod equation is given by

$$v = f(s) = \frac{1}{x} \frac{ds}{dt} = -\frac{k_m s}{K_s + s} \quad (1)$$

where s is substrate in g/l, x is biomass in g, v is uptake rate in g/gx-d, k_m is the maximum uptake rate in g/gx-d, s_i , v_i are measured data, $f(s_i)$ is the estimated uptake rate at s_i as determined using equation (1). The residual sum of square SS is defined by

$$SS = \sum_{i=1}^n (v_i - f(s_i))^2. \quad (2)$$

The derivative of f and SS become

$$\frac{\partial f}{\partial k_m} = \frac{s}{K_s + s}, \quad (3a)$$

$$\frac{\partial f}{\partial K_s} = -\frac{k_m s}{(K_s + s)^2}, \quad (3b)$$

$$\frac{\partial SS}{\partial k_m} = -\sum_{i=1}^n 2(v_i - f(s_i)) \frac{\partial f(s_i)}{\partial k_m}, \quad (3c)$$

$$\frac{\partial SS}{\partial K_s} = -\sum_{i=1}^n 2(v_i - f(s_i)) \frac{\partial f(s_i)}{\partial K_s}. \quad (3d)$$

Setting $\frac{\partial SS}{\partial k_m} = 0$ and $\frac{\partial SS}{\partial K_s} = 0$, we see from (3c) and (3d) that

$$\sum_{i=1}^n \left(v_i - \frac{k_m s_i}{K_s + s_i} \right) \frac{s_i}{K_s + s_i} = 0, \quad (4a)$$

$$\sum_{i=1}^n \left(v_i - \frac{k_m s_i}{(K_s + s_i)^2} \right) \frac{s_i}{K_s + s_i} = 0. \quad (4b)$$

Hence

$$\sum_{i=1}^n \frac{v_i s_i}{K_s + s_i} = \sum_{i=1}^n \frac{k_m s_i^2}{(K_s + s_i)^2}, \quad (5a)$$

$$\sum_{i=1}^n \frac{v_i s_i}{(K_s + s_i)^2} = \sum_{i=1}^n \frac{k_m s_i^2}{(K_s + s_i)^3}. \quad (5b)$$

Define $S(1)$, $S(2)$, $S(3)$ and $S(4)$ by

$$S(1) = \sum_{i=1}^n \frac{v_i s_i}{K_s + s_i}, \quad S(2) = \sum_{i=1}^n \frac{s_i^2}{(K_s + s_i)^3}, \quad \text{and}$$

$$S(3) = \sum_{i=1}^n \frac{v_i s_i}{(K_s + s_i)^2}, \quad S(4) = \sum_{i=1}^n \frac{s_i^2}{(K_s + s_i)^2}.$$

Then in terms of $S(i)$, $i = 1, \dots, 4$, the solution for k_m using equations (5a) and (5b) can be written as either

$$k_m = S(1)/S(4) \quad \text{or} \quad k_m = S(3)/S(2). \quad (6)$$

This implies that $S(1)S(2) = S(3)S(4)$, or equivalently,

$$\sum_{i=1}^n \frac{v_i s_i}{K_s + s_i} \sum_{i=1}^n \frac{s_i^2}{(K_s + s_i)^3} = \sum_{i=1}^n \frac{v_i s_i}{(K_s + s_i)^2} \sum_{i=1}^n \frac{s_i^2}{(K_s + s_i)^2}. \quad (7)$$

In solving equation (4) for K_s , k_m can be found by substituting K_s into either one of equations in (6).

D-2. Integrated form.

The integrated form of Monod equation is given by

$$t_i = \frac{1}{k_m x} \left[Vol \times K_s \ln \left(\frac{s_0}{s_i} \right) + Vol \times (s_0 - s_i) \right] \quad (8)$$

where t_i is the measuring time in day, Vol is reaction volume in liters. Let

$$a = \frac{K_s}{k_m x}, \quad b = \frac{1}{k_m x}.$$

Equation (8) then becomes

$$t_i = a \times Vol \times \ln \left(\frac{s_0}{s_i} \right) + b \times Vol \times (s_0 - s_i).$$

The residual sum of square is given by

$$SS = \sum_{i=1}^n \left[a \times Vol \times \ln \left(\frac{s_0}{s_i} \right) + b \times Vol \times (s_0 - s_i) - t_i \right]^2 \quad (9)$$

Setting $\frac{\partial SS}{\partial a} = 0$ and $\frac{\partial SS}{\partial b} = 0$ results in

$$\begin{aligned} a \times \sum \left[Vol \times \ln \left(\frac{s_0}{s_i} \right) \right]^2 + b \times \sum \left[Vol \times \ln \left(\frac{s_0}{s_i} \right) \right] [Vol \times (s_0 - s_i)] \\ = \sum \left[t_i \times Vol \times \ln \left(\frac{s_0}{s_i} \right) \right] \end{aligned} \quad (10a)$$

and

$$\begin{aligned} a \times \sum \left[Vol \times \ln \left(\frac{s_0}{s_i} \right) \right] [Vol \times (s_0 - s_i)] + b \times \sum [Vol \times (s_0 - s_i)]^2 \\ = \sum [t_i \times Vol \times (s_0 - s_i)]. \end{aligned} \quad (10b)$$

The solution a , b of equations (10a) and (10b) can be simplified by denoting

$$AC = t_i \times Vol \times \ln \left(\frac{s_0}{s_i} \right), \quad CD = [Vol \times (s_0 - s_i)] \left[Vol \times \ln \left(\frac{s_0}{s_i} \right) \right]$$

$$AD = t_i \times Vol \times (s_0 - s_i), \quad D = Vol \times (s_0 - s_i),$$

$$Q = \begin{vmatrix} \sum C^2 & \sum CD \\ \sum CD & \sum D^2 \end{vmatrix}.$$

Then

$$a = \frac{\begin{vmatrix} \sum AC & \sum CD \\ \sum AD & \sum D^2 \end{vmatrix}}{Q}, \quad b = \frac{\begin{vmatrix} \sum C^2 & \sum AC \\ \sum CD & \sum AD \end{vmatrix}}{Q}. \quad (11)$$

APPENDIX E

Appendix E.

Fortran program of the hydraulic-reaction-diffusion model

```

CCCCCCCCCCCCCCCCCCCCCCCCCCCCCCCCCCCCCCCCCCCCCCCCCCCCCCCCCCCC
C
C  THIS PROGRAM SEARCHES PARAMETERS TO FIT THE impluse CURVE. C
C
C  THE VARIABLE PARAMETERS ARE: D, Kl, Rtn, Vb, Db, Dp          C
C    OTHER READ-IN PARAMETERS ARE: Sbo (EITHER 0.0 OR 0.1) AND  C
C    NRCT.                                                       C
C                                                                C
CCCCCCCCCCCCCCCCCCCCCCCCCCCCCCCCCCCCCCCCCCCCCCCCCCCCCCCCCCCC
C  Specifications for Parameters
C
C  System parameters
INTEGER NSTEP, NPAR, I, J, JR, KR, I1, I2, ICR, NAL, MXIT
PARAMETER (NPAR=6)
INTEGER IC(NPAR), IP(NPAR), NC(NPAR), IFUN(NPAR, NPAR)
DOUBLE PRECISION Rl, RX, Rs, Rd, Sbo, Sbi, RAV, QAV
DOUBLE PRECISION TFINAL, Q, Td, T, Sbj
DOUBLE PRECISION D, Rf, Rtn, Vb, Db, Dp, EMIN
DOUBLE PRECISION CRf, CRtn, CVb, CDb, CDp, CD
DOUBLE PRECISION ERf, ERtn, EVb, EDb, EDp, ED
PARAMETER (NSTEP=46, TFINAL=9.0D0, Nd=20)
DOUBLE PRECISION TOL, ERROR, EDATA(10), TDATA(NSTEP)
DOUBLE PRECISION FLOAT, EXP, SQRT
LOGICAL      SCAN
INTRINSIC    FLOAT, EXP, SQRT
COMMON /PARAM/ D, Rl, RX, Rs, Rd, Sbo, Sbi, RAV, QAV, Td, Db
COMMON /QVB/ Q, Vb
C
C  Parameters used in DBVPFD
INTEGER  MXGRID, NEQNS, NINIT
INTEGER  NCUPBC, NFINAL, NLEFT
PARAMETER (MXGRID=45, NEQNS=2, NINIT=10)
PARAMETER (NLEFT=1, NCUPBC=1)
DOUBLE PRECISION TINIT(NINIT), YINIT(NEQNS,NINIT)
DOUBLE PRECISION ERREST(NEQNS), PISTEP, XFINAL(MXGRID),
&  XLEFT, XRIGHT, YFINAL(NEQNS,MXGRID)
SAVE    TINIT, YINIT

```

```

LOGICAL  LINEAR, PRINT
EXTERNAL DBVPFD, UMACH
EXTERNAL FSSBC, FCNEQN, FCNJAC, FCNPBC, FCNPEQ
C
C  Parameters used in DCSINT
INTEGER  NINTV
DOUBLE PRECISION BREAK(NSTEP), CSCOE(4,NSTEP), DCSVAL
DOUBLE PRECISION YTEMP(MXGRID)
EXTERNAL DCSINT, DCSVAL
C
C  Parameters used in DPLOTP
DOUBLE PRECISION RANGE(4), AP(MXGRID,10), XP(MXGRID)
CHARACTER  TITLE*25, XTITLE*10, YTITLE*10, SYMBOL*10
INTEGER  INC, NFUN
EXTERNAL  DPLOTP, DCONST, PGOPT
C
C  Parameters used in DIVPAG
INTEGER  NPARAM, IDO, INORM, IMETH, NEQ, MTYPE, IATYPE,
&  MITER, MXSTEP, NRCT, MXNEQ, NIN
PARAMETER (NPARAM=50, MXNEQ=1000)
DOUBLE PRECISION HINTT, PARAM(NPARAM), X,
&  TEND, Y(MXNEQ), SB(NSTEP), SD(NSTEP)
EXTERNAL  FCN, DIVPAG, FCNJ
COMMON /DIM/ NIN, NRCT, Dp
C
C  Common parameters
C
DATA EDATA/0.1D0,2.37D0,10.08D0,9.95D0,7.41D0,5.95D0,
&  2.85D0,0.74D0,0.27D0,0.22D0/
Rd=15.0D0
Rs=0.45D0
Q=0.46518D0
Sbj=17.0D0
C Define TDATA
DO 10 I=1, NSTEP
  TDATA(I) = TFINAL*FLOAT(I-1)/FLOAT(NSTEP-1)
10 CONTINUE
OPEN (UNIT=NOUT, FILE='impls.txt', STATUS='UNKNOWN')
PRINT*, 'ENTER SEARCH TYPE: 1=SCAN, 2=TEST'
READ*, I
IF (I.EQ. 1) THEN
  SCAN = .TRUE.
ELSE
  SCAN = .FALSE.
END IF

```

```

PRINT*, 'ENTER Sbo, Td AND NRCT'
READ*, Sbo, Td, NRCT
  NIN = NINIT
  NEQ = NIN+NRCT+1
  IF (.NOT. SCAN) THEN
    PRINT*, 'ENTER Kl, Rtn, Vb, Db, Dp, AND D'
    READ*, CRf, CRtn, CVb, CDb, CDp, CD
C CHANGE OTHER PARAMETERS
    PRINT*, 'ENTER RX, Rs, Sbj'
    READ*, RX, Rs, Sbj
    WRITE (NOUT, *) 'D, Dp, Db, Kl, RX, Rs, Sbj'
    WRITE (NOUT, 7000) CD, CDp, CDb, CRf, RX, Rs, Sbj
7000  FORMAT (7F9.4)
    GOTO 1010
  END IF
  PRINT*, 'ENTER INITIAL GUESS OF Kl, Rtn, Vb, Db, Dp, RX AND D'
  READ*, CRf, CRtn, CVb, CDb, CDp, RX, CD
  PRINT*, 'ENTER INITIAL STEPS OF Kl, Rtn, Vb, Db, Dp, RX AND D'
  READ*, ERf, ERtn, EVb, EDb, EDp, RX, ED
  PRINT*, 'ENTER ACCURACY LEVEL AND NUMBER OF ITERATIONS'
  READ*, NAL, MXIT
  WRITE(*, *) 'THE WINNERS ARE'
  WRITE(*, 2000)
2000 FORMAT(2X, 'KR', 3X, 'Kl', 6X, 'Rtn', 6X, 'Vb', 7X, 'Db', 7X, 'Dp',
& 7X, 'D', 8X, 'Error')
  EMIN = 100.0
  JR = 0
  KR = 0
  DO 5 I = 1, NPAR
    DO 5 J = 1, NPAR
      IFUN(I, J) = 0
5    CONTINUE
    DO 6 I = 1, NPAR
      IFUN(I, I) = 1
6    CONTINUE
100  WRITE(*, *) '(JR = ', JR, ')'
    WRITE(NOUT, *) '(JR = ', JR, ')'
    DO 12 I = 1, NPAR
      IC(I) = 3
12  CONTINUE
101  KR = KR + 1
    DO 11 I = 1, NPAR
      NC(I) = 0
11  CONTINUE
    DO 1000 I1 = 1, NPAR

```

```

      DO 1000 I2 = 1, 2
C SET COORDINATES
      DO 15 I = 1, NPAR
        IP(I) = (-1)**I2*IFUN(I, I1)
15    CONTINUE
C CHECK FOR OVERLAP
      ICR = 0
      DO 20 I = 1, NPAR
        ICR = ICR + ABS(IP(I)+IC(I))
20    CONTINUE
      IF (ICR .EQ. 0) GOTO 1000
C SET PARAMETERS
      Rf = CRf + ERf*FLOAT(IP(1))/2.0**JR
      Rtn = CRtn + ERtn*FLOAT(IP(2))/2.0**JR
      Vb = CVb + EVb*FLOAT(IP(3))/2.0**JR
      Db = CDb + EDb*FLOAT(IP(4))/2.0**JR
      Dp = CDp + EDp*FLOAT(IP(5))/2.0**JR
      D = CD + ED*FLOAT(IP(6))/2.0**JR
      Sbi = Sbj*Rtn
      Rl = Rf*600.0D0
      RAV = 1.05D0*Rl/Vb
      QAV = RAV + Q*Rtn/Vb
C CHECK FOR CONSTRAINTS
      IF (Rf .LE. 0.0D0 .OR. D .LE. 0.0D0) GOTO 1000
      IF (Rtn .GT. 1.0D0 .OR. Rtn .LE. 0.0D0) GOTO 1000
      IF (Db .LE. 0.0D0 .OR. Dp .LE. 0.0D0) GOTO 1000
C SET INITIAL CONDITION FOR S(X, T)
      IF (Sbo .LE. 0.01D0) THEN
        DO 61 I=1, NINIT
          Y(I) = Sbo
61    CONTINUE
          GOTO 5000
        END IF
C FIND Ss(X) BY DBVPFD (IN LOOP)
        DO 30 I=1, NINIT
          TINIT(I)=FLOAT(I-1)/FLOAT(NINIT-1)
          YINIT(1, I)=FLOAT(NINIT-I)/FLOAT(NINIT-1)
          YINIT(2, I)=0.0D0
30    CONTINUE
          TOL=1.D-06
          TINIT(1)=0.0D0
          TINIT(NINIT)=1.0D0
          XLEFT=0.0D0
          XRIGHT=1.0D0
          PISTEP=0.1D0

```

P
I
C
&
&
&
C Inte

40

60
C Sol
5000

50

70

```

PRINT=.FALSE.
LINEAR = .FALSE.
CALL DBVPFD (FCNEQN, FCNJAC, FSSBC, FCNPEQ, FCNPBC, NEQNS,
&    NLEFT, NCUPBC, XLEFT, XRIGHT, PISTEP, TOL, NINIT, TINIT,
&    YINIT, NEQNS, LINEAR, PRINT, MXGRID, NFINAL,
&    XFINAL, YFINAL, NEQNS, ERREST)
C Interpolate Ss(x)
  DO 40 I=1, NFINAL
    YTEMP(I) = YFINAL(1, I)
40  CONTINUE
  CALL DCSINT (NFINAL, XFINAL, YTEMP, BREAK, CSCOE)
  NINTV = NFINAL-1
  DO 60 I=1, NINIT
    Y(I) = DCSVAL(TINIT(I), NINTV, BREAK, CSCOE)
60  CONTINUE
C Solve Si(t) by DIVPAG (IN LOOP)
5000 HINIT = 1.0D-3
  INORM = 1
  IMETH = 2
  MITER = 2
  MTYPE = 0
  IATYPE = 0
  MXSTEP = 1000
  DO 50 I=1, NPARAM
    PARAM(I) = 0.0D0
50  CONTINUE
  PARAM(1) = HINIT
  PARAM(4) = MXSTEP
  PARAM(10) = INORM
  PARAM(12) = IMETH
  PARAM(13) = MITER
  PARAM(14) = MTYPE
  PARAM(19) = IATYPE
  IDO = 1
  X=0.0D0
  TOL = 1.0D-4
  DO 70 I=NIN+1, NEQ
    Y(I) = Sbo
70  CONTINUE
  SB(1) = Y(NEQ)
  SD(1) = Y(1)
  DO 80 I=2, NSTEP
    TEND = TDATA(I)
    CALL DIVPAG(IDO, NEQ, FCN, FCNJ, A, X, TEND, TOL, PARAM, Y)
    SB(I) = Y(NEQ)

```

80

I
C
C Esti
C
M
R
I

90

R
C UPD
I

400

I
1000
C CH
I
I

500

I
C UPD
I

700

C
C
C
C
C
C
C
V

2100

I
C

600

I

601


```

      SD(I) = Y(1)
80    CONTINUE
      IDO=3
      CALL DIVPAG (IDO, NEQ, FCN, FCNJ, A, X, TEND, TOL, PARAM, Y)
C Estimate the error in Sb(1, t). (IN LOOP)
      CALL DCSINT (NSTEP, TDATA, SB, BREAK, CSCOEf)
      NINTV = NSTEP-1
      ERROR=0.0D0
      DO 90 I=1, 10
        T=FLOAT(I-1)
        X=DCSVAL(T, NINTV, BREAK, CSCOEf)
        ERROR=ERROR+(X-EDATA(I))**2
90    CONTINUE
      ERROR=SQRT(ERROR)
C UPDATE MINIMUM ERROR
      IF (ERROR .LT. EMIN) THEN
        EMIN = ERROR
        DO 400 I=1, NPAR
          NC(I) = IP(I)
400    CONTINUE
        END IF
1000  CONTINUE
C CHECK IF THE CENTER IS CHANGED
      ICR = 0
      DO 500 I = 1, NPAR
        ICR = ICR + ABS(NC(I))
500    CONTINUE
      IF (ICR .EQ. 0) GOTO 600
C UPDATE CENTER
      DO 700 I = 1, NPAR
        IC(I) = NC(I)
700    CONTINUE
      CRf = CRf + ERf*FLOAT(IC(1))/2.0**JR
      CRtn = CRtn + ERtn*FLOAT(IC(2))/2.0**JR
      CVb = CVb + EVb*FLOAT(IC(3))/2.0**JR
      CDb = CDb + EDb*FLOAT(IC(4))/2.0**JR
      CDp = CDp + EDp*FLOAT(IC(5))/2.0**JR
      CD = CD + ED*FLOAT(IC(6))/2.0**JR
      WRITE (*, 2100) KR, CRf, CRtn, CVb, CDb, CDp, CD, EMIN
2100  FORMAT (I5, 7(F9.4))
      IF (KR .GE. MXIT) GOTO 601
      GOTO 101
600    JR = JR + 1
      IF(JR .LE. NAL) GOTO 100
601    PRINT*, 'THE FINAL RESULT IS'

```

W
2200
W
W
W
W
W
W
CLOC
1010
Rtr
Vb
Db
Dp
D
Sb
Rl
RA
QA
C SET

141

C FIN
DO

111
TO
TI
TI
X
X
PR
PR
LI
C
NLEF
&
&
&

```

      WRITE (*, 2200) KR, CRf, CRtn, CVb, CDb, CDp, CD, EMIN
2200  FORMAT (I5, 7(F9.4))
      WRITE (NOUT, *) 'Kl = ', CRf
      WRITE (NOUT, *) 'Rtn = ', CRtn
      WRITE (NOUT, *) 'Vb = ', CVb
      WRITE (NOUT, *) 'Db = ', CDb
      WRITE (NOUT, *) 'Dp = ', CDp
      WRITE (NOUT, *) 'D = ', CD
C LOOP FINISHED, RERUN TO FIND Sb(1, t) AND PLOT CURVES
1010 Rf = CRf
      Rtn = CRtn
      Vb = CVb
      Db = CDb
      Dp = CDp
      D = CD
      Sbi = Sbj*Rtn
      Rl = Rf*600.0D0
      RAV = 1.05D0*Rl/Vb
      QAV = RAV + Q*Rtn/Vb
C SET INITIAL CONDITION FOR S(X, T)
      IF (Sbo .LT. 0.01D0) THEN
        DO 141 I=1, NINIT
          Y(I) = 0.0D0
141    CONTINUE
        GOTO 5100
      END IF
C FIND Ss(X) BY DBVPFD
      DO 111 I=1, NINIT
        TINIT(I)=FLOAT(I-1)/FLOAT(NINIT-1)
        YINIT(1, I)=FLOAT(NINIT-I)/FLOAT(NINIT-1)
        YINIT(2, I)=0.0D0
111  CONTINUE
      TOL=1.D-06
      TINIT(1)=0.0D0
      TINIT(NINIT)=1.0D0
      XLEFT=0.0D0
      XRIGHT=1.0D0
      PISTEP=0.1D0
      PRINT=.FALSE.
      LINEAR = .FALSE.
      CALL DBVPFD (FCNEQN, FCNJAC, FSSBC, FCNPEQ, FCNPBC, NEQNS,
NLEFT,
      &  NCUPBC, XLEFT, XRIGHT, PISTEP, TOL, NINIT, TINIT,
      &  YINIT, NEQNS, LINEAR, PRINT, MXGRID, NFINAL,
      &  XFINAL, YFINAL, NEQNS, ERREST)

```

C Int
D

120
C
N
D

140
C So
510
I
I
M
M
I
M
I

130
F
F
F
F
F
F
F
F
I
X
7
I

150
S
S
I

160
I
C
C
C

C Interpolate $S_s(x)$

DO 120 I=1, NFINAL

YTEMP(I) = YFINAL(1, I)

120 CONTINUE

CALL DCSINT (NFINAL, XFINAL, YTEMP, BREAK, CSCOEFF)

NINTV = NFINAL-1

DO 140 I=1, NINIT

Y(I) = DCSVAL(TINIT(I), NINTV, BREAK, CSCOEFF)

140 CONTINUE

C Solve $S_i(t)$ by DIVPAG

5100 HINIT = 1.0D-3

INORM = 1

IMETH = 2

MITER = 2

MTYPE = 0

IATYPE = 0

MXSTEP = 1000

DO 130 I=1, NPARAM

PARAM(I) = 0.0D0

130 CONTINUE

PARAM(1) = HINIT

PARAM(4) = MXSTEP

PARAM(10) = INORM

PARAM(12) = IMETH

PARAM(13) = MITER

PARAM(14) = MTYPE

PARAM(19) = IATYPE

IDO = 1

X=0.0D0

TOL = 1.0D-4

DO 150 I=NIN+1, NEQ

Y(I) = Sbo

150 CONTINUE

SB(1) = Y(NEQ)

SD(1) = Y(1)

DO 160 I=2, NSTEP

TEND = TDATA(I)

CALL DIVPAG(IDO, NEQ, FCN, FCNJ, A, X, TEND, TOL, PARAM, Y)

SB(I) = Y(NEQ)

SD(I) = Y(1)

160 CONTINUE

IDO=3

CALL DIVPAG (IDO, NEQ, FCN, FCNJ, A, X, TEND, TOL, PARAM, Y)

C

CALL DCSINT (NSTEP, TDATA, SB, BREAK, CSCOEFF)

```

      NINTV = NSTEP-1
      WRITE (NOUT, 2300)
2300 FORMAT (7X, 'Ti', 11X, 'Sb')
      DO 165 I=1, NSTEP
        WRITE (NOUT, 2500) TDATA(I), SB(I)
2500 FORMAT (2F13.4)
165  CONTINUE
      WRITE (NOUT, *) 'EDATA(I)-Sb(T_i)='
      ERROR=0.0D0
      DO 170 I=1, 10
        T=FLOAT(I-1)
        X=DCSVAL(t, NINTV, BREAK, CSCOEf)
        WRITE (NOUT, *) EDATA(I) - X
        ERROR=ERROR+(X-EDATA(I))**2
170  CONTINUE
      ERROR=SQRT(ERROR)
      WRITE(NOUT, *) 'Error =', ERROR
      PRINT*, 'EMIN =', ERROR
C    Plot Sb(t), S(delta, t)
      NFUN = 2
      INC = 1
      SYMBOL = 'B*'
      XTITLE = 'T AXIS'
      YTITLE = 'CONCENTRATION'
      TITLE = 'D=S(delta,t), B=Sb(t)'
      RANGE(1)=0.0
      RANGE(2)=TFINAL
      RANGE(3)=0.0
      RANGE(4)=30.0
      DO 180 I=1, NSTEP
        XP(I) = TDATA(I)
        AP(I, 1) = SB(I)
        AP(I, 2) = -1.0D0
180  CONTINUE
      DO 190 I=1, 10
        J=(I-1)*5+1
        AP(J, 2) = EDATA(I)
190  CONTINUE
      CALL DPLOT (NSTEP, NFUN, XP, AP, MXGRID, INC, RANGE,
        &  SYMBOL, XTITLE, YTITLE, TITLE)
      END
C
C    SUBROUTINES USED IN DBVPFD.
C
      SUBROUTINE FCNEQN (NEQNS, T, Y, P, DYDT)

```

```

INTEGER  NEQNS
DOUBLE PRECISION  T, P, Y(NEQNS), DYDT(NEQNS)
DOUBLE PRECISION  D, Rl, RX, Rs, Rd, Sbo, Sbi, RAV, QAV, Td,
&  Db
COMMON /PARAM/ D, Rl, RX, Rs, Rd, Sbo, Sbi, RAV, QAV, Td, Db
DYDT(1) = Y(2)
DYDT(2) = P*RX*Y(1)/D/(Rs+Y(1))+2.0D0*Y(2)/(Rd-T)
RETURN
END

```

C

```

SUBROUTINE FCNJAC (NEQNS, T, Y, P, DYDPDY)
INTEGER  NEQNS
DOUBLE PRECISION  T, P, Y(NEQNS), DYDPDY(NEQNS,NEQNS)
DOUBLE PRECISION  D, Rl, RX, Rs, Rd, Sbo, Sbi, RAV, QAV, Td,
&  Db
COMMON /PARAM/ D, Rl, RX, Rs, Rd, Sbo, Sbi, RAV, QAV, Td, Db
DYDPDY(1,1) = 0.0D0
DYDPDY(1,2) = 1.0D0
DYDPDY(2,1) = P*Rs*RX/D/(Rs+Y(1))**2
DYDPDY(2,2) = 2.0D0/(Rd-T)
RETURN
END

```

C

```

SUBROUTINE FSSBC (NEQNS, YLEFT, YRIGHT, P, F)
INTEGER  NEQNS
DOUBLE PRECISION  P, YLEFT(NEQNS), YRIGHT(NEQNS), F(NEQNS)
DOUBLE PRECISION  DCONST
DOUBLE PRECISION  D, Rl, RX, Rs, Rd, Sbo, Sbi, RAV, QAV, Td,
&  Db
COMMON /PARAM/ D, Rl, RX, Rs, Rd, Sbo, Sbi, RAV, QAV, Td, Db
EXTERNAL  DCONST
F(1) = -D*YLEFT(2)+Rl*YLEFT(1)-Rl*Sbo
F(2) = YRIGHT(2)
RETURN
END

```

C

```

SUBROUTINE FCNPEQ (NEQNS, T, Y, P, DYDPDP)
INTEGER  NEQNS
DOUBLE PRECISION  T, P, Y(NEQNS), DYDPDP(NEQNS)
DOUBLE PRECISION  D, Rl, RX, Rs, Rd, Sbo, Sbi, RAV, QAV, Td,
&  Db
COMMON /PARAM/ D, Rl, RX, Rs, Rd, Sbo, Sbi, RAV, QAV, Td, Db
DYDPDP(1) = 0.0D0
DYDPDP(2) = RX*Y(1)/D/(Rs+Y(1))
RETURN

```

E
C
S
I
D

A
E
A
C
R
E

C
C
C

S
I
D
D
&
D
I
E
C
&
C
C
C

C
H
H
C
C
Y
D

&
10

Y
H

E

E
Y
C


```

END
C
SUBROUTINE FCNPBC (NEQNS, YLEFT, YRIGHT, P, DFDP)
INTEGER NEQNS
DOUBLE PRECISION P, YLEFT(NEQNS), YRIGHT(NEQNS), DFDP(NEQNS),
A
EXTERNAL SSET
A=0.0D0
CALL SSET (NEQNS, A, DFDP, 1)
RETURN
END
C
C SUBROUTINES USED IN DIVPAG.
C
SUBROUTINE FCN (NEQ, X, Y, YPRIME)
INTEGER NEQ, NIN, I, NRCT
DOUBLE PRECISION X, Y(NEQ), YPRIME(NEQ), H1, H2, C1, C2, C3, E
DOUBLE PRECISION D, Rl, RX, Rs, Rd, Sbo, Sbi, RAV, QAV, Td,
& Db, Q, Vb, Dp
DOUBLE PRECISION FLOAT, DCONST, SQRT, EXP
INTRINSIC FLOAT, SQRT, EXP
EXTERNAL DCONST
COMMON /PARAM/ D, Rl, RX, Rs, Rd, Sbo, Sbi, RAV, QAV, Td,
& Db
COMMON /QVB/ Q, Vb
COMMON /DIM/ NIN, NRCT, Dp
C
H1 = 1.0D0/FLOAT(NIN-1)
H2 = 1.0D0/FLOAT(NRCT)
C1 = 2.0D0*D/H1**2
C2 = 2.0D0*Rl/H1+2.0D0*Rl/Rd/D
YPRIME(1) = C1*Y(2)+C2*Y(NIN+1)-(C1+C2)*Y(1)-RX*Y(1)/(Rs+Y(1))
DO 10 I= 2, NIN-1
  C3 = 1.0D0/(Rd-H1*FLOAT(I-1))/H1
  YPRIME(I)=(C1/2.0D0+C3)*Y(I-1)+(C1/2.0D0-C3)*Y(I+1)-C1*Y(I)
  & -RX*Y(I)/(Rs+Y(I))
10 CONTINUE
YPRIME(NIN)=C1*Y(NIN-1)-C1*Y(NIN)-RX*Y(NIN)/(Rs+Y(NIN))
IF (X .LT. Td) THEN
  E=(Sbi-Sbo)/Td+Q*Sbo/Vb
ELSE
  E=Q*Sbo/Vb
END IF
YPRIME(NIN+1)=E-QAV*Y(NIN+1)+RAV*Y(1)
C1 = Dp/H2**2

```

C

S
I
I
I
I
I
&
C
C
I

C

D
D

10

H
H
C
C
D
D
D
D
D

C
I
I
I

20

C
DY
DY
DY
DY
C1
C2
DC
D

```

C2 = Db/H2
DO 20 I = NIN+2, NEQ-1
  YPRIME(I)=(C1+C2)*Y(I-1)-(2.0D0*C1+c2)*Y(I)+C1*Y(I+1)
20 CONTINUE
YPRIME(NEQ)=(0.5D0*C1-C2)*Y(NEQ)
YPRIME(NEQ)=YPRIME(NEQ)+(C2-C1)*Y(NEQ-1)
YPRIME(NEQ)=YPRIME(NEQ)+0.5D0*C1*Y(NEQ-2)
RETURN
END

C
SUBROUTINE FCNJ (NEQ, X, Y, DYDPY)
INTEGER NEQ, I, J, NIN, NRCT
DOUBLE PRECISION FLOAT
DOUBLE PRECISION X, Y(NEQ), DYDPY(NEQ, NEQ), C1, C2, C3,H1,H2
DOUBLE PRECISION D, Rl, RX, Rs, Rd, Sbo, Sbi, RAV, QAV, Td,
& Db, Dp
COMMON /PARAM/ D, Rl, RX, Rs, Rd, Sbo, Sbi, RAV, QAV, Td, Db
COMMON /DIM/ NIN, NRCT, Dp
INTRINSIC FLOAT

C
DO 10 I=1, NEQ
DO 10 J=1, NEQ
  DYDPY(I, J) = 0.0D0
10 CONTINUE
H1 = 1.0D0/FLOAT(NIN-1)
H2 = 1.0D0/FLOAT(NRCT)
C1 = 2.0D0*D/H1**2
C2 = 2.0D0*Rl/H1+2.0D0*Rl/Rd/D
DYDPY(1, 1)=-C1-C2-RX*Rs/(Rs+Y(1))**2
DYDPY(1, 2)=C1
DYDPY(1, NIN+1)=C2
DO 20 I=2, NIN-1
  C3 = 1.0D0/(Rd-H1*FLOAT(I-1))/H1
  DYDPY(I, I-1)=C1/2.0D0+C3
  DYDPY(I, I) = -C1-RX*Rs/(Rs+Y(I))**2
  DYDPY(I, I+1) = C1/2.0D0-C3
20 CONTINUE
DYDPY(NIN, NIN-1)=C1
DYDPY(NIN, NIN) = -C1-RX*Rs/(Rs+Y(NIN))**2
DYDPY(NIN+1, NIN+1) = -QAV
DYDPY(NIN+1, 1) = RAV
C1 = Dp/H2**2
C2 = Db/H2
DO 30 I=NIN+2, NEQ-1
  DYDPY(I, I-1) = C1+C2

```

```
DYDPDY(I, I) = -2.0D0*C1
DYDPDY(I, I+1) = C1
30 CONTINUE
DYDPDY(NEQ, NEQ-2)= C1/2.0D0
DYDPDY(NEQ, NEQ-1)= C2-C1
DYDPDY(NEQ, NEQ) = C1/2.0D0-C2
RETURN
END
```

LIST OF REFERENCES

Ag
WF

Ag:
perl
Eng

Ahr
E.C
and
Ana
2542

Ahri
meta
Micr

Ahri
therm
pp15

Alibr
sludg
Vol.

Alph
limite
Micr

Ames
applic

Andr
diges
Series

REFERENCES

- Agardy, F.J. and Shepherd, W.C.** DNA-A rational basis for digester loadings. *J. WPCF*. Vol.37, pp1236-1239, 1965
- Agardy, F.J., Cole, R.D. and Pearson, E.A.** Enzyme activity as a parameter of digester performance. pp51-65, In *Proceedings of the 18th Purdue Industrial Waste Conference*, Engineering extension series No.115, Purdue University, West Lafayette, IN, 1963
- Ahring, B.K. and Schmidt, J.E., Winther-nielsen, M., Macario, A.J.L., Macario, E.C.,** Effect of medium composition and sludge removal on the production, composition, and architecture of thermophilic (55°C) acetate-utilizing granules from an Upflow Anaerobic Sludge Blanket reactor, *Appl. Environ. Microbiol.* Vol.59, No.8, pp2538-2545, 1993
- Ahring, B.K. and Westermann, P.,** Kinetics of butyrate, acetate and hydrogen metabolism in a thermophilic, anaerobic butyrate-degrading triculture, *Appl. Environ. Microbiol.* Vol.53, No.2, pp434-439, 1987
- Ahring, B.K. and Westermann, P.,** Methanogenesis from acetate: Physiology of a thermophilic acetate-utilizing methanogenic bacteria, *FEMS Microbiol. Lett.* Vol. 28, pp15-19, 1985
- Alibhai K.R.K. and Forster, C.F.,** Physicochemical and biological characteristics of sludges produced in anaerobic upflow sludge blanket reactors, *Enzyme Microb. Technol.* Vol. 8, Oct. pp601-606, 1986
- Alphenaar, P.A., Perez, M.C. and Lettinga, G.,** The influence of substrate transport limitation on porosity and methanogenic activity of anaerobic sludge granules. *Appl. Microbiol. Biotechnol.*, Vol.39, pp276-280, 1993
- Ames, W.F.,** Numerical methods for partial differential equations. Computer Science and applied mathematics series, Ed. Rheinboldt, W., *Academic press*, New York, 1977
- Andrews, J.F. and Graef, S.P.,** Dynamic modeling and simulation of the anaerobic digestion process. *Anaerobic Biological Treatment Process.*, Advances in Chemistry Series, Vol.105, pp126-162, American Chemical Society, Washington, D.C., 1971

An
uti

An
J.

Al
19

A
cc
V

A
m
p

F
fr

V
e

I
c

Andrews, J.F., A mathematical model for the continuous culture of microorganisms utilizing inhibitory substrate. *Biotechnol. Bioeng.*, Vol.10, pp707-723, 1969

Andrews, G.F. and Tien, C. The expansion of a fluidized bed containing biomass, *AIChE J.* Vol.25, No.4, 1979

APHA–AWWA–WPCF *Standard Methods*, part 209 C & D, pp96-98, 16th edition, 1985

Asinari di San Marzano, C.M. Volatile fatty acids, an important state parameter for the control of the reliability and the productivities of methane anaerobic digestions. *Biomass.* Vol.1, pp47-59, 1981

Atkinson, B. and Davies, I.J., The overall rate of substrate uptake (reaction) by microbial films. Part I. A biological rate equation. *Trans. Inst. Chem. Engrs.*, Vol.52, pp248-259, 1974

Bae, J. and McCarty, P.L. Variation of carbon monoxide production during methane fermentation of glucose. *Wat. Environ. Res.* Vol.65, No.7, pp890-898, 1993

Bailey, J.E. and Ollis, D. F. Chapter 4, *Biochemical Engineering Fundamentals*, 2nd edition, McGraw-Hill, New York, 1986

Barnett, M. and Andrews, J.F. Expert system for anaerobic digestion process operation. *J. of Environ. Eng.* Vol.118, No.6, pp949-963, 1992

Benfield, L. and Molz, F., A model for the activated sludge process which considers wastewater characteristics, floc behavior and microbial population. *Biotechnol. Bioeng.*, Vol.26, pp352-361, 1984

Benfield, L. and Molz, F., An activated sludge model which considers toxicant concentration: simulation and sensitivity analysis. *Applied Mathematical Modelling*, Vol.9, pp454-465, 1985

Bennett, C.O. and Myers, J.E. Momentum, heat and mass transfer. Chemical engineering series, 3rd ed., McGraw-Hill, 1982

Bergmeyer, Hans Ulrich ed. *Methods of Enzymatic Analysis*, Vol.3, 1974

Berthouex, P.M. Constructing control charts for wastewater treatment plant operation. *J. WPCF*, Vol.61, No.9, pp1534-1551, 1989

Bolle, W.L., van Breugel, J., van Eybergen, G.C., Kossen, N.W.F. and van Gils, W., An integral dynamic model for the UASB reactor, *Biotechnol. Bioeng.*, Vol.28, pp1621-1636, 1985

- Bolle, W.L. et al** Modeling the liquid flow in upflow anaerobic sludge blanket reactors, *Biotechnology and Bioengineering*, Vol.28, No.11, 1986
- Bolte, J.P. and Hill, D.T.**, A comprehensive dynamic model of attached growth anaerobic fermenters. *Trans. ASAE*, Vol.36(6), pp1805-1814, 1993
- Boone, D.R., Johnson, R.L. and Lin, Y.**, Diffusion of the interspecies electron carriers H_2 and formate in methanogenic ecosystems and its implications in the measurements of K_m for H_2 and formate uptake, *Appl. Environ. Microbiol.* Vol.55, pp1735-1741, 1989
- Bornstein, B.T. and Barker, H.A.**, The energy metabolism of *Clostridium kluyveri* and the synthesis of fatty acids, *J. Biological Chemistry*, Vol.172, pp659-669, 1948
- Boscolo, A., Mangiavacchi, C., Drius, F., Rongione, F., Pavan, P. and Cecchi, F.** Fuzzy control of an anaerobic digester for the treatment of the organic fraction of municipal solid waste (MSW). *Wat. Sci. Technol.* Vol.27, No.2, pp57-68, 1993
- Braun, M., Mayer, F., Gottschalk, G.** *Clostridium aceticum* (Wieringa), a microorganism producing acetic acid from molecular hydrogen and carbon dioxide. *Arch. Microbiol.* Vol.128, pp288-293
- Brockwell, P.J. and Davis, R.A.** Time Series: theory and methods. Springer-Verlag, 1987
- Bryant, M.P., Campbell, L.L., Reddy, C.A., Crabill, M.R.**, Growth of *Desulfovibrio* in lactate or ethanol media low in sulfate in association with H_2 -utilizing methanogenic bacteria, *Appl. Environ. Microbiol.* Vol.33, pp1162-1169, 1977
- Bryant, M.P., Wolin, E.A., Wolin, M.J., Wolfe, R.S.**, *Methanobacillus omelianskii*, a symbiotic association of two species of bacteria. *Arch. Microbiol.*, Vol.59, pp20-31, 1967
- Bryers, J.D.**, Structured modeling of the anaerobic digestion of biomass particulates. *Biotechnol. Bioeng.*, Vol. 27, pp638-649, 1985
- Buhr, H.O. and Andrews, J.F.**, The thermophilic anaerobic digestion process. *Water Res.*, Vol.11(2), pp129-144, 1977
- Carr, A.D. and O'Donnell, R.C.**, The dynamic behavior of an anaerobic digester. *Prog. in Water Technol.*, Vol.9, pp727-738, 1977
- Chang, H.N.**, Numerical calculation of effectiveness factors for the Michaelis-Menten type kinetics with high thiele moduli, *J. A.I.ChE.*, Vol.28, No.6, 1982

Chang, J.E., Noike, T., Matsumoto, J. Effect of pH on methanogenesis in anaerobic digestion, *Proc. of J.S.C.E.*, No.335, pp79-87, 1983

Chang, J.E., Noike, T., Matsumoto, J. Effect of retention time and feed substrate concentration of methanogenesis in anaerobic digestion, *Proc. of J.S.C.E.*, No.320, pp67-76, 1982

Chapman, D.T. Mixing efficiency as estimated by nonlinear least squares *Canadian J. of Civil engineering*, Vol.10, pp703-712, 1983

Chartrain, M. and Zeikus, J.G. Microbial ecophysiology of whey biomethanation: Characterization of trophic populations and prevalent species composition in continuous culture, *Appl. Environ. Microbiol.*, Vol.51, pp188-196, 1986

Cholette, A. and Cloutier, L. Mixing efficiency determinations for continuous flow systems, *Canadian J. of Chemical engineering*, June, 1959

Chung, K.T. Inhibitory effects of H₂ on growth of *Clostridium cellobioparum*. *Appl. Environ. Microbiol.*, Vol.31, pp342-348, 1976

Chung, Y.C. and Neethling, J.B. ATP as a measure of anaerobic sludge digester activity. *J.WPCF* Vol.60, pp107-112, 1988

Clark, R.H. and Speece, R.E. The pH tolerance of anaerobic digestion. In *Advances in Water Pollution Research* Proceedings of the fifth International Conference on Water Pollution Research., San Francisco and Hawaii, 1970, II-27, pp1-14, Pergamon Press, Oxford UK, 1971

Colin, F. Development of an automatic equipment for the study of acid-base equilibria for the control of anaerobic digestion. In *Anaerobic digestion and carbohydrate hydrolysis of waste*. pp391-394, eds. Ferrero, G.L., Ferranti, M.P. and Naveau, H., Elsevier Applied Science Publishers, London, 1984

Cord-Ruwisch et al. , The capacity of hydrogenotrophic anaerobic bacteria to compete for traces of hydrogen depends on the redox potential of the terminal electron acceptor, *Arch. Microbiol.* Vol.149, pp350-357, 1988

Costello, D.J., Greenfield, P.F. and Lee, P.L. Dynamic modeling of a single-stage high-rate anaerobic reactor-I. Model derivation. *Water Res.* Vol. 25 (7), pp847-858, 1991a

Costello, D.J., Greenfield, P.F. and Lee, P.L. Dynamic modeling of a single-stage high-rate anaerobic reactor-II. Model verification. *Water Res.* Vol. 25 (7), pp859-871, 1991b

Dague, R.R. Application of digester theory to digester control. *J. WPCF*. Vol.40, pp2021-2032, 1968

D
E

D
C
V

D
C

R
C
I

R
C
V

R
E

R
A

R
P
V

R
S
A

C
S
I

C
d
A

C
T

Daniels, L., Sparling, R. and Sprott, G.D. The bioenergetics of methanogenesis. *Biochim. Biophys. Acta* Vol.768, pp113-163, 1984

De Beer, D., Huisman, J.W., Van den Heuvel, J.C. and Ottengraf, S.P.P., The effect of pH profiles in methanogenic aggregates on the kinetics of acetate conversion. *Wat. Res.* Vol.26 (10), pp1329-1336, 1992

Dirasian, H.A., Molof, A.H. and Borchardt, J.A. Electrode potentials developed during sludge digestion. *J.WPCF.* Vol.35, pp424-439, 1963

Eichler, B., Schink, B., Oxidation of primary aliphatic alcohols by *Acetobacterium carbinolicum* sp. nov., a homoacetogenic anaerobe., *Arch. Microbiol.*, Vol.140, pp147-152, 1984

Eikmanns, B., Thauer, R.K. Catalysis of an isotropic exchange between CO₂ and the carboxyl group of acetate by *Methanosarcina barkeri* grown on acetate. *Arch. Microbiol.* Vol.138, pp365-370, 1984

Fouda, A.E. and Capes, C.E. Hydrodynamic particle volume and fluidized bed expansion, *The Canadian J. of Chem. Engr.* Vol.55, August, 1977

Fukuzaki S., Nishio, N., Nagai, S., Kinetics of the methanogenic fermentation of acetate, *Appl. Environ. Microbiol.* Vol.56, No.10, pp3158-3163, Oct., 1990a

Fukuzaki S., Nishio, N., Shobayashi, M., Nagai, S., Inhibition of the fermentation of propionate to methane by hydrogen, acetate and propionate, *Appl. Environ. Microbiol.* Vol.56, No.3, pp719-723, Mar. 1990b

Fukuzaki, S., Nishio, N., Sakurai, H., Nagai, S., Characteristics of methanogenic granules grown on propionate in an upflow anaerobic sludge blanket (UASB) reactor. *J. Ferment. Bioeng.*, Vol. 71, No.1, pp50-57, 1991

Garside, J. and Al-Dibouni, M.R. Velocity-voidage relationships for fluidization and sedimentation in solid-liquid system, *Ind. Eng. Chem. Process Des. Dev.*, Vol.16, No 2, 1977

Graef, S.P. and Andrews, J.F., Mathematical modeling and control of anaerobic digestion. Water-1973 (Ed.G.F.Bennett), Symposium Series No. 136, Vol.70, pp101-113, AIChE, New York, New York, 1974

Gujer, W. and Zehnder, A.J.B., Conversion process in anaerobic digestion. *Water Sci. Technol.*, Vol.15, pp127-167, 1982

1
2
3

4
5

6
7

8
9
10
11

12
13
14

15
16

17
18

19
20

21
22
23
24

- Gujer, W. and Zehnder, A.J.B.**, Conversion process in anaerobic digestion, *Water Science and Technology*, Vol.15, pp127-167, 1983
- Hall, E.R.** Improving hydraulic efficiency in high rate anaerobic systems, *A seminar sponsored by Pollution Control Association of Ontario*, March, 1984, Burlington, Ontario
- Hall, E.R.** Non-intrusive estimation of active volume in anaerobic reactors, *Water Poll. Res. J. Canada* Vol.20, No.2, 1985
- Hang Min and Zinder, S.H.**, Kinetics of acetate utilization by two thermophilic acetotrophic methanogens: *Methanosarcina* sp. strain CALS-1 and *Methanotherix* sp. strain CALS-1, *Appl. Environ. Microbiol.* pp488-491, Feb. 1989
- Hamelers, H.V.M. and Koster, I.W.**, Estimation of the kinetic constants of acetoclastic methanogens from batch experiments, *Proc. EWPCA conf. on anaerobic waste water treatment. Industrial presentations.*, Amsterdam, The Netherlands, pp625-628, 1986
- Harper, S.R. and Pohland, F.G.** Enhancement of anaerobic treatment efficiency through process modification. *J.WPCF*, Vol.59, No.3, pp152-161, 1987
- Harremoës, P.**, The significance of pore diffusion to filter denitrification. *J. Water Pollu. Control. Fed.*, Vol. 48 (2), pp377-388, 1976
- Henson, J.M., McInerney, M.J., Shawn Beaty, P., Nickels, J. and White, D.C.** Phospholipid fatty acid composition of the syntrophic bacterium *Syntrophomonas wolfei*. *Appl. Environ. Microbiol.* Vol.54, pp1570-1574, 1988b
- Henson, J.M., Smith, P.H. and White, D.C.** Examination of thermophilic methane-producing digesters by analysis of bacterial lipids. *Appl. Environ. Microbiol.*, Vol.50, pp1428-1433, 1988a
- Henze, M. and Harremoes, P.**, Anaerobic treatment of waste-water in fixed film reactors-a literature review., *Wat. Sci. Technol.*, Vol.15, pp1-101, 1983
- Heyes, R.H. and Hall, R.J.**, Anaerobic digestion modelling-The role of H₂. *Biotechnol. Lett.*, Vol. 3, pp431-436, 1981
- Heyes, R.H. and Hall, R.J.**, Kinetics of two subgroups of propionate-using organisms in a anaerobic digestion, *Appl. Environ. Microbiol.* Vol. 46, pp710-715, 1983
- Hickey, R.F. and Switzenbaum, M.S.**, Behavior of carbon monoxide as a trace component of anaerobic digester gases and methanogenesis from acetate, *E.S.&T.*, Vol.24, No.11, pp1642-1648, 1990

- Hickey, R.F. and Swizenbaum, M.S.** The role of intermediate and product gases as regulators and indicators of anaerobic digestion. In *Poster Papers, Anaerobic Digestion*. pp43-47, eds. Tilche, A and Rozzi, A., Monduzzi Editore, Bologna, Italy, 1988
- Hickey, R.F., Vanderwielen, J. and Swizenbaum, M.S.** Production of trace levels of carbon monoxide during methanogenesis on acetate and methanol. *Biotechnol. Lett.*, Vol.9, pp63-66, 1987b
- Hickey, R.F., Vanderwielen, J. and Swizenbaum, M.S.** The effect of heavy metals on methane production and hydrogen and carbon monoxide during batch anaerobic sludge digestion. *Wat. Res.*, Vol.23, pp207-218, 1989
- Hickey, R.F., Vanderwielen, J. and Swizenbaum, M.S.** The effects of organic toxicants on methane production and hydrogen gas levels during the anaerobic digestion of waste activated sludge. *Wat. Res.*, Vol.21, pp1417-1427, 1987a
- Hill, D.T. and Barth, C.L.** A dynamic model for simulation of animal waste digestion. *J. Wat. Pollut. Control. Fed.* Vol.10, pp2129-2143, 1977
- Hill, D.T.** A comprehensive dynamic model for animal waste methanogenesis. *Trans. ASAE*, Vol.25, pp1374-1380, 1982
- Huser, B.A.** Methanbildung aus acetat, PhD thesis, Swiss Federal Institute of Tech. Zurich, 1981
- Inoue, Y. and Koyama, K.** Mechanism of volatile fatty acid removal in a fixed biofilm methane fermentation reactor. *Wat. Sci. Tech.* Vol. 20 (11), pp377-383, 1988
- Iza, J. et al.** Anaerobic fluidized bed reactors (AFBR): performance and hydraulic behaviour, *5th International symposium on anaerobic digestion*, 1988
- Jones, R.M. and Hall, E.R.** Assessment of dynamic models for a high rate anaerobic treatment process, *Environ. Technol. Lett.*, Vol.10, pp551-566, 1989
- Jones, R.M., MacGregor, J.F., Murphy, K.L. and Hall, E.R.** Towards a useful dynamic model of the anaerobic wastewater treatment process: A practical illustration of process identification. *Wat. Sci. Technol.*, Vol.25 (7), pp61-71, 1992
- Jones, W.J., Nagle, D.P.Jr, Whitman, W.B.** Methanogens and the diversity of archaebacteria. *Microbiol. Rev.*, Vol.51, No.1, pp135-177, 1987
- Kaspar, H. and Wuhrmann, K.** Kinetic parameters and relative turnovers of some important catabolic reactions in digesting sludge, *Appl. Environ. Microbiol.* Vol. 36, pp1-7, 1978

- Kaspar, H.F. and Wuhrmann, K.** Product inhibition in sludge digestion. *Microbial Ecol.* Vol.4, pp241-248, 1978
- Kenealy, W.R. and Zeikus, J.G.,** One-carbon metabolism in methanogens: evidence for synthesis of a two-carbon cellular intermediate and unification of catabolism and anabolism in *Methanosarcina barkeri*. *J. Bacteriol.*, Vol.151, pp932-941, 1982
- Kennedy, K.J. and Droste, R.L.,** Anaerobic fixed film reactor treating carbohydrate wastewater, *Wat. Res.* Vol.20, No.6, pp685-696, 1986
- Kissel, J.C., McCarty, P.L. and Street, R.L.,** Numerical simulation of mixed culture biofilm. *J. Environ. Eng.*, ASCE, Vol.110 (EE2), pp393-411, 1984
- Kohler, H.P.E. and Zehnder, A.J.B.,** Carbon monoxide dehydrogenase and acetate thiokinase in *Methanothrix soehngenii*, *FEMS Microbiol. Lett.*, Vol.21, pp287-292, 1984
- Koster, I.W. and Cramer, A.** Inhibition of methanogenesis from acetate in granular sludge by long-chain fatty acids, *Appl. Environ. Microbiol.* Vol.53, No.2, pp403-409, 1987
- Koster, I.W.,** Characteristics of the pH-influenced adaptation of methanogenic sludge to ammonium toxicity, *J. Chem. Technol. Biotechnol.*, Vol.36, No.10, pp445-455, 1986
- Koster, I.W., Rinzema, A.L., Lettinga, G.,** Sulfide inhibition of the methanogenic activity of granular sludge at various pH-levels, *Wat. Res.* Vol.20, No.12, pp1561-1568, 1986
- Krzycki, J.A. and Zeikus, G.** Characterization and purification of carbon monoxide dehydrogenase from *Methanosarcina barkeri*. *J. Bacteriol.* Vol.158, pp231-237, 1984
- Krzycki, J.A., Wolkin, R. and Zeikus, G.** Comparison of unitrophic and mixtrophic substrate metabolism by an acetate-adapted strain of *Methanosarcina barkeri*. *J. Bacteriol.* Vol.149, pp247-254, Jan.1982
- Kugelman, I.J. and Chin, K.K.** Toxicity, synergism and antagonism in anaerobic waste treatment processes, *Anaerobic Biological Treatment Process*, Aug. 1970
- La Motta, E.J. and Shieh, W.K.,** Diffusion and reaction on biological nitrification. *J. Environ. Eng. Div.* ASCE, Vol.105 (EE4), pp655-673, 1979
- Laanbroek, H.J., Abee, T., Voogd, J.L.,** Alcohol conversion by *Desulfobulbus propionicus* Lindhorst in the presence and absence of sulfate and hydrogen, *Arch. Microbiol.*, Vol.133, pp178-184, 1982

Le
re

Le
ox

Le
sa

Le
Ve
ag
pp

Le

Lin
me
pp

Lo
tec

Lo
App

Ma
bac
198

Ma
and

Ma
mix
A/C

Mal
Met

Mar
sludg
1989

- Lawrence, A.W. and McCarty, P.L.** Kinetics of methane fermentation in anaerobic treatment, *J. W.P.C.F.* Vol.41 No.2, Res. Suppl. R1-R17, 1969
- Lee, M.J. and Zinder, S.H.,** Hydrogen partial pressures in a thermophilic acetate-oxidizing methanogenic coculture, *Appl. Environ. Microbiol.*, Vol.54, pp1457-1461, 1988
- Lenhard, G.** A standardized procedure for the determination of dehydrogenase activity in samples from anaerobic treatment system. *Wat. Res.*, Vol.2, pp161-167, 1968
- Lens, P.N.L., De Beer, D., Cronenberg, C.C.H., Houwen, F.P., Ottengraf, S.P.P. and Verstraete, W.H.,** Heterogeneous distribution of microbial activity in methanogenic aggregates: pH and glucose microprofiles. *Appl. Environ. Microbiol.*, Vol.59 (11), pp3803-3815, 1993
- Levenspiel, O.** *Chemical reaction engineering*, 2nd edition, chapter 9. 1972
- Lin C.Y., Noike, T., Furumai, H., Matsumoto, J.,** A kinetic study on the methanogenesis process in anaerobic digestion, *Water Science and Technology*, Vol.21, pp175-186, 1989
- Locher, G., Sonnleitner, B. and Fiechter A.** Pattern recognition: a useful tool in technological processes. *Bioprocess engineering*, Vol.5, pp181-187, 1990
- Lovely, D.R.,** Minimum threshold for hydrogen metabolism in methanogenic bacteria, *Appl. Environ. Microbiol.* Vol.49, No.6, June 1985
- Macario, A.J.L. and Conway de Macario, E.** Antigenic fingerprinting of methanogenic bacteria with polyclonal antibody probes. *System. Appl. Microbiol.* Vol.4, pp451-458, 1983
- MacLeod, F.A. et al.,** Layered structure of bacterial aggregates produced in an UASB and filter reactor, *Appl. Environ. Microbiol.*, Vol.56 (6), pp1598-1607, 1990
- Macmullen, R.B. and Weber, M.** The theory of short circuiting in continuous flow mixing vessels in series and the kinetics of chemical reactions in such systems, *Trans. AIChE* Vol.31 pp409, 1935
- Mah, R.A., Smith, M.R. and Baresi, L.,** Studies on an acetate-fermenting strain of *Methanosarcina*, *Appl. Environ. Microbiol.*, Vol.35, pp1174-1184, 1978
- Manjunath, D.L. et al.** Treatment of cane sugar mill waste water in upflow anaerobic sludge blanket reactors, *Proceedings of the 44th Purdue Industrial Waste Conference*, 1989

Mc
dig
Ny

Mc
Te

Mc
wo
En

Mc

Mc
dig
Jar

Mc
ana

Mc
ana

Mc
dig

Mc
me
Tec

Nil
pro

Ols
Vo
pla

Pat
nov
198

Pau
ana
bion

McCarty P.L. One hundred years of anaerobic treatment., pp3-22, in *Anaerobic digestion*, eds. Hughes, D.E., Stafford, D.A., Wheatley, B.J., Baader, W., Lettinga, G., Nyns, E.J. and Verstraeten, W., Elsevier, Amsterdam, 1981

McCarty, P.L. and Smith, P.D., Anaerobic wastewater treatment. *Environ. Sci. Technol.*, Vol.20, pp1200-1206, 1986

McInerney, M.J., Bryant, M.P., Hespell, R.B., Costerton, J.W., *Syntrophomonas wolfei* gen. nov. spec.nov., an anerobic syntrophic fatty acid oxidizing bacterium. *Appl. Environ. Microbiol.* Vol.41, pp1029-1039, 1981

Metcalf & Eddy. Wastewater Engineering: treatment, disposal, reuse. 3rd edi.

Monteith, H.D. and Stephenson, J.P., Mixing efficiencies in full scale anaerobic digesters by tracer methods, *J. Water Pollution Control Federation*, Vol 53, pp78-84, Jan. 1981

Morgan, J.W. et al., A comparative study of the nature of biopolymers extracted from anaerobic and activated sludges, *Wat. Res.* Vol.24, No.6, pp743-750, 1990

Mosey, F.E. Kinetic description of anaerobic digestion. 3rd *International symposium on anaerobic digestion*, Boston, 1983

Mosey, F.E., and Fernandes, X.A. Patterns of Hydrogen in biogas from the anaerobic digestion of milk-sugars, *Water Science and Technology*, Vol.21, pp187-196, 1989

Mosey, F.E., Matnematical modeling of the anaerobnic digestion process: Regulatory mechanisms for the formation of short-chain volatile acids from glucose. *Water Sci. Technol.*, Vol. 15 (8), pp209-219, 1983

Nilsson, B.K. and Karlsson, H.T., Diffusion rates in a dense matrix of methane-producing microorganisms. *J. Chem. Tech. Biotechnol.*, Vol. 44, pp255-260, 1989

Olsson, G., Andersson, B., Hellstrom, B.G., Holmstrom, H., Reinius, L.G. and Vopatek, P. Measurements, data analysis and control methods in wastewater treatment plants-state of the art and future trends. *Wat. Sci. Tech.* Vol.21, pp1333-1345, 1989

Patel, G.B., Characterization and nutritional properties of *Methanothrix concilii* sp. nov., a mesophilic acetoclastic methanogen., *Can. J. Microbiol.* Vol.30, pp1383-1396, 1984

Pauss, A., Andre, G., Perrier, M. and Guiot, S. Liquid to gas mass transfer in anaerobic process: Inevitable transfer limitations of methane and hydrogen in the biomethanation process. *Appl. Environ. Microbiol.*, June, pp1636-1644, 1990b

- Pauss, A., and Guiot, S.R.** Hydrogen monitoring in anaerobic sludge bed reactors at various hydraulic regimes and loading rates. *Water Environ. Res.* Vol.65, No.3, pp276-280, 1993
- Pauss, A., Guiot, S.R., Samson, R. and Beauchemin, C.** Continuous measurement of dissolved H_2 in an anaerobic reactor using a new hydrogen air fuel cell detector. *Biotechnol. Bioeng.*, Vol.35, pp492-501, 1990a
- Peterson, S.P. and Ahring, B.K.,** Acetate oxidation in a thermophilic anaerobic sewage-sludge digester: the importance of non-aceticlastic methanogenesis from acetate, *FEMS Microbiol. Ecol.* Vol.86, pp149-158, 1991
- Phelps, T.J., Conrad, R. and Zeikus, J.G.,** Sulfate dependent interspecies H_2 transfer between *Methanosarcina barkeri* and *Desulfovibrio vulgaris* during metabolism of acetate and methanol. *Appl. Environ. Microbiol.*, Vol.50, pp589-594, 1985
- Postgate, J.R. and Campbell, L.L.,** Classification of *Desulfovibrio* species, the nonsporulating sulfate-reducing bacteria. *Bacteriol. Rev.*, Vol.30, pp732-738
- Powell, G.E. and Archer, D.B.** On line titration method for monitoring buffer capacity and total volatile fatty acid levels in anaerobic digesters. *Biotechnol. Bioeng.*, Vol.33, pp570-577, 1989
- Radian Co.** *Guidelines for the preparation of GRI quality assurance project plans*, Aug. 1990
- Rebhun, M., Argaman, Y.** Evaluation of hydraulic efficiency of sedimentation basins, *J. San. Eng. Div. Proceedings ASCE SA5*, pp37, Oct. 1965
- Richardson, J.F. and Zaki, W.N.** Sedimentation and fluidisation *Trans. Inst. Chem. Engr.*, Vol.32, No.35, 1954
- Riemer, M., Kristensen, G.H. and Harremoes, P.,** Residence time distribution in submerged biofilters, *Water Research*, Vol.14, 1980
- Rittmann, B.E. and McCarty, P.L.,** Model of steady-state-biofilm kinetics. *Biotechnol. Bioeng.*, Vol. 22, pp2343-2357, 1980
- Rittmann, B.E.,** The effect of loading fluctuations on the effluent concentration produced by fixed-film reactors. *Water Sci. Technol.*, Vol. 16, pp45-55, 1985
- Rittmann, B.E.,** The effect of shear stress on biofilm loss rate. *Biotechnol. Bioeng.*, Vol.24, pp501-506, 1982

- Robinson, J. A. and Tiedje, J.M.** Kinetics of hydrogen consumption by rumen fluid, anaerobic digester sludge, and sediment, *Appl. Environ. Microbiol.*, Vol.44, pp1374-1384, 1982
- Rozzi, A., Di Pinto, A.C. and Brunetti, A.** Anaerobic process control by bicarbonate monitoring. *Environ. Technol. Lett.*, Vol.6, pp594-601, 1985
- Rozzi, A.S., Merlinio, S., and Passino, R.,** Development of a four population model of the anaerobic degradation of carbohydrates. *Environ. Technol. Letters*, Vol.6, pp610-619, 1985
- Saez, P.B. and Rittmann, B.E.,** Improved pseudoanalytical solution for steady state biofilm kinetics, *Biotech. Bioeng.*, Vol.32, pp379-385, 1988
- Samain, E., Albaniac, G., Dubourgier, H.C., Touzel, J.P.,** Characterization of a new propionic acid bacterium that ferments ethanol and displays a growth factor dependent association with a Gram negative homoacetogen, *FEMS Microbiology Lett.* Vol.15, pp69-74, 1982
- Schauer, N.L. and Ferry, J.G.,** Metabolism of formate in *Methanobacterium formicum*. *J. Bacteriol.* Vol.42, pp800-807, 1980
- Schauer, N.L., Brown, D. P. and Ferry, J.G.,** Kinetics of formate metabolism in *Methanobacterium formicum* and *Methanospirillum hungatei*. *Appl. Environ. Microbiol.*, Vol 44, pp549-554, 1982
- Schink, B, Kremer, D.K., Hansen, T.A.,** Pathway of propionate formation from ethanol in *Pelobacter propionicus*, *Arch Microbiol* Vol.147, pp321-327, 1987
- Schink, B. and Thauer, R.K.** Energetics of syntrophic methane formation and the influence of aggregation. In Granular anaerobic sludge; microbiology and technology. *Proceedings of the GASMAT-workshop*, pp5-17, Lunteren, Netherlands, 25-27 Oct., 1987
- Schink, B., Phelps, T., Eichler, B., Zeikus, J.G.,** Comparison of ethanol degradation pathways in anoxic freshwater environments, *J. of General Microbiol.* Vol.131, pp651-660, 1985
- Schink, B.,** Fermentation of 2,3-butanediol by *Pelobacter carbinolicus* sp. nov. and *Pelobacter propionicus* sp.nov., and evidence for propionate formation from C2 compounds, *Arch Microbiol.* Vol.137, pp33-41, 1984
- Schmidt, J.E. and Ahring, B.K,** Effects of hydrogen and formate on the degradation of propionate and butyrate in thermophilic granules from an Upflow Anaerobic Sludge Blanket reactor. *Appl. Environ. Microbiol.*, Vol.59, No.8, pp2546-2551, 1993

- Schmidt, J.E. and Ahring, B.K.** Acetate and hydrogen metabolism in intact and disintegrated granules from an acetate-fed, 55°C, UASB reactor, *Appl. Microbiol. Biotechnol.* 35:pp681-685, 1991
- Schmidt, J.E. and Ahring, B.K.**, Effects of hydrogen and formate on the degradation of propionate and butyrate in thermophilic granules from an upflow anaerobic sludge blanket reactor, *Appl. Environ. Microbiol.*, Vol.59, No.8, pp2546-2551, 1993
- Schulze, D., Mehkhous, M., Fiebig, R., and Dellweg, H.** Anaerobic treatment of protein-containing waste waters: correlation between coenzyme F₄₂₀ and methane production. *Appl. Environ. Microbiol.* Vol.29, pp506-510, 1988
- Seitz, H.J., Schink, B., Pfenning, N., Conrad, R.**, Energetics of syntrophic ethanol oxidation in defined chemostat cocultures 1. Energy requirement for H₂ production and H₂ oxidation, *Arch. Microbiol.* Vol. 155, pp82-88, 1990
- Seitz, H.J., Schink, B., Pfenning, N., Conrad, R.**, Energetics of syntrophic ethanol oxidation in defined chemostat cocultures 2. Energy sharing in biomass production, *Arch. Microbiol.* Vol. 155, pp89-93, 1990
- Shrink, B.**, Energetics of anaerobic system, speech at Center of Microbial Ecology, Michigan State University, Aug.11, 1992
- Shrink, B.**, Principles and limits of anaerobic degradation: environmental and technological aspects, *Biology of anaerobic microorganisms* edi. Zehnder, 1988
- Smith, D.P.**, PhD thesis, Stanford University, 1987
- Smith, P.H. and Mah, R.A.**, Growth and methanogenesis by methanosarcina strain 227 on acetate and methanol, *Appl. Environ. Microbiol.* Vol.37, pp993-999, 1978
- Speece, R.E.**, A survey of municipal anaerobic sludge digesters and diagnostic activity assays. *Wat. Res.* Vol.22, pp365-372, 1988
- Stevens, D.K. et al.**, The effect of tracer diffusion in biofilm on residence time distributions, *Water Research*, Vol.20, No.3, 1986
- Strayer, R.F. and Tiedje, J.M.** Application of the fluorescent-antibody technique to the study of a methanogenic bacterium in lake sediments. *Appl. Environ. Microbiol.* Vol.35, pp192-198, 1978
- Stupperich, E., Hammel, K.E., Fuchs, G. and Thauer, R.K.** Carbon monoxide fixation into the carboxyl group of acetyl coenzyme A during autotrophic growth of *Methanobacterium*. *FEBS Lett.*, Vol.152, pp21-23, 1983

Switzenbaum, M.S., Giraldo-Gomez, E., Hickey, R.F. Control of anaerobic digestors. presented at the *Regional workshop and conference on anaerobic treatment of wastewater in Latin America.*, Mexico City, Mexico, Nov.6-9, 1990

Thauer, R.K., Fuchs, G. and Jungerman, K., Role of iron-sulfur proteins in formate metabolism. In *Iron Sulfur Proteins*, W. Lowenberg (Ed.), Academic Press, New York, pp121-156, 1973

Thauer, R.K., Jungermann, K. and Decker, K. Energy conservation in chemotrophic anaerobic bacteria. *Bacteriol. Rev.* Vol.41, pp100-180, 1977

Thauer, R.K., Jungermann, K., Decker, K., Energy conservation in chemotrophic anaerobic bacteria, *Bacteriological Reviews.* Vol.41, No.1, pp100-180, Mar. 1977

Thiel, P.G. and Hattingh, W.H.J. Determination of hydrolytic enzyme activities in anaerobic digestion sludge. *Wat. Res.*, Vol.1, pp191-196, 1967

Thiele, J.H. and Zeikus, J.G., Interactions between hydrogen- and formate- producing bacteria and methanogens during anaerobic digestion, *Handbook on anaerobic fermentations*, edi. Erickson, L.E. and Fung, D.Y., 1988a

Thiele, J.H. and Zeikus, J.G., Control of interspecies electron flow during anaerobic digestion: The role of formate versus hydrogen transfer during syntrophic methanogenesis in flocs, *Appl. Environ. Microbiol* Vol.54, No.1, pp20-29, 1988c

Thiele, J.H., Chartrain, M. Zeikus, J.G., Control of electron flow during anaerobic digestion: The role of floc formation in syntrophic methanogenesis, *Appl. Environ. Microbiol*, Vol.54, No.1, pp10-19, 1988b

Van der Meer, R.R. Anaerobic treatment of wastewater containing fatty acids in upflow reactors, *phD thesis*, Delft university press, 1979

Visser, F.A. et al., Diversity and population dynamics of methanogenic bacteria in a granular consortium, *Appl. Environ. Microbiol.*, Vol.57, No.6, pp1728-1734, 1991

van Lier, J.B., Crolle, K.C.F., Frijters, C.T.M.J., Stams, A.J.M. and Lettinga, G., Effects of acetate, propionate and butyrate on the thermophilic anaerobic degradation of propionate by methanogenic sludge and defined cultures, *Appl. Environ. Microbiol.*, Vol.59, No.4, pp1003-1011, 1993

van Lier, J.B., Grolle, K.C.F., Stams, A.J.M., Conway de Macario, E. and Lettinga, G. Start-up of a thermophilic upflow anaerobic sludge bed (UASB) reactor with mesophilic granular sludge. *Appl. Microbiol. Biotechnol.* Vol.37, pp130-135, 1992

Wen, C.Y. and Yu, Y.H. Mechanics of fluidization, *Chem. Eng. Process Symp. Series*, Vol. 62, 1966

Westermann, P. et al., Threshold acetate concentration for acetate catabolism by aceticlastic methanogenic bacteria, *Appl. Environ. Microbiol.*, Feb. pp514-515, 1989

Widdel, F., Wolfe, R.S., Growth of methanogenic bacteria in pure culture with 2-propanol as sole hydrogen donor, *86th Annual meeting of the American Society for Microbiology*. Abstract I126, 1986

Williamson, K. and McCarty, P.L., A model of substrate utilization by bacterial films. *J. Water Pollu. Control Fed.*, Vol.48 (1), pp9-24, 1976

Williamson, K.J. and McCarty, P.L., A model of substrate utilization by bacterial films, *J.W.P.C.F.* Vol.48, No.1, pp9-24, 1976

Wolin, M.J. Interaction between H_2 -producing and methane producing species. pp141-146, in *Microbial formation and utilization of gases (H_2 , CH_4 , CO)*. ed. Schlegel, H.G., Gottschalk, G. and Pfennig, N., Goltze, Gottingen, Federal Republic of Germany, 1976

Woods, D.D., Hydrogen lyases. The synthesis of formic acid by bacteria, *J. Biol. Chem.*, Vol.77, pp515-518, 1936

Wu, W-M, 1991(a), PhD thesis, Michigan State University

Wu, W-M, Hickey, R.F., Zeikus, J.G., 1991(b), Characterization of metabolic performance of methanogenic granules treating brewery wastewater: role of sulfate-reducing bacteria, *App. Environ. Microbiol.* Vol.57, No.12, pp3438-3449, 1991

Xu, B.J. *Principles of water supply and waste water treatment*, Qing-Hua University press, pp50-60, P.R.China, 1983

Zehnder, A.J., Ingvorsen, B.K. and Marti, T. Microbiology of methane bacteria. pp45-68, in *Anaerobic digestion*, eds. Hughes, D.E., Stafford, D.A., Wheatley, B.J., Baader, W., Lettinga, G., Nyns, E.J. and Verstraeten, W., Elsevier, Amsterdam, 1981

Zehnder, A.J.B., Huser, B.A., Brock, T.D. and Wuhrmann, K., Characterization of an acetate decarboxylating non-hydrogen-oxidizing methane bacteria, *Arch. Microbiol* Vol.124, pp1-11, 1980

Zeikus, J.G., Microbial populations in digestors, In *First International Symposium on Anaerobic Digestion*, D.A.Stafford, et al.(Ed.). A.D. Cardiff Scientific Press, Cardiff, U.K., pp75-103, 1979

Zinder, S.H. and Koch, M., Non-aceticlastic methanogenesis from acetate: acetate oxidation by a thermophilic syntrophic coculture, *Arch. Microbiol.* Vol.138, pp263-272, 1984

Zinder, S.H., Anguish, T., Lobo, A.L., Isolation and characterization of a thermophilic acetotrophic strain of *Methanothrix*, *Arch. Microbiol.* Vol.146, No. 4, pp315-322, 1987

Zinder, S.H., Cardwell, S.C., Anguish, T., Lee, M. and Koch, M., Methanogenesis in a thermophilic(58°C) anaerobic digester: *Methanothrix sp.* as an important aceticlastic methanogen., *Appl. Environ. Microbiol.*, Vol.47, No.4, pp796-807, 1984

Zinder, S.H., Conversion of acetic acid to methane by thermophiles, *FEMS Microbiology Reviews*, Vol. 75, pp125-138, 1990

Zoetemayer, R.J., Matthusen, A.J.C.M., Cohen, A. and Boelhouwer, C. Product inhibition in the acid forming stage of the anaerobic digestion process. *Wat. Res.*, Vol.16, pp633-639, 1982

MICHIGAN STATE UNIV. LIBRARIES



31293014110591